University of Lund
Department of Mineralogy and Petrology
Sölvegatan 13
S – 222 21 LUND
SWEDEN

Nordic Volcanological Institute 9901
University of Iceland
Grensásvegur 50
IS – 108 Reykjavík
ICELAND

1992-1998

Seismicity and Deformation

at

Mt. Eyjafjallajökull volcano

by

Malou Blomstrand Stinessen

A thesis
submitted to the Unversity of Lund
for
Master degree
February 1999

5103+92 s.
CODEN: SE-LUNBBS/NBGO-99/

English abstract

In this master thesis, I use seismic and geodetic data to study a period of unrest at Mt. Eyjafjallajökull volcano in South Iceland. An earthquake swarm, which occurred in 1994 was studied. Global Positioning System (GPS) geodetic measurements and optical levelling ground tilt measurements in the period of 1992 to 1998 were also analysed. Geodetic ground information measurements show that the 1994 earthquake swarm was associated with crustal deformation , probably caused by an inclined east-west oriented dyke intrusion at around 6-7 km depth beneath Mt. Eyjafjallajökull. A "Mogi"-single-point-source of pressure model cannot fully explained the data from 1992-1998, but the geodetic data rather suggest that a dyke intrusion model is more appropriate for the deformation associated with the 1994 earthquake swarm at Mt. Eyjafjallajökull. GPS measurements show that an earthquake swarm in 1996 was not associated with any significant crustal deformation. The 1996 earthquake swarm was located to the west of the 1994 earthquake swarm. It was not associated with any magmatic intrusion at shallow depth, but rather with brittle failure of the upper crust. No significant gradual deformation was observed at Mt. Eyjafjallajökull in the 1994-1998 period, indicating that Mt. Eyjafjallajökull is characterised by little deformation between episodic events of magmatic/seismic activity.

Svenskt förord

I detta examensarbete använder jag både seismiska och geodetiska data för att studera en period med seismisk aktivitet under vulkanen Eyjafjallajökull, belägen i södra Island. Lokalisering av jordbävningar i en jordbävningssvärm 1994, geodetiska data från Global Positioning System (GPS) och optiska tilt-mätningar under perioden 1992-1998 har analyserats. De geodetiska mätningarna visar att jordbävningssvärmen 1994 var associerad med krustal deformation, och orsakades av en öst-västligt orienterad mot vertikalplanet lutande magmatisk intrusion, vilken skedde på 6-7 km djup under Eyjafjallajökull. Modellering med en "Mogi"-single-point-source deformationsmodell visar emellertid att geodetiska data från tiden 1992-1998 inte fullständigt låter sig förklaras med en punktmodell. En "gångintrusion modell" verkar passa bättre med den observerade deformationen. GPS mätningarna visar vidare att en jordbävningssvärm 1996 under Eyjafjallajökull inte kan associeras med någon mätbar krustal deformation. Denna svärm inträffade längre västerut än svärmen 1994. Jordbävningarna 1996 anses inte vara förknippad med någon grund magmatisk intrusion, utan orsakades av spröd deformation i den övre delen av jordskorpan. Ingen långsam, successiv krustal deformation har kunnat observerats under perioden 1992-1998, vilket indikerar att Eyjafjallajökull är ett stabilt vulkaniskt område, där krustal deformation är nära relaterad till magmatism och/eller seismisk aktivitet.

Svensk sammanfattning (Swedish summary)

Målet med detta examensarbete i tillämpad geofysik är att öka förståelsen för geologiska och geofysiska processer och deras samspel under vulkanen Eyjafjallajökull i södra Island. På Island har sedan ett tiotal år tillbaka använts geodetiska mätningar med Global Positioning System (GPS) instrument och geodetiska tiltmätare för att påvisa krustal deformation, som orsakas av vulkanisk, annan magmatisk eller seismisk aktivitet.

Jag har behandlat och tolkat GPS- och tilt-mätningar utförda i området omkring Eyjafjallajökull sedan 1992 i detta examensarbete. Modellering med en modell med en punktformad tryckkälla föreslagen av K. Mogi 1958 har utnyttjats. Tolkning av denna modell har sedan använts för att dra slutsatser om orsaken till den uppmätta deformationen under tiden då jordbävningssvärmen 1994 ägde rum. Lokalisering av jordbävningsfoci från den för Eyjafjallajökull atypiska seismiska aktiviteten, som ägde rum under försommaren 1994 har gjorts. Vidare har en utvärdering utförts av de seismiska hastighetsmodeller, som finns för det aktuella området, och som använts för att lokalisera jordbävningarna från svärmen 1994. Jag har försökt att tolka både orsaken till den plötsliga seismiska aktiviteten under Eyjafjallajökull och relationen mellan den

observerade krustala deformationen och den seismiska aktiviteten under tidsperioden 1992-1998.

Eyjafjallajökull utgörs av en stratovulkan som är belägen i den södra delen av den östra vulkaniska zonen (EVZ, the Eastern Volcanic Zone) vid Islands södra kust. EVZ utgör tillsammans med den västra vulkaniska zonen (WVZ, the Western Volcanic Zone) en fortsättning av den mittatlantiska ryggen, som ansluter till Island vid den västligaste sydspetsen, Reykjaneshalvön. Idag anses EVZ vara den mest aktiva av de två, och 85±15% av den totala riftrörelsen anses ske i EVZ. EVZ löper från sydvästra delen av Vatnajökull till Islands södra kust i riktning mot Västmannaöarna. Vulkankonen Eyjafjallajökull bildades för ungefär 0,78 miljoner år sedan i den cirka 2 miljoner år gamla EVZ. Eyjafjallajökull är uppbyggd av alkalina basalter, men den senaste aktiviteten hade en mer sur karaktär. Lavorna domineras av ankaramiter till kvarts-trakyter.

Eyjafjallajökull ligger strax väster om den seismiskt och vulkaniskt aktiva vulkanen Katla. Mot norr påträffas ett flertal aktiva vulkaner såsom Hekla, Vatnafjöll och Torfajökull. Eyjafjallajökull har ibland även kallats "Den Tysta", vilket väl karaktäriserar den seismiska och vulkaniska aktivitet som rått under de senaste 15 åren. Den seismiska aktivitet inom EVZ är av heterogen karaktär. Det förekommer både konstant seismiskt aktiva vulkaner och områden och vulkaner som är nästan helt aseismiska. Eyjafjallajökull uppvisar en mycket periodisk seismisitet, som troligen härrör från magmatiska intrusioner eller förändringar i det rådande stressfältet i området. Två jordbävningssvärmar har ägt rum under de senaste tio åren, en 1994 samt en 1996.

En utvärdering av de tre seismiska hastighetsmodeller, som finns för området, gjordes varefter en av modellerna lyftes fram som den mest lämpliga för lokalisering av jordbävningarna under Eyjafjallajökull. Den föredragna seismiska hastighetsmodellen baseras på data från den norra delen av den i väster belägna grannvulkanen Katla (MYR-N modellen). I denna seismiska hastighetsmodell finns ingen höghastighetszon, likartad den som påträffats öster om Eyjafjallajökull i den sydisländska seismiska zonen (SISZ - South Iceland Seismic Zone) och som ingår i den andra modellen (SIL - the South Iceland Lowland model). I den tredje utvärderade modellen finns en zon med lägre seismiska hastigheter, som utgör ett tecken på fickor av magma eller magmakammare. Denna modell är baserad på data från Katlas västra del, där en magmakammare påträffades på cirka 5 km djup.

1994 års jordbävningssvärm under Eyjafjallajökull registrerades av två seismiska nätverk i området och bestod av mer än 130 "event". Dessa "event" är medel- till högfrekvensjordbävningar, som inträffade strax norr om Eyjafjallajökull. Av dessa har totalt 67 lokaliserats i denna studie. Magnitudintervallet sträcker sig från M_L 0,59 till 2,27 och jordbävningarna klassificerades därför som mikrojordbävningar.

Jordbävningssvärmen började plötsligt den 23:e maj och pågick drygt en och en halv månad fram till den 3:e juli 1994. Majoriteten av jordbävningarna skedde på fyra till sju kilometers djup och uppvisade en tydlig öst-västlig trend, vilken väl överensstämmer med det lokala stressfältet, som anses råda under Eyjafjallajökull, men som ännu ej funnit sin slutliga förklaring. Fokalmekanismerna uppvisar en homogen trend med vertikala T-axlar, horisontella P-axlar och öst-västligt orienterade nodalplan. P-axlarnas orientering varierar dock, vilket har tolkats antingen som en effekt av det heterogen stressfält, som råder under Eyjafjallajökull, eller att stressfältet skulle ha varierat under tiden för jordbävningssvärmen. Den mer regionala seismiska trend, som observerats i anslutning till EVZ, är orienterad i en mer nordöstlig-sydvästlig riktning. Sett över längre tid verkar den seismiska aktiviteten under Eyjafjallajökull vara närmare sammankopplad med detta regionala stressfält. De få jordbävningar som inträffar är troligen inte betingade av magmatiska intrusioner utan snarare av små justeringar av det regionala stressfältet, vilket orsakas av plattornas rörelser. Med hjälp av de GPS-mätningar, som gjorts under åren 1994 till 1998, och som analyserats i detta examensarbete, kan ingen mätbar deformation i Eyjafjallajökull påvisas, trots den jordbävningssvärm som intr_ffade 1996. Denna svärm anses därför inte vara relaterad till någon magmatisk intrusion, som skulle kunna generera mätbar deformation i jordskorpan. Däremot är jordbävningssvärmen 1994 associerad med mätbar deformation i jordskorpan. Den senare seismiska aktiviteten och deformationen tolkas som resultat av en

magmatisk intrusion, en skivformad gång, intruderad på 6-7 km djup i öst-västlig riktning under vulkanens norra flank. Denna intrusion anses vara liten. Som förut föreslagits har den en begränsad längd och mindre än fem meters bredd.

Modellering med den modell med en punktformad källa som föreslagits av Mogi indikerar att jordbävningssvärmen under Eyjafjallajökull 1994 troligen orsakats av en gångintrusion snarare än en magmakammare. Denna tolkning beror på att den största uppmätta deformationen inte skedde direkt över det t_nkta deformationscentrumet, som Mogis modell föreslår, utan snarare söder om Eyjafjallajökull. Tiltmätningar under tiden 1993-1994 uppvisar en tilt-vektor, som inte är riktad direkt mot deformationscentrumet (Mogimodellen) utan istället pekar mot ett deformationscentrum söder eller sydväst om Eyjafjallajökull. Detta indikerar vidare att en gång-intrusionsmodellen bättre skulle passa de geodetiska data och den uppmätta deformationen än en modell grundad på Mogis modell.

Eyjafjallajökull karaktäriseras av ringa seismisk aktivitet. Den intensifierade seismisitet, som inträffat under de senaste 15 åren är episodisk och plötslig. Jordbävningssvärmen 1994 orsakades troligen av en magmatisk intrusion medan den under våren 1996 inte kan relateras till någon magmatism, eftersom ingen observerbar krustal deformation förekom under denna tid. Den deformation som uppmätts under mätperioden 1992-1998 anses vara nära knuten till magmatisk och/eller seismisk aktivitet under Eyjafjallajökull. Geodetiska mätningar (GPS och tilt-mätningar) under åren 1994 (efter 1994 års "event") och 1998, visar att ingen långsam mer kontinuerlig mätbar deformation sker under Eyjafjallajökull.

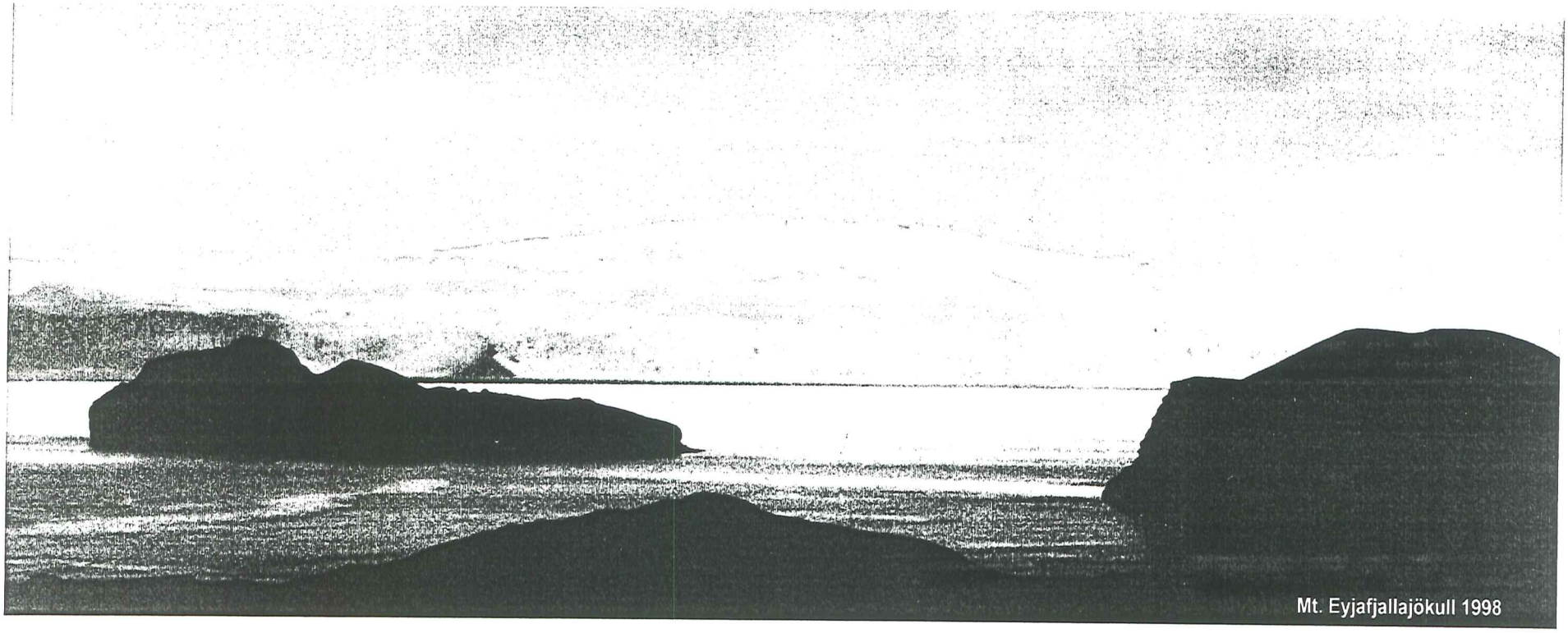

Mt. Eyjafjallajökull 1998

ACKNOWLEDGEMENTS

The work described here was conducted while I was a research fellow at the Nordic Volcanological Institute in 1998-1999. It would have been impossible to do without my supervisors Dr. Freysteinn Sigmundsson at the Nordic Volcanological Institute and Bryndís Brandsdóttir at the Science Institute of the University of Iceland. Thank you Freysteinn and Bryndís for all discussions, the advice, expertise, support and help with all kind of problems.

Most of the earthquake data used in this study had been collected earlier by the Science Institute, University of Iceland, the Nordic Volcanological Institute and the Iceland Meteorological Office. I acknowledge access to all the data and thank all the individuals involved in the collection of these data. The GPS measurements were conducted by the Nordic Volcanological Institute and the Science Institute. The Nordic Volcanological Institute supported me with salary for eight months and a great environment to work within.

I also would like to thank my supervisor in Sweden, Dr. Anders Lindh at the University of Lund, for making this cooperation with the Nordic Volcanological Institute possible and for support and encouragement.

Thanks to Sigrún Hreinsdóttir for GPS support and friendship. I also want to mention Jan Rées for helping me with everything with the thesis structure and supporting me all the time.

There are so many people who I want to thank. THANK YOU ALL !!!

CONTENTS

LIST OF TABLES

LIST OF FIGURES

FIGURE TEXTS

Figure 1:

Magnetic Field Anomaly map based on the DNAG and Iceland aeromagnetic gridded data. From Maps of Gravity, Bathymetry and Magnetics for Iceland and Surroundings. Orkustofnun/National Energy Authority, by H. Eysteinssson and K. Gunnarsson, 1995.

Figure 2:

Geology map of Iceland by Ármann Huskuldsson

Figure 3:

The volcanic zones of Iceland. Map provided from the Nordic Volcanological Institue. Included are the ridge spreading rates (NUVEL- 1) by DeMets et al. 1990.

Figure 4:

Geographical map of Iceland with the names of the major volcanoes in Iceland. From Nordic Volcanological Institute.

Figure 5:

Simplified crustal geology structure map of the southern part of the Eastern Volcanic Zone. From N.Óskarsson et al., 1982. The high grade amphibolite layer (between 2 and 3) is the one now interpreted to be generating the thick crust, and should therefore be thicker than in this figure.

Figure 6a:

Seismicity map of Iceland in 19950101-19981231, with all the earthquakes with magnitudes over ML=2 and well located. The different seismic zones in the text are shown as well as the volcanic zones.

Figure6b:

Epicentres and focal mechanisms of earthquakes in Iceland. Epicentres are derived from the earthqauek list (PDE) of the U.S . Geological Survey for the time period 1963-1987. From Einarsson , 1991.

Figure 7.

High- and low frequency earthquakes from the Vatnafjöll earthquake in 21 December 1992 (high frequency events - lower figure), and low frequency events fromthe

neighbouring Hekla volcano in 4 August 1994 - upper part of the figure. From Soosaluand Einarsson, 1997.

Figure 8a:

vertical and horizontal deformation associated with a single point source Mogi model. From Sigmundsson, 1994??????

Figure 8b:

Dyke intrusion, as figure 8a.

Figure 9:

Geology map of the southern part of Iceland including Mt. Eyjafjallajökul and the Hekla, Katla, Torfajökull volcanoes and more. From the geology map from Landmælingar……..

Figure 10:

Geology map fo Mt. Eyjafjallajökull. From Jónsson, 1998.

Figure 12:

the results from the 2-D seismic undershooting at the Katla volcano. From Guðmundsson et al., 1994.

Figure 12:

Epicentres in the southern part of the Eastern Volcanic Zone, within the time period 1979ö1985. From Einarsson, 1991.

Figure 13:

Earthquake activity at Torfajökull and Hekla during the time period 1991-1995. From Soosalu and Einarsson, 197.

Figure 14:

Seismic activity registred by the South Iceland Lowland network (SIL) for the Eyjafjöll volcanic system region during the time period 1991-1998. From the Veðurstofa(Meteorological Office in Iceland.

Figure 15.

Earthqukae locations by the SIL network for the 1994 earthquake swarm at Mt. Eyjafjallajökull. From the same source as figure 14.

Figure 16:

Magnitude versus time plotted for the events plotted in Figure 15. Source, see Figure 14 and 15.

Figure 17:

Magntidue versus depth for the seismic events in Figure 14-16. Source, see Figure 14-16.

Figure 18:

Orientations of P-and T-axes for the microearthquake in the 1994 swarm at Mt. Eyjafjallajökull, derived by Dahma and Brandsdóttir, 1997.

Figure 19:

The two seismic networks operative during the earthquake swarm at Mt. Eyjafjallajökull 1994. Coordinates from source as Figure 14-17.

Table 1:

Coordinates for the seismic stations within the two seismic networks. Source, see Figure 19.

Table 2:

Seismic stations and the distance, azimuth, angle and number of recorded events for each individual seismic station.

Figure 20:

Suggested seismic velocity model derived from the 2-D undershooting profile over the Katla volcano, deriving the data for the MYR-V and the MYR-N velocity models used to relocate the seismic events during the 1994 earthquake swarm at Mt. Eyjafjallajökull. Source see Figure 12.

Figure 21:

Differences of the three velcoity models used in this study to relocate seismic events. From Guðmundsson et al. 1994; and Bjarnason et al., 1983?????

Table 3:

Seismic velocities of the different velocity models with depths. From sources as Figure 21.

Figure 22:

Rms versus number of earthquakes for the 1994 earthquake swarm at Mt. Eyjafjallajökull. Data was derived from the relocations of the earthquake with the program HYPOINVERSE (Klein1978).

Table 4:

Estimated parameters for re spective velocity model, derived as from the same source as Fiugre 22.

Figure 23a-c:

Locations of the earthquakes for the swarm 1994 at Mt. Eyjafjallajökull for the three different velocity models MYR-N,. MYR-V and SIL. Source, see Figure 22.

Figure 24a-b:

Latitude versus time, see Figure 23.

Figure 25a-b:

Longitude versus time, see Figure 23.

Figure 26a-b:

Depth versus time, see Figure 23.

Figure 27a-b:

Depth versus latitude, see Figure 23.

Figure 28a-b:

Depth versus longitude, see Figure 23.

Table 5:

Affected rock volume calculated for the different velocity models, source see Figure 23.

Figure 29:

Plot of the analysed earthquake according to the whole swarm. Source as Figure 17 for ex.

Table 6:

Figure 30:

Magnitude versus depth, see Figure 23.

Figure 31:

Magntidue versus Latitude, see Figure 23.

Figure 32:

Magntidue versus Longitude, see Figure 23.

Figure 33:

Magnitude versus time, see Figure 23.

Figure 34:

GPS measurements in the years 1992, 1993 and 1994 respecitvely, conducted in the Eastern Volcanic Zone. From Jónsson et al., 1995.

Table 7:

GPS and tilt stations: coordinates and station numbers. From ???????????

Table 8:

GPS measurements ; scaling factos and errors for each campign. From calculated GPS estimattions with the BERNES …

Figure 35:

Map of the GPS stations measured in 1998.

Table 9:

GPS stations measured in 1992-1998 around Mt. Eyjafjallajökul. Dates. From ???????

Figure 36a:

Repeatability plot for the 1994Aa GPS campaign.

Figure 36b:

Scatter plot for the 1994Aa GPS camping.

Table 10:

Final coordinates for all the GPS stations within each GPS campaing during 1992-1998 around Mt. Eyjafjallajökull

Figure 3a:

Repeatability plot for the 1994Ab GPS campaign.

Figure 37b:

Scatter plot for the 1994A GPS camping.

Figure 38a:

Repeatability plot for the 1994B GPS campaign.

Figure 38b:

Scatter plot for the 1994B GPS camping.

Figure 39a:

Repeatability plot for the 1998 GPS campaign.

Figure 39b:

Scatter plot for the 1998 GPS camping.

Table 11:

1 simga minor and major axis of uncertanty ellipsoids in the GPS measurements

Figure 40:

GPS displacement vectors for 1992-1994B

Figure 41:

GPS displacement vectors for 1992-1998

Figure 42:

GPS displacement vectors for 1994Ab-1994B

Figure 43:

GPS displacement vectors for 1994Ab-1998

Figure 44:

GPS displacement vectors for 1994B-1998

Figure 45:

Tilt stations around Mt. Eyjafjallajökull measrued in 1992-1998

Figure 46:

Tilt displacement vectors for 1992-1993 Fimmvörðuháls

Figure 47:

Tilt displacement vectors for 1993-1994 Fimmvörðuháls

Figure 48:

Tilt displacement vectors for 1994-1995 Fimmvörðuháls

Figure 49:

Tilt displacement vectors for 1994-1995 Dagmálafjall

Figure 50:

Figure 51:

Figure 52:

Figure 53:

Figure 54:

Figure 55:

Table 12:

GPS displacements between 1992 and 1998

Table 13:

Table 14:

1. Introduction

Several physical and chemical geological processes may cause earthquakes at volcanoes, such as inflation/deflation of shallow crustal magma chambers, magmatic intrusion/extrusions into the upper crust or thermal cracking due to heating or cooling of brittle, crustal material. Seismological studies can give important information about the dynamics and the structure of volcanoes, and the upper crust. Earthquake locations provide information of the event characteristics. Seismic waves propagating through the roots of volcanoes carry valuable information on the physical state of the rocks, e.g. molten or solid phases, probable pockets or even chambers of magma.

The aim of this Master Thesis is to provide a better understanding of the behaviour of the Mt. Eyjafjallajökull volcano or "The Quiet One" and in particular the seismicity that occurred there in 1994 and 1996. Crustal deformation associated with the 1994 earthquake swarm was measured by Global Posisitoning System (GPS) geodetic measurements. A comparison of the 1994 and 1996 earthquake swarms is given, as well as an interpretation of their probable cause. The first part of the thesis gives an introduction to the general tectonics and geology of Iceland, and the Eyjafjöll volcanic system including Mt. Eyjafjallajökull. The second and third part include the analyses of the earthquake data and the geodetic measurements respectively. The fourth part contains a

discussion, followed by conlcusions.

1.1 Tectonics and geology of Iceland

Iceland is situated on the Mid Atlantic Ridge, the oceanic plate boundary between the diverging American and Eurasian plates (**Figure 1**). Iceland consists of oceanic crust, still being formed along a plate boundary, in the vicinity of one of the major hotspots found on Earth. The North Atlantic Mantle Plume activity began around 130 Myears ago northwest of Greenland (Lavwer and Müller, 1994). Around 60 Myears ago, this hot spot activity caused a jump of the spreading ridge, initiating an episode of rifting and eruptions of voluminous basalts between Greenland and Europe (Hill, 1991). The Iceland Plateau in the North Atlantic Ocean, was formed during the interaction between the North Atlantic mantle plume and the Mid-Atlantic Ridge activity. At the latitude of south Iceland, the Mid-Atlantic Ridge spreading rate is 19.4 mm/year in direction N104°E, according to the NUVEL-1 global plate motion model (DeMets et al., 1990). The oldest exposed Tertiary basalts in Iceland are around 16 million years old (Sæmundsson, 1979) and are located in the northwestern part of the country (**Figure 2**).

The Mid-Atlantic Ridge plate boundary in Iceland (**Figure 3**) is expressed

as a series of volcanic and seismic zones (Einarsson, 1991), and postglacial activity in Iceland is confined to these zones of activity. The Reykjanes Penisula oblique rift and the Western Volcanic Zone (WVZ) are the onland extensions of the submarine Mid-Atlantic Ridge. The Eastern Volcanic Zone (EVZ) is subparallel to the WVZ, with the South Icelandic Seismic Zone (SISZ) linking these two volcanic zones together. The EVZ runs southwest from Vatnajökull to Vestmannaeyjar and changes from being a rift zone in the north, to a flank zone with volcanism but little evidence of rifting in the south (Sæmundsson, 1978). It has been suggested to be a southward propagating rift, now successively replacing the Western Volcanic Zone due to an eastward jump of the spreading axis 2 Myears ago, towards the current centre of the North Atlantic Plume (Einarsson, 1991). Four major rift-volcanic episodes have occurred in the EVZ, during the last 1100 years and (Þórarinsson, 1975). The Northern Volcanic Zone (NVZ) is the northward continuation of the Eastern Volcanic Zone, striking from Vatnajökull to the northern coast of Iceland. There, the plate boundary is offset again westwards, across the Tjörnes Fracture Zone (TFZ) to the Kolbeinsey Ridge. The Snæfellsnes Volcanic Zone (SVZ) and the Öræfajökull-Snæfell Volcanic Zone (OSVZ) are volcanic flank zones in the western and the south-eastern part of Iceland (see Figure 2). These are characterised by older rocks, low magma supply rate, and poorly developed tensional features (Sæmundsson, 1978). The southern part of the EVZ is also a flank zone, but only 2 Myears old. The complicated geometry of the Mid-Atlantic Ridge plate boundary in Iceland is a

result of the repeated ridge jumps, which have taken place throughout the geological history of Iceland (Sæmundsson, 1979; 1986).

The volcanic zones in Iceland are divided into volcanic systems, each consisting of a fissure swarm, up to 200 km in length, and a central volcano associated with high temperature geothermal activity and acidic rocks (Einarsson, Þ., 1994). Some of the central volcanoes have developed a caldera. The volcanic systems are aligned in an *en-echelon* arrangement. This is especially pronounced in the Reykjanes Peninsula, and in the northern part of the NVZ (see Figure 2).

Spreading in South Iceland is more complicated than in North Iceland, because there it is divided between the two volcanic zones in the area. GPS measurements conducted in 1986-1992 indicated a spreading rate in South Iceland of 21 ± 4 mm/year in direction N117 ± 11° E (Sigmundsson et al., 1995), which is consistent with the spreading rats inferred by DeMets et al. (1990). The WVZ has been active since 7 Myears ago, while the southern part of the EVZ was activated around 2 Myears ago (Sæmundsson, 1978). The GPS measurements suggest that currently the region north of the SISZ is moving together with the American plate to the west and the area to the south of the SISZ moves to the east together with the Eurasian plate. The GPS measurements suggest also that the WVZ is not as active as the EVZ, and only 15 ± 15% of the total extension is accomodated by that zone, while 85 ± 15% is focused on the EVZ (Sigmundsson et al., 1995). The theory that the EVZ is now overtaking the role as the active volcanic zone is also supported by the fact that very little volcanic activity has taken place in the WVZ

during the last 2000 years, while there have been four rifting episodes in the EVZ associated with volcanism. Unlike most of the volcanoes in Iceland, the crust in the southern part of the EVZ can support high topographic features such as Mt. Eyjafjallajökull and the Hekla volcano.

Mt. Eyjafjallajökull is located in the southernmost Eastern Volcanic Zone. Other volcanoes in this region include Hekla, Katla (beneath the Mýrdalsjökull glacier), Tindfjöll, Torfajökull and the Vestman Islands (**Figure 4**). The southern part of the EVZ is characterized by thicker crust than in the north (**Figure 5**), and more alkaline eruptive products are generated there due to larger depth of melt (Óskarsson et al., 1982). Mt. Eyjafjallajökull is dominated by alkaline basalts, but the latest activity was acidic (Kristjansson et al., 1988). The lavas are dominated by transitional alkali basalts, but a range from ankaramitic to quartz trachytic lavas have been documented (Loughlin, 1995). The nearby Katla volcano is dominated by Fe-Ti-rich transitional alkali basalts (Meyer et al., 1985), but small volumes of rhyolite also exist (Carswell, 1983). It seems that the high Fe/Ti lavas erupting from Katla, have also been erupted from Mt. Eyjafjallajökull (Loughlin, 1995). Hekla is one of the most active volcanoes in Iceland, a ridge built up by repeated eruptions on a volcanic fissure striking in an ENE-WSW direction, oblique to most fissures in the EVZ. The lavas and the tephras are of intermediate to acid composition (Grönvold et al., 1983). Tindfjallajökull has a large summit caldera and is built up of ignmibrites – the Þórsmörk Ignimbrite (Jörgensen, 1980). Torfajökull is dominated by peralkaline and postglacial subalkaline

rhyolites (McGarvie, 1984). It has been suggested that the Torfajökull lavas are derived from a large, shallow magma chamber (MacDonald et al., 1990). The Vestman Islands and the Heimey central volcano have erupted intermediate compositions and Meyer et al. (1985) suggested that the mantle plume influence should be minimal here.

1.2 Crustal structure beneath Iceland

Numerous studies have been undertaken to explore the crustal structure beneath Iceland. The first refraction experiment was along a 250 km long profile in 1960 in northwestern Iceland (Båth, 1960). It resolved a three layered 28 km thick crust, with v_p = 7.34 km/s just above the Mohorovicic (Moho) discontinuity, the boundary between the lower crust and the upper mantle. Refraction measurements made by Pálmason (1971) produced a five-layer-model, with the lowermost layer (layer 4) reaching down to 16 km depth with v_p = 7.2 km/s. This layer was interpreted as being the upper mantle.

Two theories have developed since the 1970s; *the thin crust theory* and the *thick crust theory*. The first model suggests a thin (~10 km thick) and hot crust underlain by partially molten, low-velocity mantle. Magnetotelluric measurements show a low resistivity layer at depth of 10-20 km beneath Iceland

Beblo et al., 1983). This layer has been interpreted in support of the thin crustal model (Beblo and Björnsson, 1980) and was suggested to consist of partially molten ultramafic rocks, belonging to the upper part of the mantle. Temperature gradient extrapolations from some shallow (< 2000 m deep), geothermal bore-holes, also support this theory, according to the temperature gradient extrapolations calculated by Flóvenz and Sæmundsson (1993). The interpretation of Pálmason (1971) agrees with this model. The second theory, the thick crust theory, has been accumulating more and stronger evidence during the last few years. Refraction seismic studies in several areas in Iceland including the first study conducted by Båth, have revealed a clear Moho boundary between crust and mantle at a depth of 20-40 km (Bjarnason et al., 1993; Menke et al., 1996; Staples et al., 1997; and Darbyshire et al., 1998). Observed earthquake hypocenters at 6-8 km depth (beneath volcanic zones such as the southern part of the WVZ), and at 12-14 km depth in off-rift regions such as the South Iceland Lowland (Stéfansson et al., 1993, Bjarnason and Einarsson, 1991) also indicate a thick crust. This is because earthquakes do not occur if the temperature exceeds 400-800°C (Menke et al., 1995). Good transmission of shear waves in the 12-25 depth range is also in agreement with a thick crust. Shear wave quality factors, at 12-25 km depth, in range of 100-2000 are compatible with temperatures at least 200-300°C below solidus (Menke and Levin, 1994; Menke et al., 1995). Shear wave data from Gebrande et al. (1980) reinterpreted by Menke et al. (1996), and a crustal accretion model by Menke and Sparks (1995), are also in favor of a thick crust

model.

The crust in the southernmost part of the EVZ, where Mt. Eyjafjallajökull is situated, is about 20 to 30 km thick (Menke et al., 1996). Reinterpretation of the RRISP-77 shear wave data collected by Angenheister et al. (1980), shows that the crust thickens from 20-24 km in south-west to 30 km in central Iceland, to 35 km near the eastern coast (Menke et al., 1996). This interpretation is in agreement with petrological studies made by Óskarsson et al. (1982), indicating deep source of melts (alkaline eruptive products) in the southernmost part of the EVZ.

The maximum depth of earthquakes at central volcanoes is also in good agreement with a thick crust in the southernmost part of the EVZ. Earthquakes occur at 12 km depth at Mt. Eyjafjallajökull (earthquake swarm in 1994). The seismic activity at 20-30 km depth beneath the Hekla volcano (Soosalu and Einarsson, 1997), and earthquake locations from Torfajökull at 17 km depth (Soosalu and Einarsson, 1997), all support the thick crust theory.

1.3 Seismic activity in Iceland

Seismic activity in Iceland is highly variable (**Figure 6**). Most of the larger earthquakes in Iceland occur within the transform fault zones (Einarsson, 1991), the South Icelandic Seismic Zone (SISZ) and the Tjörnes Fracture Zone (TFZ). In the south, a 10-15 km wide east trending hypocentral belt generates

earthquakes on N-S striking right lateral faults (Einarsson, 1991). In the north, three hypocentral belts have been identified (Einarsson, 1991). They are subparallel and strike in a NW direction. Seismic activity within the volcanic zones is characterised by spatial clustering of located earthquakes (Einarsson, 1991). Most of the clusters coincide with central volcanoes. Each central volcano develops its own seismic characteristics. Rifting features such as normal faults and fissure swarms are normally aseismic, except during rifting periods and magmatic events. Most earthquakes occurring in Iceland are of high frequency type, with short coda duration, caused by brittle failure (Brandsdóttir and Einarsson, 1992).

However, some of the earthquakes associated with volcanoes in Iceland, lack the higher frequencies, and are called low-frequency events. They are characterised by less power in the higher frequencies and longer coda duration, which makes their amplitude/duration ratio much lower than for high frequency earthquakes. A number of low-frequency earthquakes in volcanic regions are associated with flow of magma through cracks (Chouet, 1996), or with fluid transport in magmatic or hydrothermal systems associated with volcanoes and magmatic intrusions/extrusions (Brandsdóttir and Einarsson, 1992). Low-frequency earthquakes may also be a result of attenuation on a wave path (propagation effects). Because of their different origin, they vary significantly in shape. Some of them have the shape of the so called "Minakami b-type" earthquakes, while others look like the "m-type" or "l-type" earthquakes recorded

at Mount St. Helens (Brandsdóttir and Einarsson, 1992). The low-frequency earthquakes are often very hard to locate because of emergent P-waves and unclear or absent S-waves. In addition to high- and low-frequency earthquakes, a third type of seismicity occurs in Iceland, socalled volcanic tremor. During all eruptions in Iceland, volcanic tremor of two types has been identified, one associated with eruptions and one with intrusions (Brandsdóttir and Einarsson, 1992). Usually earthquakes are superimposed on the tremor during the beginning of an eruption, as was the case for the Hekla eruption in January 1991. The amplitude of the volcanic tremor seems to follow the vigor of the eruptions (Einarsson, 1991; Brandsdóttir et al., 1992). The differences between typical high- and low-frequency earthquakes and volcanic tremor are shown in **Figure 7**.

The seismic active areas in Iceland show different behaviour. Some areas show a consistent seismic activity, whereas others show intermittent or even seasonal seismic activity. The seismicity map (Figure 5) shows the numerous areas of high seismicity in Iceland. The main seismic characters for each of the active zone are presented below.

The *Reykjanes Penisula* shows persistent seismic activity on the southern half of the penisula, with earthquakes occurring mainly at depths between one to five kilometres, not located on one particular fault (Einarsson, 1991). Near the tip of the peninsula, earthquake swarms occur and normal faulting is there the most common fault mechanism (Einarsson, 1991). Toward the east, the seismicity is more of mainshock-aftershock character and strike–slip faulting becomes more

prominent (Einarsson, 1991).

The *Hengill* triple junction is a region of current high seismic activity. The Hengill central volcano with its fissure swarm, is the centre of some of the seismicity but not all. Some earthquakes occur over a much wider area, and at depth between one to seven km (Einarsson, 1991). Some earthquakes show normal or strike-slip faulting but others have a non-double-couple component (Foulger, 1988a; Foulger, 1988b). Much of the background seismicity is caused by active heat extraction from hot crust in geothermal areas where circulating ground water causes cooling and contraction of rock (Björnsson et al., 1982). Since 1994 there has been continuous enhanced seismic activity in the Hengill area, related to the uplift of a broad area centred on Mt. Ölkelduháls (Sigmundsson et al., 1997a). Two M5 earthquakes occurred in the area in 1998. On June 4, 1998, an $M_L = 5.1$ earthquake occurred close to Litla-Skarðsmýrarfjall at a depth of about 4.6 km (Ágústsson, 1998). In November 1998, on Friday the 13th, an $M_L = 5.0$ earthquake occurred west of Hjalli in Ölfus at a depth of 5.3 ± 0.3 km (Rögnvaldsson et al., 1998). Aftershock activity continued for several days, the largest aftershock being a $M_L = 4.7$ event on the 14th of November. The November earthquakes indicate rupture on N-S oriented faults (Rögnvaldsson et al., 1998).

The *South Icelandic Seismic Zone* takes up transform motion between the Reykjanes Peninsula and the EVZ. It is a zone of overall left-lateral transform motion, but this motion is accomodated by parallel right-lateral strike-slip faulting

on an array of NS oriented faults, and a counter clockwise rotation of the blocks in between, so called bookshelf faulting (Sigmundsson et al., 1995). Major earthquakes (M7) seem to occur in the SISZ, at an interval of 80-120 years (Einarsson et al., 1981). The most recent earthquake since 1912 was the Vatnafjöll earthquake in 1987, with a magnitude of M_s = 5.8 (Bjarnason and Einarsson, 1991). It occurred at a depth of 11 ± 3 km with the associated earthquake sequence occurring at 6-14 km depth (Bjarnason and Einarsson, 1991). According to locations of fore- and aftershock events, this earthquake was associated with right-lateral strike-slip on a nearly vertical N-striking fault (Einarsson, 1991).

The *Northern Volcanic Zone* with the Krafla and Askja volcanoes among others, is the extension of the EVZ north of Vatnajökull. This zone is characterised by low background seismicity, mostly confined to the two mentioned volcanoes. The Krafla volcano was very active during its 1974-1985 rifting episode. Seismicity was then influenced by two processes: 1) inflow of magma into a shallow crustal magma chamber at about 3 km depth and 2) rifting of the plate boundary (Einarsson, 1991; Tryggvason et al., 1986).

The seismicity of the Eastern Volcanic Zone is confined to the central volcanoes in the area. Some of the volcanoes such as Katla show persistent activity, whereas others, such as Hekla, are nearly aseismic except during eruptions. Mt. Eyjafjallajökull shows periodic seismic activity aligned in an E-W direction, in agreement with the local stress field in that region. Two earthquake

swarms have taken place at Mt. Eyjafjallajökull during the last 15 years, in 1994 and 1996. Two well defined clusters of earthquakes occur beneath the Mýrdalsjökull ice cap, one beneath the southeastern part of the Katla volcano and the other beneath the southwestern part (Figure 8). One poorly constrained fault plane solution from the southeastern cluster reveals strike-slip faulting, indicative of deflating magma chamber (Einarsson, 1991). A pronounced annual cycle of seismicity occurs at Mýrdalsjökull, with the main part of the events occurring in the fall (Einarsson, 1991). The explanation seems to be that the melted ice from each summer increases the pore pressure triggering slip on faults above the magma chamber (Einarsson and Brandsdóttir, in press).

The Torfajökull central volcano shows high and persistent seismic activity (Soosalu and Einarsson, 1997), with both high- and low frequency events as well as earthquake swarms. It has vigorous geothermal activity in the western part of its caldera (Sæmundsson, 1972; Sæmundsson, 1982), where nearly all of the present-day seismicity is located (Einarsson, 1991; Soosalu and Einarsson, 1997). This more or less persistent seismic activity is related to heat extraction, following cooling, contraction and cracking of the rocks, as has been suggested for the Hengill area. The seismicity of Torfajökull is thought to be caused by minor magma movements in the roots of the volcano (Brandsdóttir and Einarsson, 1992), but this volcano has not generated an eruption for a few centuries (Brandsdóttir et al., 1992).

The Hekla volcano (see Figure 8) has erupted several times during the last

30 years (May 1970, August 1980, April 1981 and January 1991). This volcano shows little or no sign of long-term precursory activity before it erupts. The earthquakes during the eruptions are often superimposed on the volcanic tremor (Brandsdóttir and Einarsson, 1992), even though the tremor activity and the earthquake activity have been varying during the different events. The low seismicity associated with the eruptions of Hekla, may indicate that the eruptions are fed by a magma chamber in the lower crust. Pressure changes at this depth cause crustal strains over a wide region in the stressed crust above the magma chamber, but this stress may not be sufficient to generate earthquakes (Brandsdóttir and Einarsson, 1992).

1.4 Crustal deformation at volcanoes

Geodetic monitoring of volcanic areas is important to understand and predict volcanic and seismic activity, and to improve our understanding of volcano dynamics. Sources of crustal deformation at volcanoes include: i) pressure changes in high-level magma storage areas and conduits, ii) magmatic intrusions, iii) earthquakes and iv) thermal changes. The physical and chemical changes within a volcano, as a result of magmatic or seismic activity, may be observed and measured. Dormant volcanoes show deformation rates of up to few

cm/year, while during an eruption, deformation can exceed one meter.

The most commonly used model to interpret crustal deformation at volcanoes, is the so called Mogi model (Mogi, 1958). This model assumes a small sphere of varying pressures, *a point source*, within an elastic half-sphere. The elastic Lamé coefficients are assumed to be equal. By using elasticity theory, the deformation caused by such a single point source can be calculated. Anderson (1936) solved the mathematical problem, but it was not until 1958 that the equations were applied to volcanic deformation by Mogi. A Mogi source will cause a maximum uplift directly above the source. The uplift then decays with distance away from the source (**Figure 8a**). A Mogi source causes also horizontal surface displacements, radially away from the source (see Figure), with maximum amplitude some distance away form the source. Surface deformation caused by a Mogi source model, is radially symmetric on the surface (Mogi, 1958), and is given in cylindrical polar coordinates r, ϕ and z:

Vertical displacement : $u_z = C\, d/(d^2+ r^2)^{3/2}$

Horizontal radial displacement : $u_r = C\, r/(d^2+ r^2)^{3/2}$

Tilt : $\delta = \partial u_z / \partial r = C\, (-3dr)/(d^2+ r^2)^{5/2}$

where

d = source depth

r = horizontal (radial) displacement

C = source strength parameter

Four free parameters occur in the model; latitude, longitude and depth for the location of the source and the fourth for the source strength. The source strength parameter is in turn given by ;

$C = (3a^3\Delta P)/(4\mu)$

where

ΔP = change in fluid pressure within the sphere

a = the radius of the sphere

μ = the rigidity of the crust surrounding the sphere

It is not possible to infer the source radius or the pressure change directly, only the value for C. The Mogi model is valid as long as $(a/d)^5 << 1$ (McTigue, 1987).

The ground deformation accompanying earthquakes and dike intrusions is unfortunately not as easy calculated as for a single point Mogi source, but a set of equations is given by Okada (1985). A planar dike will cause uplift at its flanks, and a central subsidence (**Figure 8b**), with the exact deformation field depending on the location and dimension of the dike itself. Pollard et al. (1983) reviewed deformation associated with dike intrusions.

A number of geodetic techniques are used to detect crustal deformation at volcanoes. Global Positioning System (GPS) geodesy is one of the techniques, and the one primarily used in the work presented here. That technique is

discussed in Chapter 3.1. Other techniques include levelling, tilt measurements, electronic distance measurements (EDM) and satellite radar interferomtery (SAR). These techniques are presented shortly below, but general reviews are e.g. given by Bilham (1991) and Sigmundsson (1994):

Levelling: By using a set of graduated rods and a level, the elevation difference between two points space 50 m or less apart can be measured with a standard deviation of about 0.1 mm. The elevation difference between any two points, can be measured incrementally by summation of separately determined elevation increments obtained during each individual setup (Sigmundsson, 1994). As a result of random errors, the standard deviation of and observed elevation difference, will increase with the square root of the levelling line distance. If L is the length of a levelling line (km), the accuracy of a levelling measurement can be as good as $0.2\text{mm}\sqrt{L}$.

Tilt: Repeated elevation measurements along short profiles provides a way to measure surface tilt of volcanoes, e.g. to detect inflation/deflation periods. Such measurement are termed dry tilt measurements, optical levelling tilt and spririt-level tilt measurement. The accuracy of such tilt measurements, especially if the tilt signal is small, can be better than 1 μrad if a T-or L-shaped benchmark configuration is used (Tryggvason, 1994). Another way of measuring tilt is to use electronic shallow-borehole tiltmeters. These have been used in Iceland, but unfortunately they are very sensitive for strain as a result of temperature changes (freeze-thaw-problems) and rainfall, which in Iceland has derived tilt signals of

more than 20 μrad. Such errenous signals can very easily mask long-term deformation. During the Krafla rifting event in 1975-1984, more than 20 sequences of "magmatic breathing" accompanying eruptions, could be detected thanks to tilt measurements (Tryggvason, 1991).

EDM: By using a geodimeter transmitting a modulated light placed at one end of a baseline, and a reflector in the other end detecting and sending back the light signal, deformation can be measured. The best conventional geodimeters in use will give accuracies of $5mm+10^{-6}L$, where L is the length of the baseline (Sigmundsson, 1996).

SAR: This is a new technique that relies on measuring phase shifts between two images acquired by radar satellites. Review of the technique is given by Massonet and Feigl (1998). The technique has been applied in Iceland by Vadon and Sigmundsson (1997), and Sigmundsson et al. (1997b).

1.5 Previous research and studies of ground deformation

Iceland may be the best place on Earth to study the mechanism of crustal spreading on land. After the acceptance of the plate tectonics theory in the 1960s, geodetic measurements to monitor deformation, have been conducted nearly annually in Iceland, using a variety of techniques. These measurements have significantly advanced the knowledge about the style of deformation, and active

processes, at divergent plate boundaries.

The first crustal deformation project in the Eastern Volcanic Zone was conducted in 1967 (Decker et al., 1971), to detect crustal widening across the zone. Distance measurements along a 60 km long EDM-profile were conducted, from the fissure swarm of the Hekla volcano, east across the Bárðarbunga fissure swarm and the Eldgjá fissure. Remeasurements on this profile, including measurements directly after the eruptions of 1980-1981 Hekla, indicate episodic movements, more related to the seismic and volcanic activity rather than the overall divergent motion of the plates (ref-------).

Global Positioning System (GPS) geodetic measurements were first conducted in Iceland in 1986 with the purpose of establishing a geodetic control within the SISZ, enabling future studies of destructive earthquakes in the area (Foulger et al., 1993). This GPS-network was remeasured and expanded in 1992 (Sigmundsson et al., 1995). These measurements have shown how crustal strain is accumulating across the SISZ. Little or no spreading is observed across the southernmost part of the EVZ, including Mt. Eyjafjallajökull. In South Iceland, GPS measurements have been used since 1986 at individual volcanoes, including Hekla, Mýrdalsjökull and Mt. Eyjafjallajökull, to monitor the ground deformation. During and after the 1991 eruption of Hekla, two measurement campaigns were conducted. The results indicated that the eruption was associated with a surface deflation volume of about 0.1 km^3. The depth to the magma reservoir was calculated to be 9 km ± 6.5 km (Sigmundsson et al., 1992). The campaign in

1994 indicated a uniform extension across the EV (Jónsson, 1996: Jónsson et al., 1997). Minor deformation was observed along the rift zone and stress seems to be accumulating in the SISZ.

1.6 The Eyjafjöll volcanic system

Mt. Eyjafjallajökull is a glaciated stratovolcano located on the western side of the EVZ (**Figure 9**), near the south coast of Iceland. It belongs to the Eyjafjöll volcanic system. The Eyjafjallajökull glacier of about 80 km^2 area, covers the upper part of the mountain. The highest peak on the rim of a 2.5-km-wide summit crater reaches 1666 m.a.s.l. The Eyjafjöll volcanic system, the EVS, strikes in an east-west direction, being 30 km long and 8 km wide. It has been active for the at least 0.78 Myear (Kristjánsson et al., 1988). The EVS, along with Mýrdalsjökull (the Katla volcano) and the Vestman Islands mark the southern tip of the propagating part of the EVZ (see Figure 12). The Eyjafjöll volcanic system is surrounded by the inudated river area Markarfljót to the north, the high plateau of Fimmvörðuháls Pass connecting Mt. Eyjafjallajökull with the Mýrdalsjökull glacier to the east. The flat lowlands of Eyjafjallasandur and Skógasandur enclose the area to the south, and the highlands of Seljalandsheiði among others to the west (see Figure 12).

The structural evolution of Mt. Eyjafjallajökull has been described by

Kristjansson et al. (1988) as follows. More than 600 Kyears ago the volcanic system began building up. Lavas were erupted from the central area of the volcano and not along an E-W trend as later activity. These lavas originated from NE-SW orientated sheets (Kristjansson et al., 1988). Lavas with an age of 600 Kyears were erupted from E-W radial dykes and sheets. This might be caused by the close presence of the Katla volcano or an influence from the SISZ (Kristjánsson et al., 1988). The two volcanoes are connected by east-west striking faults and eruptive fissures, which are part of the radial dyke system of each volcano (Dahm and Brandsdóttir, 1997).

Fieldwork conducted by Loughlin (1995) showed that the Eyjafjöll volcanic system consists of subaerial, subglacial and submarine deposits (**Figure 10**), which has been built up during six glacial and six interglacial periods. The youngest rocks are exposed at the western end of the radial fissure system and the stratigraphy suggests that the volcanic activity has migrated westwards during the last 0.3Ma. The youngest rocks originate from an eruption in 1821 - 23 and were acidic (Kristjansson et al., 1988). The intrusive rocks of the area is dominated by inclined sheets, a term used for discordant, usually discontinuous intrusions associated with central volcanoes (Loughlin, 1995). These sheets may dip inwards towards the volcanic centre with an angle of about 45° (cone sheets), or may dip outwards (ring sheets). All of the rocks within the Eyjafjöll volcanic system range in chemical composition from dacites to basaltic ankaramites.

Several inclined and NE-SW striking sheets build up the core of the Eyjafjöll

volcanic system, as well as E-W oriented radial sheets. The sheets of Mt. Eyjafjallajökull can be divided into three categories (Loughlin, 1995), according to their concurrent stress regimes: i) radial (magmatic, especially common in the eastern part of the volcano), ii) E-W oriented, and iii) NE-SW oriented (regional, located in the southern and central part of the volcano). Petrological evidence suggests that the NE-SW oriented were formed, as a result of tapping different sources or that they generated from a long-lived fissure system connected to an evolving magma chamber. Only one composite dyke has been identified in the Eyjafjöll system. Such dykes are, however, a common feature in other Tertiary central volcanoes in eastern Iceland (Walker, 1963; Furman et al., 1992; Loughlin, 1995). Also, inward dipping inclined sheets, common in other volcanoes in Iceland, has only been found dipping outwards at Mt. Eyjafjallajökull.

The occurrence of a summit crater, acid and intermediate rocks, hydrothermal alteration and numerous inclined sheets in the core of the volcano, indicates that the Eyjafjallajökull volcano is partly fed by a shallow crustal magma chamber (Kristjansson et al., 1988). The central crater may mark its present position. Existence of such shallow magma storage at the neighbouring Katla volcano has been confirmed by seismic studies of Gudmundsson et al (1994). They showed that the Katla magma chamber is 5 km across, along their refraction profile (**Figure 11**). Only the bottom of the magma chamber was clear from the refraction data. It occurs at a depth of 3 km below the surface of the glacier, but the height of the magma chamber must be at least 1 km. The magma chamber of

Katla may contain as much as 5 km^3 of melt, but if Mt. Eyjafjallajökull has a shallow magma chamber, it is probably smaller than the one beneath Katla. Postglacial activity at Mt. Eyjafjallajökull has been interpreted as being derived from a shallow magma chamber. According to the diversity of lavas, the abundance of vertical NE-SW sheets in the core of the volcano and petrological studies (Loughlin, 1995), the magma seems to have been erupting from several crustal magma chambers at different depths, and these magma chambers might be or have been connected. A connection with the Katla magma chamber might also exists, as Mt. Eyjafjallajökull and the Katla volcano are connected by east-west striking faults and eruptive fissures. These fissures and faults are part of the radial dyke system of each volcano (Dahm and Brandsdóttir, 1997; Einarsson and Brandsdóttir, in press).

The last 13,000 years have been characterised by little volcanic activity (Guðmundsson, 1996). During the last glaciation, the Markarfljót glacier formed in the Markafljót valley north of Mt. Eyjafjallajökull. Two subaerial lavas on the western flanks of Mt. Eyjafjallajökull have been documented, the Kambagilshraun and the Hamragarðarhraun lava flows, both erupted from the western end of the fissure system (Kjartansson, 1958; Jónsson, 1998). Johannesson (1985) showed that the Kambagilshraun lava is covered with moraines, indicating that it has been overriden by the Markarfljót glacier at least 12000 years ago. The Hamragarðarhraun lava lies on striated ground and was probably erupted after the retreat of the Markarfljót glacier (Johannesson, 1985). Therefore, it is probably

younger than the Kambagilshraun lava. The Eyjafjallajökull volcano has only had two known historical eruptions, one in 1612 on a subglacial summit fissure and a second one in 1821-1823 (Dahm and Brandsdóttir, 1997). The eruption characteristics are quite different from the nearby Katla volcano, which has erupted frequently during historical time (Þórarinsson, 1975) and is among the most active volcanoes in Iceland. The Katla volcano had its last eruption in 1918, except a possible subglacial eruption in 1955 (Þórarinsson, 1975).The extrusives of transitional-alkaline rocks from Eyjafjallajökull indicate that the postglacial eruptive activity resulting in fissures radiating away from the summit crater, were most likely fed by dyke intrusions from one or several crustal magma chambers at shallow depth (Dahm and Brandsdóttir, 1997).

2. Earthquakes

2.1 Previous Earthquake studies within the Eastern Volcanic System

Several central volcanoes are located in the close vicinity of Mt. Eyjafjallajökull, such as the Katla and the Torfajökull volcanoes (**Figure 12**). The

Mýrdalsjökull volcanic area with the Katla volcano has shown persistent seismic activity for more than four decades (Einarsson and Brandsdóttir, in press). Except for a possible subglacial volcanic eruption in 1955, no volcanic activity has been detected (Tryggvason, 1960). Seismic data show two hypocentral clusters, one within the caldera of the Katla volcano and the other centred in the Goðabunga area, to the west of the caldera rim (Einarsson and Brandsdóttir, in press). The Goðabunga earthquakes show typical volcanic behaviour with emergent P-waves and poor S-waves. Most of the earthquakes in both clusters are located in the uppermost 5 km. Both clusters have been interpreted as being derived from two separate magma chambers (Einarsson and Brandsdóttir, in press). The occurrence of a zone of low P-velocities and high S-wave attenuation, interpreted as a magma chamber at a depth of less than 3 km, has been suggested as being the source of these earthquakes (Gudmundsson et al., 1994).

Torfajökull to the northeast of Mt. Eyjafjallajökull, was seismically active in late 1985 and in 1986 with four low-frequency earthquake swarms (Brandsdóttir and Einarsson, 1992). The first began in early March 1986 and lasted nearly a month. This swarm consisted of around five earthquakes per day, while the next swarm from early May lasting a couple of days showed more than 20 events per day. In July the daily number of earthquakes was rather constant, around five to twelve events per day, but suddenly in late August it increased to more than 40 events per day and lasted throughout September. This was the biggest low-frequency earthquake swarm in the area so far known. The fourth

swarm occurred in November 1986. The seismicity of Torfajökull is thought to be caused by minor magma movements in the roots of the volcano, due to the fact that this volcano has not generated an eruption for a few centuries (Brandsdóttir and Einarsson, 1992). It could also be a result of thermal cracking due to a cooling magma body (Soosalu and Einarssson, 1997). During the volcanically quiet period between 1991 and 1995, Soosalu and Einarsson (1997) have studied the background seismicity of the Hekla and the Torfajökull volcano to the north of Mt. Eyjafjallajökull (**Figure 13**). The Hekla volcano was generally aseismic during this period. At Torfajökull, the magnitude M_L range was between 0.4 and 2.8 and the earthquakes were located between the surface and a depth of 14 km, with the densest hypocentral cluster between 5-12 km depth. Low-frequency earthquakes were also studied and they indicate a swarmlike behaviour. These swarms seem to be normal for the volcanically quiet period in 1991-1995, with no clear temporal pattern. Swarm activity of low-frequency earthquakes seems normal for Torfajökull, with often an abrupt beginning with the highest activity peak already reached in a single day (Soosalu and Einarsson, 1997). There is no apparent temporal or spatial correlation between the occurrence of low- and high frequency earthquakes. At the Vatnafjöll volcano, seismic activity occurred mainly in two N-S lineaments extending northward toward the Hekla volcano.

Prior to an earthquake swarm in 1994, Mt. Eyjafjallajökull had been seismically very quiet (Einarsson, 1991). The 1994 earthquake swarm studied in this thesis will be described further below.

2.2 The 1994 earthquake swarm at Eyjafjallajökull

The aim with the project of placing out portable seismometers in the area of the Eyjafjöll volcanic system including Mt. Eyjafjallajökull, was to provide and improve the depth determinations for seismic events occurring in the southern part of the Eastern Volcanic Zone. The South Iceland lowland regional seismic network only does not provide sufficiently good depth determinations of earthquakes, even though the horizontal errors are accurate enough. With this follows also a better understanding of the seismic properties within the crust in this region.

Prior to the earthquake swarm in 1994 (**Figure 14**), Mt. Eyjafjallajökull had not shown any noticable seismic activity during the last ten years (Einarsson and Björnsson, 1987). The 1994 earthquake swarm at Mt. Eyjafjallajökull began on May 29 and faded out in late June, with more than 130 micro-earthquakes (**Figure 15**) recorded by a local network (SIL – the South Iceland Lowland network). The seismic activity consisted of a cluster of earthquakes, without any signs of foreshock, mainshock and/or aftershock events (**Figure 16**). It was a rather typical behaviour for an *earthquake swarm* within the volcanic zones in Iceland, a sequence of seismic events with small magnitudes and no main- or

aftershock events. The magnitude ranged from 0.59 to 2.27 M_L, with a constant magnitude pattern with time (**Figure 17a** and **b**).

Dahm and Brandsdóttir (1997) derived moment tensors for 15 of the best recorded earthquakes during this earthquake swarm. The study revealed focal solutions with nearly vertical T-axes and horizontal P-axes, and E-W oriented nodal planes (**Figure 18**). The variable orientation of the P axis azimuths indicated that the local stress field within the volcano varied during the swarm, or that there is a heterogenous stress field beneath the volcano. Moment tensors for the main part of the events studied, show a positive isotropic component, between 2 and 44 % of the total moment tensor, indicating a coseismic expansion due to, for example, tensile cracking (Dahm and Brandsdóttir, 1997). The mechanism behind the earthquake swarm was interpreted as a vertical intrusion of magma into a confined region at the northern flank of the volcano. This interpretation was based on the spatial and temporal seismic pattern, the small magnitude range, the focal mechanism, and the depth range (Dahm and Brandsdóttir, 1997). Isotropic source component indicating coseismic expansion appeared in some of the events studied. Three methods of moment were used to derive tensors, the single event method, the multiple event method and the first motion method. The first two gave thrust mechanism with E-W striking nodal lines. The first motion method cannot give any solutions of the focal mechanism but the nodal lines derived from this method is consistent with the other two methods. Two types of double-couple focal solutions were derived from the first motion method, thrust mechanism

similar to the inversion results above and a pure ~90° dip-slip mechanism (Dahm and Brandsdóttir, 1997)

2.3 Data, methods and processing

I have used data from two seismic station networks to study the 1994 earthquake swarm. The first is the South Iceland Lowland (SIL) network which in 1994 consisted of 12 three component digital seismic stations, distributed across South Iceland (Stefánsson et al., 1993). The second seismic network was a temporary one, portable seismometers installed in response to the 1994 seismic activity (**Figure 19**). Six portable three-component stations were deployed. The stations consisted of Scintrex model PRS-4 recorders with Rugby and Omega synchronised clocks and Mark Products Model L22D three-component geophones (with a flat response to ground velocity above their 2 Hz corner frequency). The data were sampled at 100 Hz with a dynamic range of 132 dB and a resolution of 3.67 nm/s. The sampling accuracy was ± 10 ms. The P- and S- arrivals of the earthquakes were read with the Scientific Spread Sheet Software, Sun Version 3.4 (Menke, 1988). A three-pole Butterworth band-pass filter was used to frequency-filter out the noise, first band-passing from 1 to 15 Hz and the second from 2 to 12 Hz. All three components, vertical, north and east were analysed. The P-arrivals were mainly determined from the vertical component, whereas the S-arrivals were read mostly from the northern, or the eastern components.

Both the networks recorded the 1994 earthquake swarm, while only the SIL network recorded another earthquake swarm in 1996. Seven stations within the SIL network, have been used – ASM, HAU, MID, SAU, SKH, SNB and SOL. The second seismic network, the temporary, consisted of six different stations – GIJ, HRU, LMB, MSK, SKO and STE (**Table 1**). The portable stations were not all six collecting data at the same time.

The two seismic networks give a good configuration of stations recording earthquakes from within the Eyjafjallajökull region (Figure 19). Stations GIJ and STE (and HRU) were located in the close to the seismic activity, but no station was located directly above the hypocentral region, nor at a close distance to the east of the earthquake swarm. Because of that the main part of the earthquakes were located at 4-6 km depth, the nearby stations STE and GIJ within the 4 km range horizontally, resulted in small vertical errors. Earthquake depth estimates would not be significantly better constrained with stations closer to the hypocentral region. The distance range to each station from the 1994 earthquake hypocentres is shown in **Table 2**.

The SIL network recorded more than 130 micro-earthquakes from the swarm in 1994 (**Appendix 1**). Of these 72 events were recorded by both networks (Figure 16). To locate earthquakes, readings from at least four stations are necessary as four unknown variables are to be solved simultaneously (latitude, longitude, depth and origin time). More stations are preferred to minimise horizontal and vertical errors. Only 67 earthquakes fulfilled the criteria of being

recorded by at least four stations, including at least one station from the portable network. These earthquakes occurred from June 3 (day 154 of the year) until June 22 (day 173). The portable network was only in operation from June 2 (day 153) until July 3 (day185). Unfortunately, part of the data set from the portable network (the last deployment from day 178 to day 185) was not backed up from the field computer before it was erased. The last earthquake from this swarm recorded and still readable is from the 26th of June (day 178).

By using only data from the SIL-stations, the earthquake location solutions will differ significantly, from the solutions incorporating data from the temporary network. This confirms the necessity of having a dense network recording the earthquakes, providing a good cover of the area. The SIL-stations are mainly located to the west of the earthquake swarm and will thereby drag the locations towards them to the west. The SIL-stations are also located further away from the source than the temporary stations, and will therefore NOT give the same accuracy in the earthquake depth parameter, so the vertical errors will be larger. The comparisons between the different earthquake locations determined by using SIL-stations versus a solution incorporating data from both the SIL- and the temporary network, is given in Chapter 2.5.

2.4 Velocity models and seismic velocities

The crust beneath Mt. Eyjafjallajökull is not well known, due to lack of

refraction data within the region. The seismic velocity models used to determine the hypocentres for the earthquakes, are appropriate velocity models for adjacent regions, to find a model most suitable for the area. Earthquake hypocentres were determined using the program HYPOINVERSE (Klein, 1978) and using three different velocity models. The three models are:

i) MYR-N (without a low velocity zone) or Mýrdalsjökull North model, derived by Gudmundsson et al. (1994),

ii) MYR-V (including a low velocity zone) or Mýrdalsjökull West model, also derived by Gudmundsson et al. (1994) and

iii) SIL model derived by Bjarnason et al. (1993) for the South Iceland Seismic Zone and the South Iceland Lowlands.

The MYR-N and the MYR-V velocity models were derived from 2-D seismic undershooting on a profile across Mýrdalsjökull, to reveal a possible magma chamber beneath the Katla volcano. Guðmundsson et al. (1994) defined 1-D piece-wise-linear velocity models for three different regions of the volcano, the northern (N), the western (V) and the southern (S) region (**Figure 20**). In the south, the uppermost crust shows a low velocity zone at more than 2 km depth. This is in agreement with results from Pálmason (1971), with his interpretation including a 4.5-km-thick Layer 2 with a velocity of 4.5km/s, extending from a depth of 2.7 km. In the north, the velocity continues to increase with depth, agreeing with models calculated by Flóvenz (1980) and Flóvenz and Gunnarsson (1991), appropriate for the Iceland neovolcanic zone with uneroded, upper crust.

The SIL velocity model is derived from a part of the 170 km long South Iceland Seismic Tomography (SIST) profile (Bjarnason et al., 1993). The profile extends from the western coast, across the Mid-Atlantic Ridge spreading centre in the WVZ, and throughout the SISZ to the western edge of the EVZ. The upper crust, layer 2A, shows significant lateral and thickness (0.7-3 km) variations in the southeast. Thicker upper crust can only be formed (in Iceland), where lava is overlaying older crust with a temperature gradient lower than 100°C, as a consequence of ridge jumps or propagation of rifts through older crust (Bjarnason et al., 1993). The thicker upper crust in the SISZ and the western part of the EVZ, is probably a result of the ridge jump from the WVZ to the EVZ. Layers 2B and 2C, with velocites of 5.0 km/s and 6.5 km/s respectively, show large lateral variations, being thicker further to the east of the WVZ (Bjarnason et al., 1993). The depth to the lower crust, is defined by a sharp decrease in the velocity gradient at ~6.5 km/s. The depth to the lower crust is relatively constant beneath the WVZ (3.0-4.0 km), but increases to the east of the WVZ to 6.0-7.0 km (Bjarnason et al., 1993). The total thickness of the crust in south Iceland is 20-24 km, with a sharp reflector at the bottom interpreted as a Moho (v_P = 7.7 km/s). This is in agreement with layer 4 from the Palmason profile (1971), with a velocity of 7.2 km/s interpreted as the lowest part of the crust underlain by the Moho boundary.

The three seismic velocity models I have used, MYR-N, MYR-V and SIL, are shown in **Figure 21** and **Table 3**. The SIL and the MYR-N velocity models

show similar velocities between 0.5 to 4.5 km depth. At larger depths, the SIL velocity model shows higher velocities and therefore it locates earthquakes at shallower depth than the MYR-N velocity model. The MYR-V velocity model shows lower velocities than both of the other models.

2.5 Earthquake analyses

In total, 67 earthquakes from the 1994 earthquake swarm (**Appendix 2**), with magnitudes M_L between 0.59 to 2.27, were located with the HYPOINVERSE program (Klein, 1978). The magnitudes were derived from the SIL stations. In total, more than 130 micro-earthquakes (see Appendix 1) were recorded by the SIL-and the portable network. By adding the readings from the automatically read SIL stations to our data, I relocated 67 earthquakes. Of these, 65 of the earthquakes gained a root means square (rms) deviation less than 0.10 (**Figure 22**) using the SIL velocity model, or the MYR-N velocity model.

Several parameters are calculated with the HYPOINVERSE program, such as latitude/longitude, depth, observed arrival times and their correlation with the calculated arrival times, vertical and horizontal errors and number of readings for each located earthquake. Five of these parameters are used to further evaluate a quality for the location for each individual earhquake (**Table 4**). The different parameters are weighted together for each earthquake and a quality factor (Q), ranging from *a* to *d*, is derived. The best located earthquakes will gain the quality

factor a. Only the a- and b-quality earthquakes have been further used in this study. The range of the quality parameters for the a- and b-quality earthquakes is given as follows:

Rms	the root mean square error	≤ 0.10
Z	the vertical error	$\pm$ 1.0 km (a), $\pm$ 2.5 km (b)
H	the horizontal error	$\pm$ 0.5 km (a), $\pm$ 1.25 km (b)
Gap	the gap*	$\leq 90°$ (a), $\leq 135°$ (b)
Nwr	the number of readings	$\geq$ 6 nwr (a, b, c)

*: the largest angle between two stations and the hypocentre

The MYR-N and the SIL model seem to fit better for Mt. Eyjafjallajökull, than the MYR-V velocity model, as we obtain smaller errors and better quality factors using the MYR-N and SIL velocity models (see Table 6). The rms for all 67 earthquakes relocated in this study, with a satisfactory rms of not more than 0.10 (two of these earthquake derived rms of 0,11 and 0,12 respectively, due to bad arrival times for the P-wave from the station Lambafell).

2.5.1 Latitude and longitude

By comparing the calculated errors derived using the three different velocity models, we eliminated model MYR-V on the bases of it yielding higher errors and

more hypocentral scatter that the other two models (**Figures 23**). The MYR-V model incorporates a low velocity zone, which clearly does not exist beneath Mt. Eyjafjallajökull, thus producing a much poorer fit to the earthquake data. Using the MYR-V model the hypocentral zone has a more southward trend and the E-W lineation resolved by the other models does not appear. The SIL model gave the smallest horizontal (ERH)) and vertical (ERZ) errors. Hypocentral maps produced using the SIL and MYR-N models are so similar that one cannot distinguish between them, based on the earthquake locations. The average horizontal error becomes larger if we only use the SIL stations(which are situated further away to the east), and much poorer depth determinations are gained. Using only the SIL stations, the hypocentres are shifted northwards and further to the west (Figure 24). The best determined locations delineate an hypocentral zone, **which covers XX km E-W and YY km N-S, and a total of ZZ km^2.**

The western border of this zone lies just east of the Gígjökull glacier outlet and the eastern boundary stretches just south of the more easterly lying Steinholtsjökull outlet glacier, except for one earthquake further to the east. The velocity models SIL and MYR-N both reveal a pronounced trend striking E-W, subparallel to the E-W striking faults and eruptive fissures existing in the Eyjafjöll volcanic system. This trend has not been fully explained, but is clearly apparent in the overall shape of the Eyjafjöll volcanic system, as well as on the eastern and the western sides of Mt.Eyjafjallajökull. Here the dykes are propagating to east and to the west from the centre. Earthquake migration with time can not be seen,

neither in latitude nor longitude (**Figure 24-25**).

2.5.2 Earthquake depths

The earthquake hypocentres exhibit no temporal migration during the study period. Earthquake depths converge best using the MYR-N velocity model. Most of the earthquakes occur at 4-6 km depth throughout the swarm. The SIL asnd the MYR-N velocity models show, however, a significant difference in earthquake depths (**Figure 26**). Using the SIL model gives shallower depth locations due to the higher velocities in the model, and also the earthquakes are located in two clusters at 1-3 and 4-6km depth respectively. The SIL model locates the earthquakes in the beginning of the swarm at both depths, while most of the earthquakes of the swarm occur at 4-6 km depths. The third model, the MYR-V model, also shows similar scatter as the SIL model does, but it locates nearly all the earthquakes deeper due to the low velocity zone incorporated in this model and in two clusters, one at 5-8 km depth and a second one at 9.5-11.5 km depth. The second, deeper cluster is more poorly constrained and occurs in the beginning of the earthquake swarm, as was the case for the upper cluster of the SIL model.

The smallest horizontal and vertical errors occur for the earthquakes located within the 4-6 km depth range for all three models. The deepest located

earthquakes occur in the middle of the swarm around –19.57 longitude. A correlation between the hypocentral latitude and depth of earthquakes can be seen. The deepest located earthquakes are located in the northernmost part of the hypocentral region. Also, a trend with an increase in depth towards the east, using the SIL and MYR-N velocity model is obvious (**Figure 27** and **28**). The deepest earthquakes occur away from the visible summit crater and a possible dyke E-W striking intrusion in the northern part of the volcano, may cause such a distribution pattern of seismic events.

Based on earthquake distribution in latitude, longitude and depth, for the two best fitting models, (SIL and MYR-N), an hypocentral rock volume (a- and b-quality earthquakes only) has been calculated (**Table 5**). Including the C-quality earthquakes compared to a calculation only including A- and B quality earthquakes, gives nearly the same rock volume for the SIL model, while it is much larger for the MYR-N model (see Table 9). Though the largest difference occurs for the MYR-V velocity model.

The depth scatter obtained using only the SIL-stations and the SIL velocity model is larger, than if data from the temporary stations is used as well. Indeed the reason for installing the portable network was to obtain more accurate earthquake depth determinations in the area. The two sub-clusters shown in the SIL model solution, do not appear using only the SIL-seismic stations. Instead a homogenous scatter over depth occurs, but the average vertical error is larger.

University of Lund
Department of Mineralogy and
Petrology
Sölvegatan 13
S – 222 21 LUND
SWEDEN

Nordic Volcanological
Institute 9901
University of Iceland
Grensásvegur 50
IS – 108 Reykjavík
ICELAND

1992-1998
Seismicity and Deformation
at
Mt. Eyjafjallajökull volcano

by

Malou Blomstrand Stinessen

A thesis
submitted to the Unversity of Lund
for
Master degree
February 1999

2.5.3 Time

Most of the earthquakes occurred in the beginning and middle of the swarm, which is the same earthquake swarm pattern as the neighbouring Torfajökull volcano showed in 1991-1995 (Soosalu and Einarsson, 1997). The western- and easternmost located earthquakes occur in the beginning of the earthquake swarm (Figure 25). The southernmost located earthquakes occur in the beginning and in the end of the swarm while the northernmost earthquakes occur in the middle around June 9 and 10 (Figure 26). As mentioned before, only a slight trend towards shallower depths occur with time (Figure 27).

2.5.4 Magnitude

Magnitudes of the earthquakes were derived automatically by the SIL system only, because the portable stations were not calibrated to measure the magnitude (**Figure 29**).

Earthquake magnitude is defined as follows (Richter, 1935);

$M_L = \log(a/T) + f(\Delta, h) + C_s + C_r$

M_L = magnitude (Richter)

a = amplitude (microns = 0.001 mm)

T = wave period (s)

F = funktion correcting for the effects of distance and depth (different for different waves and wave components)

Δ = the distance to E (degrees)

h = focal depth (km)

C_s = station correction (local differences for special stations)

C_r = regional correction (different earthquake regions)

Only 56 of the total 67 earthquakes were used, excluding the quality c-earthquakes, whereof another two earthquakes failed to give the magnitude. The 1994 earthquake swarm generated Richter magnitudes between 0.59 to 2.27 M_L.

Comparisons between the magnitude and other seismic parameters will be described as follows. The rms compared to the magnitude shows a wide scatter. The largest rms difference occurs at a magnitude of around 1.1 ML. No earthquakes with magnitude over 1.61 occur in the 4-6 km depth interval (**Figure 30**). A trend with slightly larger magnitudes with increasing depth (**Figure 31**) may be seen, using the MYR-N velocity model. The longitude versus the magnitude (**Figure 31**) shows a trend with larger earthquakes occurring further to the north away from the summit crater. Magnitude compared to latitude is plotted in Figure 32, and shows a consistent distribution over the latitudinal range. The largest scatter in magnitude occurs in the beginning of the swarm and then the magnitude scatter seems to decrease and becomes more concentrated around 1.2 M_L (**Figure 33**).

2.5.5 Record section plots and seismogram characteristics

Earthquake locations were derived, with satisfactory results, i.e. with observed P-wave arrivals deviating less than ±0.10 seconds, from the HYPOINVERSE program, and the S wave arrivals deviating less than ±0.15 seconds from the calculated arrival time. Record sections were plotted for individual stations and earthquake seismograms were plotted. Record section plots for the portable seismometer stations with all the recorded earthquakes for each station are shown in **Appendix 3**.

For some selected earthquakes, the record section (RSX) program was used to plot the readings from each stations recording the earthquakes (**Appendix 4**). The selected earthquakes were selected according to the following criteria;

i) the fit of the arrival times from each of the recording stations

ii) where the number of stations recording the earthquake was as high as possible

iii) where the stations recording the earthquake, were a good mixture of stations from both of the networks

iv) and finally to show the typical behaviour of the 1994 earthquake swarm at Mt. Eyjafjallajökull

The seismometer stations showed individual seismic characteristics. The portable stations show clearer P- and S-waves and higher signal-to-noise ratio,

making them easier to read. The seismogram characteristics from each station are shown in **Appendix**. The earthquakes seem to be similar to the high- and medium frequency earthquakes occurring at Mt. St. Helens, as classified by Malone (1983). No further frequency analysis of the Eyjafjallajökull earthquakes has been conducted.

The seismic wave pattern for one of the seismic stations, SKO, sometimes show an additional P-wave arriving before the S-wave. This extra P-wave could be a reflection from the surface or from a geological boundary within the crust beneath Mt. Eyjafjallajökull. This is the only station showing this specific pattern, and the high topographical relief in the station area may affect the wave paths, enabling a re-reflection of the waves from the hypocentral region.

The earthquake data in this study does not provide evidence for the existence of a magma chamber nor a low velocity zone beneath Mt. Eyjafjallajökull, down to 12 km depth within the studied horizontal hypocentral region of the 1994 earthquake swarm. Attenuation of the seismic waves does not seem to occur, except for the seismic station LMB. This stations sometimes have very emergent S-waves, especially in the end of the swarm.

2.6Uncertainties

The crust in the area is heterogeneous and no refraction study in the area has been conducted, except for the nearby Katla volcano (Gudmundsson et al., 1994).

No sign of a magma chamber beneath Mt. Eyjafjallajökull, is visible from the 1994 earthquake swarm data. No detectable low velocity zones due to patches of magma, appears when locating earthquakes beneath Mt. Eyjafjallajökull. The attenuation of the S-waves is not apparent as for the Katla volcano, though the stations Lambafell shows attenuation.

A rather large uncertainty in the data comes from the SIL-stations and their readings. The automatically read readings from the SIL-stations, were therefore read manually again. The SIL-stations MID, HAU and SNB seem to be correct, whereas the SIL-stations ASM, SAU, SOL and SKH were very difficult to read. Automatical readings of the SIL-station SKH were most often wrong, probably because of low signal-to-noise ratio. The SIL-station MID, which is closest to the hypocentral region, was correctly read, but the clock seem to be wrong causing the missfit of the readings from this station (**Table 6**).

2.7Choice of the best fitting seismic velocity model

Of the three seismic velocity models, the Mýrdalsjökull North (MYR-N) and the SIL models better suit the Eyjafjöll volcanic system, because:

i) The scatter of the three models became smallest when using the MYR-N model.

ii) The main localised depth occurred at 4-7 km depth, with a slight preference for shallower located earthquakes using the SIL velocity model.

This depth interval is in agreement with the crustal deformation measured by GPS and tile measurements. No clustering except a vague trend of two sub-cluster when using the SIL velocity model, has been derived.

iii) The rms for these two models was less than the MYR-V model.

iv) The horizontal and the vertical error were smaller than for the MYR-V model.

v) The quality of the earthquakes ranging from the best located a-earthquakes to the worst located c-earthquakes was best for the SIL model. The MYR-V model only calculated four a-earthquakes, compared to eleven and twelve for the MYR-N and the SIL model respectively.

Finally, the MYR-N velocity model was determined to be the most appropriate velocity model for the area with the smallest errors in vertical and horizontal and also the best concentration of the hypocentral region. This model does not incorporate the high velocity zone (included in the SIL model), nor the low velocity zone indicating patches of magma (included in the MYR-V model).

3. GPS AND LEVELLING MEASUREMENTS

3.1 GPS – An Introduction

GPS – the Global Positioning System is a navigation system based on satellites constructed for military purpose by the United States Department of Defense. The system can give absolute positions accurate to tens of metres and better if corrections are applied. The system may also be utilised by civilians for high precision geodesy. The fundamental principle of the GPS system is to measure the distance between several satellites and a receiver. By taking the difference in time between the transmission of a signal from the satellites and the reception of the same signal at the receiver, and then multiply the time difference by the velocity of light, the distance can be calculated. Because the positions of the GPS-satellites are known, estimations of a position for a receiver can be conducted. The main observable in GPS measurements is the pseudo-range, R, from receiver A to satellite j expressed as (Hofmann-Wellenhof et al., 1994):

$$R = c\,(t_A - t^j) = c\,(t_{A(GPS)} - \delta_A) - (t^j_{(GPS)} - \delta^j)$$

$$= c(\Delta t_{(GPS)} + \Delta\delta) = \vartheta^j_A + c\,(\Delta\delta + \delta_p)$$

where

c = velocity of light

t_A = time of reception at station A

t^j = time of transmission from satellite j

$t_{A\,(GPS)}$ =

$t^j_{\,(GPS)}$ =

$\Delta t_{(GPS)} = t_{A(GPS)} - t^{j}_{(GPS)}$

δ^{j} = corresponding error in the satellite clock

δ_A = error in the receiver clock

$\Delta\delta = \delta^{j} - \delta_A$

$\vartheta^{j}_{A} = c(\Delta t_{(GPS)} + \delta_p)$

ϑ^{j}_{A} = real distance between satellite and receiver

δ_p = delay associated with all error sources due to ion- and tropospheric propagation effects.

The system receives signals from 24 satellites distributed in six different orbital trajectories with inclination of 55° to the equator of the Earth. The satellite orbital planes are about 20000 km over the Earth´s surface, with orbital periods of about 12 hours duration. This constellation of the satellites makes it possible to receive more than four satellite signals whenever and wherever on Earth. GPS geodetic measurements can therefore be made any time everywhere on Earth.

The satellite signal is controlled by atomic time standards, two rubidium clocks and two cesium clocks onboard each of the GPS satellites, with long term stability. These frequency standards generate the socalled fundamental frequency f_0 of 10.23MHz. The f_0 is then used to create two transmission waves so called *carrier waves*, L1 (f_0 154 =1575.42 MHz) and L2 (f_0 120 = 1227.60 Mhz), which correspond to 19.0 cm and 24.4 cm wavelength respectively. Two code sequences

of +1 or –1 signals, the C/A- and the P-code, are used to modulate the carrier waves. GPS navigation instruments use the code signals to calculate absolute locations. The C/A-code is used for civilian purpose and is repeated every millisecond while the P-code is often encrypted for military use and repeats itself once every 37 weeks. An information code is added to the two, containing navigation information, such as satellite orbit parameters and satellite clock corrections.

The complete GPS signal can be described by the following equations (Dixon, 1991):

$$S1(t) = A_{P1}*P(t)*D(t)*\cos(2\pi f_1 t) + A_C*C(t)*D(t)*\sin(2\pi f_1 t)$$

$$S2(t) = A_{P2}*P(t)*D(t)*\cos(2\pi f_2 t)$$

where:

S1(t) = Modulated L1 carrier wave

S2(t) = Modulated L2 carrier wave

P(t) = P-code

C(t) = C/A-code

D(t) = Navigation information

A_P = Relative amplitudes of the P-code

A_C = Relative amplitude of the C/A-code

GPS geodetic receivers record both the S1(t) and S2(t) signals from all

GPS satellites in view. These signals can provide a measure of the pseudo-range from ground to satellite, and they can be used to calculate accurate relative position of receivers.

Beginning in 1987, the WGS-84 (World Geodetic System 1984), system was used as a reference frame for GPS (Decker, 1986). It is a geocentric (centre of origin in the same point as the Earth´s mass centre) x, y, and z system. Precision of coordinate determinations increases with observation time length at the GPS stations. In Iceland, station occupation time of about 24 hours has been used in much of the crustal deformation studies. It provides an accuracy of few mm. The errors in the satellite orbits will cause baseline errors in GPS data processing, but use of post-computed precise orbits minimises these errors. Details on GPS error sources, are given by Segall and Davis (1997).

3.2 GPS data, processing and methods

I have processed GPS data from the measurements conducted around Mt. Eyjafjallajökull in 1994 (1994 spring and 1994 autumn campaigns) and in 1998. I have also compared my results with the results of measurement conducted in 1992. The GPS-data was collected with three Trimble 4000 SST GPS-receivers, owned by the Nordic Volcanological Institute. Data were collected from four different campaigns described separately below (subchapters 3.4.1.1-3.4.1.3).

3.2.1 Measurements

3.2.1.1 The 1992 campaign

GPS measurements in the Eyjafjallajökull area in 1992 were a part of a larger survey. A regional GPS network set up in South Iceland 1986 and densified in 1989, was then re-measured. Details of this campaign are given in Sigmundsson et al. (1992b; 1995). Two sessions were measured each individual day, both being about 12 hours long (**Table 7**). Each station was measured for at least four sessions. In total 41 stations were measured during this campaign. Three stations (HAMR, REYN and SKOG) were located in the close vicinity of Mt. Eyjafjallajökull (**Figure 34**).

3.2.1.2 The 1994 campaigns (spring and autumn campaign)

The GPS measurements around Mýrdalsjökull and Eyjafjallajökull in 1994 were a part of a larger campaign in the Eastern Volcanic Zone. Details are given by Jónsson et al. (1995); Jónsson (1996); and Jónsson et al. (1997).

The Mýrdalsjökull volcanoes (Katla and Goðabunga) and Mt. Eyjafjallajökull network consisted of totally 17 GPS points. The main part of the points had been measured before but several points were added around Eyjafjallajökull (**Table 8**) due to the seismic unrest there during May and June the

same year (Figure 34). The measurements were conducted during eleven days, from the 27th of May until the 6th of June (days 147-157 of the year). The second measurement period lasted from the 18th to the 22nd of September 1994 (days 261-265of the year).

3.2.1.3 The 1998 campaign

The 1998 campaign lasted for six days from 2nd of July to 7th of July (days 183-187 of the year). The campaign was carried out by Halldór Ólafsson and Erik Sturkell from the Nordic Volcanological Institute, and Sigrún Hreinsdóttir from the Science Institute, University of Iceland. Three Trimble 4000 SST receivers owned by the Nordic Volcanological Institute, were used. Seven points were measured in 1998 (**Figure 35**). One new point, Dagmálafjall (DAGM), was measured for the first time, other stations were re-measured (Table 7). The Dagmálafjall station is a part of an optical levelling tilt station. Each measurement day was divided into three measurement sessions, numbered 0, 1 and 2, respectively. Each station was measured for at least four sessions.

3.2.2 Data processing

I used the BERNESE GPS software version 4.0 (Rothacher and Mervart,

1996), to analyse GPS data. Each individual processing step will be discussed below. This software reduces errors and eliminate biases in the measurements, using signal phase differences. The single difference uses differences between two receivers, the double difference takes the differences between a two coupled satellites and a pair of receivers and finally the triple difference calculates the differences between two different epochs t_1 and t_2.

3.2.2.1 Data transfer

The raw data from the receivers were transferred to the RINEX format, which stands for Receiver Independent Exchange format. This is done by the program TRRINEXO, especially made for data from the Trimble manufacturer. Two different RINEX files are created, an observation file a navigation file. Each RINEX observation data file contains only information from one receiver, and consists of a header section with auxiliary station and receiver information. The navigation message file includes broadcast message for all satellites collected during the different sessions.

Next step in the data transfer is to converting the RINEX files into the Bernese format. This is done with the program RXOBV3. The RINEX format is an ASCII format, but the Bernese format is a binary one. Binary files are used to enhance the speed of the transfer. The navigation message files are also converted to the Bernese format. Four observation files are created for each RINEX file,

with different name extension names:

*.PZH: Phase zero-difference header file containing information about the station , receiver, antenna and ambiguities.

*.PZO: Phase zero-difference observation file containing phase observation information.

*.CZH: Code zero-difference header file including the similar information as the *.PZH-file.

*.CZO: Code zero-difference observation files with code observations

All of the antenna information in each file with the extension *.DAT, is checked manually with the field notes and corrected if not agreeing with each other. The *.DAT file contains information like sitename/number, observation agency, receiver type/number and antenna information (height, number and E/N).

3.2.2.2 Orbit processing

In my data analysis I used socalled "IGS final orbits" orbit information from CODE, the Center for Orbit Determination in Europe. These orbits are based on the best available data. Precise orbit files are then created in two steps, by using the programs PRETAB and ORBGEN. The first program takes the precise orbit format – the SP3 format – containing precise satellite clock information with a sampling rate of 15 minutes and precise orbit information, and converts into the Bernese format. This program generates socalled tabular orbit

files, and aslo satellite clock files, by fitting the satellite clock information in the precise files within intervals of several hours with two degree polynomial within intervals of 12 hours. The second program, ORBGEN, creates socalled standard arc orbits for each individual day. It computes the standard orbits by using the satellite positions in the tabular orbit files generated by PRETAB, with numerical integration of the equations of motion.

3.2.2.3 Data pre-processing

Three pre-processing programs have been used to prepare the data for the main GPS estimation programs. These programs are CODSPP, SNGDIF and MAUPRP.

The receiver clock has to be synchronised with GPS time. The first program, CODSPP, uses the zero-differences code measurements to calculate the receiver clock error with about 1μs accuracy, and to calculate preliminary receiver coordinates. The CODSPP will use the P-code if possible, but even the C/A-code is sufficient enough for this purpose.

The second program, SNGDIF generates the phase single difference between receivers at points, which are measured simultaneously. The Bernese GPS software uses double differences as the basic observables, the single differences being created in SNGDIF and stored in files, and the double differences are generated in the program GPSEST.

In the last program, MAUPRP will search for and correct, cycle slips (temporary loss of the satellite phase signal). A receiver can measure the difference in phase of the satellite transmitted carrier signal, and its replica created intermally within a receiver. This measure will give a value between 0 and 1 phase cycle (0 and 2π). After the receiver has been activated, an integer counter is initialised and the tracking of the counter is incremented by one as soon as the fractional phase will change from 2π to 0. The accumulated phase for every epoch will thereby represent the sum of the directly measured fractional phase and the integer count. The initial integer number n^i_{Fk} of cycles between the satellite i and the receiver k is an unknown and has to be estimated. If no loss of signal lock occurs, the initial phase ambiguity will remain the same, but a loss of it will cause a jump in the accumulated phase by an integer numbers of cycle. If there is a difference between two times, t_1 and t_2 in the initial integer number, a cycle slip has occurred between t_1 and t_2. The cause of such cycle slips include;

i) Obstruction of the satellite signal due to trees, buildings etc.

ii) Low-signal-to-noise ratio due to rapidly changing ionospheric conditions, multipaths, high receiver dynamics or low satellite elevation.

iii) Failure in the receiver software.

iv) Malfunctioning of the satellite oscillator.

Therefore all observations are checked and all time intervals (t_1 - t_2) with occurring cycle slips are detected and repaired if possible, by estimating the difference during the time intervals.

The MAUPRP will do three pre-processing steps. The first step is to find the time intervals NOT containing any cycle slips, by checking whether the double difference phase observations are smooth functions of time. These intervals are then used to compute the triple difference solution to enable estimation of a fair approximation of the coordinates. This is done by using a standard least square adjustment for each baseline. The second step in the MAUPRPR, the "clear" time interval data, a triple difference solution is calculated using the standard least-squares adjustment for each baseline, where the first station´s coordinates are kept fixed on their priori values while the second station´s coordinates are estimated. The triple difference residuals are computed for all observations even the ones containing cycle slips. This residuals are then stored into a file. MAUPRP´s third step, corrects big jumps on the single difference level occurring due to the receiver clocks (clock jumps). The residuals from the second step are inspected to enable detection of cycle slips. MAUPPRP will also give the information of the ambiguities set up, with each satellite having one ambiguity corresponding to the first epoch. All changes are then saved into a certain file. After the MAUPRP processing step, the data is ready for final parameter estimation, with the GPSEST program.

3.2.2.4 Coordinate estimation

A special set of programs is used for final estimation of station coordinates

and other parameters. The first run of the precise parameter estimation program GPSEST, will use least square adjustment to calculate coordinates, resolve the initial integer phase ambiguities, model the ionosphere and model the local troposphere. An estimation of the coordinates of the observation points, using a socalled ionosphere free linear combination (L_3) is conducted and then saved to a file to enable good a priori coordinates for the next step. In the next step the GPSEST program keeps the estimated coordinates from the last step fixed and resolves the phase ambiguities using a so-called wide-lane linear combination (L_5) on the double difference level for the phase observations. The third step includes a final coordinate solution for each point, where the fixed wide-lane (L_5) ambiguities are introduced as input. A solution for the narrow-lane ambiguities is made, by using the ionospheric free linear (L_3) combination. With the fourth run of the GPSEST, socalled normal equation files (*.NEQ) are used to calculate the final coordinate combination for each measurement session.

Finally, as a last step a program called ADDNEQ is used to combine the results from individual sessions into a single multi-session solution. By using statistically correct combination of the single session solution from the GPSEST, calculation of accurate coordinates and their uncertainties are computed.

3.3 GPS analyses and uncertainties

The different GPS campaigns in the area around Mt. Eyjafjallajökull had

somewhat different aims, and different set of stations was measured in each of them. Stations measured in the earliest campaign in 1994 (1994Aa) have not been re-measured. This campaign was however processed to provide future reference. The earlier campaigns were not aimed specifically at detecting crustal deformation of Mt. Eyjafjallajökull, but were rather parts of larger projects concerning regional deformation within the EVZ and deformation of the Katla volcano.

In the following I present results of my GPS-data analyses for the different GPS-data sets. During each of the measurement campaings, at least two sessions, each 7:55 hours long, were measured at each GPS station. Each session was separately processed and the combination program ADDNEQ (least square estimation solution), was used to derive a final solution providing the best estimated coordinate values.

The final estimation processing step for each session was done by the estimation program GPSEST. Coordinate values and formal error are calculated. These indicate the phase scatter of the data set. Systematic errors and mismodeled parameters are not taken into account, and experience wutg tge BERNESE Software suggest that the formal error provided byt the GPSEST programs may be unrealistic. The weighted session-to-session corrdinate scatter and repeatability will give a better estimation of the error. For the GPS campaigns in this study, more than three sessions for each GPS point were processed (two for the 1992 campaign). The ADDNEQ program uses the scatter of the whole network solution to get closer to the realistic errors. The program calculates a scaling

factor for all the formal errors from the GPSEST program, and a scaled sigma for the geocentric coordinates (x, y and z) is derived.

With the program version used to process the GPS data for this study, the Bernese software, version 4.0, the ADDNEQ does not calculate the scaled sigma for the ellipsoid coordinates (latitude, longitude and height). Instead, the program DYNAP (Dynamic Adjustment Program) from the National Geodetic Survey USA, was used. It uses the same methods as the ADDNEQ program,to calculate a scaling factor between realistic and formal errors,and the scaled sigma for the ellipsoid coordinates. The derived scaling factor was added to the unscaled formal uncertainty ellipse, to derive a more realistic uncertainty of the error ellipses. The scaling factor for each campaign was calculated and can be seen in **Table 8**, together with the avearages of the formal error, the session-to-session coordinate repeatability, and the scaled error into each coordinate component.

One source of error has not been mentioned, possible systematic errors due to the antenna position. The antenna height was measured tvice, before and after the measurements were conducted, in order to minimise antenna position errors.

In the following paragraphs, the scatter and the repeatability plot and the coordinates for each of the GPS data sets are presented. The scatter plots show how coordinate estimates from each inidvidual session solutionss deviate from a weighted average solution. The repeatability plot shows how the session-to-session scatter for each station. A low repeatability value is good. It shows that the coordinate estimates for individual sessions are consistent, and that the

coordinate estimates are accurate.

3.3.1 The 1994 GPS campaigns

The 1994 GPS measurement were actually collected curing three different time periods, and were therefore analysed as separate campaigns – 1994Aa, 1994Ab and 1994B representing day 147-151 (27th to 31st of May), 153-157 (2nd of June to 6th of June) and 261-265 (18th to 22nd of September) respectively (**Table 9**) with all of the measured stations.

3.3.1.1 The 1994Aa campaign

This campaign does not include any stations measured in other campaings, so a comparison is not possible, until those stations have been measured again. This campaign was processed to provide a future reference for deformation around Mýrdalsjökull. Station Reynisfjall was kept fixed as the reference station during this campaign. After three runs of GPSEST and ADDNEQ, the repeatability and the scatter were plotted and these are shown in **Figure 36 a** and **b**. The coordinates are given in **Table 10**.

The scatter plots show that the scatter of individual solutions from their wieghted average, does not exceed ±1.0 cm for the length. The scatter is less than 0.9 cm in north-south component. The east-west componenet shows a scatter of

less than 1.5 cm. The height shows a scatter of ±2.7 cm. The repeatability plots show for the length, N-S and E-W solutions not more than 0.8 cm and 1.7 cm for the height.

3.3.1.2 The 1994Ab campaign

This campaign used the station SELJ as a fixed reference station. Only three stations, HAMR, SELJ and STEI were measured during this campaign. The coordiantes for SELJ were the ones derived from the 1994B campaign. GPSEST estimation programs and ADDNEQ were run four times to get good a priori coordinates. Final coordiantes are given in Table 10.

The scatter plots indicate good qualtiy of the data with an uncertainty of less than ± 0.25 cm, except for the session STEI1551 (short session) for the length, N-S, and E-W, and ±1.4 cm for the height (**Figure 37a**). The repeatability plots show small uncertainties for the data set, with an uncertainty of only 0.15 cm for length, N-S and E-W and 0.6 cm for the height (**Figure 37b**).

3.3.1.3 The 1994B campaign

This subcampaign used again the REYN as a reference station. The GPSEST estimation programs and the program ADDNEQ was run two times. Coordinates are given in Table 10.

The scatter plot shows the following results; ±0.25 cm for the length, ±0.9 cm for the N-S, ±0.7 cm for the E-W and finally ±3 cm for the height (**Figure 38a**)..

The repeatability plots show less than ±0.5 cm for the length and the E-W, ±0.6 for the N-S and finally 1.9 cm for the height (**Figure 38b**).

3.3.1.4 The 1998 campaign

HAMR was the reference station and was measured during the whole subcampaign. Because of lack of data for the HAMR station in sessions 1852 and 1862, these sessions were excluded from the final solution. Therefore the GPSEST estimation programs and ADDNEQ was run in three different steps, 1841-1851, 1860-1861 and 1870-1881. The GPSEST estimation programs and ADDNEQ program were run three times (Table 10).

The scatter plots give an indications of good results with a scatter of ±0.5 cm for the length, ±0.6 cm for the N-S ±0.5 cm (except for REYN1841) for the E-W and ±2.0 cm for the height (**Figure 39a**). The repeatability plots indicate an uncertainty of less than 0.7 cm, 0.8 cm and 0.3 cm for the length, N-S and E-W respectively. The height is less than 1.0 cm (**Figure 39b**).

3.4 Crustal deformation

The programs within the BERNES GPS Software, version 4.0, the

program ADDNEQ does not calculate the scaled sigma for the ellipsoid coordinates. Instead it derives the unscaled formal uncertainty ellipsoids for each GPS point. The program DYNAP (Dynamic Adjustment Program), from the Natinal Geodetic Survey in USA, uses the same method as the program ADDNEQ does, but it calculates the scaled sigma for the ellipsoid coordinates. The scaling factor is applied to the unscaled formal uncertainty ellipse, to derive a more realistic final uncertainty ellipsoid – a scaled sigma for the ellipsoid coordinates. The scaling factor is x.xx, 7.44, 12.92 and 8.74 for the 1992, 1994Ab, 1994B and the 1998 GPS campaign respectively.

3.4.1 1992-1994B

REYN was used as the reference station, but the coordinates were shifted in order to calculate displacement relative to the HAMR station (fixed station in all my presentations). Two stations were compared to HAMR, namely REYN and SKOG (**Table 12**). The most significant crustal deformation occurred at SKOG, with more than 51 mm of movement to the east and 22 mm to the south. The station REYN showed a slight uplift of 13 mm. Only the REYN station showed any detectable movement in height, but still very small (**Figure 40**).

3.4.2 1992-1998

REYN was still the reference station, but again the coordiantes were shifted so station HAMR appears stationary. Two stations, REYN and SKOG were compared to HAMR (Table 12). The movements in height were larger but still very small except for the station SKOG, which showed an uplift of 25 mm. The REYN showed for the same period also an uplift of more than 15 mm. The horizontal movements were for both the stations are towards the SE, as in the 1992-1994B solution. REYN showed 14 mm displacement to the east, whereas SKOG showed 46 mm to the east and 22 mm to the south (**Figure 41**).

3.4.3 1994Ab-1994B

SELJ was used as the reference station, but displacements are estimated relative to the HAMR station (Table 12). STEI and SELJ showed the following results: STEI showed 22 mm subsidence, while SELJ resulted in a movement of 18 mm to the south, 15 mm to the west and an uplift of 29 mm (**Figure 42**).

3.4.4 1994Ab-1998

Displacements relative to the HAMR station are the following: uplift of 17 and 36 mm for STEI and SELJ, respectively (Table 12). STEI showed no detectable movement in the horizontal, while SELJ showed movement of 18 mm to the south and 13 mm to the west (**Figure 43**).

3.4.5 1994B-1998

HAMR was used as the reference station (Table 12). The 1998 GPS stations FIMM, REYN, STEI SKOG and SELJ were compared to the 1994B. Little detectable movements occurred, during this time period, but station STEI and station SKOG showed an uplift of 39 and 27 mm respectively (**Figure 44**).

3.5 Ground tilt measurements and analyses

Tilt measurements have been used in several studies to observe and estimate the ongoing crustal deformation at volcanoes in Iceland, including Hekla (Tryggvason, 1994) and Mýrdalsjökull (Tryggvason, 1973a or b).

Two tilt stations are located in the close vicinity of Mt. Eyjafjallajökull, namely Fimmvörðuháls and Dagmálafjall (**Figure 45**). The Fimmvörðuháls station was established and initially surveyed in 1992, whereas Dagmálafjall station was initially measured in 1994. Each station is a T-shaped array of about 12 benchmarks spaced about 50 metres apart. The raw measurement data is a set of precisely measured elevation differences between the benchmarks (**Figure 46**). Such precise elevation measurements between the benchmarks have been conducted nearly annuallyby the staff of the Nordic Volcanological Institute. The raw data was processed with a software prepared by Eysteinn Tryggvason, at the

Nordic Volcanological Institute. Raw data is used to generate an output file with estimates of ground tilt between successive measurements. Ground tilt is given in units of μrad, where 1 μrad is equal to 1 cm relative uplift between stations spaced 10 km apart. The program used gives the north and east component of ground tilt.

The inferred annual ground tilt between the years 1992, 1993, 1994, 1995 and 1998 for the tilt stations FIMM and DAGM are shown in **Figure 47-50**. The tilt between the 1992 to 1993 and 1994 to 1995 is very similar, while the calculated tilt between 1993 and 1994 is significantly different. The 1993-1994 tilt vector points almost directly to the W, instead of NW. The angle between the two vectors is 40-45°. The size of the 1993-1994 tilt vector is also much larger than for the other year comparisons. The vector for the annual comparison between 1993 and 1994 including the time period for the 1994 earthquake swarm, is 12 μradians compared to 2-3 for the other comparisons. In special, the northern component shows significant differences (**Figure 51**).

1993-1994 ground tilt at the Fimmvörðuháls station, is in broad agreement with a single Mogi point source at the location of the 1994 earthquake swarm. Predicted tilt according to the model is:

$$\text{Tilt} = 3 * \Delta h_0 + D^3 r * R^5$$

where

$$R^2 = (D^2 + r^2)$$

D = Depth to the source

r = 11.0 km, horizonal distance from the earthquake swarm to the FIMM tilt station

Δh_0 = vertical displacement directly above the source

I try to fit a Mogi model to the vector component of the 1993-1994 ground tilt that points *directly* to the source (the calculated mean hypocentre of 1994 earthquake swarm). This component is 9.08 μrad. By varying the depth parameter between 0 and 15 km with a one-kilometer-intervall, and by varying Δh_0, an estimate of the model tilt at Fimmvörðuháls was infered. In **Figure 52**, the model parameters capable of producing the observed tilt (9.08 ±1 μrad), are plotted. This figure shows curves of 8.08, 9.08 and 10.08 μrad, respectively, calculated for 11.0 km source distance. The figure shows that for each Δh_0 (m), an acceptable ground tilt (9.08 ±1 μrad), can be derived for a certain depth value. The value of Δh_0 will decrease with increasing depth to a critical value of 11 km depth. The earthquakes located with the MYR-N velocity model, occur at 4-7 km depth. As can be seen in the figure 52, with a tilt of 10 μrad, a depth value of 4 km will give a maximum uplift at the surface, directly above the single point Mogi source, of about 0.85 metres. A depth value of 7 km would result in a maximum uplift of about 0.30 metres, with the same tilt measured. The similar values for a tilt of 8 μrad, would be 0.80 and 0.35 metres respectively. Modelling of horizontal and vertical displacement, associated with a Mogi source, at the GPS stations at Mt. Eyjafjallajökull, at the time of the 1994 earthquake swarm, is

shown in **Figure 53**. The GPS stations are pointed out on the x-axes and their values plotted, in an attempt to search for the best curve, for the observed deformation at the time of the earthquake swarm in 1994. The modelling will only be indicative, because the lack of number of stations (being only three, namely HAMR, SELJ and STEI). Together with earthquake data and interpretation of the pattern of crustal deformation at Mt. Eyjafjallajökull, further suggestions of the probable cause can be drawn (see more in the discussion and conclusion).

Maximum deformation directly above the modelled point source by Mogi, and the distance to the GPS statons plotted on the xaxis, suggest that the observed deformation at each individual GPS point is not in good agreement with a Mogi model. An increased deformation source depth, would generate a better fit for the observed crustal deformation, with a source at about 7 km and a smaller h_0 of 0.20 metres (**Figure 54a** and **b**). The closest, to the deformation source located station, STEI, is not showing a large uplift, as would be expected for a single Mogi point source. Rather this station shows subsidence, indicative of that a better fit for the data sets would be a dyke intrusion model with the maximum deformation occurring on the flanks of the dyke intrusion, and not directly above the modelled source of deformation.

4. Conclusions and Discussion

The earthquake swarm in 1994 at Mt. Eyjafjallajökull was an unusual event, as the mountain has been characterised by low background seismicity during the last 15 years ("the Quiet One"). The 1994 earthquake swarm pattern shows a typical Icelandic earthquake swarm behaviour, similar of the seismic swarm activity within the Torfajökull during 1991 to 1995 (Soosalu and Einarsson, 1997). The seismicity shows an abrupt beginning that soon reaches its maximum in a few days and then decreases with time. The magnitude range was between 0.59 to 2.27 M_L. The earthquake swarm lasted from the 27th of May until the 3rd of July 1994, and was registred by, in total, 13 seismometers, with a good seismic network configuration, including two stations less than 4 km away from the epicentral region.

The main part of the relocated events occur at a depth of 4-7 km just SSE of the Steinholtsjökull glacier outlet, NNE of the summit crater. The relocations are good, with small horizontal and vertical errors. The deepest located earthquakes occurred furthermost to the north, away from the summit crater situated in the centre of the volcano. The most northwars located earthquakes are the largest earthquakes in the swarm as well. This could, as has been suggested before (Dahm and Brandsdóttir, 1997), indicate an opening of a crack at 6-7 km depth. This crack will open up when intrusion of magma occurs, causing the crack to widen with time. The slight trend in migration to shallower depth with time further supports this indication.

The intrusion, suggested to be a dyke intrusion beneath the norhtern flank

of the volcano, seems to have been intruding in an east-west lineation. Temporal and spatial seismic pattern (after relocation), small magnitude range and type and orientation of focal mechansims of the Mt. Eyjafjallajökull earthquakes are all indicative of intrusive activitity SSE of the summit crater. The study by Dahm and Brandsdóttir (1997) showed that all the derived focal solutions have nearly vertical T-axes and horizontally oriented P-axes, and 75 % of the 15 studied events have E-W oriented nodal planes, which further supports a magmatic intrusion in an E-W direction. Relocation of 67 earthquake, indicate a well defined hypocentral region at 4-7 km depth with a clear E-W orientation of the earthquake swarm distribution in latitude and longitude.

The 1994 earthquake swarm was associated with crustal deformation measured by GPS and ground tilt measurements. The geodetic measurements show that the surface crustal deformation between 1992 and autumn of 1994, and between 1994 spring and the autumn of 1994, was nearly identical. This indicates that the crustal deformation in the area was closely related to the earthquake swarm in 1994, because the main part of measured deformation occurred at the time of the 1994 earthquake swarm. The geodetic measurements does not show any detectable crustal surface deformation between the autumn 1994 and the summer 1998, despite the earthquake swarm activity in early 1996. This indicates that an earthquake swarm in 1996 at Mt. Eyjafjallajökull, was not associated with any crustal surfcae deformation and was therefore not caused by any magmatic intrusion at shallow depth. The 1994 and the 1996 earthquake swarms show some

similar patterns, with the 1996 earthquake swarm being located furthermore to the west. Depth locations for the 1996 events are very poor, due to that only the SIL seismic netork further away from the mountain recorded the 1996 seismic activity. Relocations of only one day of the 1996 earthquake swarm indicates that the very deep located earthquakes in the 1996 swarm, may have occurred at a similar depth as the 1994 earthquake swarm. Though similar seismic characteristics and behaviour (magnitude range, temporal distribution and longitudinals pattern), the geological processes seem to be different for the two earthquake swarms.

The earthquakes themselves ($M_L \geq 2.27$) are too small to generate enough slip on faults at depth, to generate the crustal deformation observed by GPS and ground tilt measurements at the surface associated with the 1994 earthquake swarm. According to slip calculations for micro-earthquakes by Rögnvaldsson (1994), the mircro-earthquakes within the 1994 earthquake swarm at Mt. Eyjafjallajökull, are likely to have only generated a few mm deformation on the surface. A magmatic intrusion at shallow depth could, on the other hand, explain well the deformation pattern at Mt. Eyjafjallajökull, and such an intrusion probably caused the 1994 seismic activity at Mt. Eyjafjallajökull as well. A vertical or inclined dyke intrusion of limited dimensions is likely to have occurred. The suggested dyke intrusion model of Dahm and Brandsdóttir (1997) with up to 5 metres dyke-opening, is of too large dimension probably the dyke opening was an order of magnitude smaller than suggested by Dahm and Brandsdóttir (1997).

Although an earthquake swarm occurred in Goðabunga in 1992, the measured crustal deformation measured at Mt. Eyjafjallajökull between 1992 and 1998, is suggested to be closely related to the earthquake swarm there in 1994. This is supported by first of all the timing of the obe-served crustal deformation. The main deformation detected by GPS measurments occurred between May and September 1994, the time interval for the earthquake swarm being late May to early July 1994. Small or no detectabel deformation in the area has been measured by geodetic measurements. The indicative stable Mt. Eyjafjallajökull, according to these measurements, show no measurable deformation from September 1994 to July 1998. This is suggested to be the typical "deformation pattern" for Mt. Eyjafjallajökull. The second evidence is that the horizontal displacement show expansion across Mt. Eyjafjallajökull. Because of this expansion, it is natural to interpret the ground tilt results at Fimmvörðuháls as indicative of uplift of the Eyjafjallajökull massif. The third an last evidence for that the observed crustal deformation at Mt. Eyjafjallajökull in the summer of 1994 is not related to activity beneath the Katla or Goðabunga volcanoes, is that the ground tilt vector derived between September 1993 and September 1994 pointing towards a possible source at the western part of Mt. Eyjafjallajökull, was derived within the same time interval as the 1994 earthquake swarm occurred. Also, the this ground tilt vector is four to six times larger than the measured ground tilt for the other year comparisons in 1992-1993 and 1994-1995 are. Therefore it is unlikely that the observed crustal deformation relates to processes

taking place beneath Mýrdalsjökull, rather the source of deformation must lie beneath Mt. Eyjafjallajökull.

The geodetic measurements conducted at Mt. Eyjafjallajökull in May/June and September 1994 respectively is inidicative of a sudden crustal deformation occurring in the summer of 1994, in close relation with the time for the 1994 earthquake swarm. The horizontal displacements observed by GPS measurements at Mt. Eyjafjallajökull, suggest an overall stable long-term pattern of no or little crustal deformation. Small horizontal displacements for all stations except STEI between September 1994 and the summer 1998, all suggest a stable non-deforming pattern for Mt. Eyjafjallajökull. STEI, on the other hand, show both detectable horizontal movement and uplift. The station SKOG also shows uplift, though just very small according to the horizontal errors for the measurements between 1994B and 1998. The station SKOG is the GPS point in the GPS measurements in 1992-1994B and 1992-1998 respectively, which shows a significant horizontal deformation, but no vertical deformation was measured at this station during these time intervals. Nearly all or 93% of the total observed deformation occurred in the time interval 1992-1994B, including the earthquake swarm activity at Mt. Eyjafjallajökull. SKOG shows very little evidence of horizontal deformation from the autumn 1994 to the summer 1998. The SELj station measured in 1994Ab, 1994B and in 1998, shows an interesting pattern with large horizontal and vertical deformation between the two GPS measurements in 1994 and in the time period 1994Ab-1998, with nearly equal

deformation for the two time periods. The uplift is though larger for the longer time period being 3.7 cm, compared to 3.0 cm respectively. The other GPS station measured during the same campaigns, STEI, shows a major subsidence in the summer of 1994, being the only station showing detectable subsidence. This station is closest station to the average epicentral region for the 1994 earthquake swarm at Mt. Eyjafjallajökull. After the earthquake swarm, an uplift of the area seems to be continous for this station. No major horizontal displacement seems to occur at this GPS point during the time spans mentioned above, except for a horizontal deformation (norht component) at STEI between September 1994 and July 1998.

The model by Mogi for a single point source only partly fit the seismic and geodetic data in this study. A model with a dyke intrusion, with the maximum vertical displacement not above the centre of the deformation source, but rather at the flanks of the dyke intrusion (see Figure 8a and b), would possibly better model the observed crustal deformation at Mt. Eyjafjallajökull and the 1994 earthquake swarm. The sudden crustal deformation pattern and the fact that the closest station to the epicentral region, STEI, shows subsidence while the other GPS station measured at the same time, SELJ, instead shows a signifcant uplift and horizontal displacement, could suggest a better fit with a dyke intrusion model. Also, the ground tilt vector calculated for the 1993-1994 period including the swarm activity, does not point directly to the centre of the located earthquakes at the northern part of the mountain, but rather point towards a possible source of

deformation just south of the other tilt station Dagmálafjall, to the west of the volcano around 16.9 km SSW of the epicentral average position. An inclined dyke intrusion would, instead of generating a symmetric deformation pattern, result in an asymmetry within the deformation style as suggested by Sigmundsson et al., (1999, in press) for the Reunion Island Piton de la Fournaise volcano. Interferomteric analysis of SAR images, showen an asymmetric deformation associated with an inclinded dyke in the roots of the volcano. Instead of having a symmetric deformation at the surface, the area closest showed a different pattern on each side of the the inferred dyke. The area on the "foot-wall" side of the intrusion showed no uplift, but rather subsidence, while the area on the "hanging-wall" side of the dyke, generated a significant uplift closest to the dyke intrusion successively decreasing with distance from the dyke (**Figure 55**). The measured subsidence at the GPS station STEI at MT. Eyjafjalajökull during the 1994 earthquake swarm, might be a result of an inclinde sheet oriented in an E-W direction, dipping towards the south or southwards. The ground tilt vector pointing to the south of the epicentral region for the 1994 earthquake swarm at Mt. Eyajfjallajökull, westwards from the tilt station Fimmvörðuháls, might be explained if not fully but partly by a dyke intrusion of this character.

The thick crust in the southern part of the EVZ is capable of supporting large loads as topographical large volcanoes as Mt. Eyjafjallajökull and the Katla volcano for example. The scattered GPS signal between the autumn 1994 and summer 1998 may probably suggest general stability and nealry no deformation of

the area in recent years. According to the GPS measurements conducted in the period 1992-1998, no long-term gradual. Observable subsidence or expansion/contraction has occurred at Mt. Eyjafjallajökull. The crustal deformation measured, seems to be closely related to the seismic and magmatic activity during the 1994 earthquake swarm. Although, some vertical deformation at the GPS station STEI (the closest one to the epicentral region of the 1994 earthquake swarm) occurs between June and September 1994, we have no evidence for gradual inflation/deflation ("magmatic breathing") of the volcano in the 1994-1998 period. This is in contrast with the behaviour of Krafla and Askja in the Northern Volcanic Zone, which both show ongoing subsidence and contraction in recent years after volcanic activity in the middle of 1980s. the conclusion drawn from the 1994-1998 GPS comparisons is that between magmatic/seismic activity , Mt. Eyjafjallajökull appears rather stable with no or very small deformation rates of less than 2.5 mm/year horizontally and 1cm/year for the vertical displacement. The deformation at Mt. Eyjafjallajökull can be described as sudden, without any observable long-term gradual deformation, occurring in close relation with seismic or magmatic activity beneath the mountain.

FUTURE WORK

refraction study

modelling with a dyke intrusion model

7 References

Angenhiester, G., Björnsson, S., Einarsson, P., Gebrande, P., Goldflam, W., Jacoby, R., Litvineko, I. V., Loncarevic, B., Miller, H., Pálmason, G., Pavlenkova, N. I., Richard, S., Solomon, S. C., Wigel, W. and Zverev, S. M. (1980). Reyjanes Ridge Iceland seismic experiment (RRISP 77), *J. Geophys.*, **47**, 228-238.

Andersson, E. M. (1936). The dynamics of the formation of cone-sheets, ring-dykes, and cauldron subsidences, *Proc. R. Soc. Edinburgh*, **56**, 128-157.

Águstsson, K. (1998). Stefnur og strik í landslagi á Hellisheiði og í Hengli, *Veðurstofa Íslands Greinargerð*, **VÍ-G98037-JA05**, Reykjavík.

Águstsson, K. (1998). Jarðskjálftahrina á Hellisheiði og í Hengli í maí-júlí 1998, *Veðurstofa Íslands Greinargerð*, **VÍ-G98040-JA06**, Reykjavík.

Baueršima, I. (1983). NAVSTAR (Global Positioning System (GPS), II.

Mitteilungen der Satelliten-Beobachtungsstation Zimmervald, No. 10, Astronomical Institute, University of Berne.

Beblo, M., and Björnsson, A., (1980). A model of electrical resistivity beneath NE-Iceland, correlation with tempearture, *J. Geophys.*, **47**, 184-190.

Beblo, M., Björnsson, A., Árnason, K., Stein, B., and Wolfgram, P. (1983). Electrical conductivity beneath Iceland – Constraints imposed by magnetotelluric results on temperature, partial melt, crustal and mantle structure, *J. Geophys.*, **53**, 16-23.

Beutler, G. (1992). The Impact of the International GPS Service for Geodynamics on the Surveying and Mapping Community, In: *International Union of Surveying and Mapping (IUSM) Presented Papers of the Working Group Sessions*, 84-94.

Bilham, R. (1991). Earthquakes and sea level: space and terrestrial metrology on a changing planet, *Reviews of Geophysics*, **29**, 1-29.

Bjarnason, I. Þ., and Einarsson, P. (1991). Source mechanism of the 1987 Vatnafjöll earthquake in South Iceland, *J. Geophys. Res.*, **96**, 4313-4324.

Bjarnason, I. Þ., Menke, W., Flóvenz, O. G. and Caress, D., (1993). Tomographic

image of the Mid-Atlantic plate boundary in southwestern Iceland, *Geophys. Res. Letters*, **98**, 6607-6622.

Björnsson, H., Björnsson, S. and Sigurgeirsson, Þ. (1982). Penetration of water into hot rock boundaries of magma at Grímsvötn, *Naure*, **295**, 580-581.

Brandsdóttir, B. and Einarsson, P. (1992). Volcanic tremor and Low-frequency earthquakes in Iceland, In: Gasparini, p., Scarpa, R. and Aki, K (eds.), *Volcanic seismology*, Springer, Berlin, Heidelberg New York,, **vol.3**, 212-222.

Brandsdóttir, B., Menke, W., Einarsson, P., White, R. and Staples, R. (1995). Crustal structure of the Krafla central volcano in the Northern Volcanic Zone of Iceland as determined through seismic observations, The Science Institute of the University of Iceland, report **RH-05-95**, 79 pp.

Brandsdóttir, B., Menke, W., Einarssson, p., White, R. S. Staples, R. K. (1997). Færoe-Iceland Ridge Experiment 2. Crustal structure of the Krafla central volcano, *J. Geophys. Res.*, **vol.102**, No.**B4**, 7867-7886.

Brandsdóttir, B. and Einarsson, P. (in press). Earthquakes in the Mýrdalsjökull area, Iceland, 1978-1985: Seasonal correlation and relation to volcanoes, in press.

Båth, M. (1960). Crustal structure of Iceland, *J. Geophys. Res.*, **65**, 1793-1807.

Båth, M. (1970). Introduktion till seismologin, Natur och kultur, Victor Pettersons Bokindustri AB.

Carswell, D. A. (1983). The volcanic rocks of the Sólheimajökull area, southern Iceland, *Jökull*, **33**, 61-71.

Cawer and Muller, 1994.Geology.

Chouet, B. (1996). Long-period volcano seismicity: its source and use in eruption forecasting, *Nature*, **380**, 309-316.

Dahm, T. and Brandsdóttir, B. (1997). Moment tensors of microearthquakes from the Eyjafjallajökull vocano in South Iceland, *Geophys. J. Int.*, **130**, 183-192.

Davies, J. L., Prescott, W. H., Svarc, J. L. and Wendt, K. J. (1989). Assessment of Global Positioning System measurements for studies of crustal deformation, *J. Geophys. Res.*, **94**, 13635-13650.

Decker, B. L. (1986). World Geodetic System 1984, Proceedings of the Fourth International Geodetic Symposium on Satellite Positioning, Austin, Texas, April

28-May 2, **vol.1**, 69-92.

Decker, R. W. P., Einarsson, P., and Mohr, P. A. (1971). Rifting in Iceland: New geodetic data, *Science*, **173**, 530-533.

DeMets, C., Gordon, R. G., Stein, S. and Argus, D. F. (1990). Current plate motions. *Geophys. J Int.*, **101**, 425-478.

Dixon, T. H. (1991). An introduction to the Global Positioning System ans some geological applications, *Reviews of Geophysics*, **29**, 249-276.

Einarsson, P., Björnsson, S., Foulger, G., Stéfansson, R. and Skaftadóttir, Þ. (1981). Seismicity pattern in the South Iceland Seismic Zone. In: D. Simpson and P. G. Richards (Editors) Earthquake Prediction – and International Review. Am. Geophys. Union, Maurice Erwing Ser., **4**: 141-151.

Einarsson, P and Eiriksson, J. (1982). Earthquake fractures in the districts Land Rangárvellir in the South Iceland Seismic Zone, *Jökull*, **32**, 113-120.

Einarsson, P. and Björnsson, S., (1987). Jarðskjálftamælingar á Raunvísindastofnun Háksólans, In: Þ. Sigfússon (ed.), Íhlutarins eðli: Festschrift for Þorbjörn Sigurgeirsson, Menningarsjóður, Reykjavík, 251-278.

Einarsson, P. (1989). Intraplate earthquakes in Iceland, Earthquakes at North Atlantic Passive Margins: Neotectonic and Postgalcial Rebound, Kluwer, Dordrecht, The Netherlands, pp329-344.

Einarsson, P. (1991). Earthquakes and present-day tectonism in Iceland, *Tectonophysics*, **189**, 261-279.

Einarsson, Þ. (1994). Geology of Iceland, Mál og menning.

Eysteinsson, H. and Hermance, J. F. (1985). Magnetotelluric measurements across the Eastern Volcanic Zone in South Iceland, *J. Geophys. Res.*, **90**, 10093-10103.

Flóvenz, o. G. (1980). Seismic structure of the Icelandic crust above layer three and the relation between body wave velocity and the alteration of the basaltic crust, *J. Geophys. Res.*, **47**, 211-220.

Flóvenz, O. G. and Gunnarsson, K. (1991). Seismic crustal structure in Iceland and surrounding area, *Tectonophys.*, **189**, 1-17.

Flóvenz, O. G. and Sæmundsson, K. (1993). Heat flow and geothermal processes

in Iceland, *Tectonophys.*, **225**, 123-138.

Foulger, G. R. (1988). Hengill triple junction, SW. Iceland: 1. Tectonic structure and spatial and temporal distribution of local earthquakes, *J. Geophys. Res.*, **93**, 13493-13506.

Foulger, G. R. (1988). Hengill triple junction, SW. Iceland: 2. Anomalous earthquake focal mechansims and implications for processes within the geothermal reservoir and at accretionary plate boundaries, *J. Geophys. Res.*, **93**, 13507-13523.

Foulger, G. R., Beutler, G., Bilham. R., Einarsson, P., Fankhauser, S., Gurtner, W., Hugentobler, U., Morgan, W. J., Rothacher, M., Thorbergsson, G. and Wild, U. (1993). The Iceland 1986 GPS geodetic survey; tectonic goals and data processing results, *Bull. Géodésique*, **67**, 148-172.

Furman, T., Frey, F. A and Meyer, P. S. (1992). Petrogenesis of Evolved Basalts and Rhyolites at Ásturhorn, Southern Iceland: the Role of Fractional Crystallisation, *J. Petrol.*, **33**, 1405-1445.

Furman, T. (1992). Evolution of Icelandic central volanoes: evidence from the Ásturhorn, Southern Iceland, *Bull. Volcanol.*, **55**, 45-62.

Gebrande, H., Miller, H. and Einarsson, P. (1980). Seismic structure of Iceland along the RRISP-profile 1, *J. Geophys.*, **47**, 239-249.

Grönvold, K., Larsen, G., Einarsson, P., Þórarinsson, S. and Sæmundsson, K. (1983). The Hekla eruption 1980-1981, *Bull. Volanol.*, **46**, 349-363.

Gudmundsson, O., Brandsdottír, B. and Sigvaldsson, G. E. (1994). The crustal magma chamber of the Katla volcano in south of Iceland revealed by 2d-seismic undershooting, *Geophys. J. Int.*, **119**, 277-296.

Gudmundsson, O. (1996).

Helgason, J., 1984. Frequent shifts of the volcanic zone in Iceland, *Geology*, **12**, 212-216.

Helgason, J., 1985. Shifts of the plate boundary in Iceland; some aspects of tertiary volcanism, *J.Geophys.Res.*, **90 No.B12**, 10084-10092.

Hill, R. I., 1991. Starting plumes and continental break-up. *Earth planetary Science Letters*, **104**, 398-416.

Hofmann-Wellenhof, B., Lichtenegger, H. and Collins, J., (1994). Global Positioning System, Theory and Practice, 3. ed. Springer-Verlag, Wien, 355 pp.

Johannesson, H. (1985). On the ages of two recent lava flows in Eyjafjöll and the late glacial terminal moraines in south Iceland, *Jökull*, **35**.

Jónsson, S., Einarsson, P., Sigmundsson, F., Pálsson, K. and Ólafsson, H. (1995). GPS Experiments in the Eastern Volcanic Zone, South Iceland, in 1994, The Science Institute of the University of Iceland, report **RH-11-95**, 54pp.

Jonsson, S. (1996). Crustal deformation across a divergent ðlate boundary, the Eastern Volcanic Rift Zone, South Iceland, 1967-1994, using GPS and EDM. Master thesis of the University of Iceland.

Jörgensen, K. A. (1980). The eruption of the Þórsmörk ignimbrite, south Iclenad: the structure of the magma chamber deduced from the eruption products, *Nordic Volcanological Institute Report (NVI)*, **RH-8103**.

Kjartansson, G. (1958). Endaslepp hraun undir Eyjafjöllum (Lava flows deprived of their distal ends in Eyjafjöll, South Iceland), *Natt. fræd.*, **28**, 127-140.

Klein, F. W. (1978). Hypocenter location program HYPOINVERSE, U.S.

Geological Survey Open file Rep., **78-694**, 113 pp.

Kristjansson, L., Johannesson, H., Eiriksson, J. and Gudmundsson, A. I. (1988). Brunhes-Matuyama paleomagnetism in three lava sections in Iceland, *Can, J. Earth Sci.*, **25**, 215-225.

Kurz, M. D., Meyer, P. S. and Sigurdsson, H. (1985). Helium isotope systematics within the neovolcanic zones of Iceland, *Earth and planetary Science Letters*, **74**, 291-305.

Langbein, J. O., Linker, M. F., McGarr, A. F. and Slater, l. E. (1987). Precision of two-colour geodimeter measurements: Results from 15 months of observations, *J. Geophys. Res.*, **92**, 11644-11656.

Loughlin, S. C. (1995). The evolution of the Eyjafjöll volcanic system, southern Iceland – PhD thesis, University of Durham.

MacDonald, R., McGarvie, D. W., Pinkerton, H., Smith, R. L. and Palacz, Z. A. (1990). Petrogenic evolution of the Torfajökull volcanic complex, Iceland i. Relationship between the magma types, *J. Petrol.*, **31**, 429-459.

Malone, S. D. (1983). Volcanic earthquakes; Example from Mt. St. Helens, In.

Kanamori H., Ital. Fisica, bologna, Italy, 436-455.

Massonet, D. and Feigl, K. L. (1998). Radar interferometry and its application to changes in the Earth's surface, *Review of Geophysics*, **vol.36**, **No.4**, 441-500.

Minatakami, T. (1984). Seismology of volacnoes in Japan, In: Civetta, L., Gasparini, P., Luongo, G. and Rapolla A. (eds.), *Physical Volcanology*, Dev. Solid Earth geophys., Elsevier, Amsterdam, **6**, 1-27.

McGarvie, D. W. (1984). Torfajökull: a volcano dominated by magma mixing, *Geology*, **12**, 685-688.

McTigue, D. F. (1987). Elastic stress and deformation near a finite spherical magma body: Resolution of the point source paradox, *J. Geophys. Res.*, **92**, 12931-12940.

Menke, W. (1988). (Scientist Spread Sheet, Version 3.4)

Menke, W. and Levin, V. (1994). Cold crust in a hot spot, *Geophys. Res. Lett.*, **21**, 1967-1970.

Menke, W., Levin, V. and Sethi, R. (1995). Seismic attenuation in the crust at the

mid-Atlantic plate boundary in southwest Iceland, *Geophys. J. Int.*, **122**, 175-182.

Menke, W. and Sparks, D. (1995). Crustal accretion model for Iceland predicts "cold"crust, *Geophys. Res. Lett.*, **22**, 1673-1676.

Menke, W., Brandsdóttir, B., Einarsson, P. and Bjarnason, Þ. (1996). Re-interpretation of the RRISP-77 Iceland shear wave profiles, *Geophys. J. Int.*, **126**, 166-172.

Meyer, P. S, Sigurdsson, H & Schiling, J. G. (1985). Petrological and geochemical variations along the Iceland's neovolcanic zones, *J. Geophs. Res.*, **90**, 10043-10072.

Mogi, K. (1958). Relations between the eruptions of various volcanoes and the deformation of the ground surfaces around them, *Bull. Earthquake Res.*, Inst., *Univ. Tokyo*, **36**, 99-134.

Okada, Y. (1985). Surface deformation due to shear and tensile faults in a half space, *Bull. Seism. Soc. Am.*, **75**, 1135-1154.

Óskarsson, N., Sigvaldsson, G. E. and Steinþórsson, S. (1982). A dynamic model of rift zone petrogenesis and the regional petrology of Iceland, *J. Petrol.*, **23**, 28-

74.

Pálmason, G. (1971). Crustal structure of Iceland from Explosion Seismology, Soc. Sci. Isl., Reykjavík, 187 pp.

Pollard, D. D., Delaney, P. T., Duffield, W. A., Endo, E. T. and Okamura, A. T. (1983). Surface deformation in volcanic rift zones, *Tectonophys.*, **94**, 541-584.

Richter, C. F. (1935). An instrumental earthquake magnitude scale, *Bull. Seism. Soc. Am.*, **25**, 1-32.

Rothacher, M. and Mervart, L. (1996). *BERNES GPS Software Version 4.0*, Astronomical Institute, University of Berne.

Rögnvaldsson, S. Þ., Árnadóttir, Þ., Águstsson, K., Skftadótti, Þ., Guðmundsson, G. B., Björnsson, G., Vogfjörð, K., Stéfansson, R., Böðvarsson, R., Slunga, R., Jakobsdóttir, S. S., Ragnarsson, S., Halldórsson, p., Þorkelsson, B. and Ásgerisdóttir, M. (1998). Skjálftahrina í Ölfusi í nóvember 1998, *Veðurstofa Íslands Greinargerð*, **VÍ-G98046-JA09**, Reykjavík.

Saastamoinen, J. (1972). Atmospheric correction for the troposphere and stratosphere in radio ranging of satellites in The use of artificial satellites for

geodesy, Geophysical monograph 15, Americal Geophysical Union, Washington, D. C., 64, 674.

Segall, and Davis (1997).

Sigmundsson, F., Einarsson, P., and Bilham, R. (1992). Magma chamber deflation recorded by the Global Positioning System: The Hekla 1991 eruption. *Geophys. Res. Lett.*, **19**, 1483-1486.

Sigmundsson, F., Einarsson, P., Bilhan, R., and Sturkell, E. (1992). South Iceland 1992 GPS-measurements: Summary and daily observation logs. Nordic Volcanological Institute, report **9201**, 19 pp.

Sigmundsson, F. (1994b). GPS monitoring of volcanic deformation in Iceland, *Cahiers du Centre Europeén de Géodynamiques et de Séismologie*, **5**,

Sigmundsson, F. (1994a). Crustal deformation at volcanoes, In: *Proceedings of the course The mitigation of volcanic hazards*, **EUR 16804**, 237-258.

Sigmundsson, F., Einarsson, P., Bilham, R. and Sturkell, E. (1995). Rift-transform kinematics in South Iceland: Deformation from Global Positioning System measurements, 1986 to 1992, *J.Geophys. Res.*, **100**, 6235-6248.

Sigmundsson, F., Einarsson, P., Rögnvaldsson, S. Þ., Foulger, G. R., Hodgkinson, K. M. and Þorbergsson, G. (1997). The 1994-1995 seismicity and deformation at the Hengill triple junction, Iceland: Triggering of earthquakes by minor magma injection in a zone of horizontal shear stress, *J. Geophys. Res.*, **vol.102**, No. **B7**, 15151-15161.

Sigmundsson, F., Vadon, H. and Massonet, D. (1997a). Readjustment of the Krafla spreading centre segment to crustal rifting measured by satellite radar interferometry, *Geophys. Res. Lett.*, **24**, 1843-1846.

Soosalu, H. and Einarsson, P. (1997). Seismicity aroung the Hekla and Torfajökull volcanoes, Iceland, during a volcanically quiet period, 1991-1995, *Bull. Volcanol.*, **59**, 36-48.

Stéfansson, R., Böðvarsson, R., Slunga, R., Einarsson, P., Jakobsdóttir, S., Bungum, H., Gregersen, S., Havskov, J., Hjelme, J. and Korhonen, H. (1993). Earthquake prediction research in the South Iceland Seismic Zone and the SIL project, *Bull.seism. Soc. Am.*, **83**, 696-716.

Sæmundsson, k. (1972). Geological notes on the Torfajökull area (in Icelandic9, *Natt. fræd.*, **42**, 81-99.

Sæmundsson, K. (1982). Calderas in the neovolcanic zones of Iceland (in Icelandic), In . Eldur er í norðri, Festschrift for Sigurður Þórarinsson, Sögufélag, Reykjavík, 221-239.

Sæmundsson, K., (1978). Fissure swarms and central volcanoes of the neovolcanic zones of Iceland, *Geol. J.*, Spec. Issue, **10**, 415-432.

Sæmundsson, K., (1979). Outline of the geology of Iceland, *Jokull*, **29**, 7-28.

Sæmundsson, K., (1986). Subaerial volcanism in the western Northern Atlantic, in Vogt, p. P., and Tucholke, B. E., eds., The Geology of North America, Volume M, Th Western North Atlantic Region: The Geological Society of America.

Sæmundsson, K. et al. Hengill

Þórarinsson, S and Sigvaldsson, G. E. (1972). The Hekla eruption of 1970, *Bull. Volcanol.*, **36**, 1-20.

Tryggvason, E. (1969). Earthquakes, jökulhlaups and subglacial eruptions, *Jökull*, **10**, 18-22.

Tryggvason, E. (1973). Surface deformation and crustal continental and oceanic rift zones, In: *Contintental and Oceanic Rifts* (edited by g. pálmason), AGU,

Washington, *Geodynamic Series*, **8**, 17-29.

Tryggvason, E. (1991). Magnitude deformation of active volcanoes in Iceland, *Cahiers du Centre Europeén de Géodynamique et de Séismologie*, **4**, 37-49.

Tryggvason, E. (1994). Program for the tilt measurements.

Tryggvason, E. (1994). Observed ground deformation at Hekla, Iceland prior to and during the eruptions of 1970, 1980-1981 and 1991, *J. Volcanol. Geotherm. Res.*, **61**, 281-291.

Vadon, H. and Sigmundsson, F. (1997). 1992-1995 Crustal deformation at Mid-Atlantic ridge, SW Iceland, mapped by radar interferometry, *Science*, **275**, 194-197.

Walker, G. P. L. (1963). The Breiðdalur central volcano eastern Iceland, *Quart. J. Geol. Soc. Lond.*, **119**, 29-63.

University of Lund
Department of Mineralogy and Petrology
Sölvegatan 13
S – 222 21 LUND
SWEDEN

Nordic Volcanological Institute 9901
University of Iceland
Grensásvegur 50
IS – 108 Reykjavík
ICELAND

1992-1998
Seismicity and Deformation at Mt. Eyjafjallajökull volcano

by

Malou Blomstrand Stinessen

A thesis
submitted to the Unversity of Lund
for
Master degree
February 1999

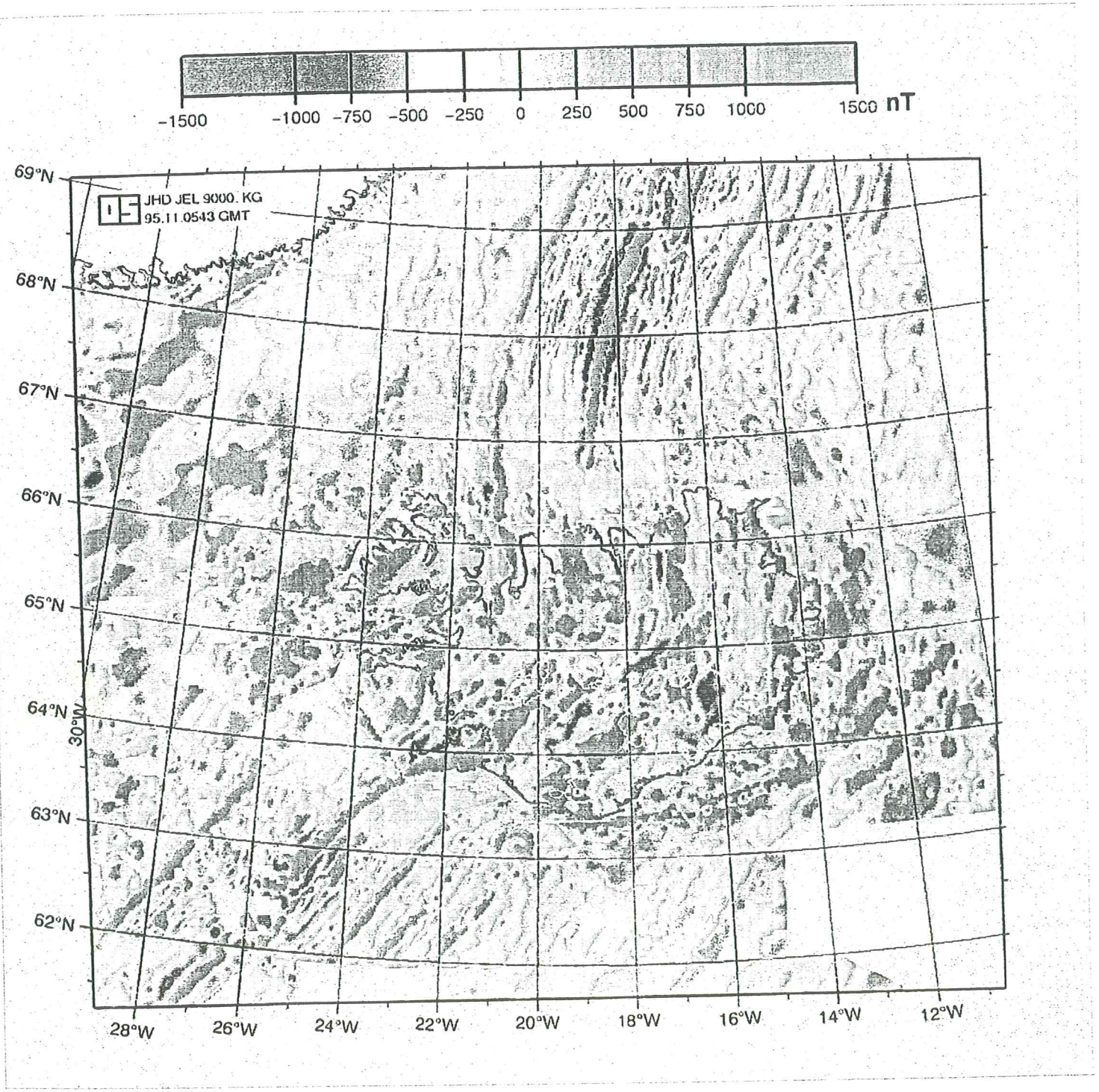
-1500
-1000
-750
-500
-250
0
250
500
750
1000
1500 nT
JHD JEL 9000. KG
95.11.0543 GMT
69°N
68°N
67°N
66°N
65°N
64°N
63°N
62°N
30°W
28°W
26°W
24°W
22°W
20°W
18°W
16°W
14°W
12°W

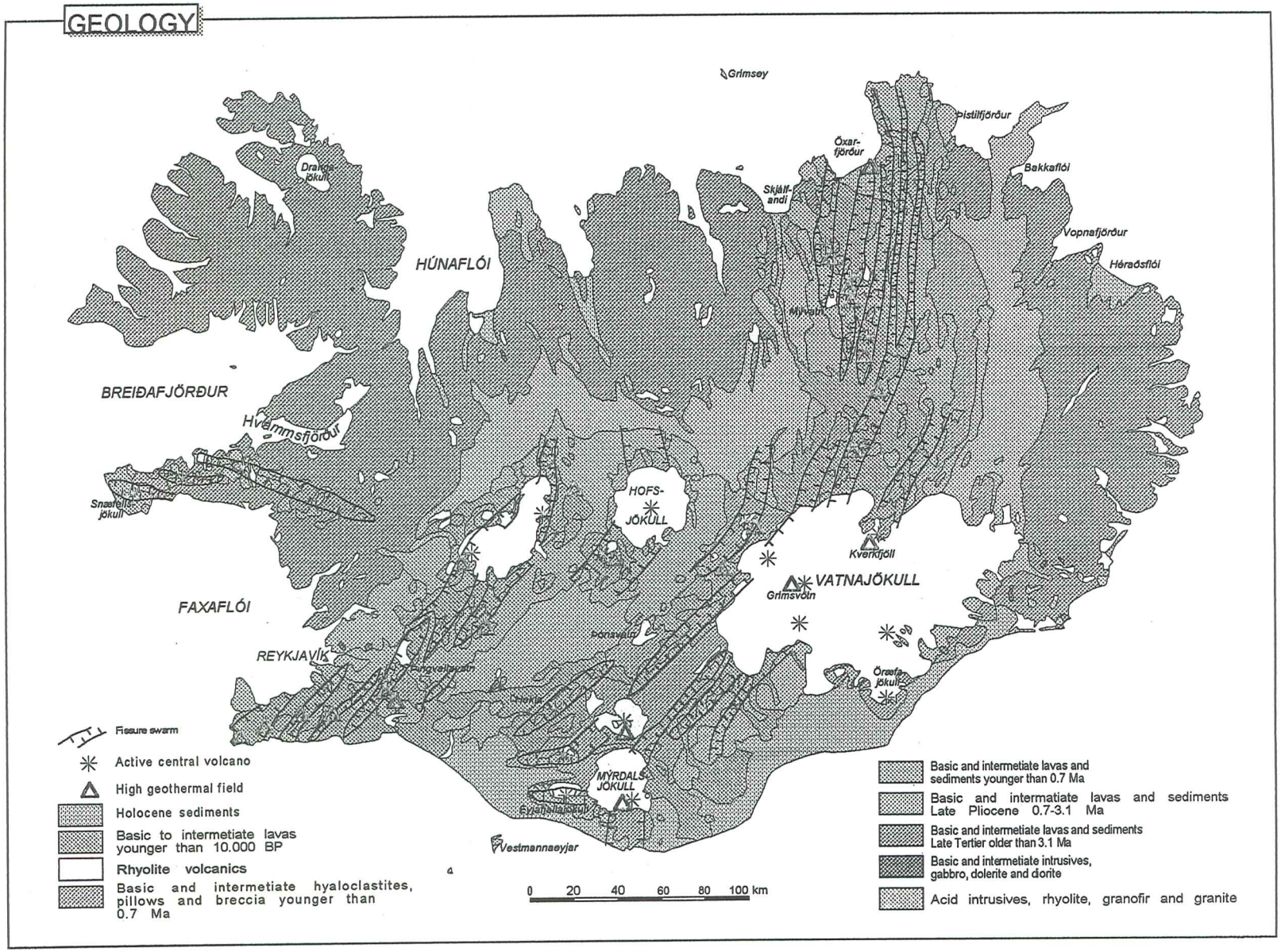
GEOLOGY
Grímsey
Þistilfjörður
Öxarfjörður
Bakkaflói
Skjálfandi
Vopnafjörður
Héraðsflói
HÚNAFLÓI
Mývatn
Drangajökull
BREIÐAFJÖRÐUR
Hvammsfjörður
Snæfellsjökull
HOFSJÖKULL
Kverkfjöll
VATNAJÖKULL
Grímsvötn
FAXAFLÓI
REYKJAVÍK
Þingvallavatn
Hekla
Öræfajökull
MÝRDALSJÖKULL
Eyjafjallajökull
Vestmannaeyjar
0 20 40 60 80 100 km
Fissure swarm
Active central volcano
High geothermal field
Holocene sediments
Basic to intermetiate lavas younger than 10.000 BP
Rhyolite volcanics
Basic and intermetiate hyaloclastites, pillows and breccia younger than 0.7 Ma
Basic and intermetiate lavas and sediments younger than 0.7 Ma
Basic and intermatiate lavas and sediments Late Pliocene 0.7-3.1 Ma
Basic and intermetiate lavas and sediments Late Tertier older than 3.1 Ma
Basic and intermetiate intrusives, gabbro, dolerite and diorite
Acid intrusives, rhyolite, granofir and granite

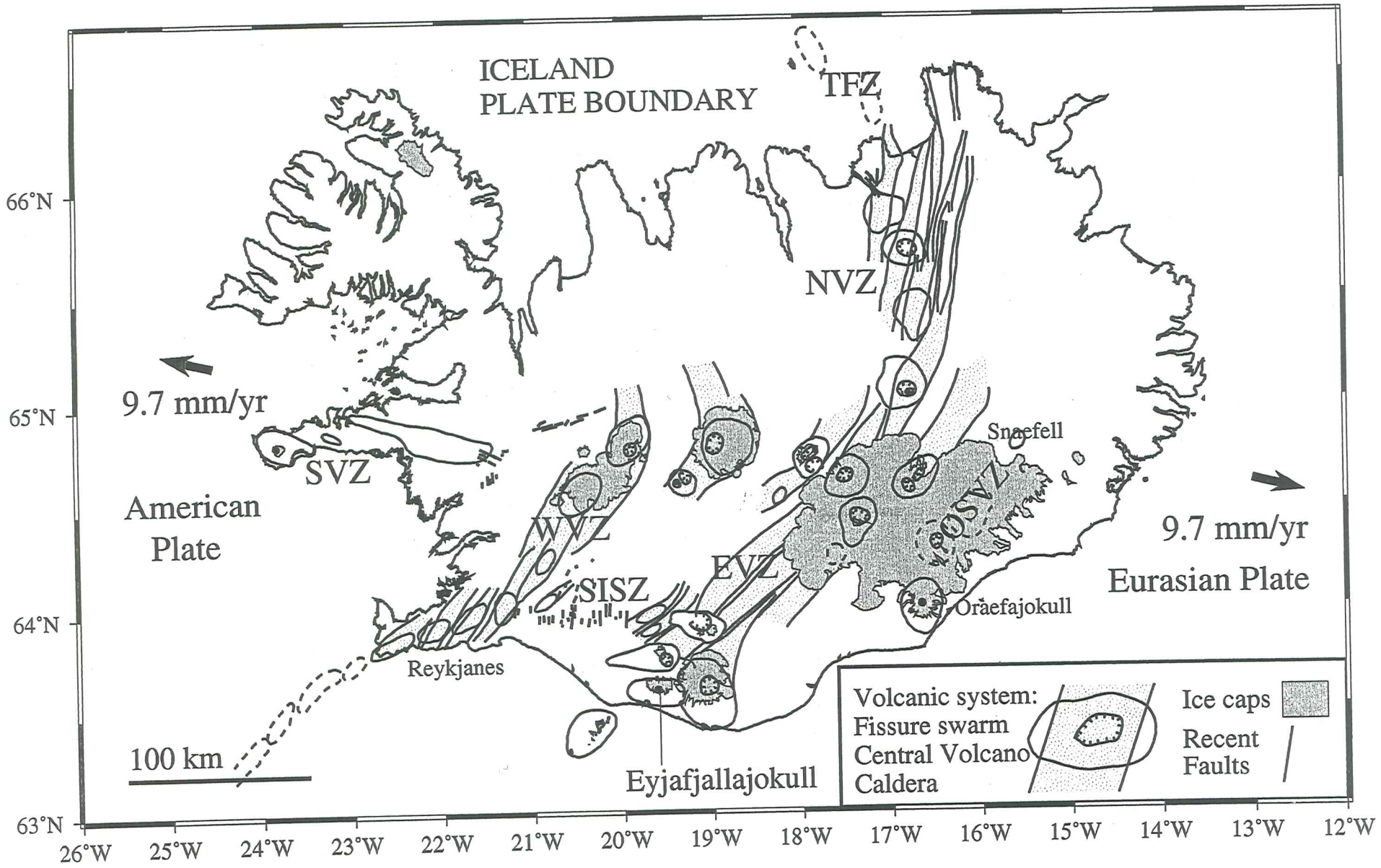
ICELAND
PLATE BOUNDARY
TFZ
NVZ
SVZ
WVZ
SISZ
EVZ
ÖSVZ
9.7 mm/yr
American
Plate
9.7 mm/yr
Eurasian Plate
Snaefell
Öraefajokull
Reykjanes
Eyjafjallajokull
100 km
Volcanic system:
Fissure swarm
Central Volcano
Caldera
Ice caps
Recent
Faults
66°N
65°N
64°N
63°N
26°W
25°W
24°W
23°W
22°W
21°W
20°W
19°W
18°W
17°W
16°W
15°W
14°W
13°W
12°W

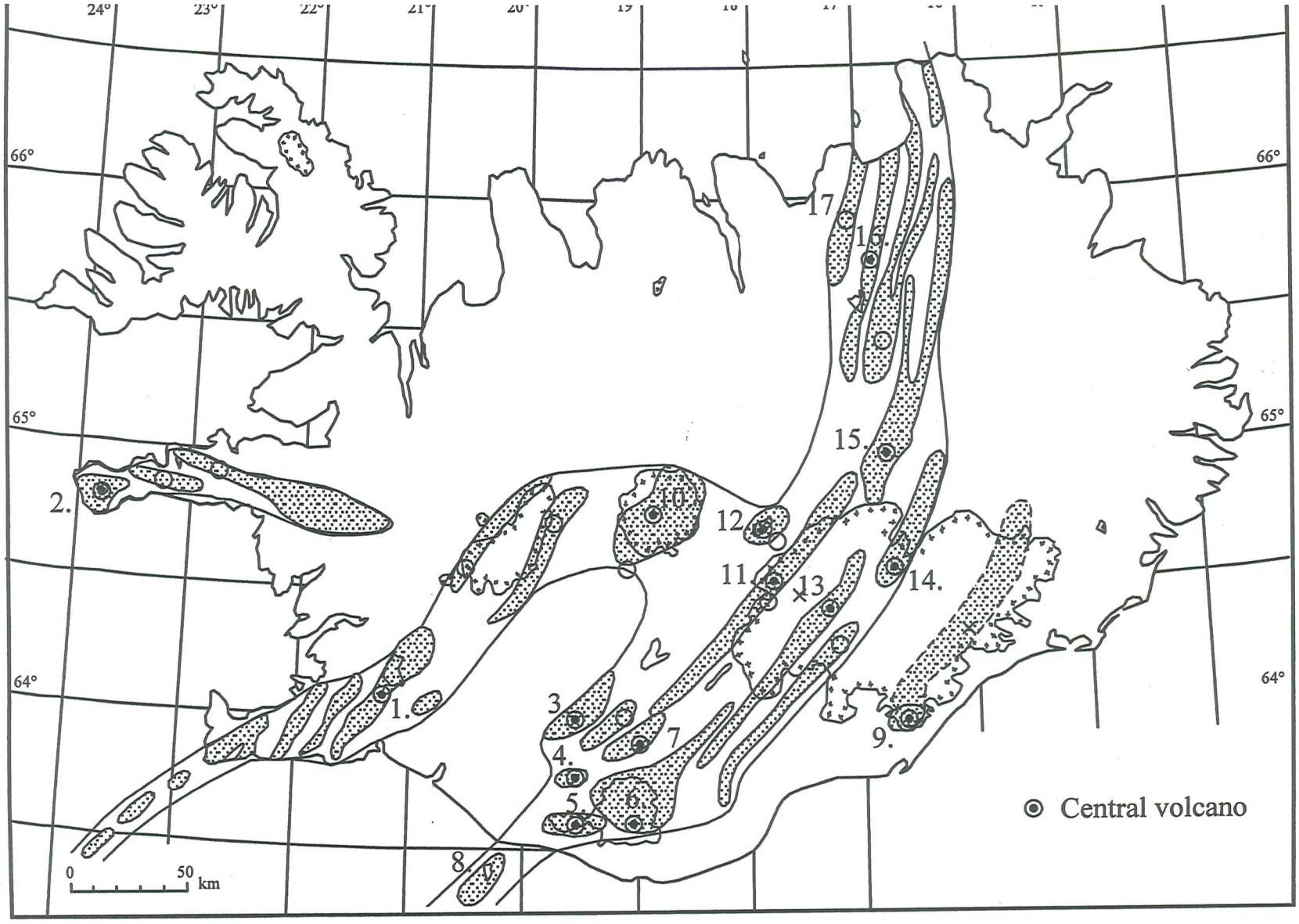

1. Hengill
2. Snæfellsjökull
3. Hekla
4. Tindfjallajökull
5. Eyjafjallajökull
6. Katla
7. Torfajökull
8. Vestmannaeyjar
9. Öræfajökull
10. Hofsjökull
11. Bárdabunga
12. Tungnafellsjökull
13. Grímsvötn
14. Kverkfjöll
15. Dyngjufjöll
16. Krafla
17. Theistareykir

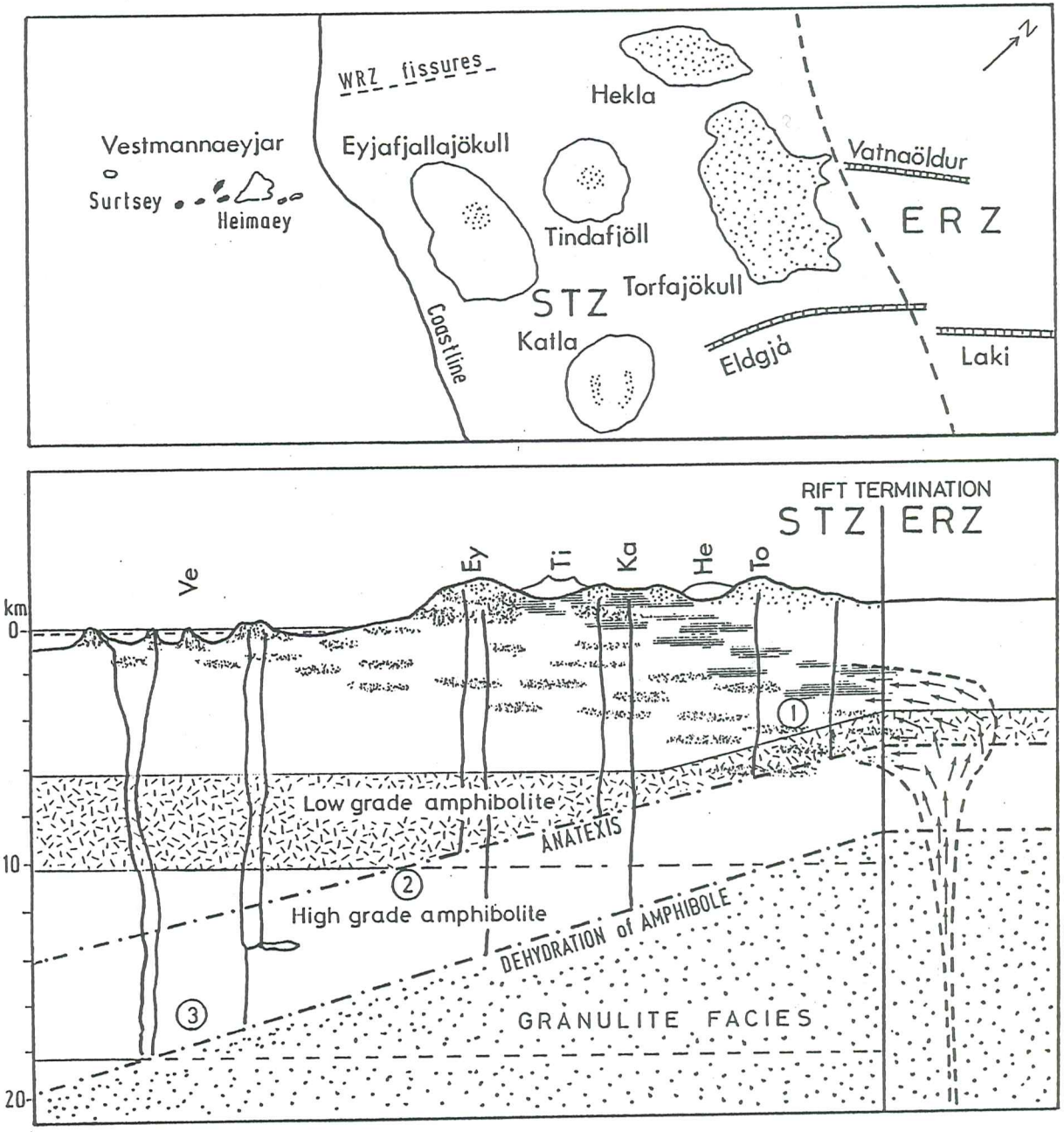
WRZ fissures
Hekla
Vestmannaeyjar
Surtsey
Heimaey
Eyjafjallajökull
Tindafjöll
Vatnaöldur
ERZ
STZ
Torfajökull
Coastline
Katla
Eldgjá
Laki
RIFT TERMINATION
STZ
ERZ
Ve
Ey
Ti
Ka
He
To
km
0
10
20
Low grade amphibolite
ANATEXIS
High grade amphibolite
DEHYDRATION of AMPHIBOLE
GRANULITE FACIES
1
2
3

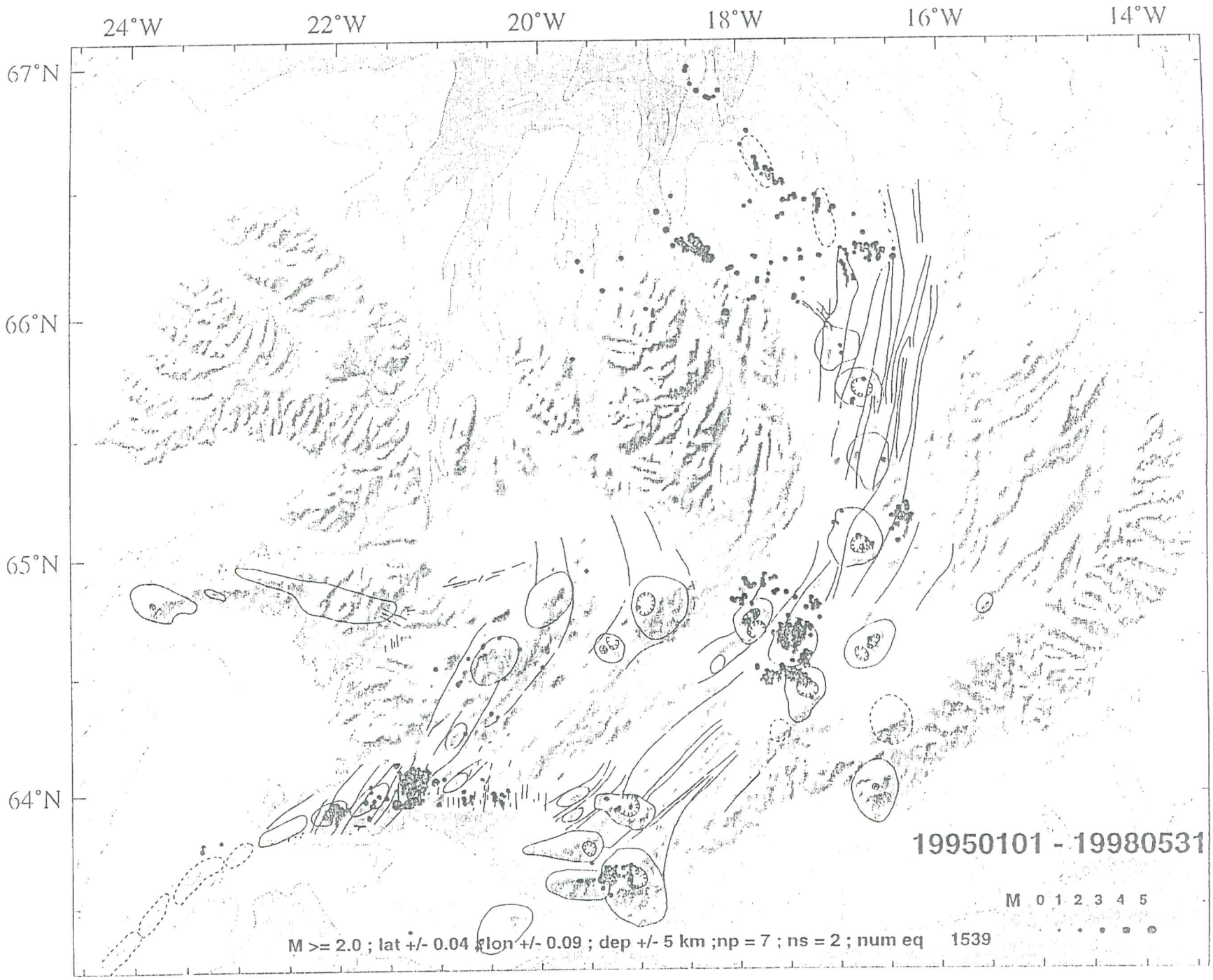
24°W
22°W
20°W
18°W
16°W
14°W
67°N
66°N
65°N
64°N
19950101 - 19980531
M 0 1 2 3 4 5
M >= 2.0 ; lat +/- 0.04 ;lon +/- 0.09 ; dep +/- 5 km ;np = 7 ; ns = 2 ; num eq 1539

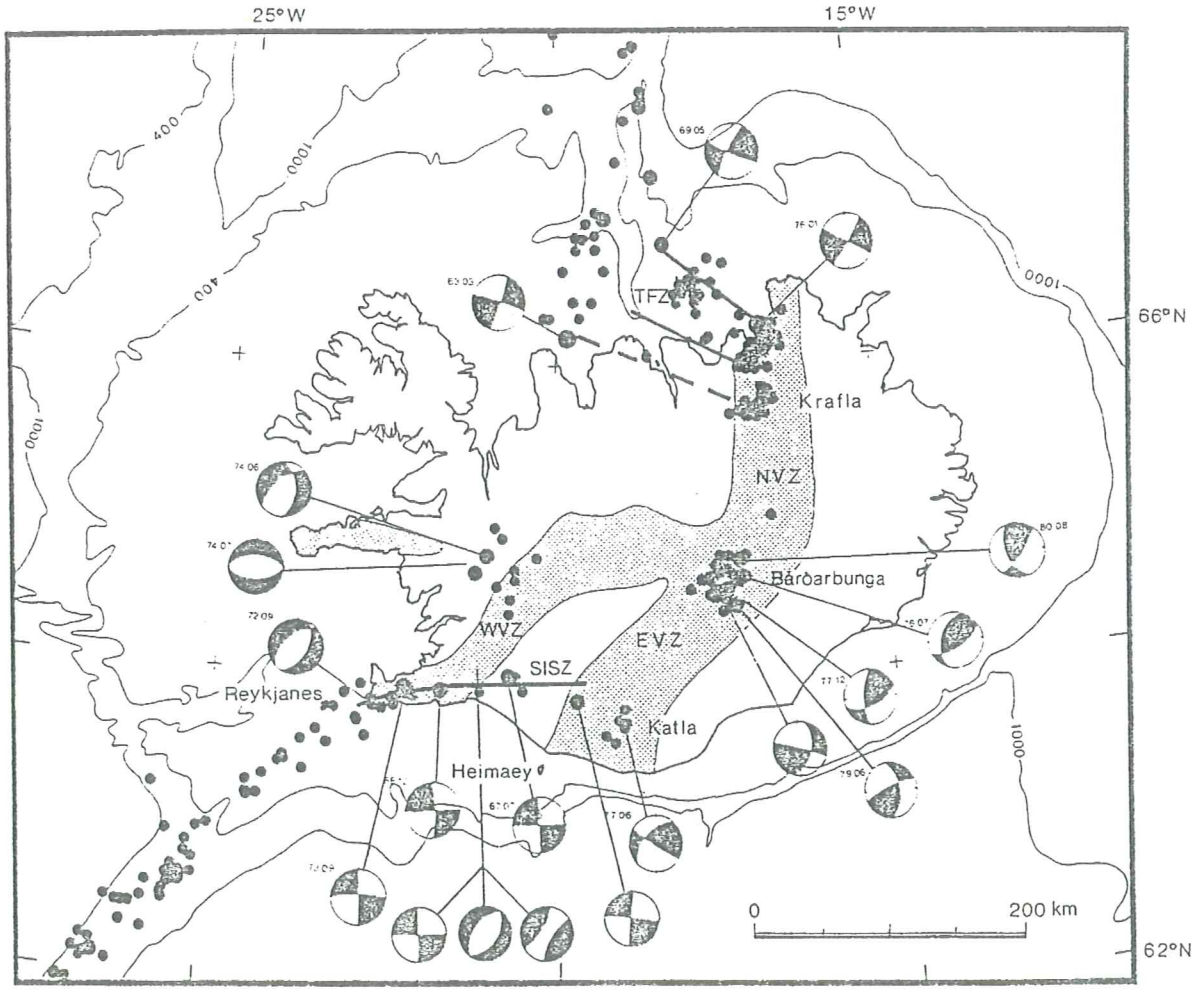
25°W
15°W
66°N
62°N
400
1000
TFZ
Krafla
NVZ
Bárðarbunga
WVZ
EVZ
SISZ
Reykjanes
Katla
Heimaey
0
200 km

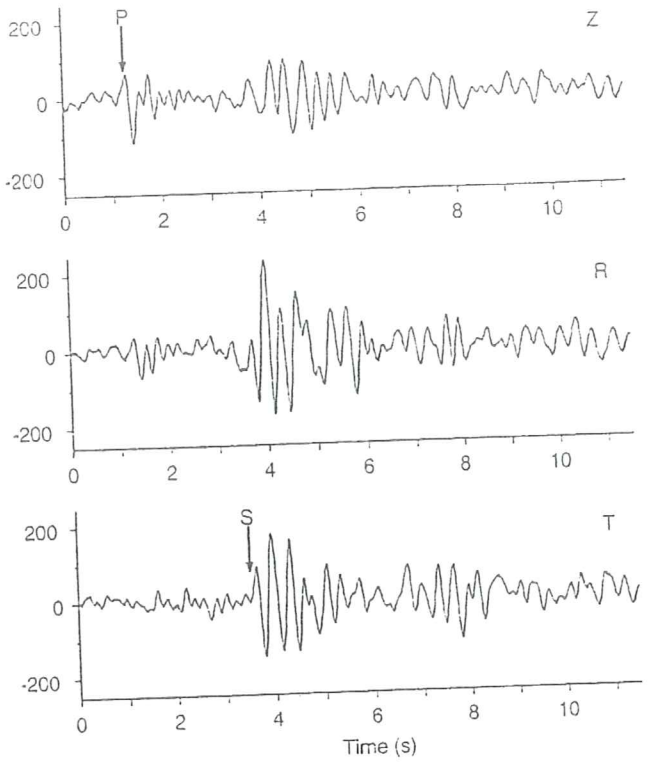
P
Z
200
0
-200
0
2
4
6
8
10
R
S
T
Time (s)

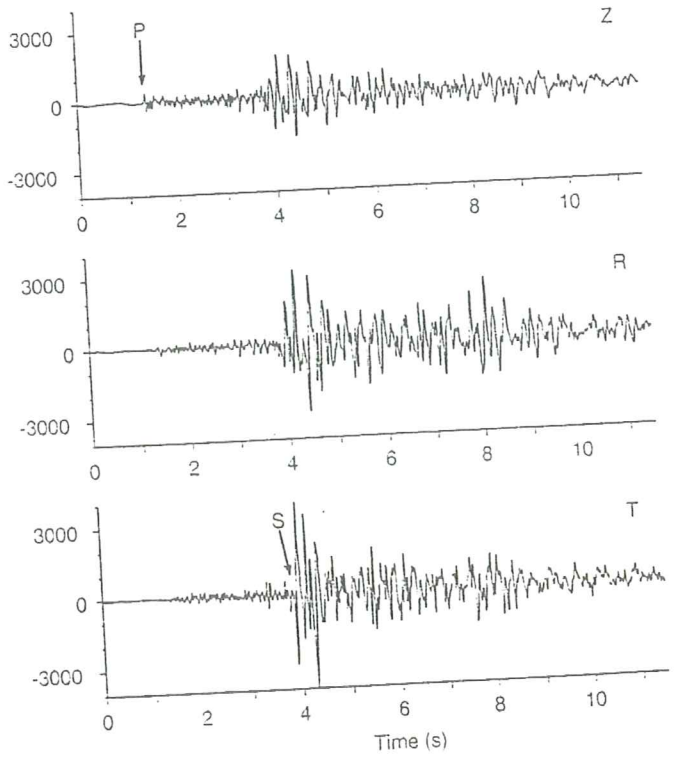
Z
P
3000
0
-3000
R
S
T
Time (s)

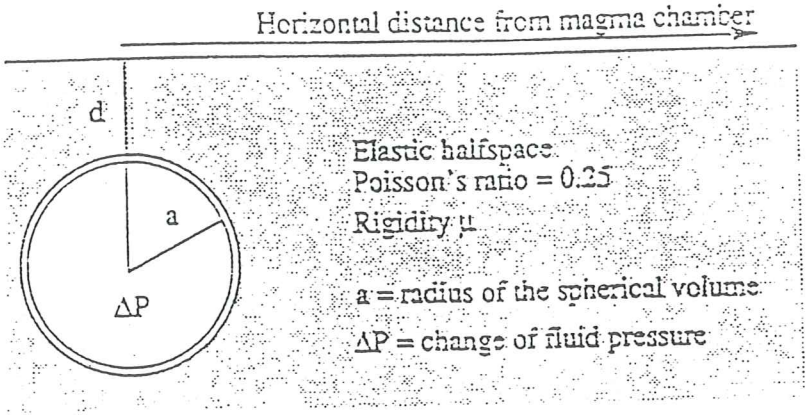
Horizontal distance from magma chamber
d
a
ΔP
Elastic halfspace
Poisson's ratio = 0.25
Rigidity μ
a = radius of the spherical volume
ΔP = change of fluid pressure

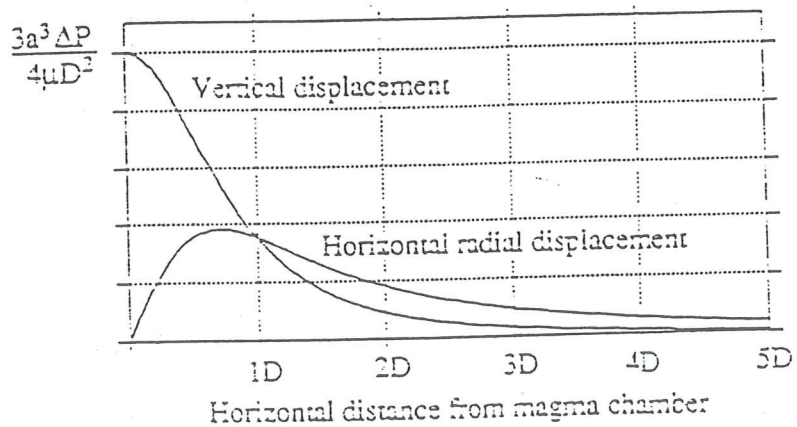
3a³ΔP / 4μD²
Vertical displacement
Horizontal radial displacement
1D
2D
3D
4D
5D
Horizontal distance from magma chamber

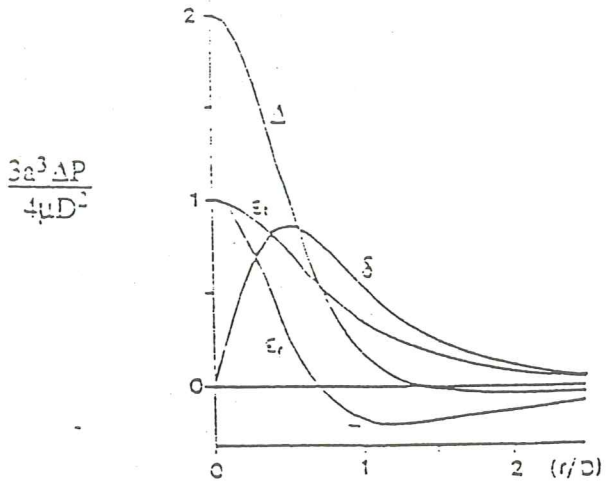
3a³ΔP / 4μD²
2
1
0
Δ
ξr
ξ
εr
0
1
2
(r/D)

(A)
VERTICAL DISPLACEMENT, $\frac{v\mu}{\Delta P d(1-\nu)}$
DISTANCE, x/d
z/d = 1.0
0.9
0.7
0.5
0.3
(B)
HORIZONTAL DISPLACEMENT, $\frac{u\mu}{\Delta P d(1-\nu)}$
DISTANCE, x/d
z/d = 1.0
0.9
0.7
0.5
0.3

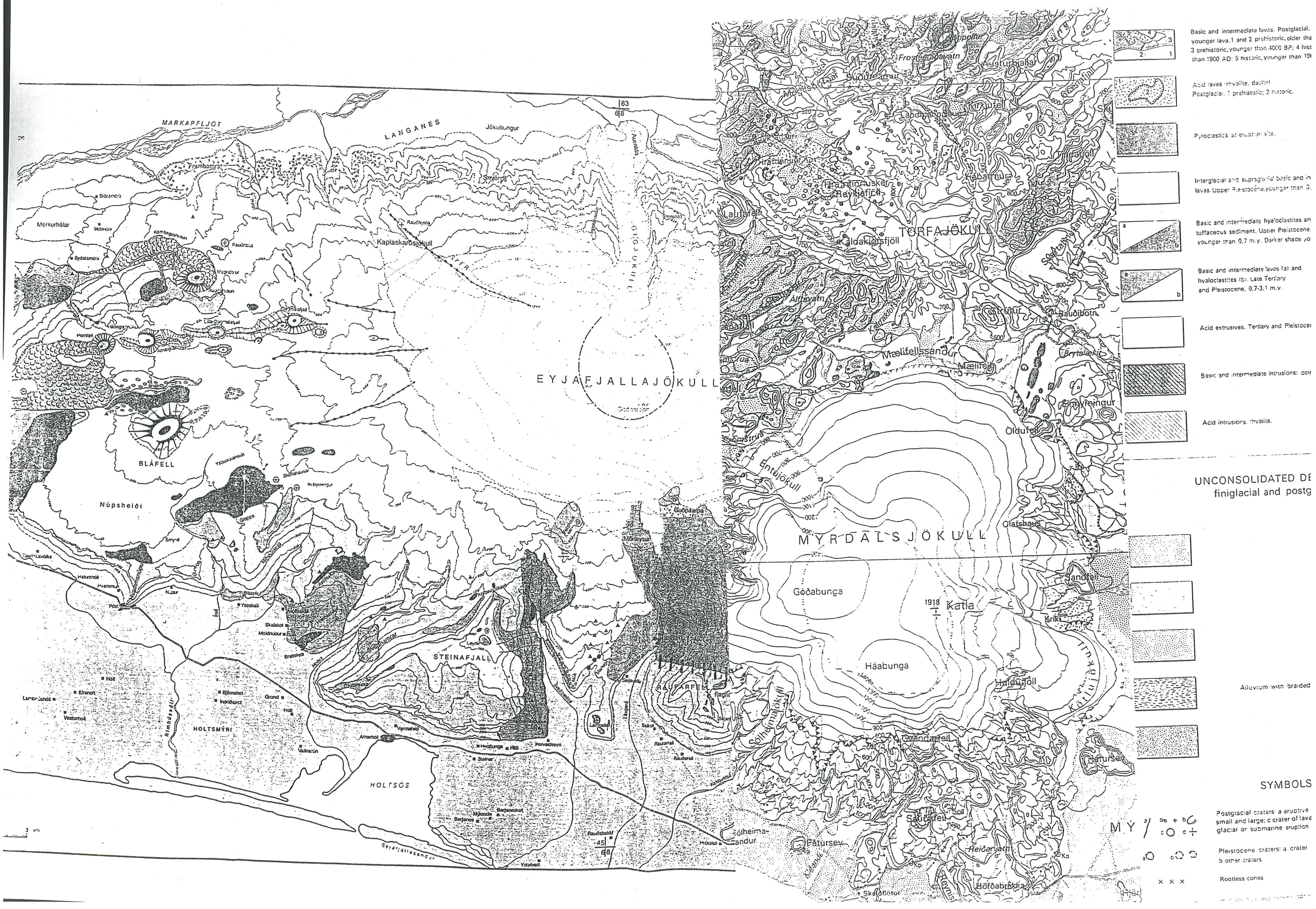

MARKARFLJÓT
LANGANES
Jökultungur
Stóramörk
Mörkurhólar
Syðstamörk
Kaplaskarðsjökull
EYJAFJALLAJÖKULL
BLÁFELL
Núpsheiði
STEINAFJALL
HOLTSMÝRI
HOLTSÓS
Eyjafjallasandur
Raufarfell
Sólheimasandur
Pétursey
Frostastaðavatn
Austurhallar
Kirkjufell
Hrafntinnusker
Reykjafjöll
Laufafell
TORFAJÖKULL
Álftavatn
Mælifellssandur
Mælifell
Rauðibotn
Brytalækir
Einhyrningur
Öldufell
Entujökull
MYRDALSJÖKULL
Goðabunga
1918 Katla
Háabunga
Sandfell
Sólheimajökull
Höfðabrekka
Heiðarvatn
Basic and intermediate lavas. Postglacial. younger lava.1 and 2 prehistoric, older than 3 prehistoric, younger than 4000 BP; 4 historic than 1900 AD; 5 historic, younger than 19
Acid lavas (rhyolite, dacite) Postglacial. 1 prehistoric; 2 historic.
Pyroclastics at eruption site.
Interglacial and supraglacial basic and in lavas. Upper Pleistocene, younger than 0.
Basic and intermediate hyaloclastites an tuffaceous sediment. Upper Pleistocene, younger than 0,7 m.y. Darker shade yo
Basic and intermediate lavas (a) and hyaloclastites (b). Late Tertiary and Pleistocene. 0.7-3.1 m.y.
Acid extrusives. Tertiary and Pleistocen
Basic and intermediate intrusions: dole
Acid intrusions: rhyolite.
UNCONSOLIDATED DE
finiglacial and postg
Alluvium with braided
SYMBOLS
Postglacial craters: a eruptive small and large; c crater of lava glacial or submarine eruption
Pleistocene craters: a crater b other craters
Rootless cones

Basic and intermediate lavas. Postglacial. Bars in younger lava. 1 and 2 prehistoric, older than 4000 BP 3 prehistoric, younger than 4000 BP; 4 historic, older than 1900 AD: 5 historic, younger than 1900 AD.

Acid lavas (rhyolite, dacite) Postglacial. 1 prehistoric; 2 historic.

Pyroclastics at eruption site.

Interglacial and supraglacial basic and intermediate lavas. Upper Pleistocene, younger than 0.7 m.y.

Basic and intermediate hyaloclastites and tuffaceous sediment. Upper Pleistocene, younger than 0.7 m.y. Darker shade younger (b)

Basic and intermediate lavas (a) and hyaloclastites (b). Late Tertiary and Pleistocene. 0.7-3.1 m.y.

Acid extrusives. Tertiary and Pleistocene.

Basic and intermediate intrusions: dolerite.

Acid intrusions, rhyolite.

UNCONSOLIDATED DEPOSITS
finiglacial and postglacial

Pumice

Till

Alluvium

Alluvium with braided river courses

Aeolian sand

SYMBOLS

Postglacial craters: a eruptive fissure. b crater, small and large; c crater of lava shield; d subglacial or submarine eruption site

Pleistocene craters: a crater of lava shield; b other craters

Rootless cones

MÆLIKVARÐI (SCALE 1:250000

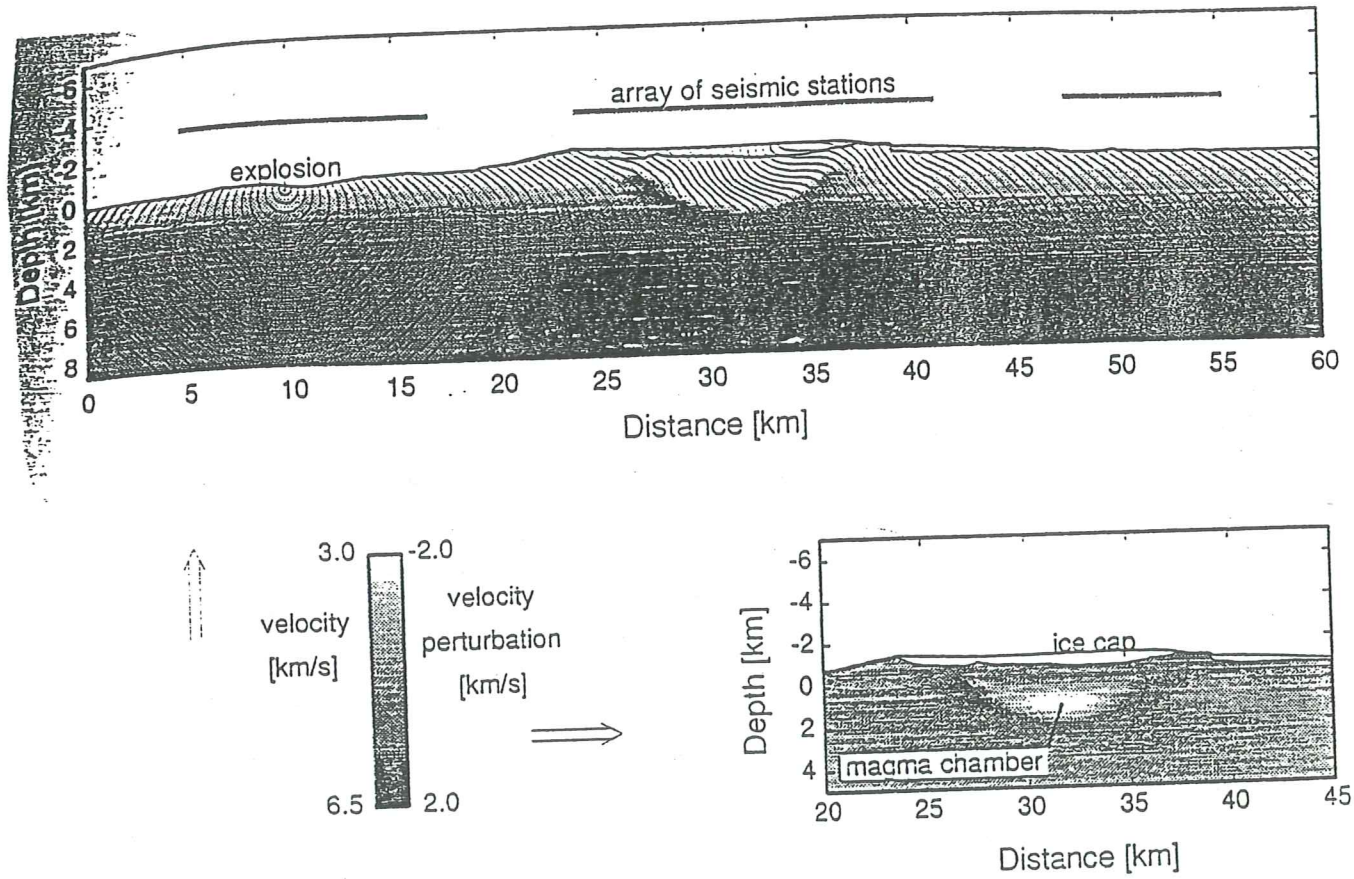
array of seismic stations
explosion
Depth [km]
-6
-4
-2
0
2
4
6
8
0
5
10
15
20
25
30
35
40
45
50
55
60
Distance [km]

3.0
-2.0
velocity
[km/s]
velocity
perturbation
[km/s]
6.5
2.0

Depth [km]
-6
-4
-2
0
2
4
ice cap
magma chamber
20
25
30
35
40
45
Distance [km]

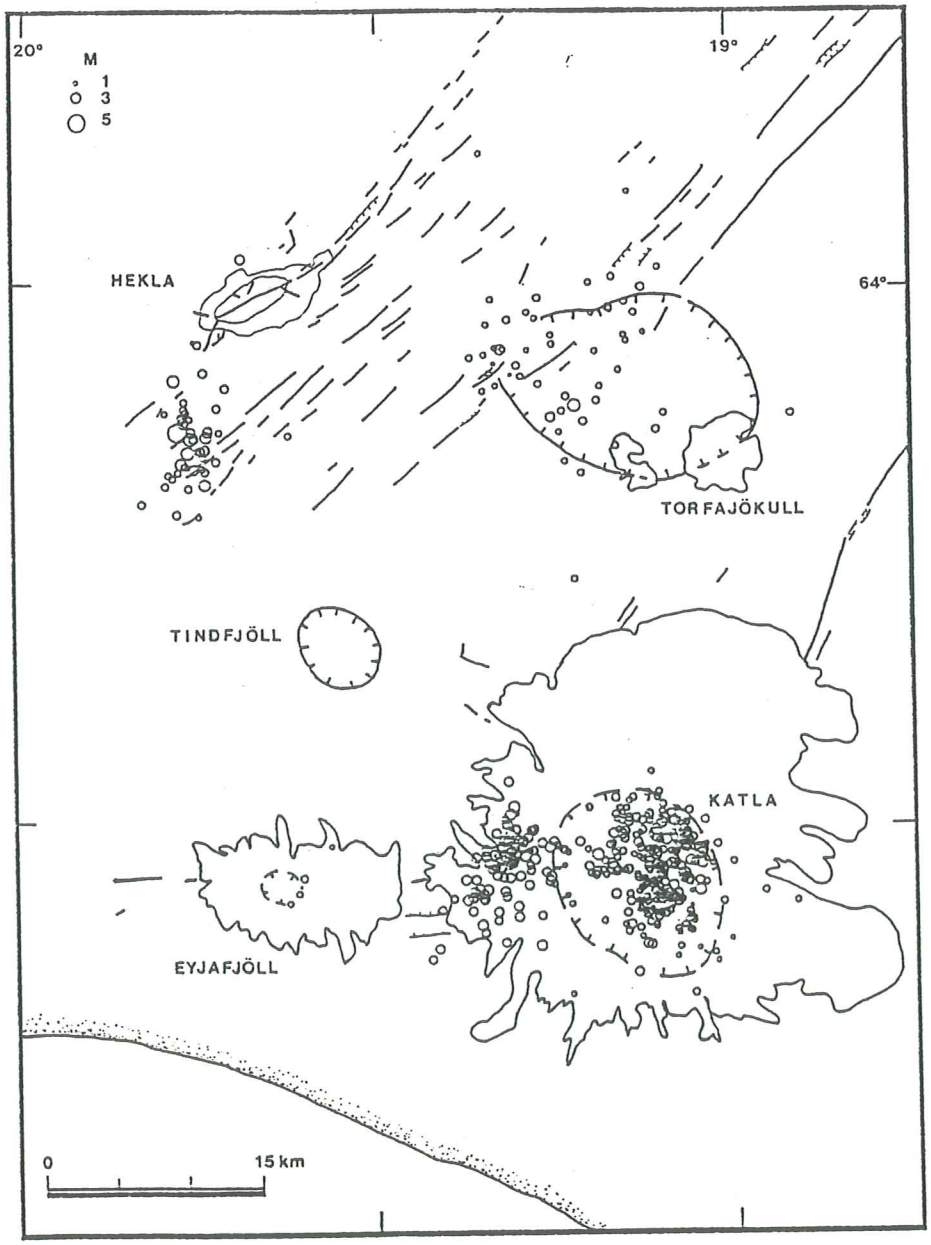
20°
19°
M
1
3
5
HEKLA
64°
TORFAJÖKULL
TINDFJÖLL
KATLA
EYJAFJÖLL
0
15 km

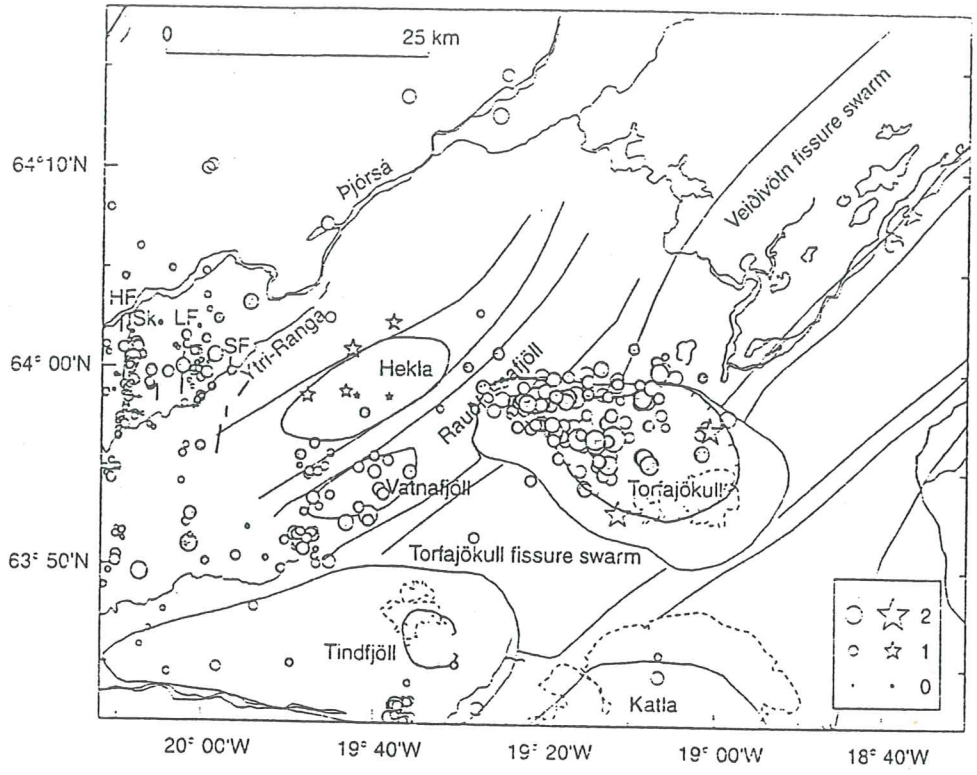
0
25 km
64°10'N
64° 00'N
63° 50'N
Þjórsá
Veiðivötn fissure swarm
HF
Sk.
LF
SF
Ytri-Rangá
Hekla
Rauðufjöll
Vatnafjöll
Torfajökull
Torfajökull fissure swarm
Tindfjöll
Katla
2
1
0
20° 00'W
19° 40'W
19° 20'W
19° 00'W
18° 40'W

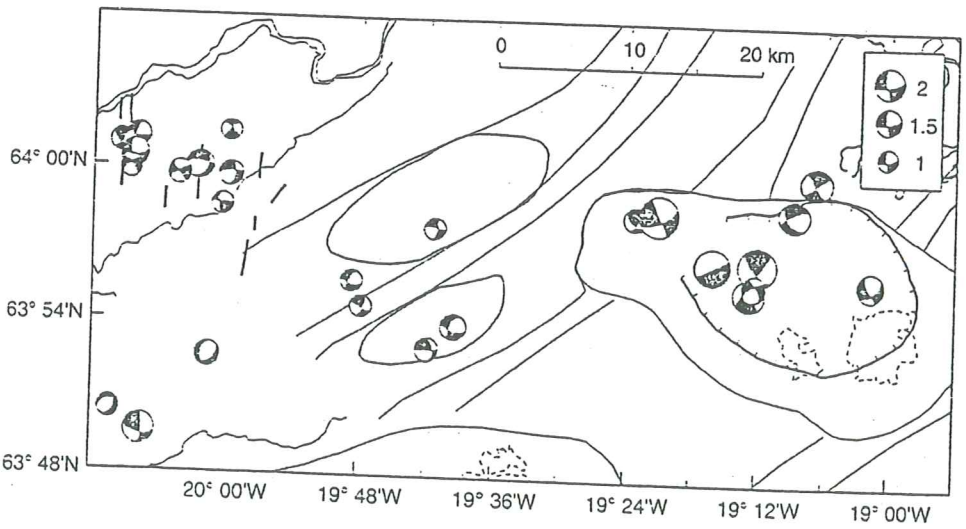
0
10
20 km
64° 00'N
63° 54'N
63° 48'N
2
1.5
1
20° 00'W
19° 48'W
19° 36'W
19° 24'W
19° 12'W
19° 00'W

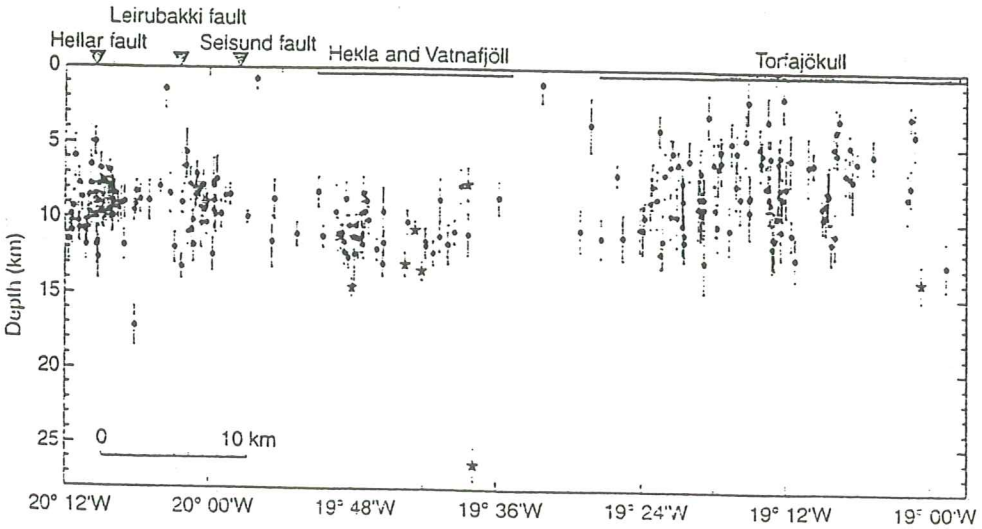
Leirubakki fault
Hellar fault
Selsund fault
Hekla and Vatnafjöll
Torfajökull
Depth (km)
0
5
10
15
20
25
0
10 km
20° 12'W
20° 00'W
19° 48'W
19° 36'W
19° 24'W
19° 12'W
19° 00'W

Seismic activity at Mt. Eyjafjallajökull 1991-1998

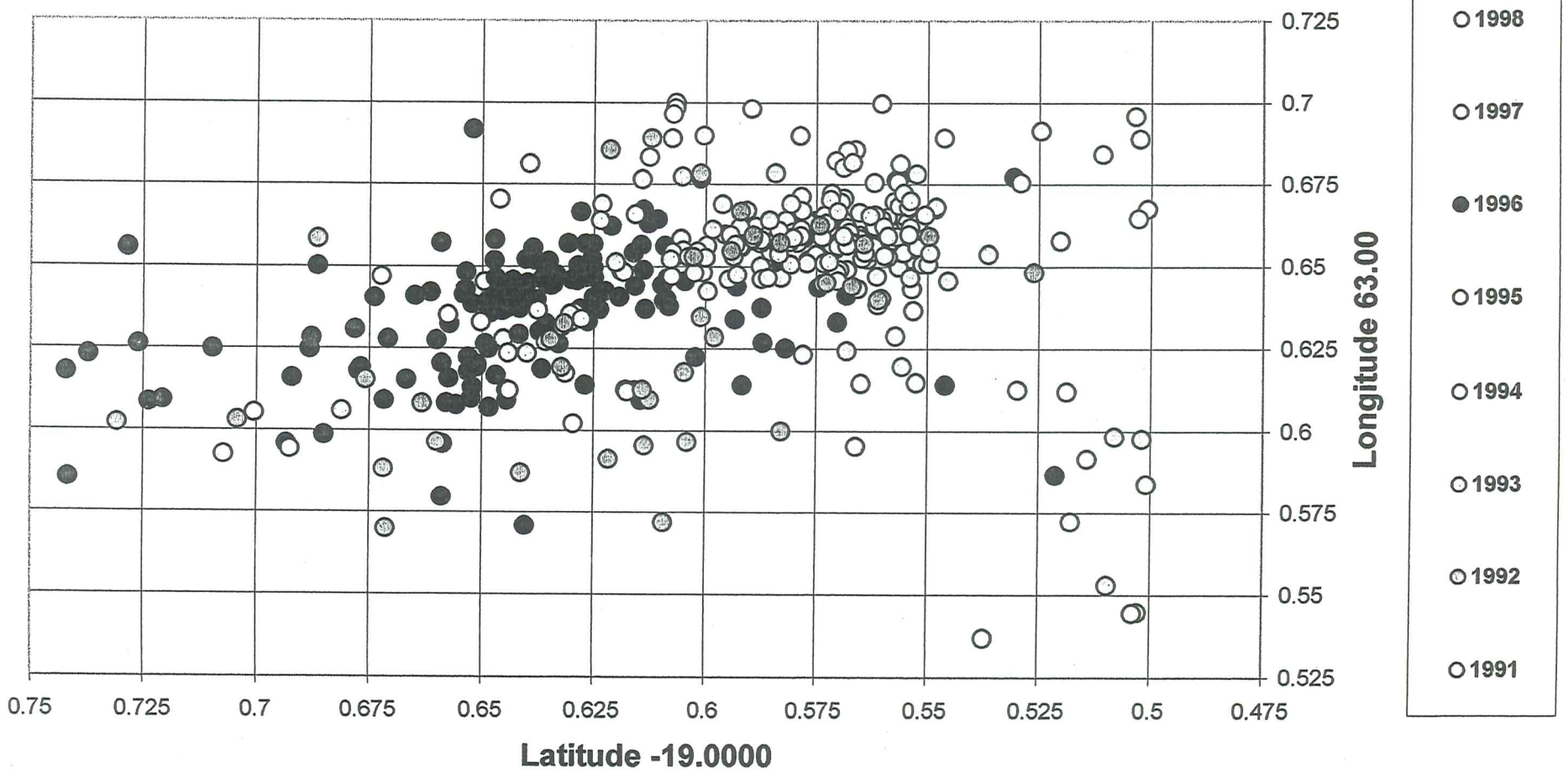

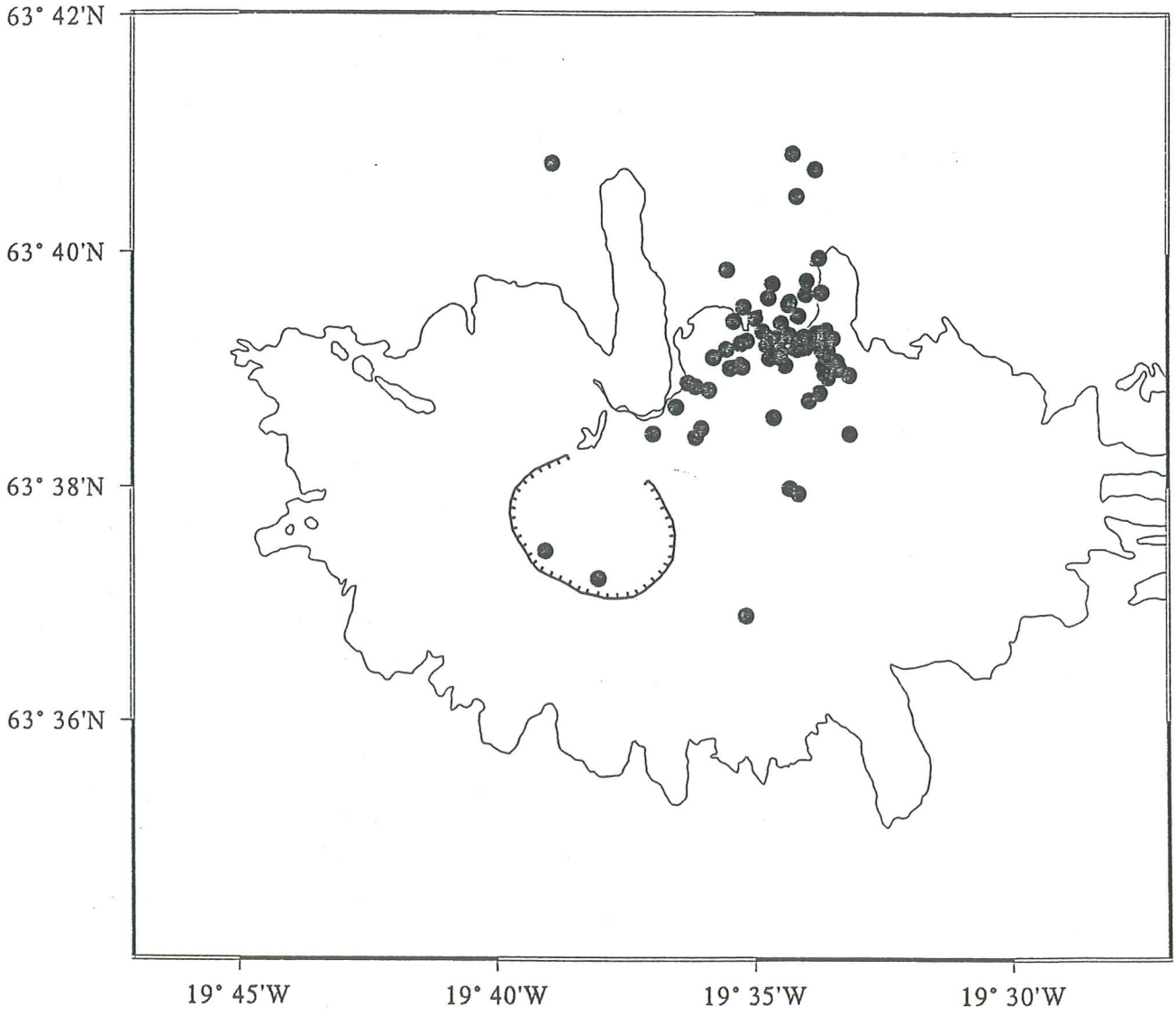
63° 42'N
63° 40'N
63° 38'N
63° 36'N
19° 45'W
19° 40'W
19° 35'W
19° 30'W

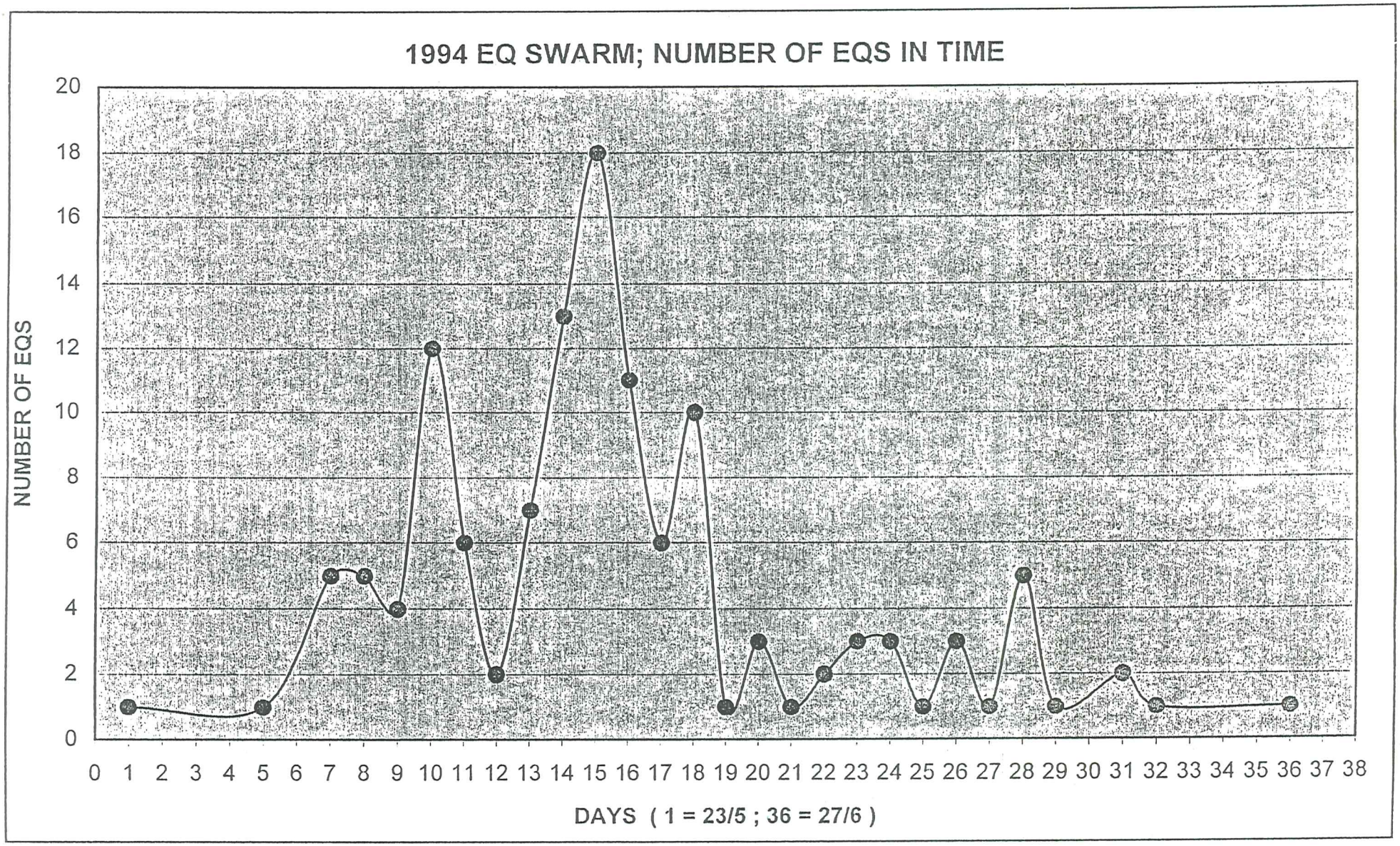
1994 EQ SWARM; NUMBER OF EQS IN TIME
NUMBER OF EQS
0
2
4
6
8
10
12
14
16
18
20
0 1 2 3 4 5 6 7 8 9 10 11 12 13 14 15 16 17 18 19 20 21 22 23 24 25 26 27 28 29 30 31 32 33 34 35 36 37 38
DAYS (1 = 23/5 ; 36 = 27/6)

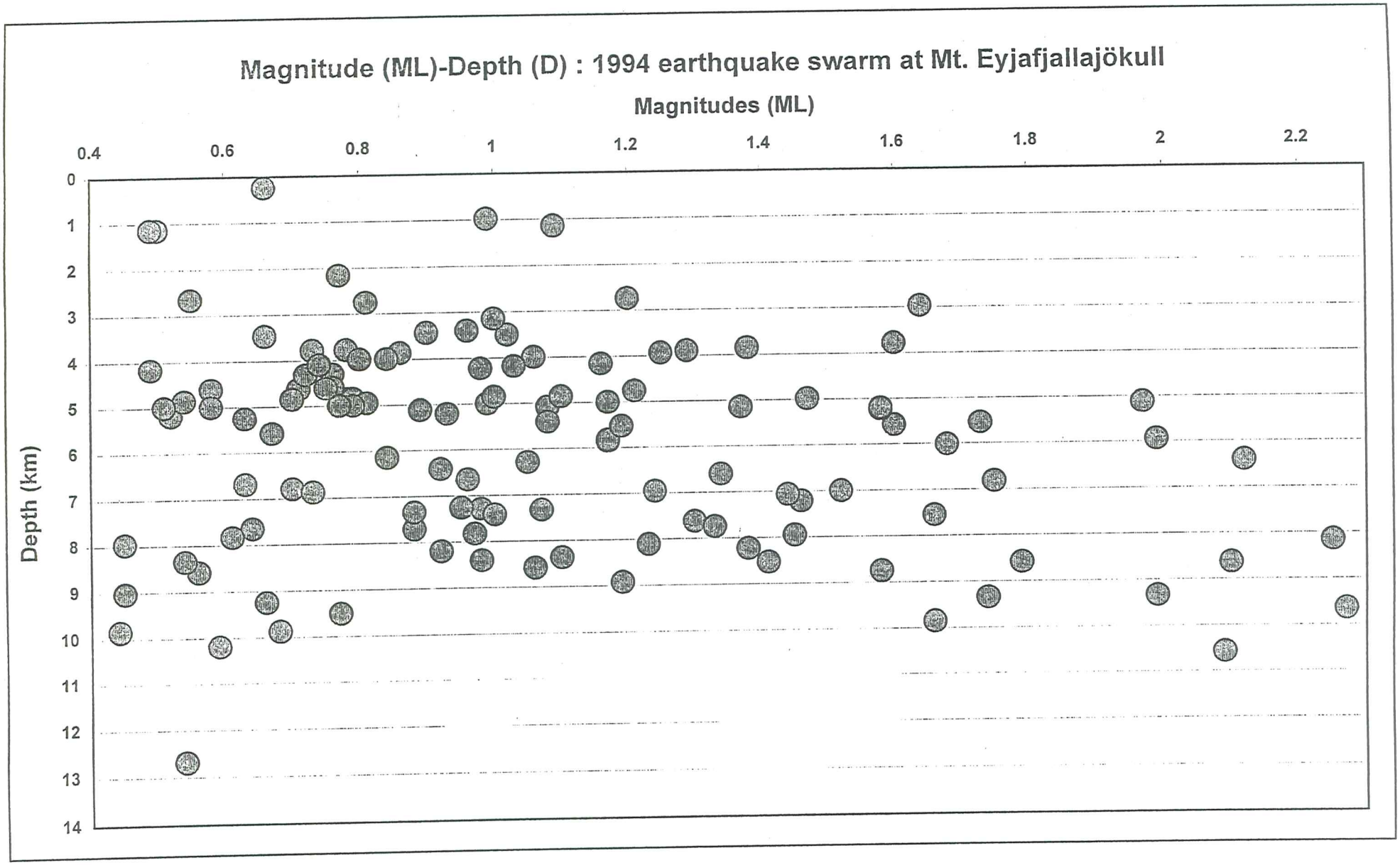
Magnitude (ML)-Depth (D) : 1994 earthquake swarm at Mt. Eyjafjallajökull
Magnitudes (ML)
0.4
0.6
0.8
1
1.2
1.4
1.6
1.8
2
2.2
Depth (km)
0
1
2
3
4
5
6
7
8
9
10
11
12
13
14

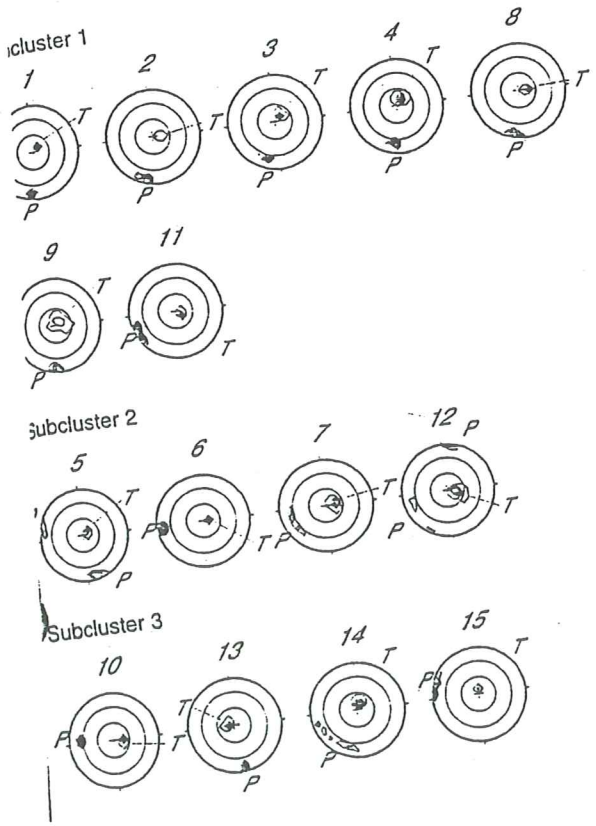
ıcluster 1
1
2
3
4
8
9
11
Subcluster 2
5
6
7
12
Subcluster 3
10
13
14
15
T
P

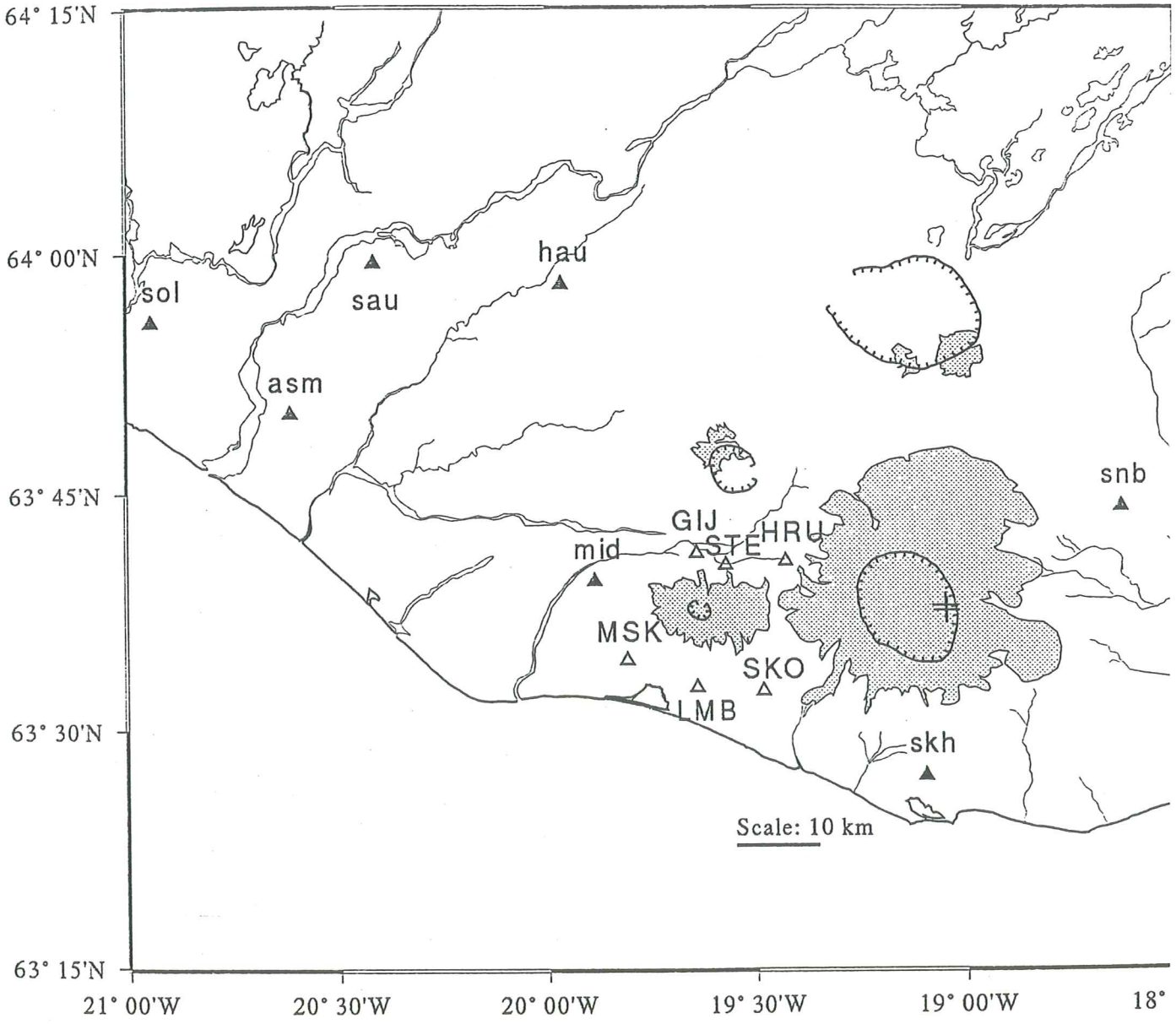
64° 15'N
64° 00'N
63° 45'N
63° 30'N
63° 15'N
21° 00'W
20° 30'W
20° 00'W
19° 30'W
19° 00'W
18°
sol
sau
hau
asm
snb
GIJ
STE
HRU
mid
MSK
SKO
LMB
skh
Scale: 10 km

Seismometers		Latitude	Longitude	Latitude	Longitude
		(63 00.00)	(1X 00.00)	-63.0000	(-19.0000)
SIL (South Iceland Lowland)					
asm	Ásmúli	63 50.038	20 24.893	63.8340	20.4149
hau	Haukardálur	63 58.131	19 57.915	63.9689	19.9653
mid	Mið	63 39.5	19 53.144	63.6583	19.8857
sau	Sau	63 59.408	20 24.936	63.9901	20.4156
skh	Skammadalsheiði	63 27.21	19 05.67	63.4535	19.0945
snb	Snæbýli	63 44.17	18 37.83	63.7362	18.4063
sol	Sólheiði	63 55.758	20 56.649	63.9293	20.9442
Portable seismometers					
GIJ	Gigjökull	63 41.25	19 38.49	63.6875	19.6415
HRU	Hrúna	63 40.75	19 25.5	63.6792	19.4250
LMB	Lambafell	63 32.78	19 38.49	63.5463	19.6415
MSK	Miðskáli	63 34.51	19 48.57	63.5752	19.8095
SKO	Skógaheiði	63 32.55	19 28.82	63.5425	19.4803
STE	Steinsholt	63 40.5	19 34.21	63.6750	19.5702

Station	distance (km)	azimuth	angle	no.of rec.
asm	53.7-56.0	290-294	48-73	49
hau	38.2-41.3	330-335	48-76	57
mid	13.6-17.5	265-279	53-85	52
sau	54.3-54.7	311-312	53-54	2
skh	30.2-33.3	128-134	45-77	48
snb	45.7-49.6	76-79	44-73	49
sol	73	294	54	1
GIJ	4.5-7.3	313-346	69-138	34
HRU	7.3-9.9	60-70	93-112	11
LMB	10.6-14.2	188-202	62-107	45
MSK	12.1-15.6	231-239	62-87	44
SKO	11.9-13.5	153-164	62-105	42
STE	2.3-4.1	0-359	123-159	21

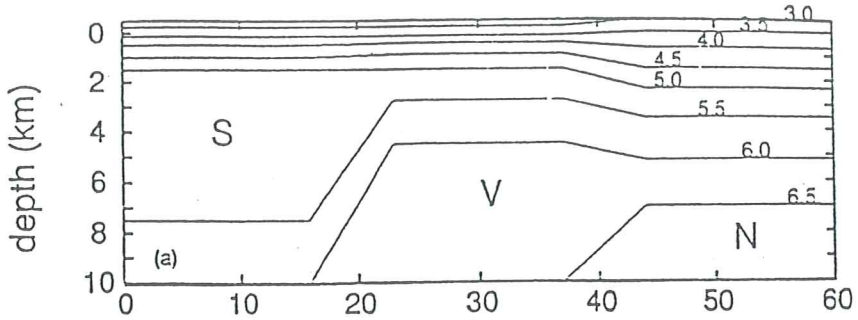
depth (km)
0
2
4
6
8
10
0
10
20
30
40
50
60
3.0
3.5
4.0
4.5
5.0
5.5
6.0
6.5
S
V
N
(a)

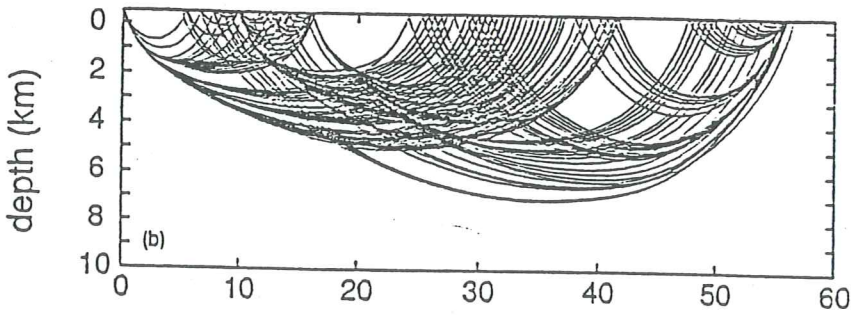
depth (km)
0
2
4
6
8
10
0
10
20
30
40
50
60
(b)

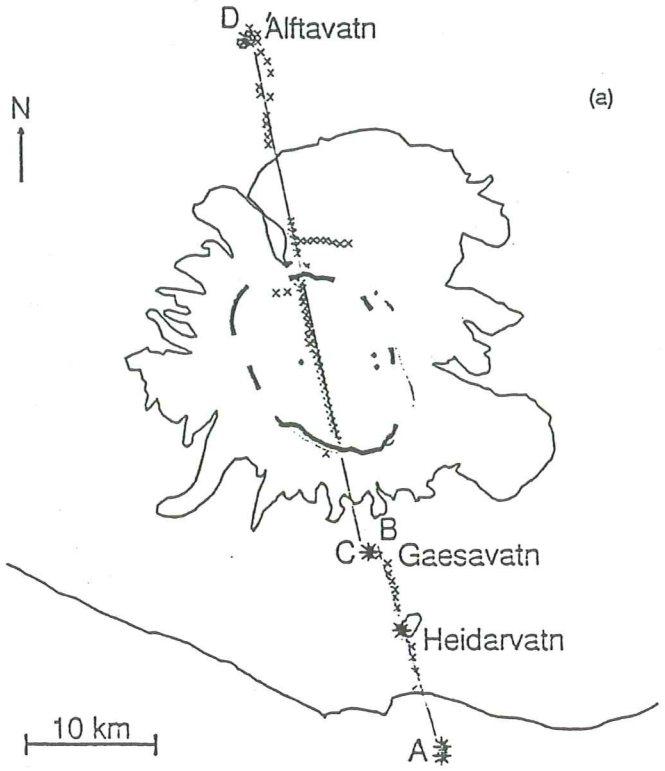
D
Álftavatn
(a)
N
B
C
Gaesavatn
Heidarvatn
10 km
A

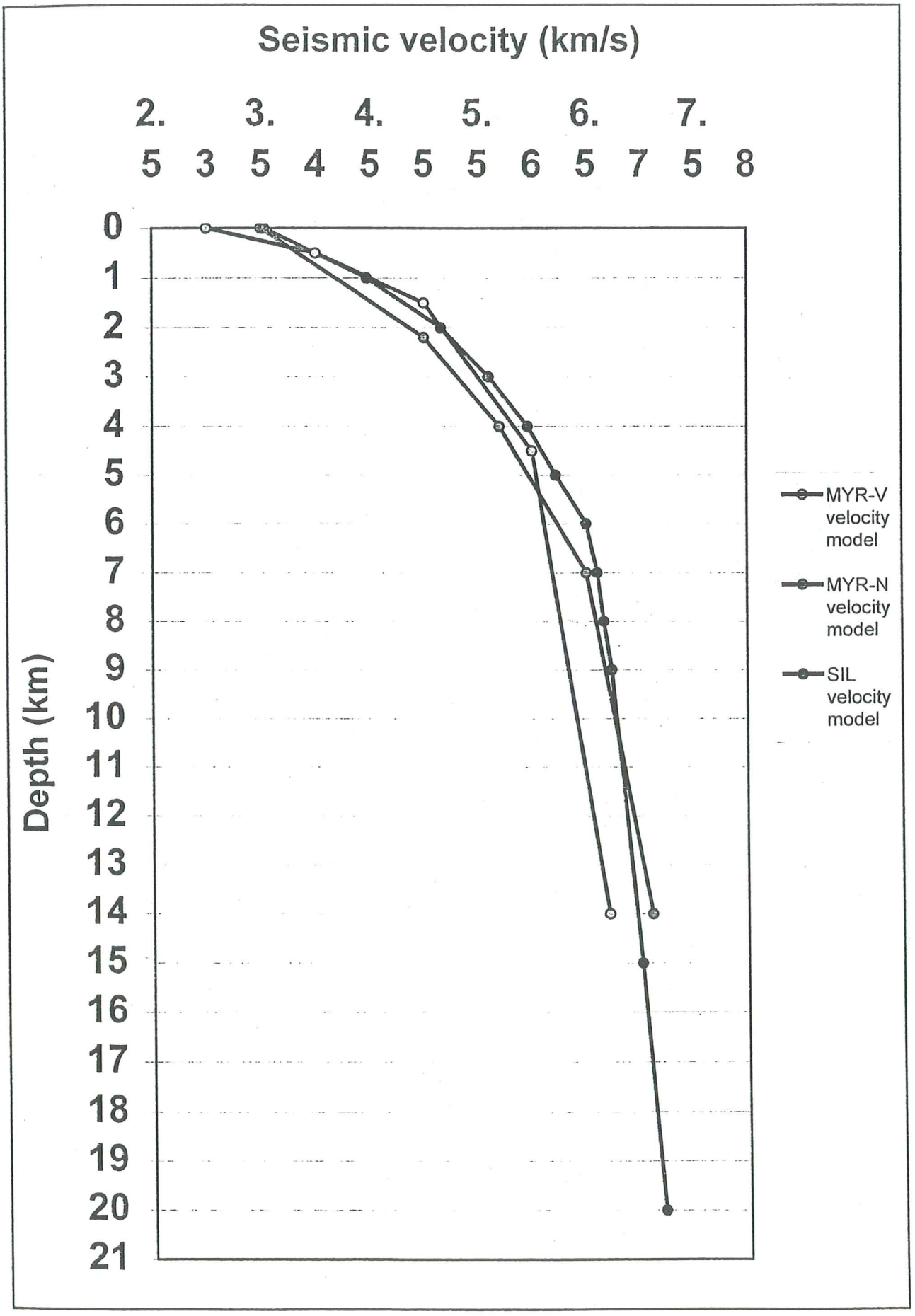
Seismic velocity (km/s)
2.5
3.5
4.5
5.5
6.5
7.5
8
0
1
2
3
4
5
6
7
8
9
10
11
12
13
14
15
16
17
18
19
20
21
Depth (km)
MYR-V velocity model
MYR-N velocity model
SIL velocity model

Crustal velocity models

SIL	SIL	MYR-N	MYR-N	MYR-V	MYR-V
D (km)	*v* (km/s)	D (km/s)	*v* (km/s)	D (km/s)	*v* (km/s)
0	3.53	0	3.5	0	3
1	4.47	2.2	5	0.5	4
2	5.16	4	5.7	1.5	5
3	5.6	7	6.5	4.5	6
4	5.96	14	7.1	14	6.7
5	6.22				
6	6.5				
7	6.6				
8	6.66				
9	6.73				
15	7				

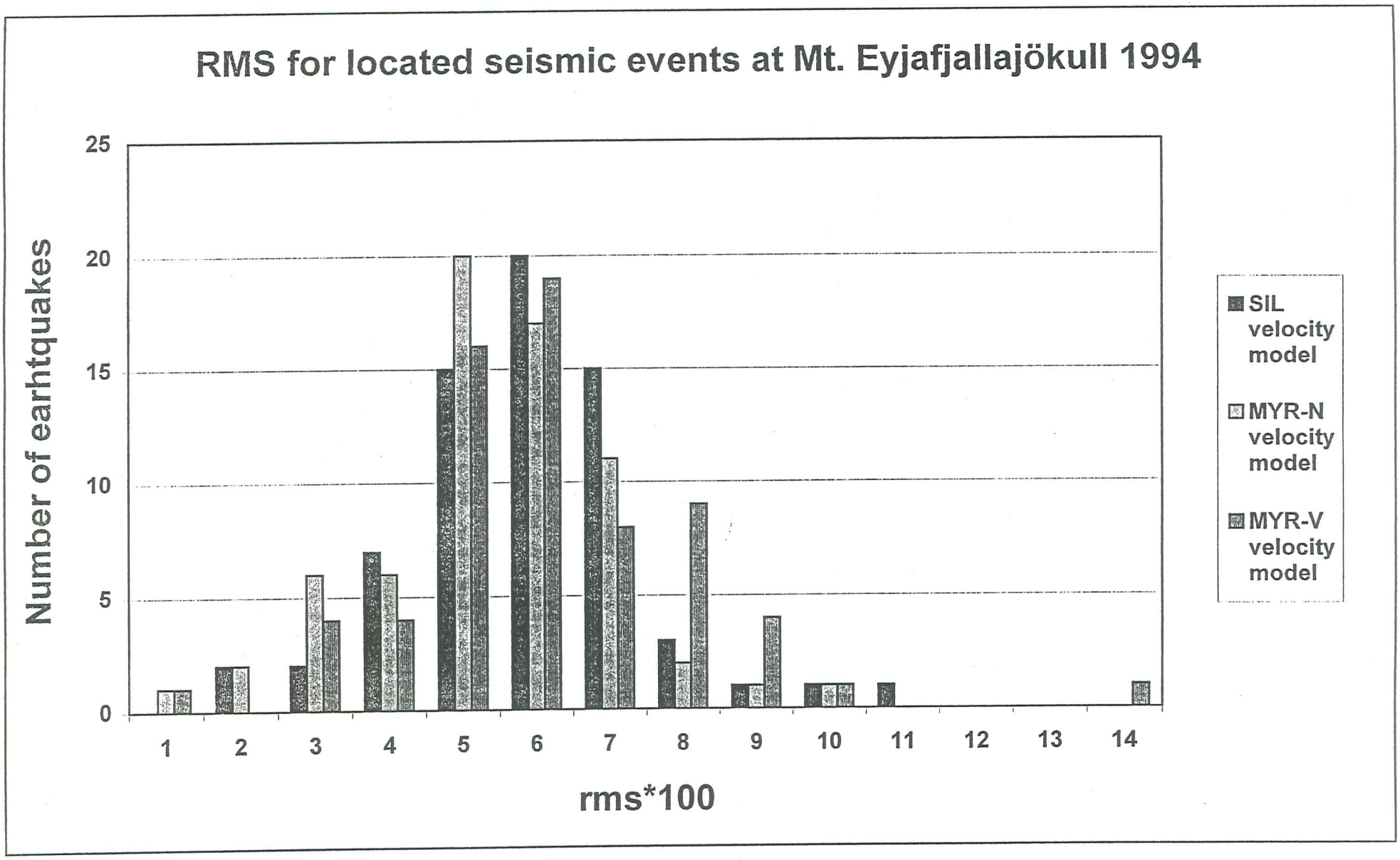
RMS for located seismic events at Mt. Eyjafjallajökull 1994
Number of earhtquakes
0
5
10
15
20
25
1
2
3
4
5
6
7
8
9
10
11
12
13
14
rms*100
SIL velocity model
MYR-N velocity model
MYR-V velocity model

Estimated parametres for the velocity models

	A+B	A+B+C
Latitude		
SIL	63 38.42 - 63 40.25	63 38.42 - 63 40.25
MYR-N	63 38.51 63 40.14	63 37.86 - 63 40.92
MYR-V	63 38.13 - 63 39.65	63 38.13 - 63 41.12
Longitude		
SIL	19 32.01 - 19 36.84	19 32.00 - 19 36.84
MYR-N	19 31.72 - 19 36.84	19 31.72 - 19 36.84
MYR-V	19 30.98 - 19 36.35	19 30.98 - 19 37.44
Depth (km)		
SIL	1.30 - 7.35	1.30 - 7.35
MYR-N	2.29 - 9.64	2.29 - 9.64
MYR-V	1.88 - 12.30	1.88 - 12.30
nwr		
SIL	8-19	8-19
MYR-N	8-19	8-19
MYR-V	8-19	7-19
gap		
SIL	75 - 177	75 - 240
MYR-N	57 -177	37 - 222
MYR-V	60 - 173	60 - 230
dmin		
SIL	2.3 - 15.1	2.3 - 15.1
MYR-N	2.4 - 14.0	2.4 - 14.9
MYR-V	1.7 - 13.3	1.7 - 14.6
rms		
SIL	0.03 - 0.12	0.03 - 0.12
MYR-N	0.03 - 0.11	0.03-0.11
MYR-V	0.04 - 0.15	0.02 - 0.15
error h		
SIL	0.2 - 0.9	0.2 - 1.2
MYR-N	0.2 - 1.2	0.2 - 1.4
MYR-V	0.2 - 1.4	0.2 - 1.7
error z		
SIL	0.3 - 1.8	0.3 - 2.1
MYR-N	0.3 - 2.1	0.3 - 5.1
MYR-V	0.3 - 3.2	0.3 - 4.1
qualtity		
SIL	12 + 48	12 + 48 + 7
MYR-N	11 + 43	11 + 43 + 13
MYR-V	4 + 51	4 + 51 + 12

Fig 23

a-c

Scale: 5 km

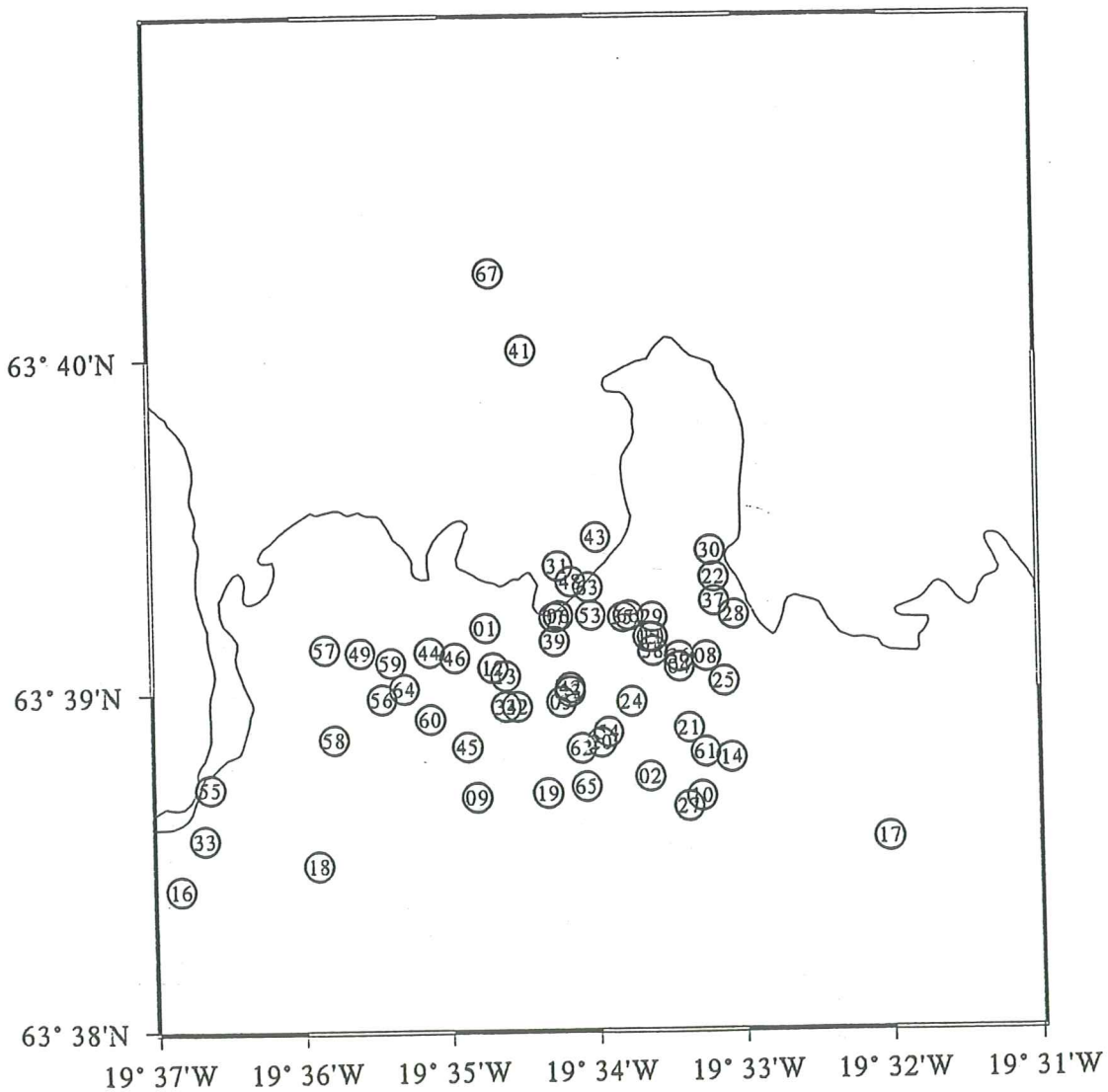

Scale: 5 km

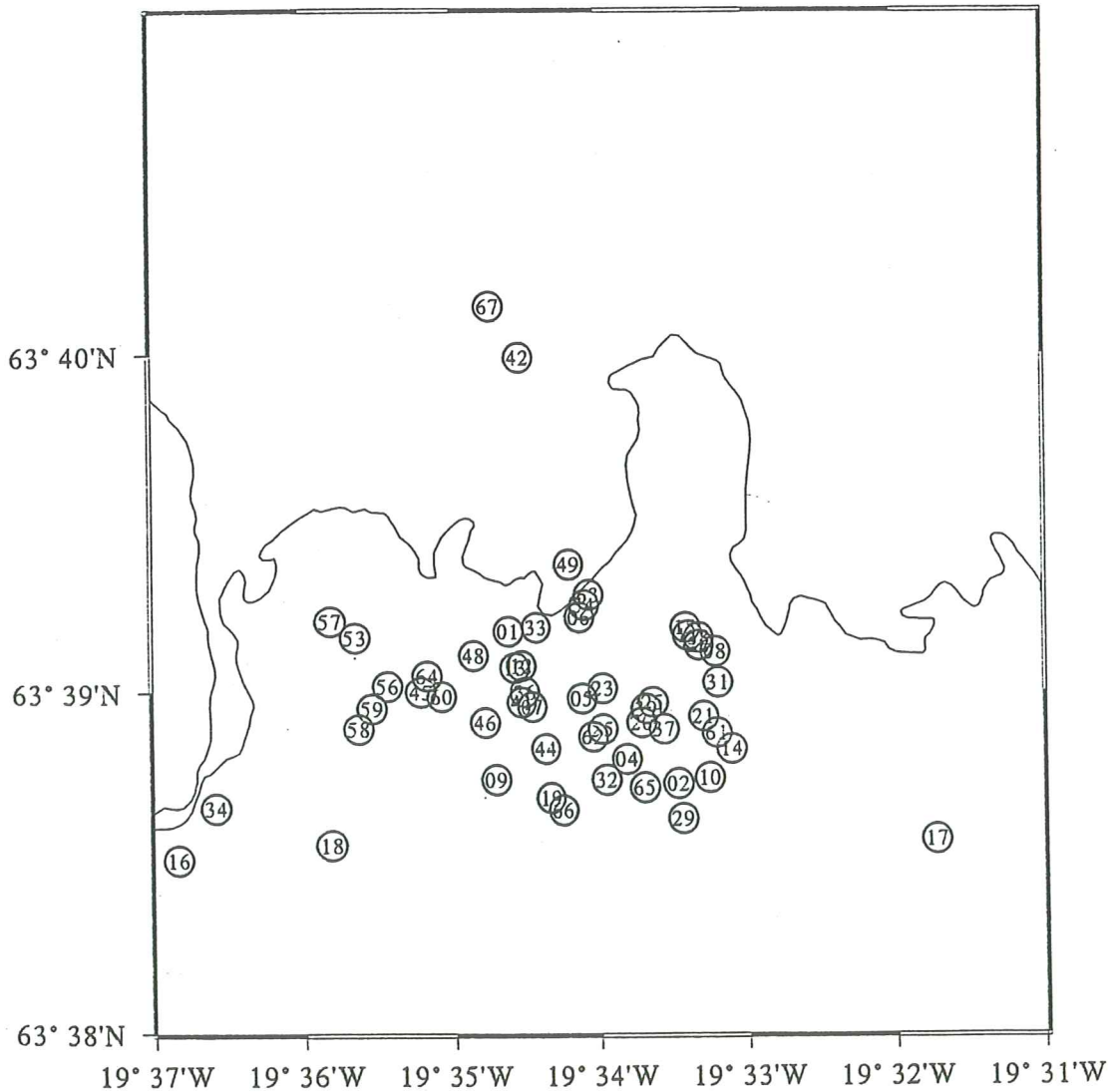
63° 40'N
63° 39'N
63° 38'N
19° 37'W
19° 36'W
19° 35'W
19° 34'W
19° 33'W
19° 32'W
19° 31'W

Scale: 5 km

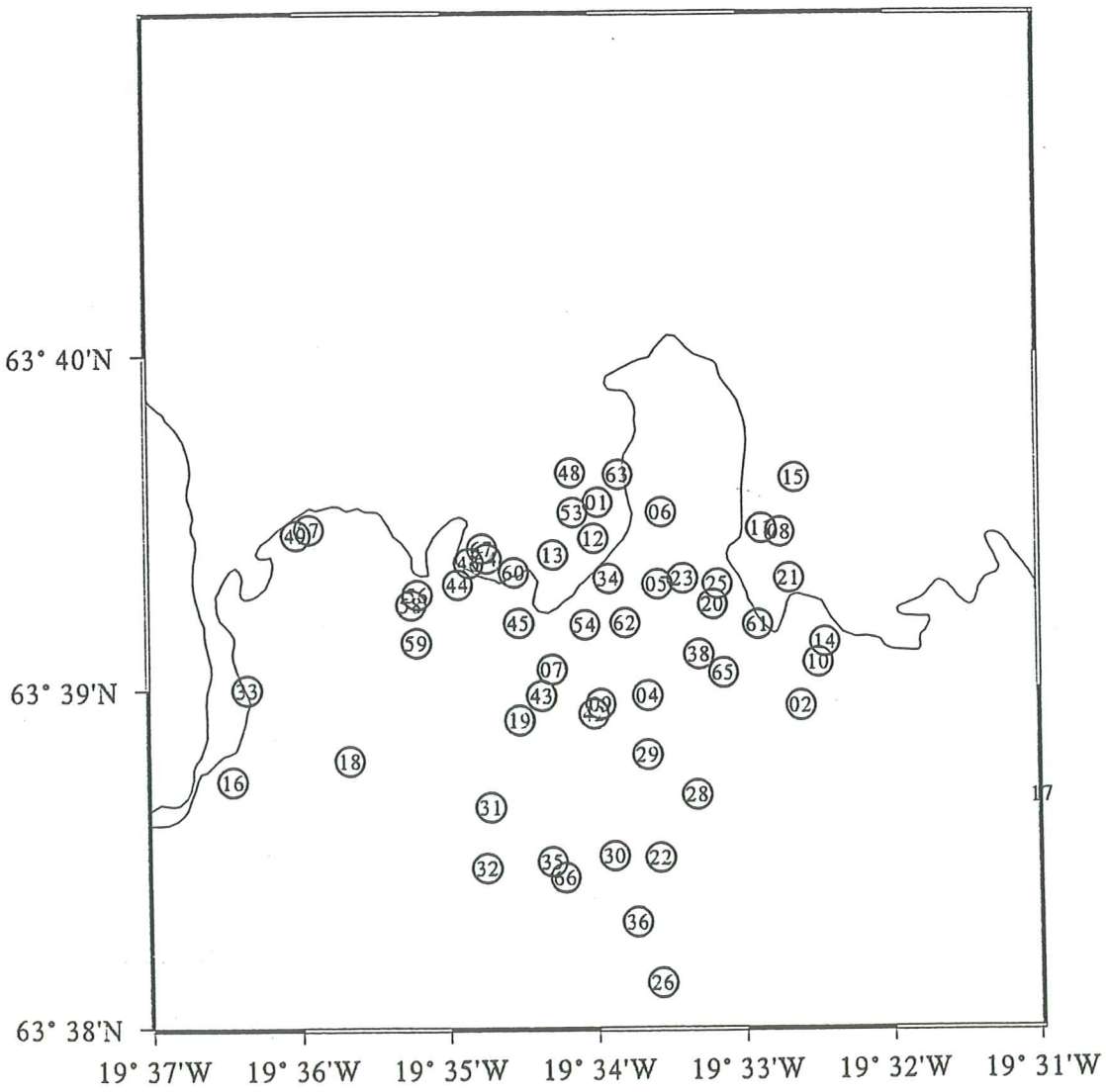
63° 40'N
63° 39'N
63° 38'N
19° 37'W
19° 36'W
19° 35'W
19° 34'W
19° 33'W
19° 32'W
19° 31'W

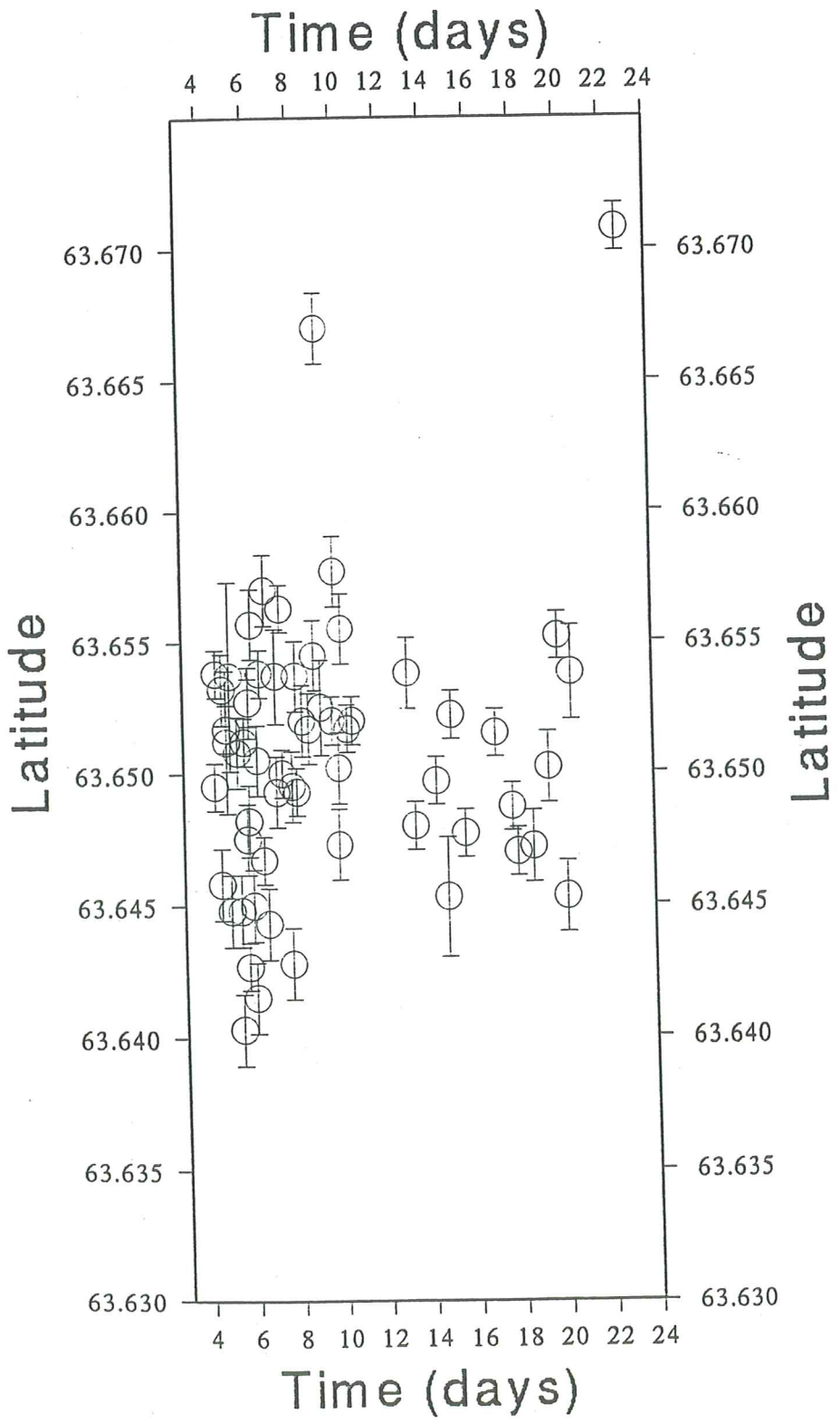
Time (days)
4 6 8 10 12 14 16 18 20 22 24
63.670
63.665
63.660
63.655
63.650
63.645
63.640
63.635
63.630
Latitude
Time (days)

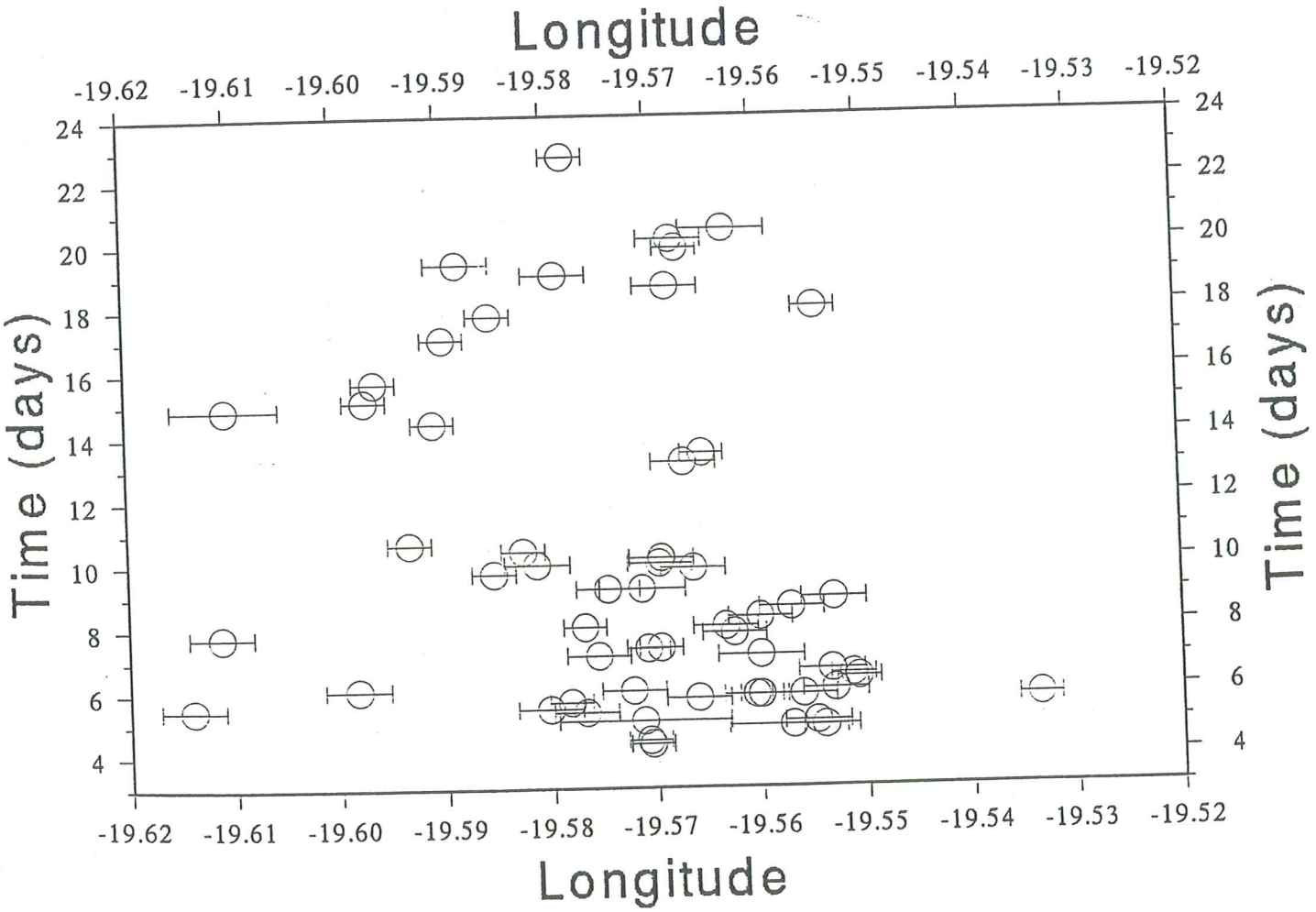
Longitude
-19.62 -19.61 -19.60 -19.59 -19.58 -19.57 -19.56 -19.55 -19.54 -19.53 -19.52
Time (days)
24 22 20 18 16 14 12 10 8 6 4
Longitude
-19.62 -19.61 -19.60 -19.59 -19.58 -19.57 -19.56 -19.55 -19.54 -19.53 -19.52
Time (days)
24 22 20 18 16 14 12 10 8 6 4

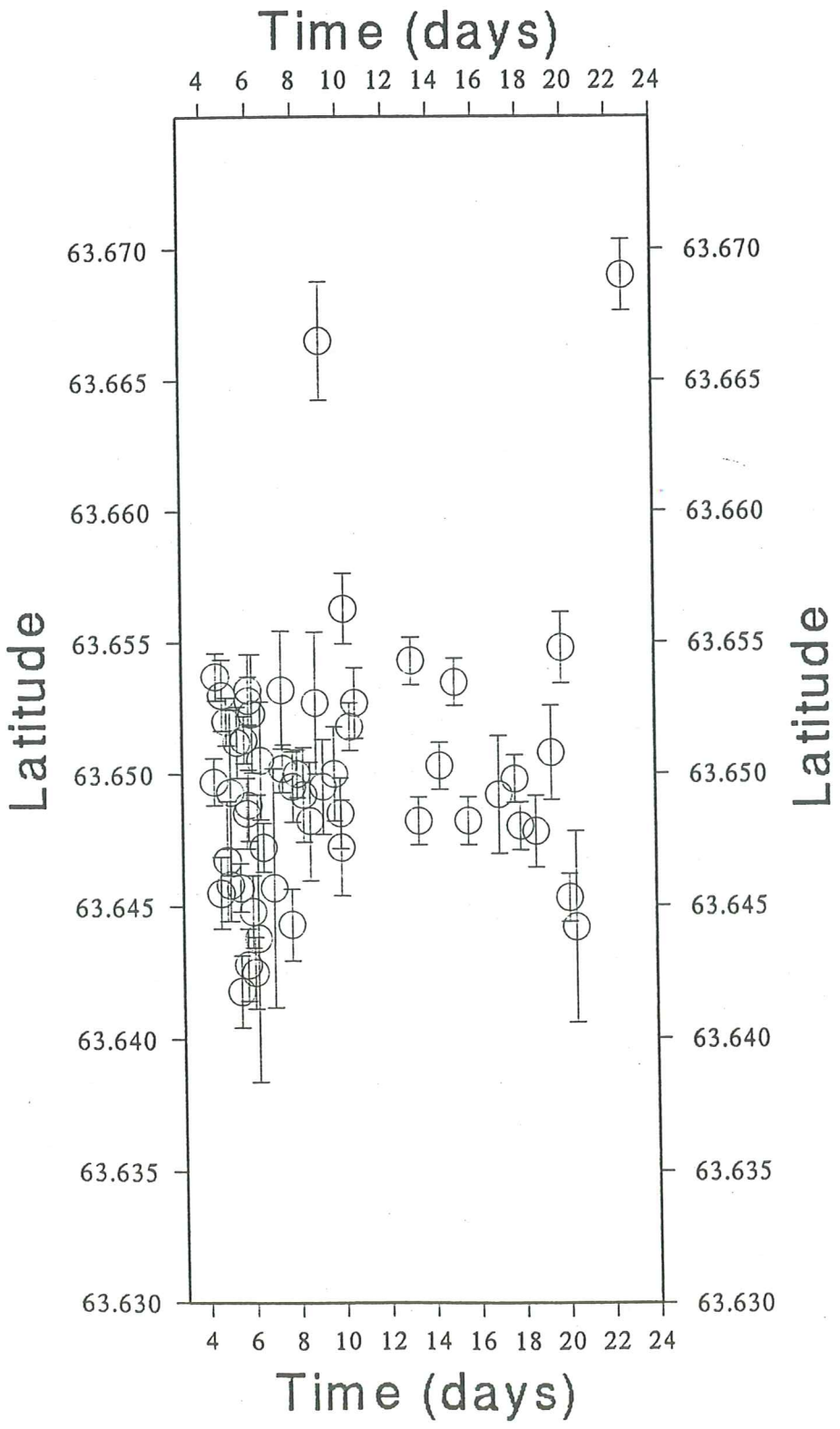
Time (days)
4 6 8 10 12 14 16 18 20 22 24
63.670
63.665
63.660
63.655
63.650
63.645
63.640
63.635
63.630
Latitude
Latitude
Time (days)

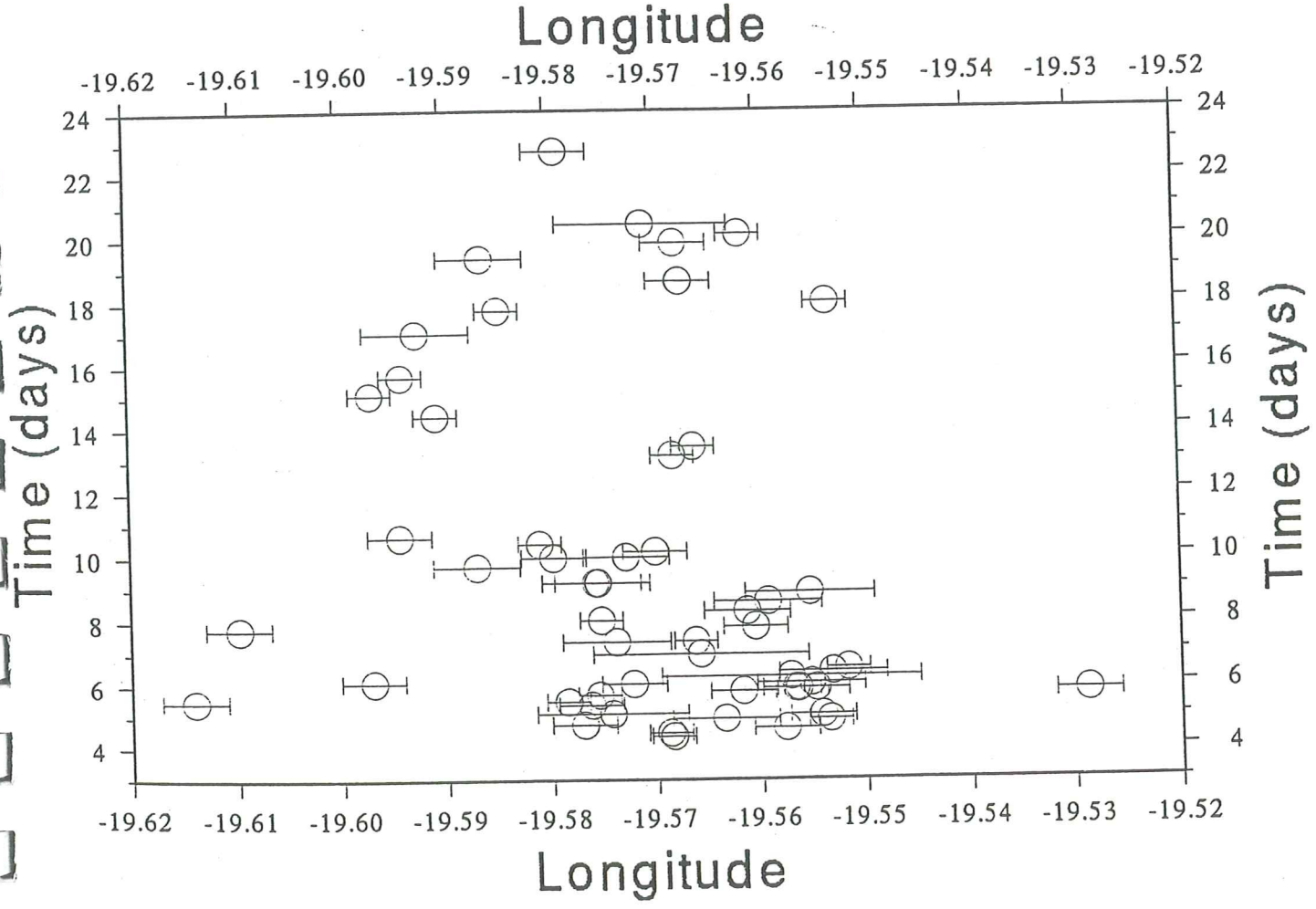
Longitude
-19.62 -19.61 -19.60 -19.59 -19.58 -19.57 -19.56 -19.55 -19.54 -19.53 -19.52
Time (days)
24 22 20 18 16 14 12 10 8 6 4
Longitude
-19.62 -19.61 -19.60 -19.59 -19.58 -19.57 -19.56 -19.55 -19.54 -19.53 -19.52
Time (days)
24 22 20 18 16 14 12 10 8 6 4

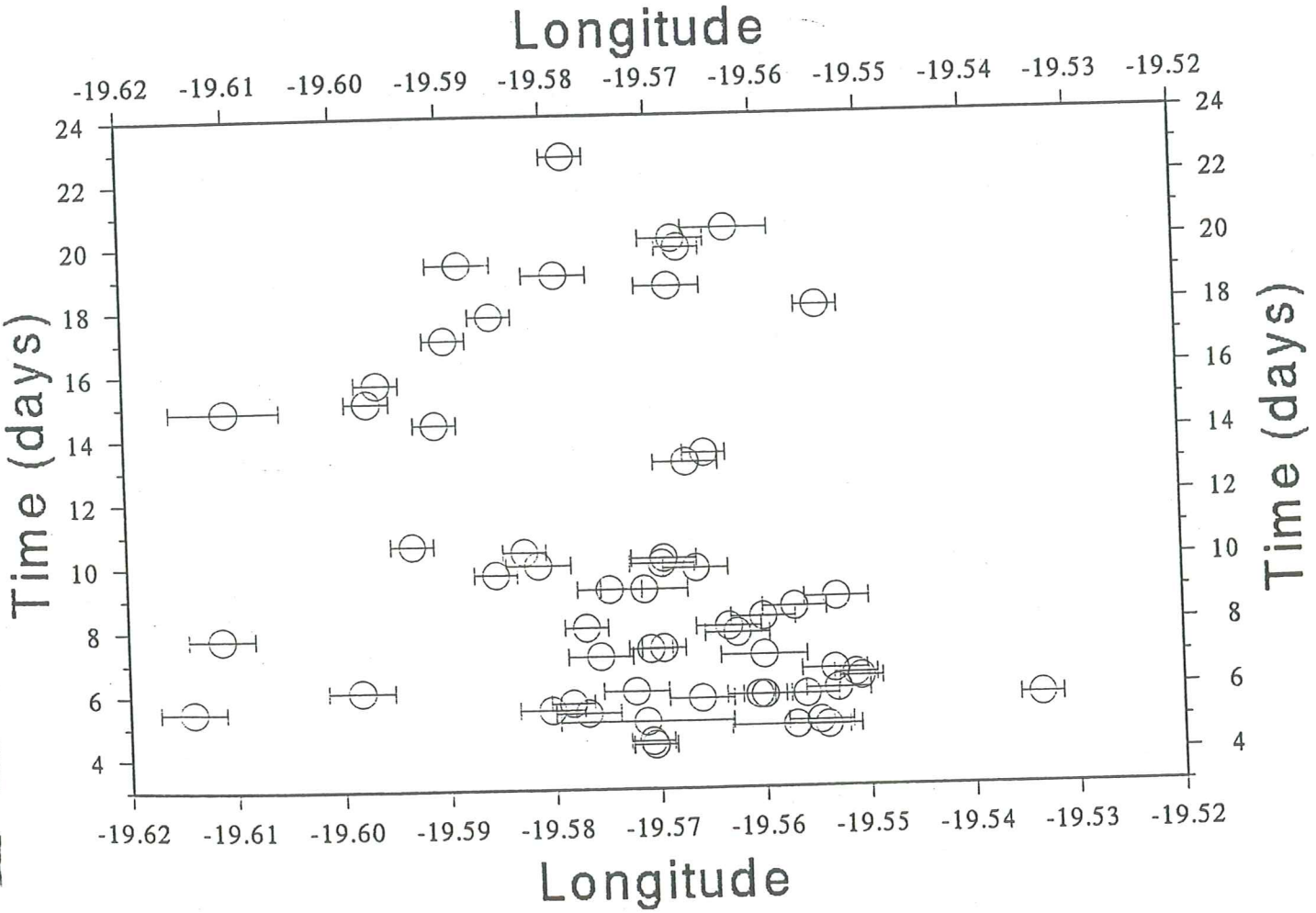
Longitude
-19.62 -19.61 -19.60 -19.59 -19.58 -19.57 -19.56 -19.55 -19.54 -19.53 -19.52
Time (days)
24 22 20 18 16 14 12 10 8 6 4
Longitude
-19.62 -19.61 -19.60 -19.59 -19.58 -19.57 -19.56 -19.55 -19.54 -19.53 -19.52
Time (days)
24 22 20 18 16 14 12 10 8 6 4

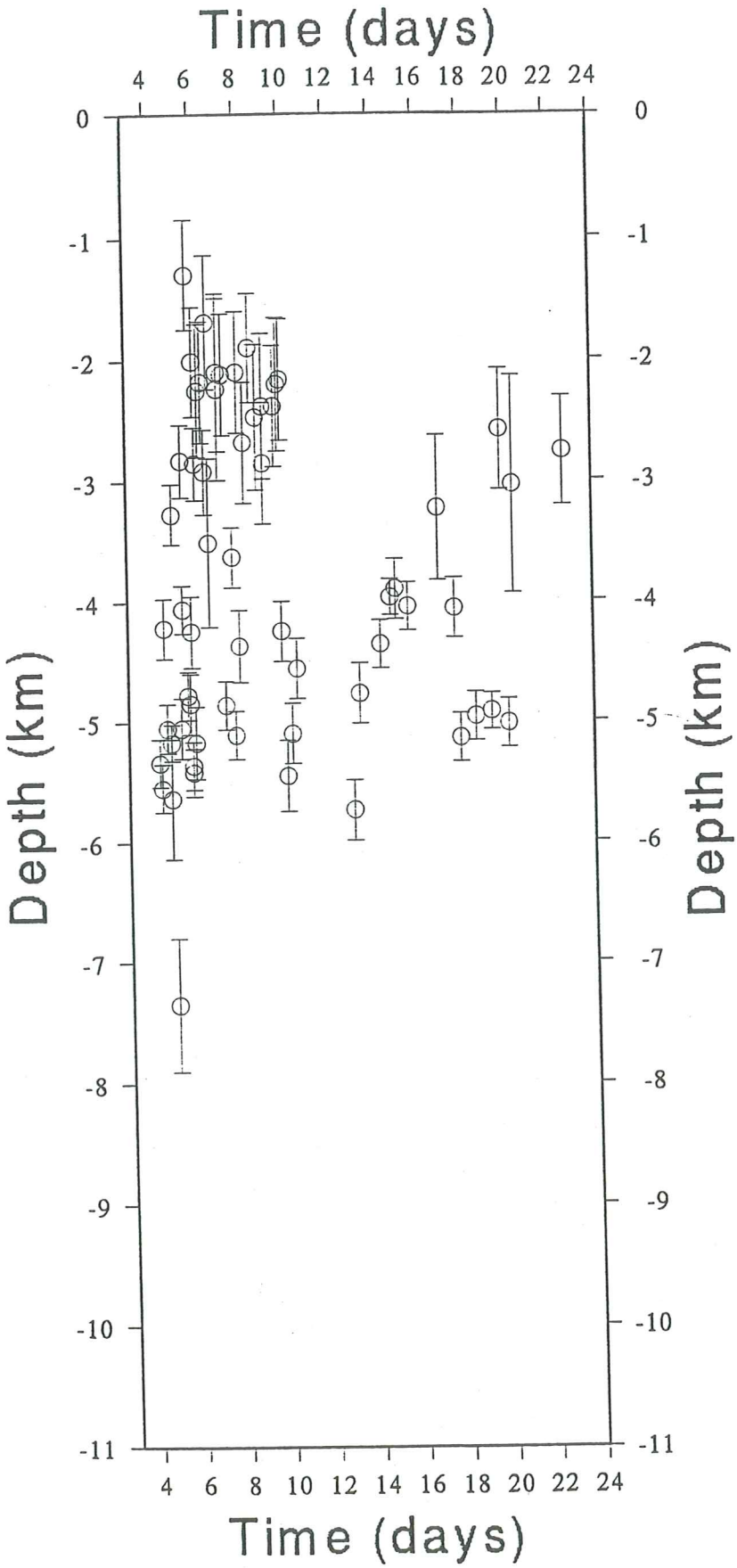
Time (days)
4 6 8 10 12 14 16 18 20 22 24
0 -1 -2 -3 -4 -5 -6 -7 -8 -9 -10 -11
Depth (km)
Depth (km)
4 6 8 10 12 14 16 18 20 22 24
Time (days)

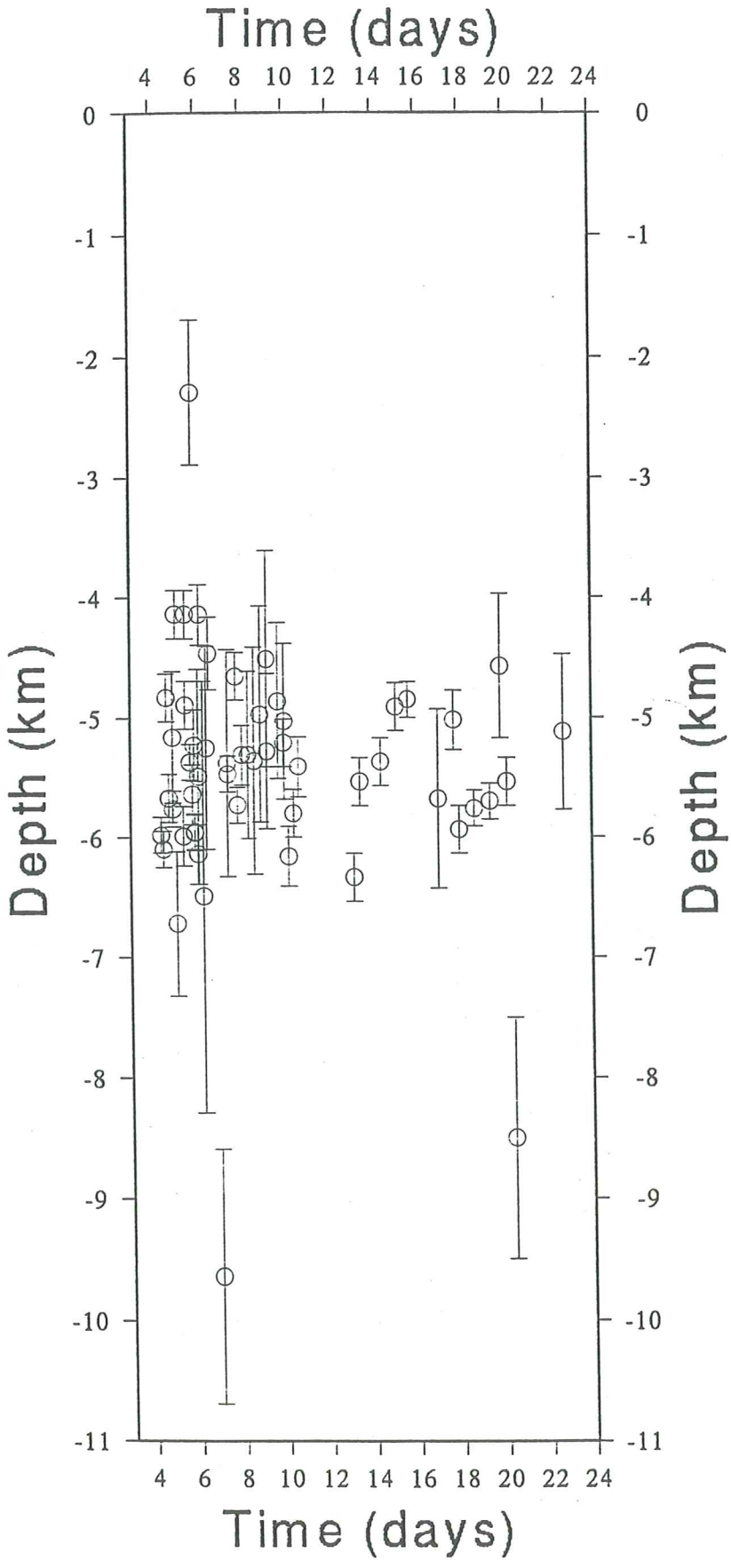
Time (days)
4 6 8 10 12 14 16 18 20 22 24
0 -1 -2 -3 -4 -5 -6 -7 -8 -9 -10 -11
Depth (km)
Depth (km)
4 6 8 10 12 14 16 18 20 22 24
Time (days)

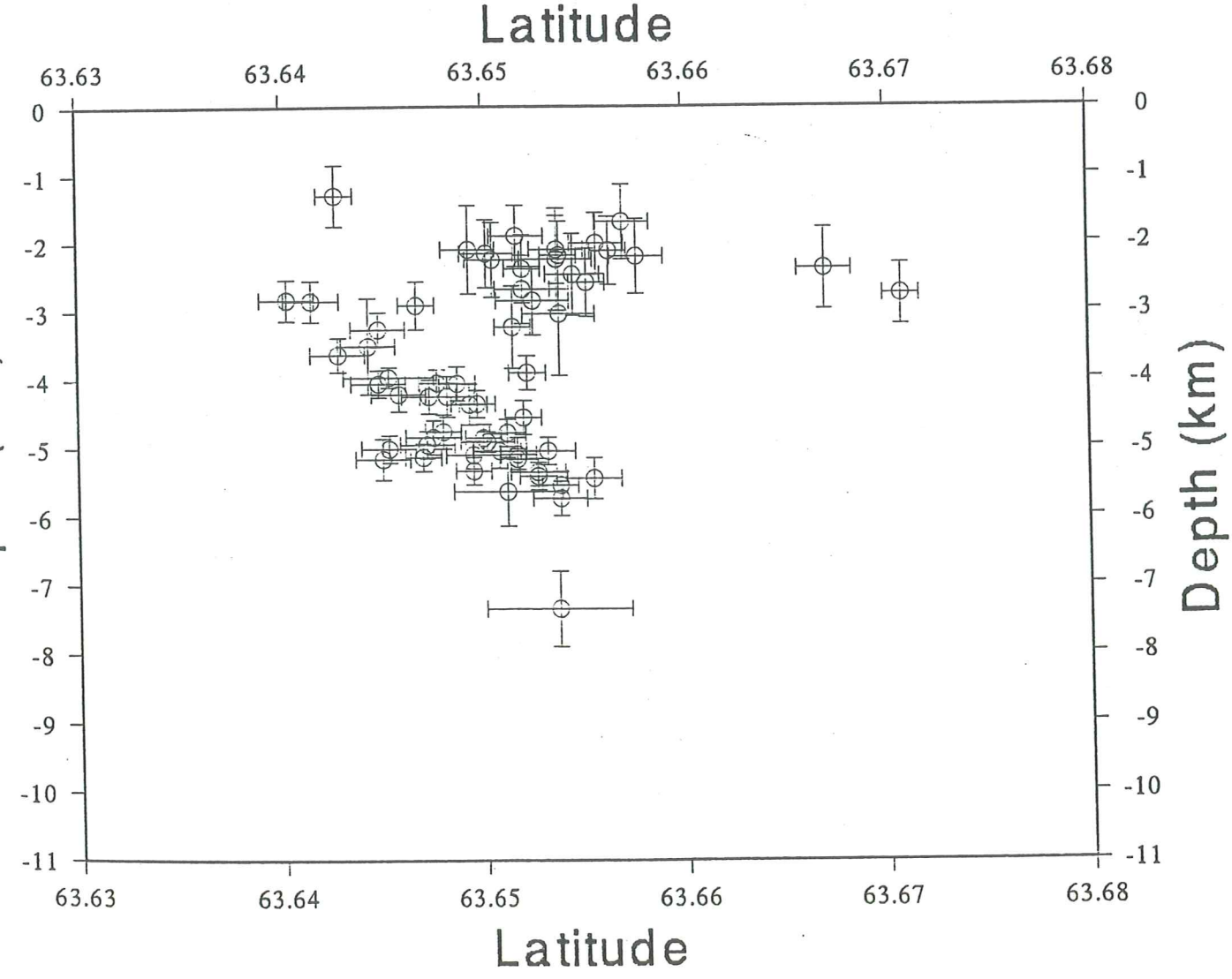
Latitude
63.63
63.64
63.65
63.66
63.67
63.68
0
-1
-2
-3
-4
-5
-6
-7
-8
-9
-10
-11
Depth (km)
Depth (km)
Latitude

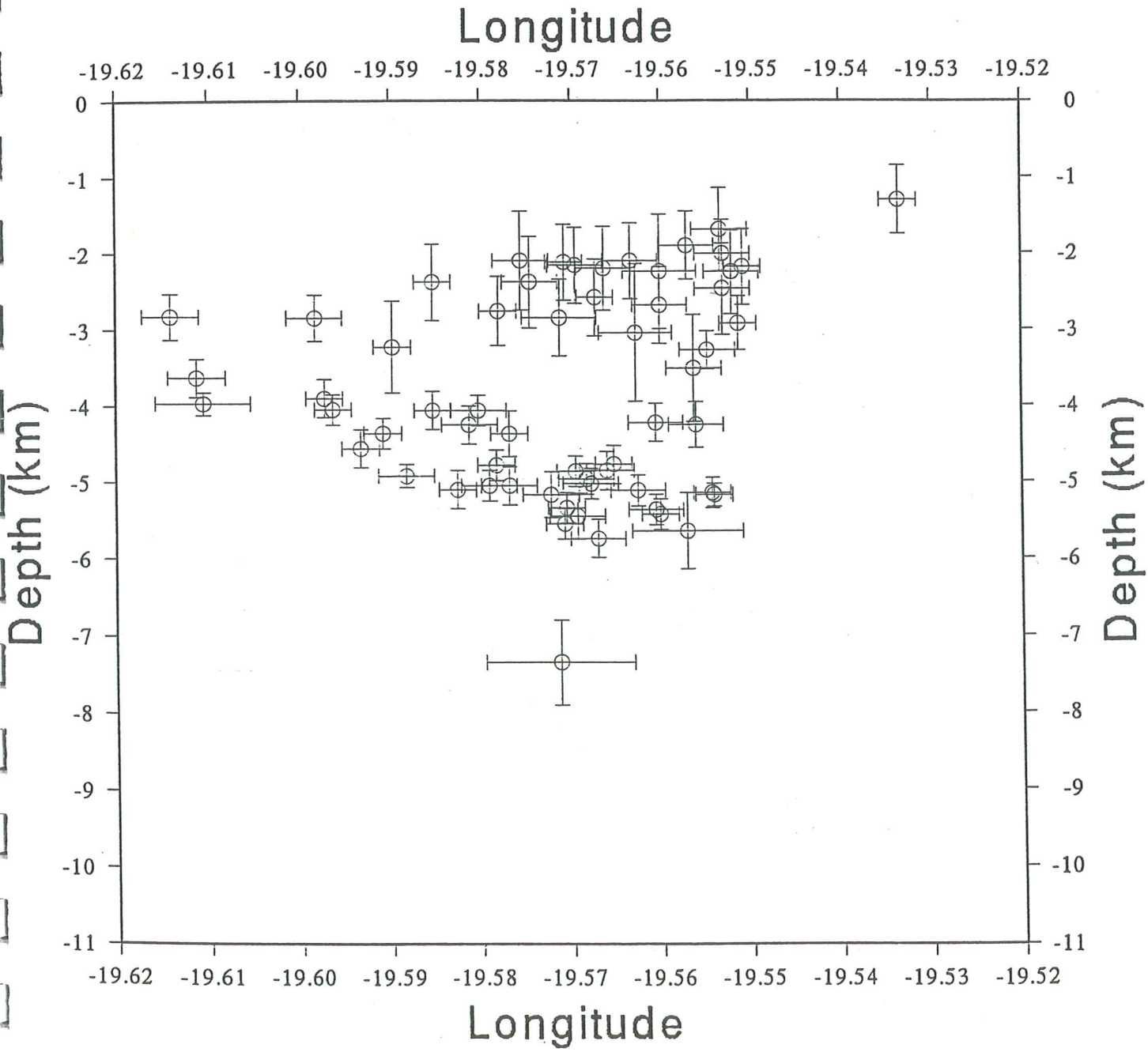
Longitude
-19.62 -19.61 -19.60 -19.59 -19.58 -19.57 -19.56 -19.55 -19.54 -19.53 -19.52
0 -1 -2 -3 -4 -5 -6 -7 -8 -9 -10 -11
Depth (km)
Depth (km)
-19.62 -19.61 -19.60 -19.59 -19.58 -19.57 -19.56 -19.55 -19.54 -19.53 -19.52
Longitude

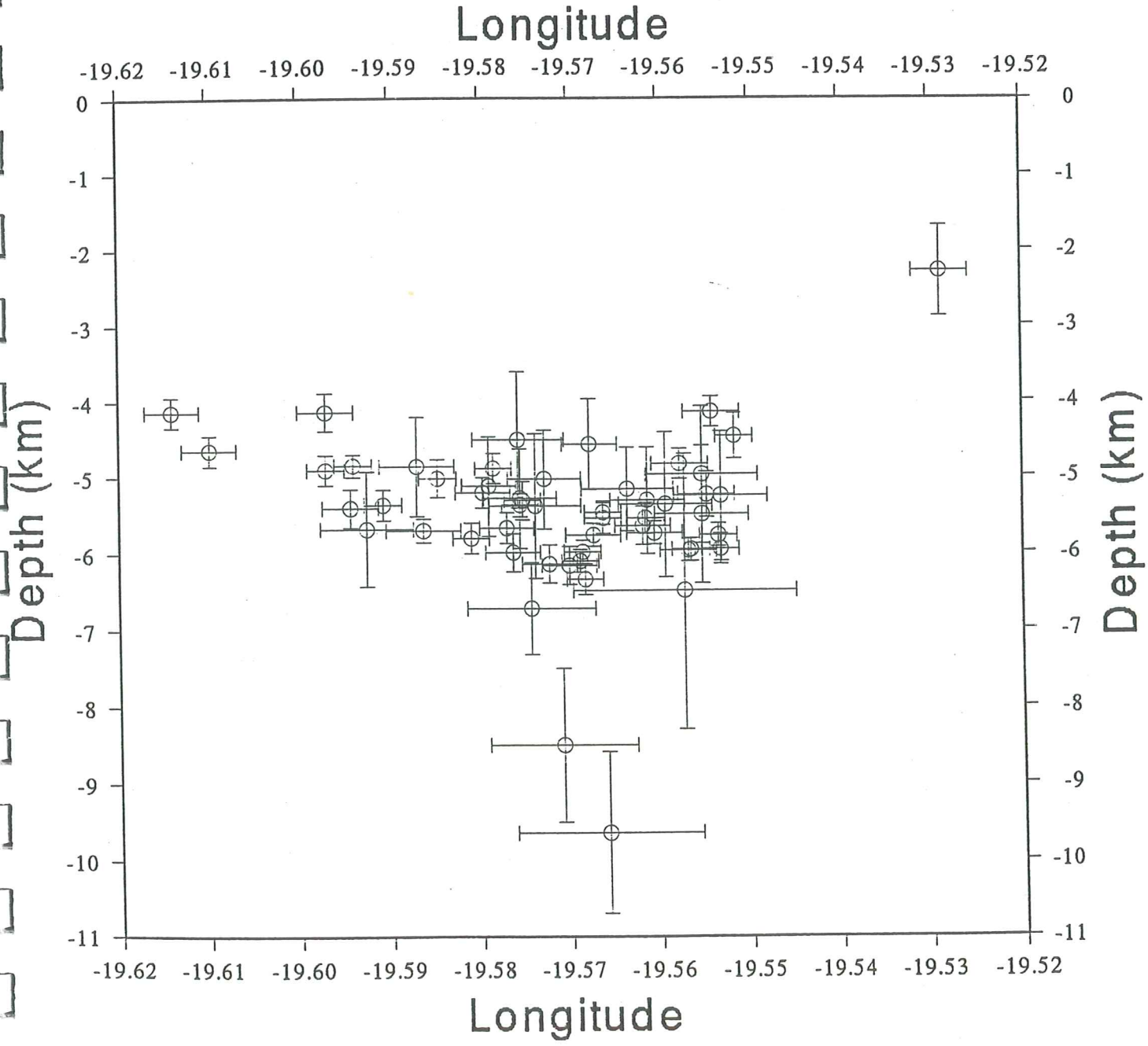
Longitude
-19.62 -19.61 -19.60 -19.59 -19.58 -19.57 -19.56 -19.55 -19.54 -19.53 -19.52
0 -1 -2 -3 -4 -5 -6 -7 -8 -9 -10 -11
Depth (km)
Depth (km)
-19.62 -19.61 -19.60 -19.59 -19.58 -19.57 -19.56 -19.55 -19.54 -19.53 -19.52
Longitude

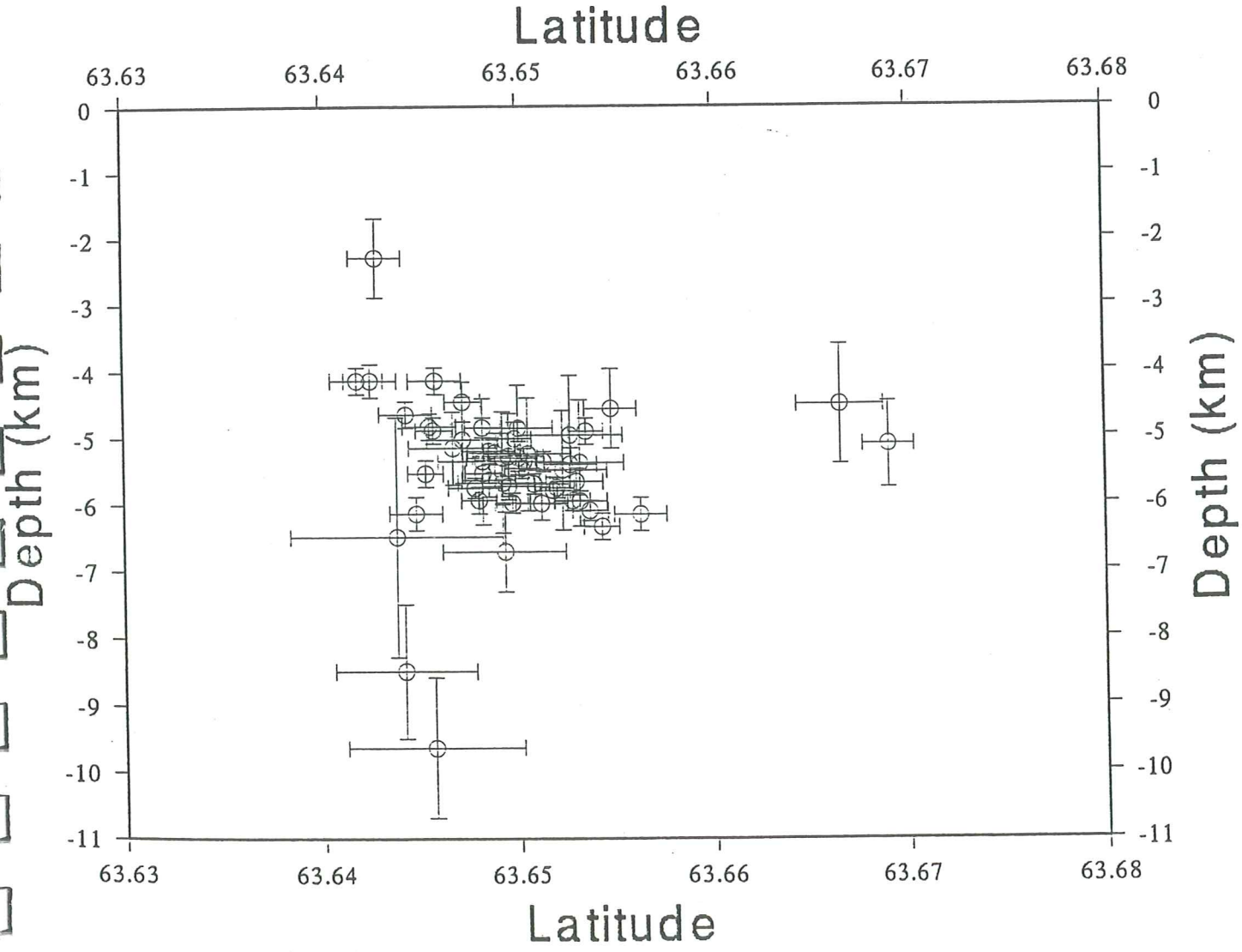
Latitude
63.63
63.64
63.65
63.66
63.67
63.68
0
-1
-2
-3
-4
-5
-6
-7
-8
-9
-10
-11
Depth (km)
Depth (km)
Latitude

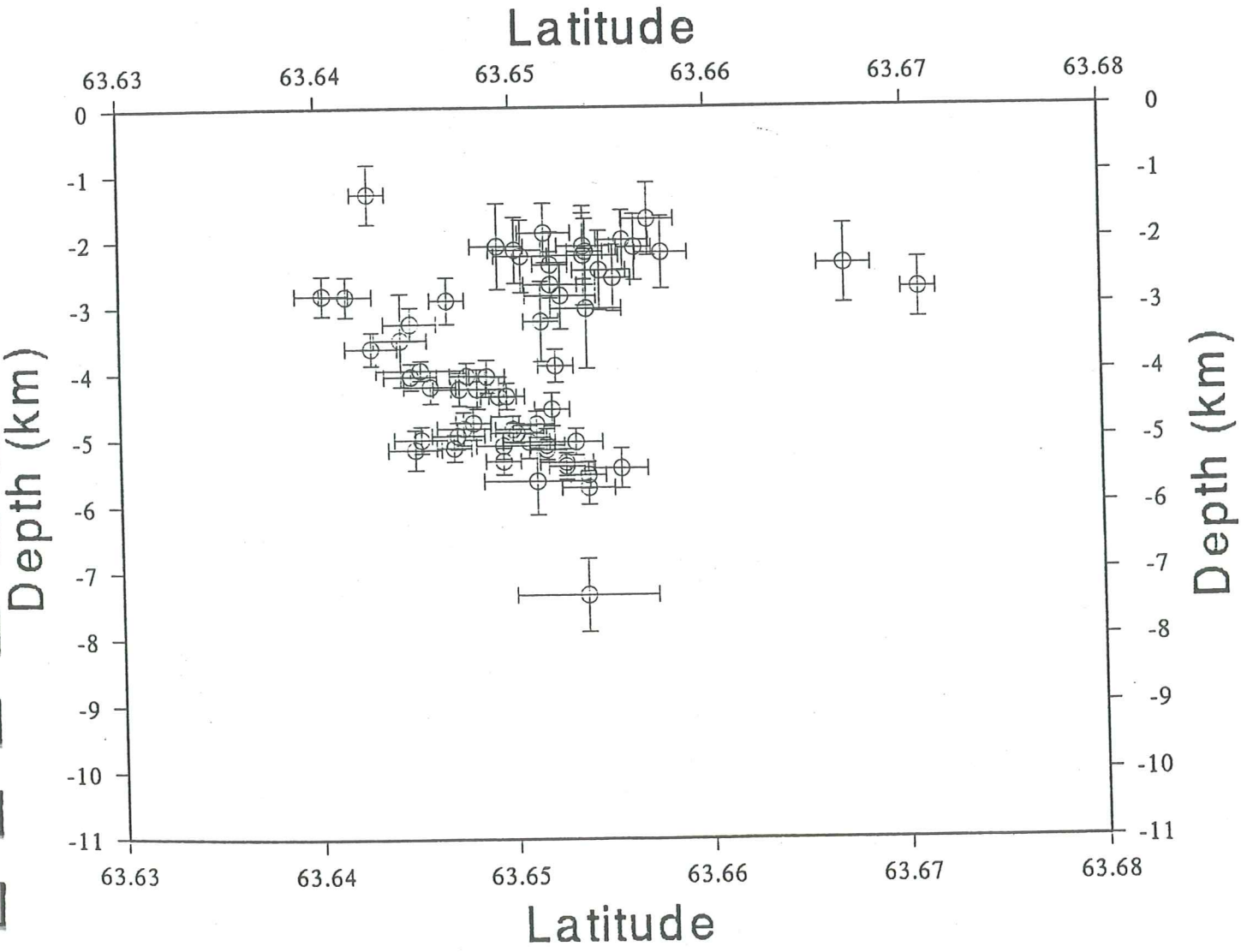
Latitude
63.63
63.64
63.65
63.66
63.67
63.68
0
-1
-2
-3
-4
-5
-6
-7
-8
-9
-10
-11
Depth (km)
Depth (km)
Latitude

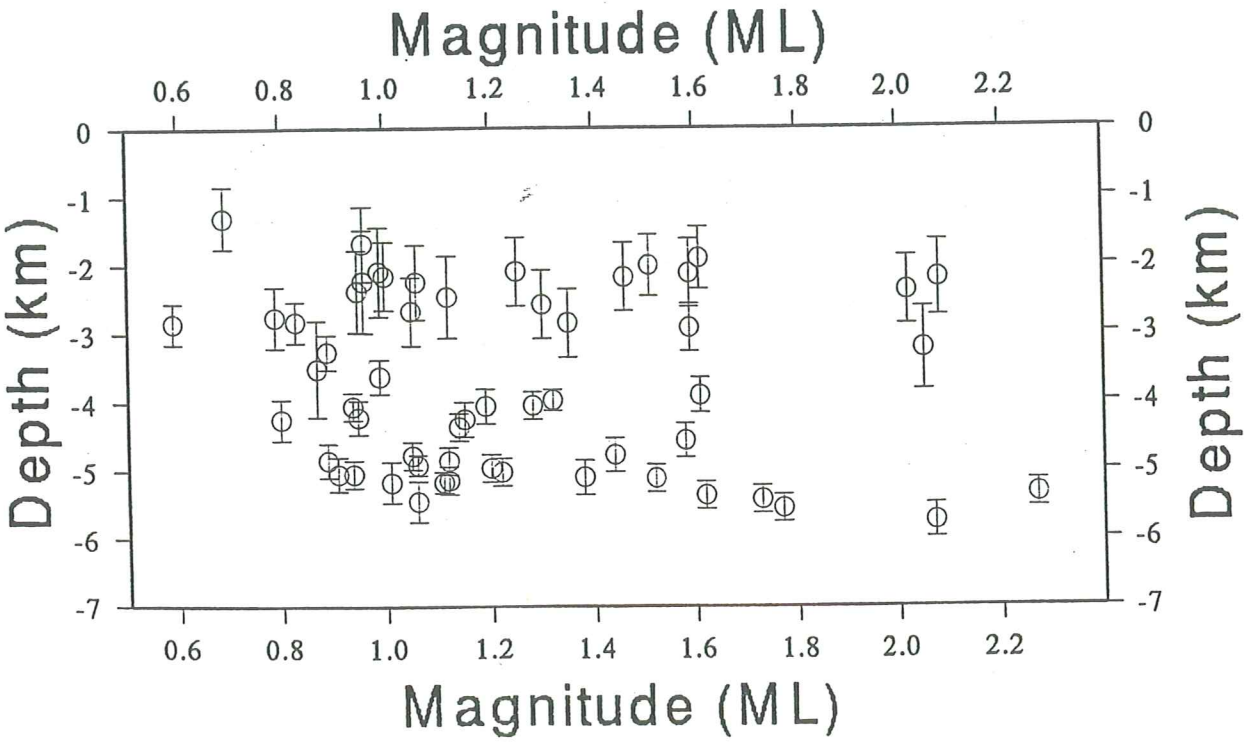
Magnitude (ML)
0.6
0.8
1.0
1.2
1.4
1.6
1.8
2.0
2.2
0
-1
-2
-3
-4
-5
-6
-7
Depth (km)
Depth (km)
Magnitude (ML)

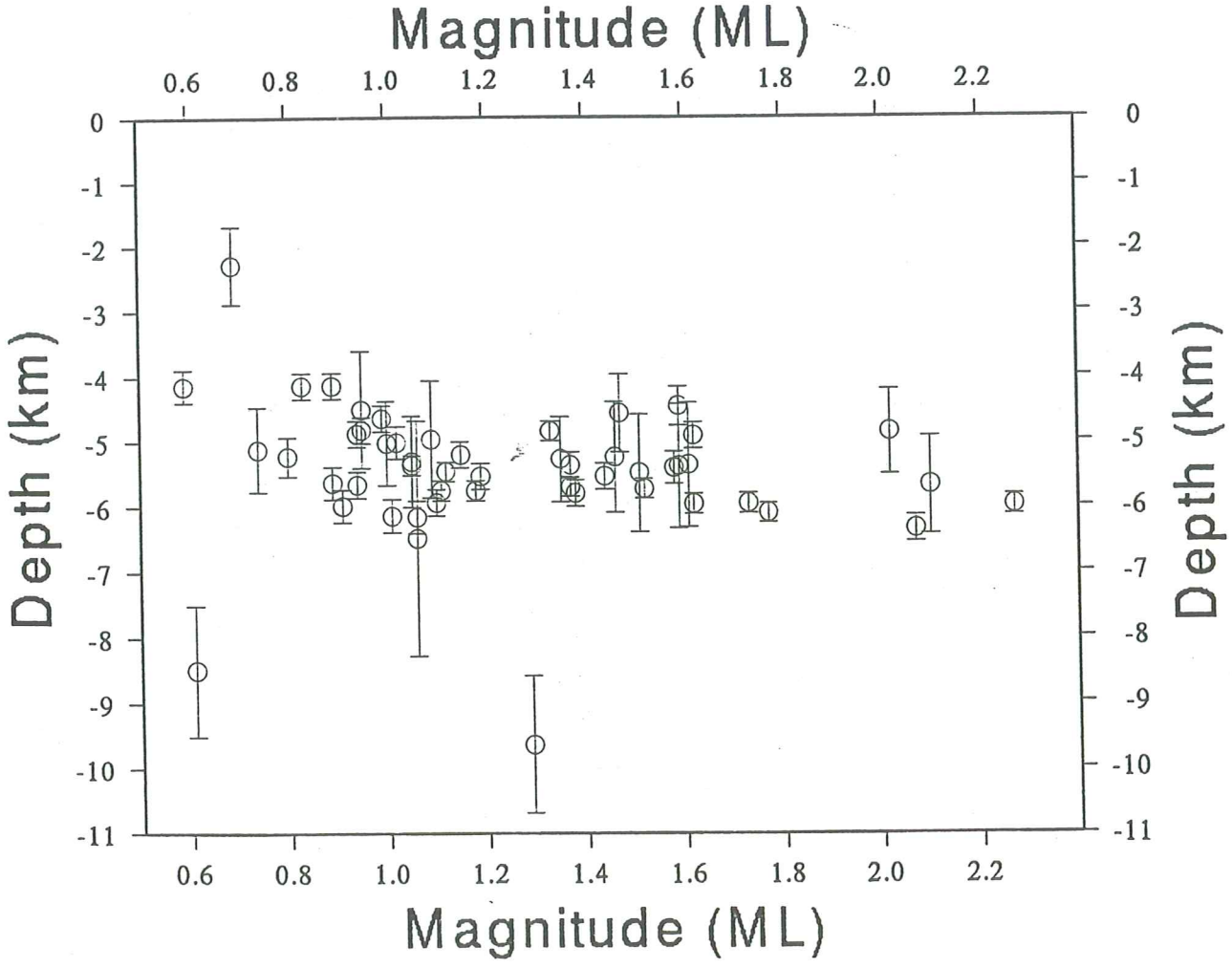
Magnitude (ML)
0.6
0.8
1.0
1.2
1.4
1.6
1.8
2.0
2.2
0
-1
-2
-3
-4
-5
-6
-7
-8
-9
-10
-11
Depth (km)
Magnitude (ML)
Depth (km)

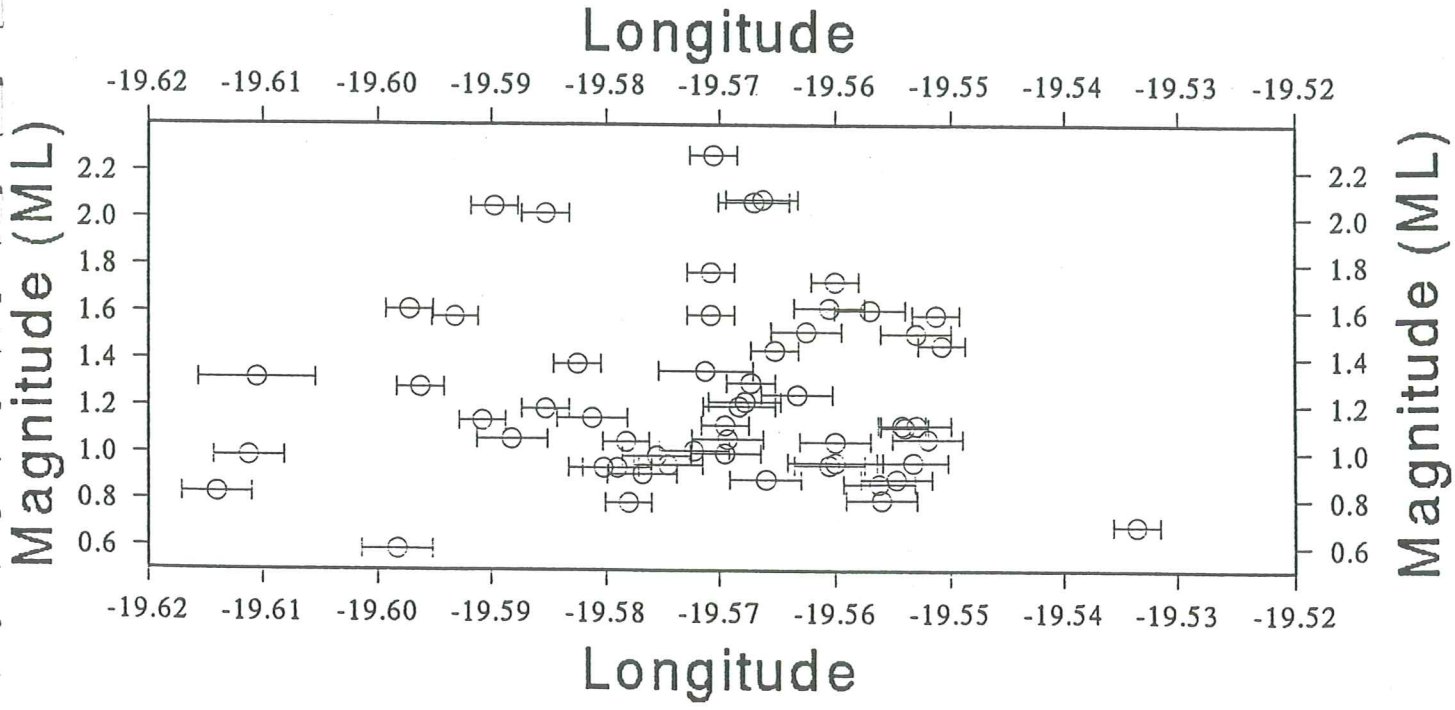
Longitude
-19.62
-19.61
-19.60
-19.59
-19.58
-19.57
-19.56
-19.55
-19.54
-19.53
-19.52
Magnitude (ML)
2.2
2.0
1.8
1.6
1.4
1.2
1.0
0.8
0.6
Longitude
Magnitude (ML)

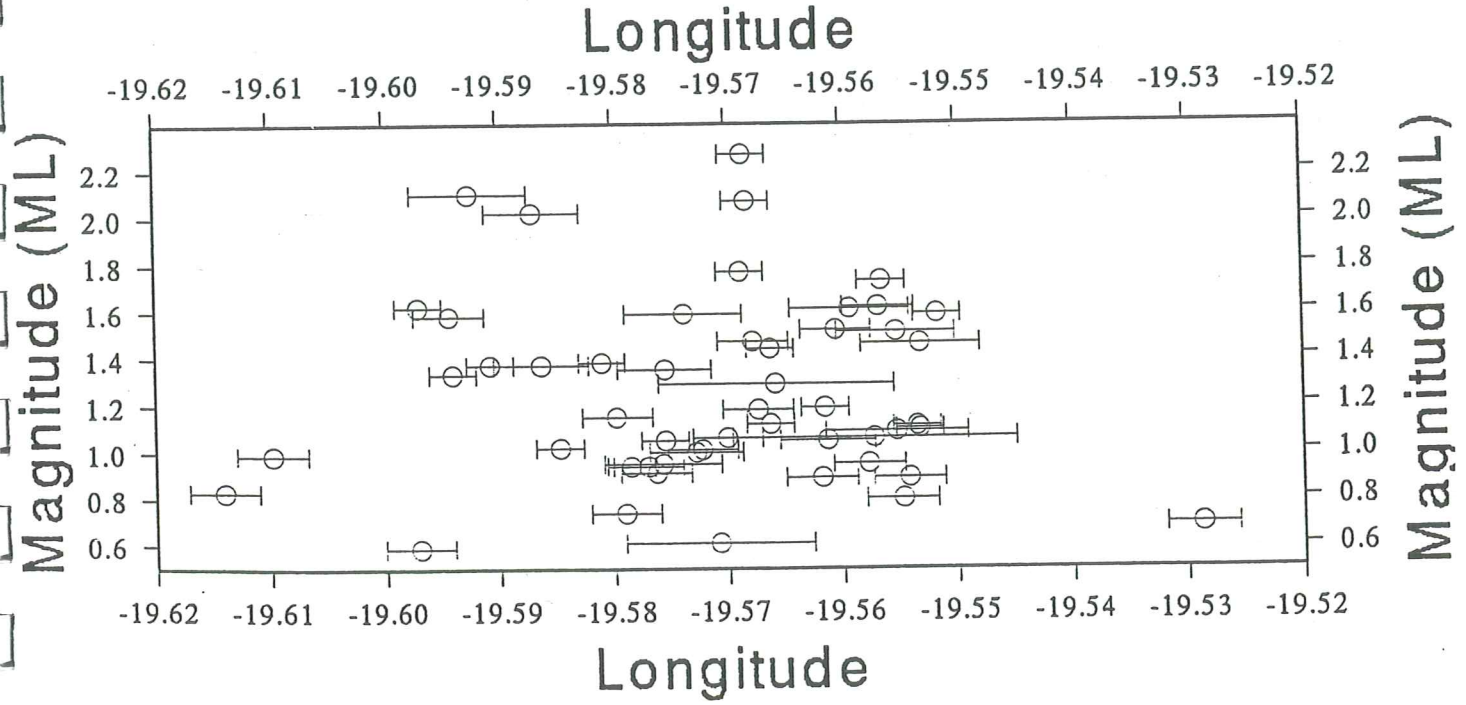
Longitude
-19.62 -19.61 -19.60 -19.59 -19.58 -19.57 -19.56 -19.55 -19.54 -19.53 -19.52
Magnitude (ML)
2.2 2.0 1.8 1.6 1.4 1.2 1.0 0.8 0.6
Magnitude (ML)
2.2 2.0 1.8 1.6 1.4 1.2 1.0 0.8 0.6
-19.62 -19.61 -19.60 -19.59 -19.58 -19.57 -19.56 -19.55 -19.54 -19.53 -19.52
Longitude

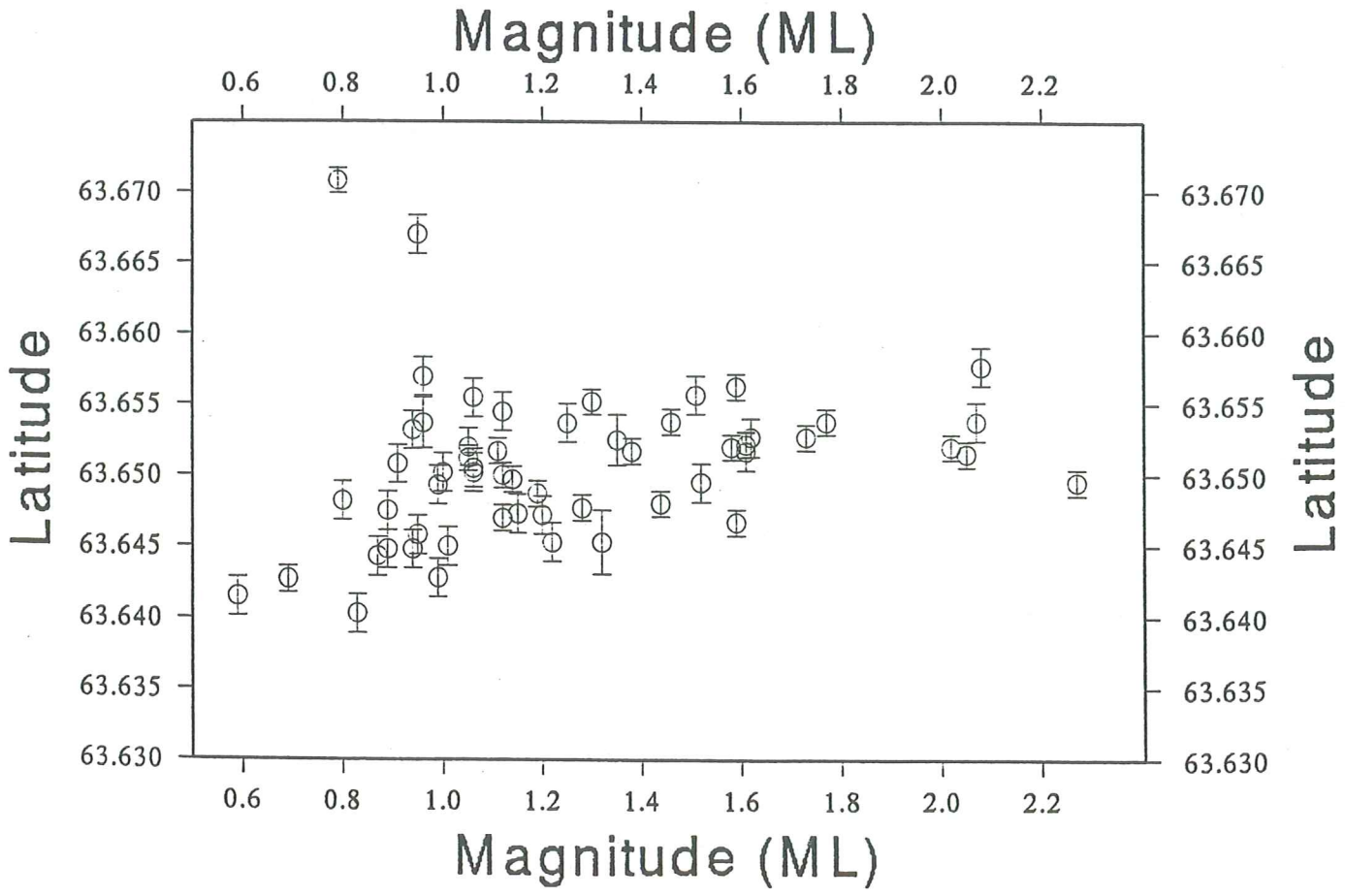
Magnitude (ML)
0.6
0.8
1.0
1.2
1.4
1.6
1.8
2.0
2.2
Latitude
63.670
63.665
63.660
63.655
63.650
63.645
63.640
63.635
63.630
Magnitude (ML)
Latitude

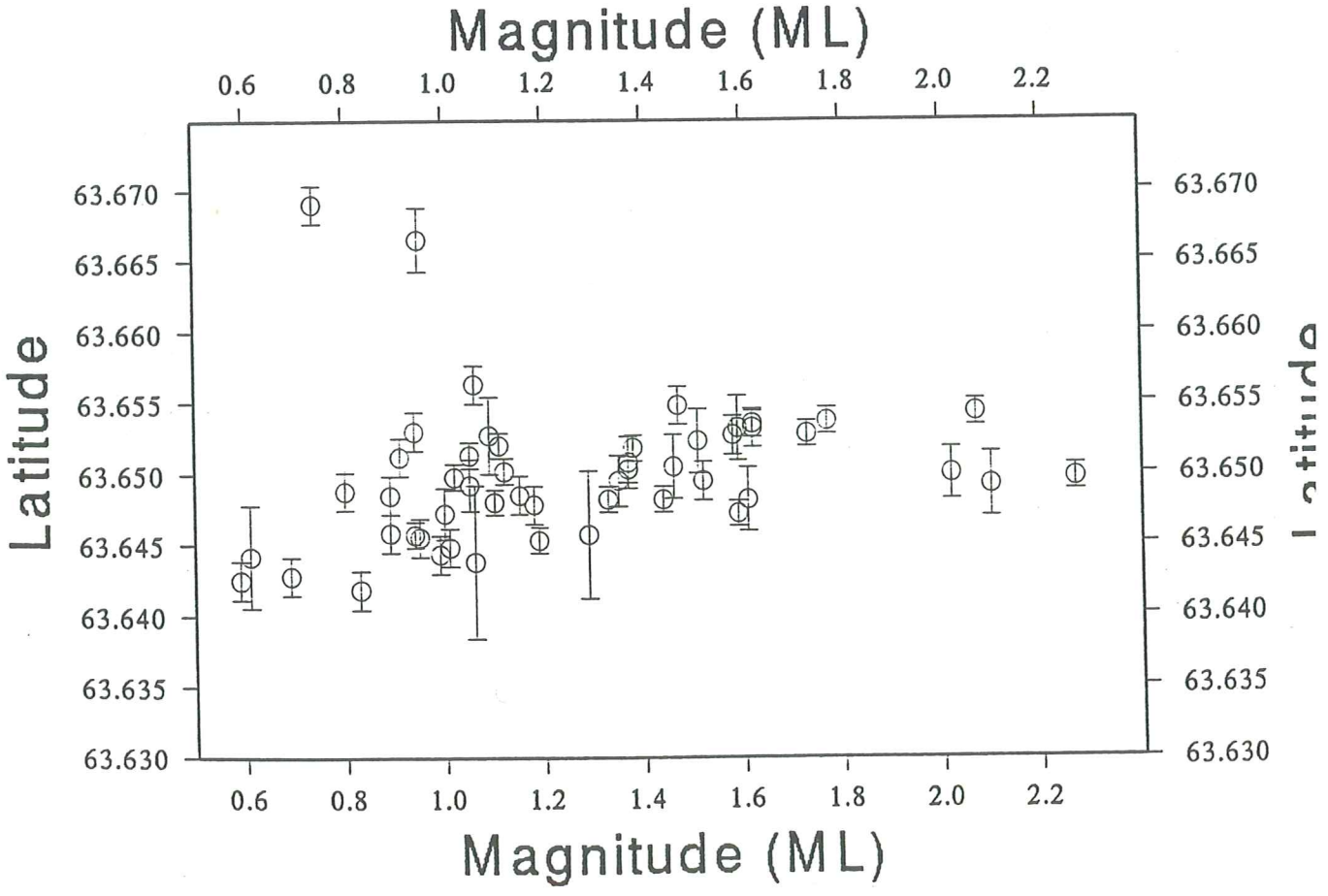
Magnitude (ML)
0.6
0.8
1.0
1.2
1.4
1.6
1.8
2.0
2.2
Latitude
63.670
63.665
63.660
63.655
63.650
63.645
63.640
63.635
63.630
Magnitude (ML)

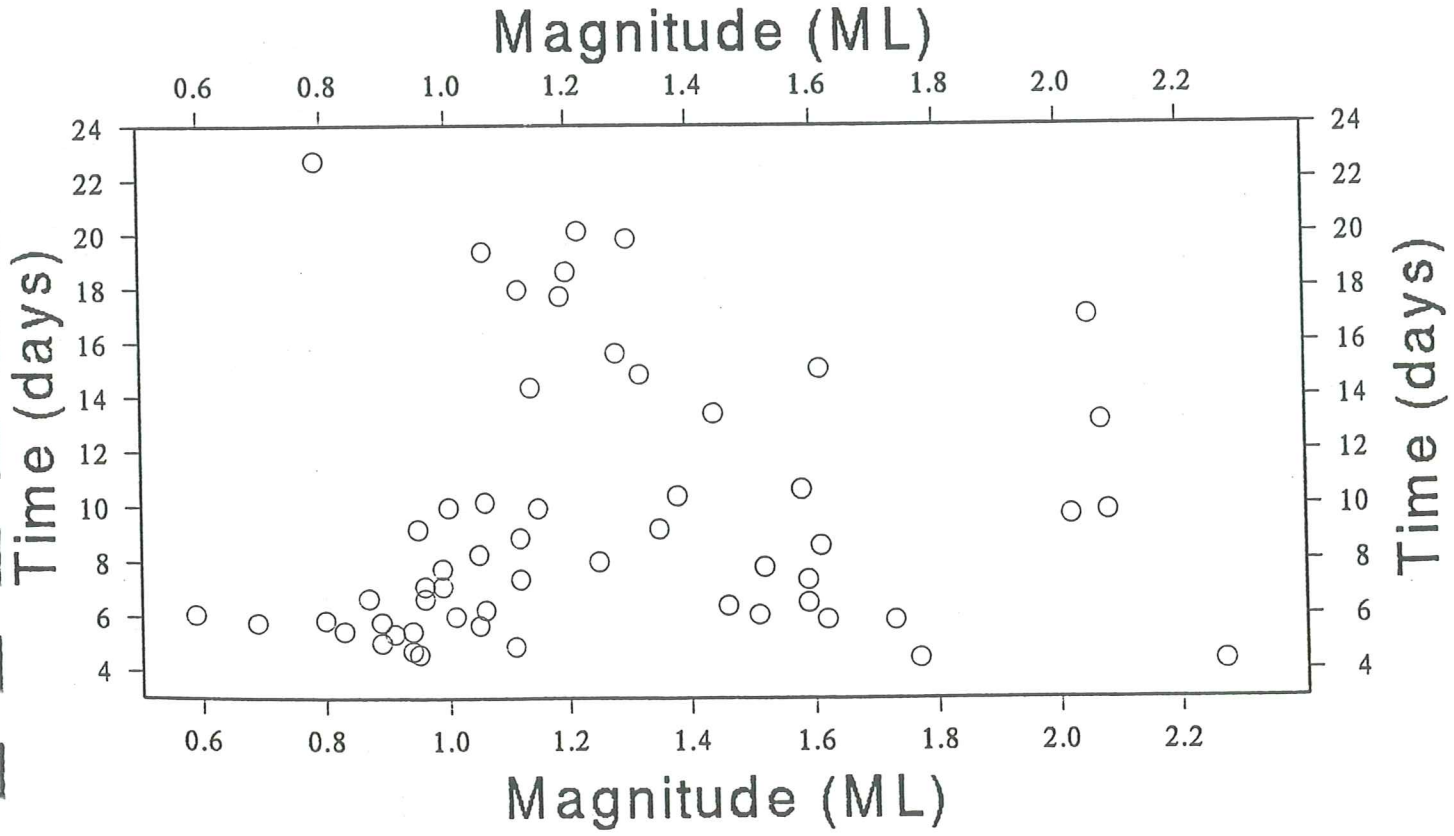
Magnitude (ML)
0.6
0.8
1.0
1.2
1.4
1.6
1.8
2.0
2.2
Time (days)
4
6
8
10
12
14
16
18
20
22
24
Magnitude (ML)
Time (days)

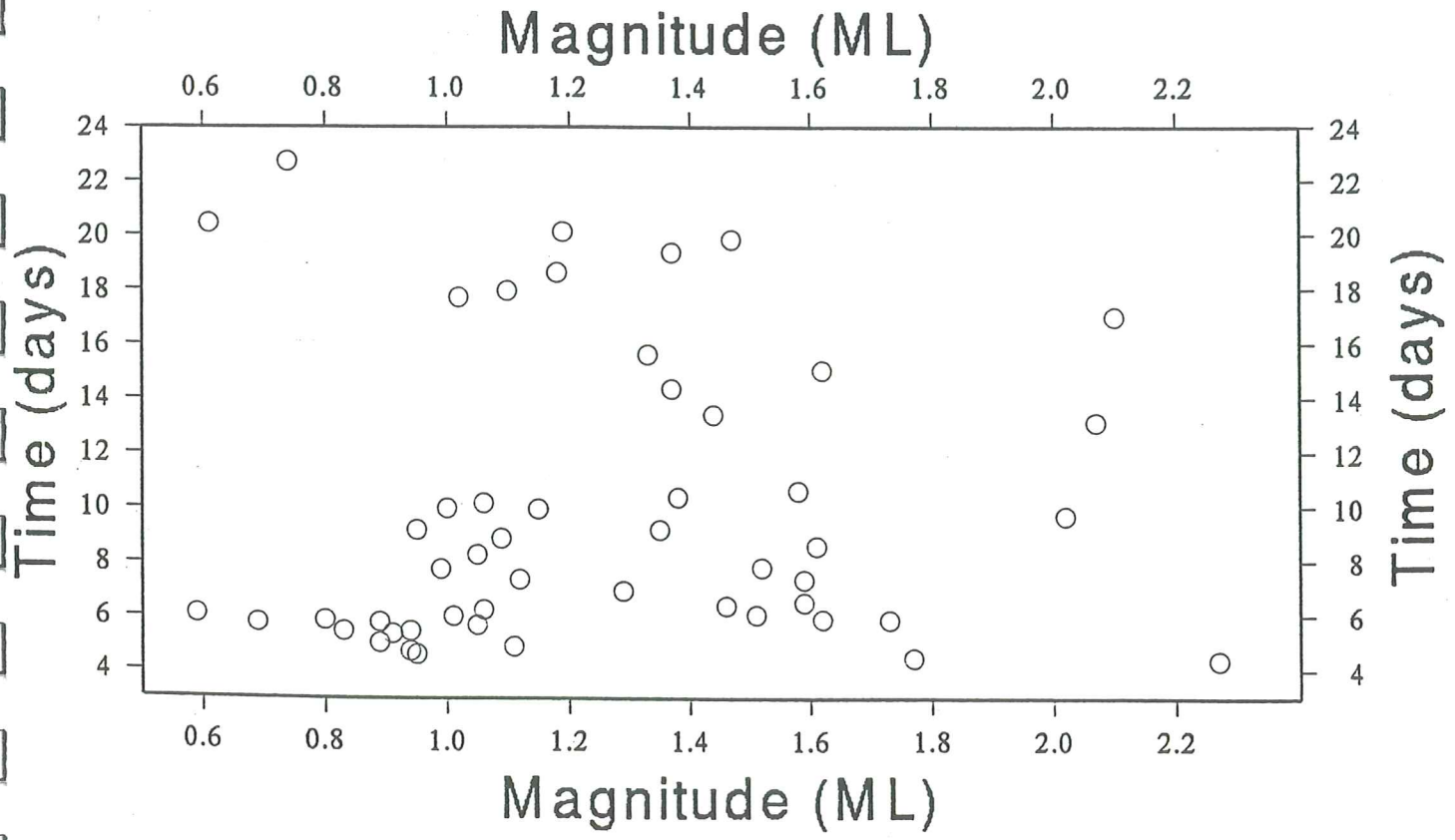
Magnitude (ML)
0.6
0.8
1.0
1.2
1.4
1.6
1.8
2.0
2.2
Time (days)
4
6
8
10
12
14
16
18
20
22
24
Magnitude (ML)
Time (days)

Gps-and tilt stations: coordinates and station numbers

GPS-stations

Code	Station name	Number	Lat	Lat	Lat	Lon	Lon	Lon
ALFT	Álftagróf	NE9213	63	29.22	63.487	19	10.38	19.173
AUST	Austmannsbunga	NE9304	63	40.27	63.67117	19	4.5	19.075
ENTA	Enta	Iron rod	63	42.04	63.70067	19	10.56	19.176
FIMM	Fimmvörðuhals	NE9203	63	36.24	63.604	19	26.15	19.43583
HAMR	Hamragarðar	OS7487/S34	63	37.2	63.62	19	59.08	19.98467
HOFD	Höfðabrekkuheiði	704	63	30.31	63.50517	18	52.13	18.86883
HRIS	Hríshóll	NE9202	63	27.38	63.45633	18	52.38	18.873
KJAL	Kjalnater	NE9306	63	36.58	63.60967	18	29.39	18.48983
KRIK	Kriki	726	63	37.35	63.6225	18	48.55	18.80917
OLAF	Ólafshaus	746	63	40.47	63.6745	18	46.56	18.776
REYN	Reynisfjall	OS7377/S16	63	25.06	63.41767	19	1.38	19.023
RJUP	Rjúpnafell	NE9303	63	37.08	63.618	18	52.13	18.86883
SELJ	Seljavellir	NE94004	63	33.45	63.5575	19	37.57	19.62617
SKOG	Skógaheiði	OS7486/S35	63	34.35	63.5725	19	26.43	19.4405
SOHH	Sólaheimaheiði	NE9214	63	32.54	63.54233	19	15.29	19.25483
SOLH	Sólheimar	NE9215	63	30.26	63.50433	19	18.19	19.30317
STEI	Steinsholt	NE94005	63	40.37	63.67283	19	36.31	19.60517

Tiltstations

Code	Station name	Number	Lat	Lat	Lat	Lon	Lon	Lon
fimmv	Fimmvörðuháls	NE9203	63	36.24	63.604	19	26.15	19.43583
dagm	Dagmálafjall	NE9414	63	37.53	63.6255	19	49.29	19.8215

University of Lund
Department of Mineralogy and
Petrology
Sölvegatan 13
S – 222 21 LUND
SWEDEN

Nordic Volcanological
Institute 9901
University of Iceland
Grensásvegur 50
IS – 108 Reykjavík
ICELAND

1992-1998
Seismicity and Deformation
at
Mt. Eyjafjallajökull volcano

by

Malou Blomstrand Stinessen

A thesis
submitted to the Unversity of Lund
for
Master degree
February 1999

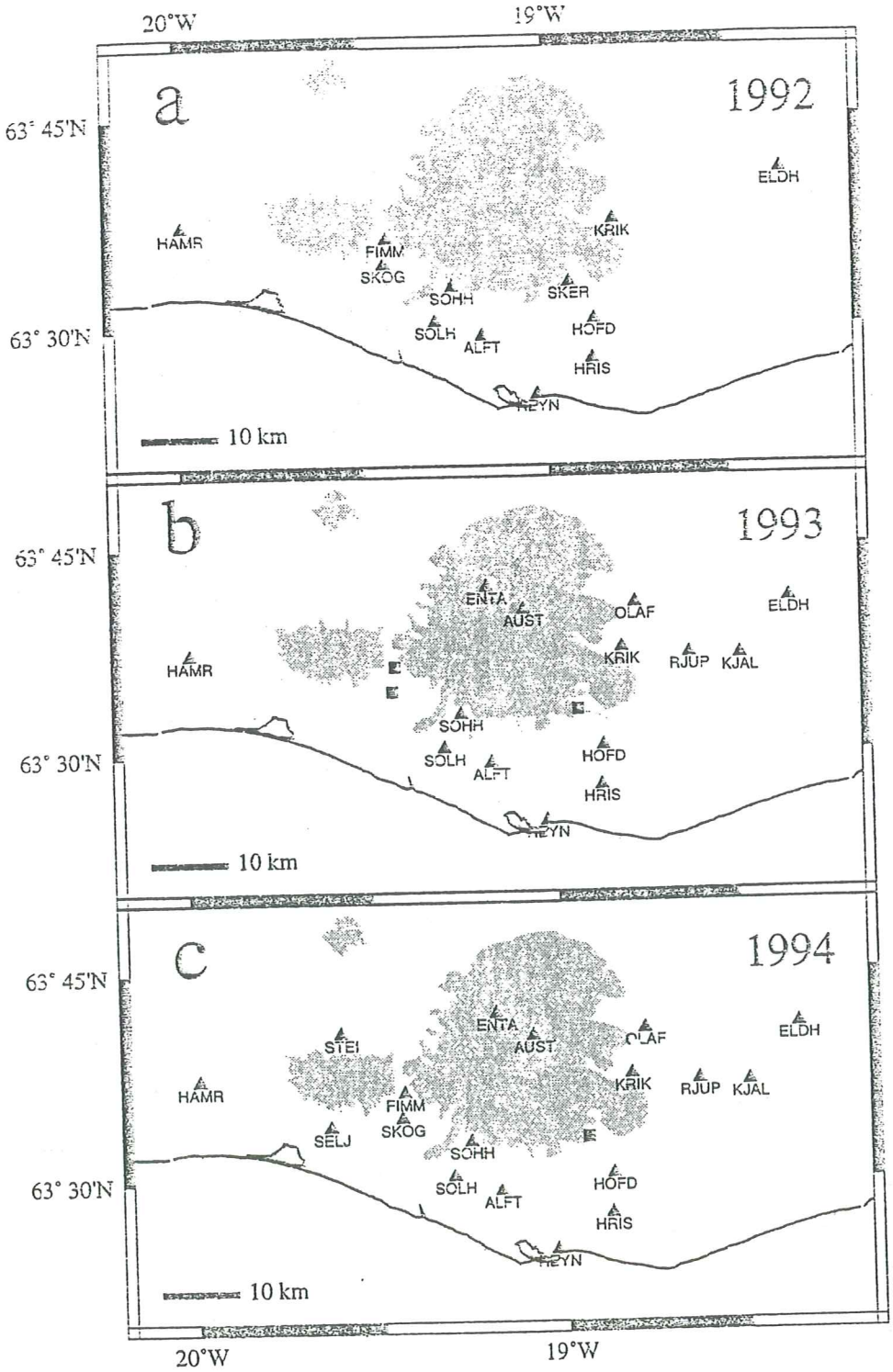

Figure 2.2: a) Points occupied in 1992. b) The whole network in 1993, three points were not measured that year (squares). c) The network was all measured in 1994, except one point (square).

GPS measurments: scaling factors and errors

1992				
Hamr		0.002	0.0027	0.011
Skog		0.002	0.0027	0.011
Reyn		0.002	0.0027	0.011
1994Ab				
Hamr	Selj	0.001	0.001	0.003
Stei	Selj	0.001	0.001	0.003
1994B				
Fimm	Reyn	0.003	0.002	0.014
Hamr	Reyn	0.003	0.003	0.015
Stei	Reyn	0.003	0.003	0.015
Selj	Reyn	0.002	0.002	0.011
1998				
Fimm	Hamr	0.001	0.001	0.008
Reyn	Hamr	0.002	0.002	0.01
Stei	Hamr	0.002	0.001	0.008
Skog	Hamr	0.002	0.002	0.01
Dagm	Hamr	0.001	0.001	0.001
Selj	Hamr	0.001	0.001	0.006

GPS stations measured in 1992, 1994 and 1998 around Mt. Eyjafjallajökull

1992

92	219	220	221	222	223	224	225
HAMR				0.1	0.1	0.1	0
REYN	1	0.1	0.1				
SKOG			0.1	0.1			

*: two 12hour-sessions / day

1994

94Aa	147	148	149	150	151
REYN	1.2	0.1.2	0.1.2	0.1.2	0.1.2
AUST	1.2	0.1.2			
ENTA	1.2	0.1			
KJAL			2	0.1	
KRIK			2	0.1.2	
OLAF				2	0.1
RJUP				2	0.1
SOHH		2	0.1		
SOLH		2	0.1		

*: three 7:55hour-sessions / day

94Ab	153	154	155	156	157
HAMR	2	0.1.2	0.1.2	0.1.2	0.1.2
SELJ	2	0.1.2	0.1.2	0.1.2	0.1.2
STEI		0.1.2	0.1.2	0.1.2	0.1.2

*: three 7:55hour-sessions / day

94B	261	262	263	264	265
REYN	1.2	0.1.2	0.1.2	0.1.2	0.1.2
ALFT				2	0.1
FIMM		2	0.1		
HAMR			2	0.1	
HOFD	2	0.1			
HRIS	1.2	0.1			
SELJ				2	0.1
SKOG		1.2	0		
STEI			2	0.1	

*: three 7:55hour-sessions / day

1998

98	184	185	186	187	188
HAMR	1.2	0.1.2	0.1.2	0.1.2	0.1
DAGM			2	0.1.2	0.1
FIMM	1.2	0.1			
REYN	1.2	0.1			
SELJ				1.2	0.1
SKOG		1.2	0.1		
STEI		1.2	0.1.2	0	

*: three 7:55hour-sessions / day

EYJAFJALLAJOKULL 1994Aa

Scatter Plot

Height

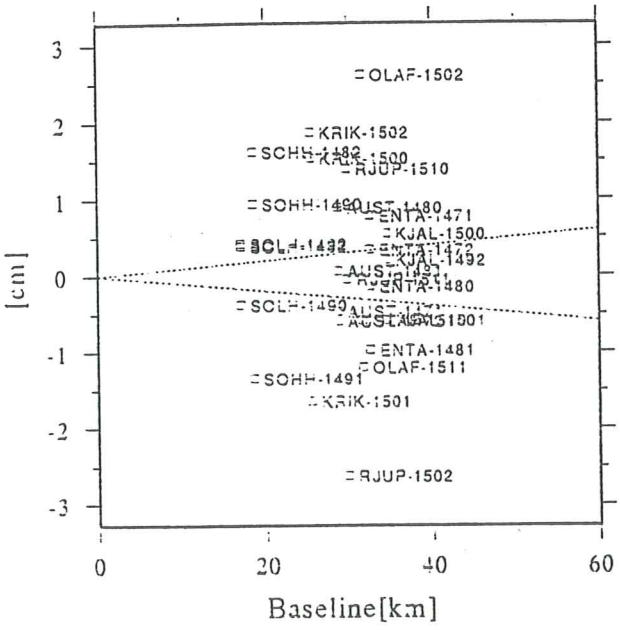

Length

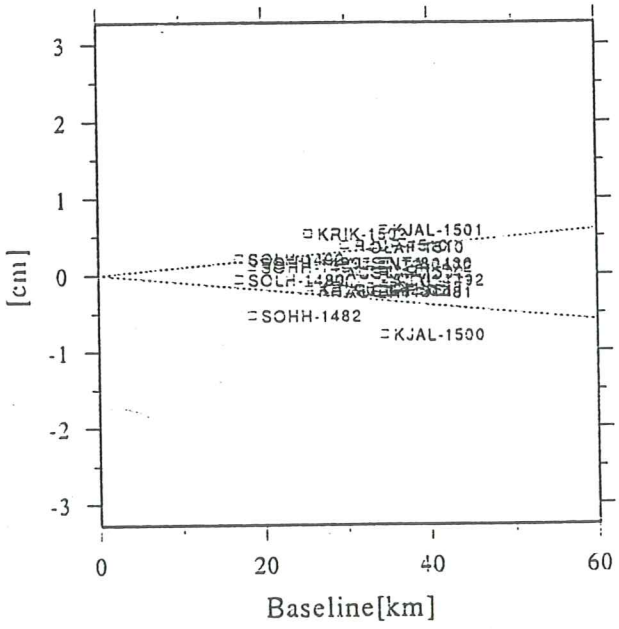

N-S

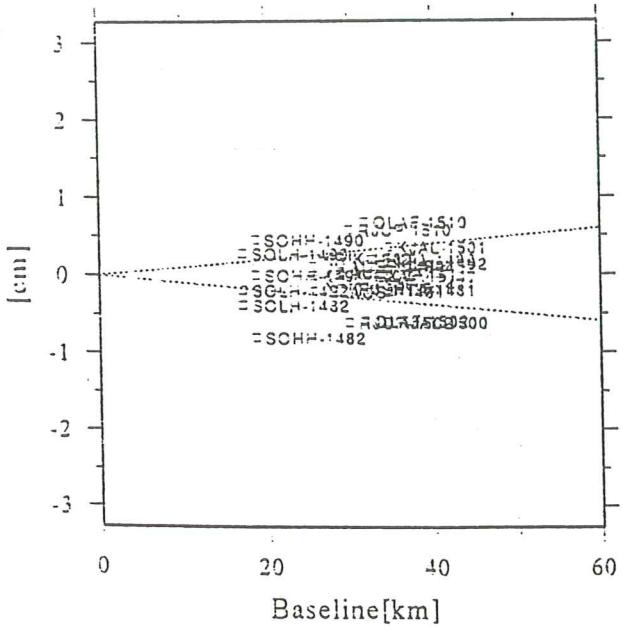

E-W

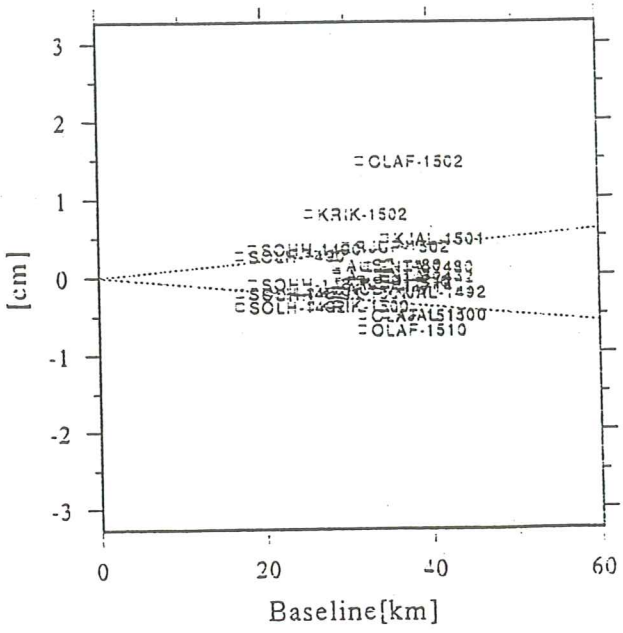

EYJAFJALLAJOKULL 1994Aa

Repeatabilities

Height

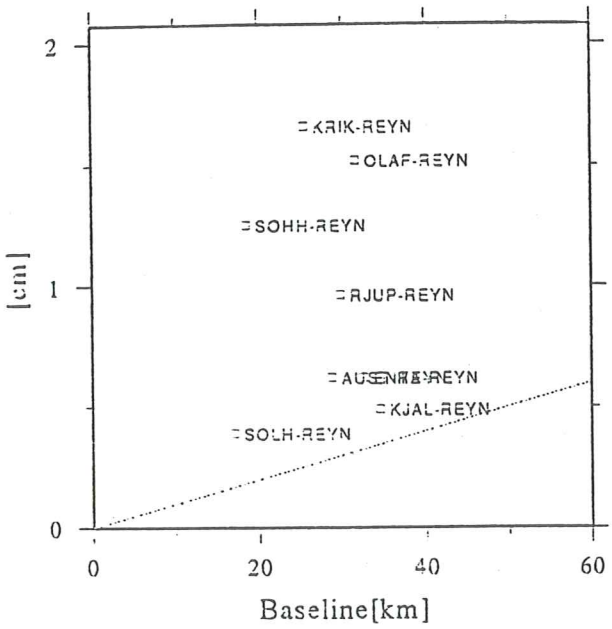

Length

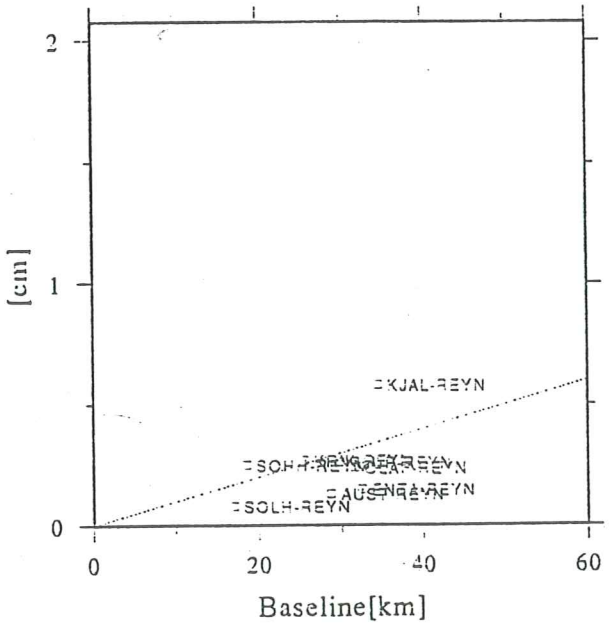

N-S

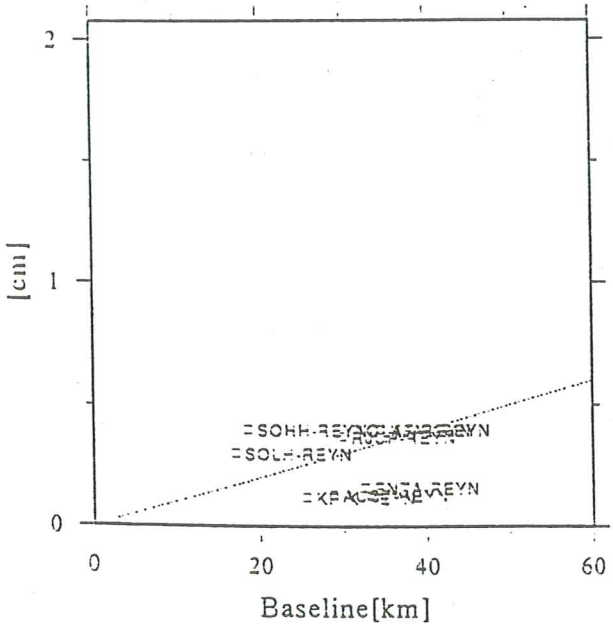

E-W

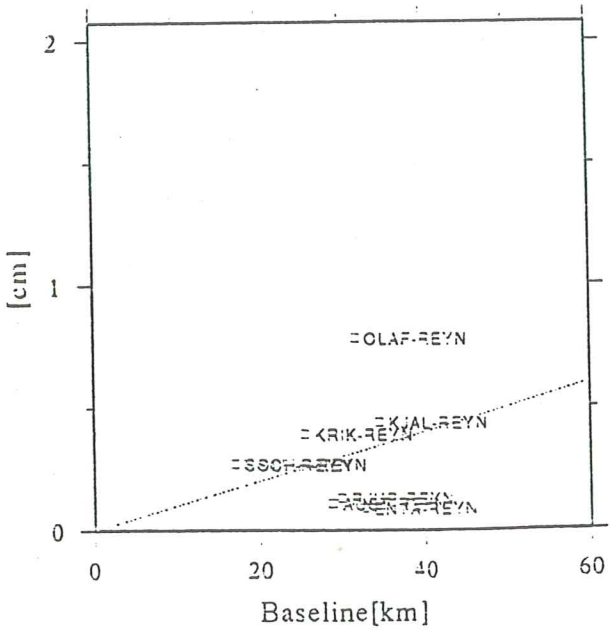

9294Ab98HAMR.CRD
1992 EYJAFJALLAJOKULL 22-SEP-98 16:

LOCAL GEODETIC DATUM: WGS - 84 EPOCH: 1992-07-05 13:03:00

NUM	STATION NAME	X (M)	Y (M)	Z (M)	FLAG
3	HAMR	2670302.5494	-971158.2182	5691289.1915	F
4	REYN	2705472.8456	-933012.9067	5681273.9634	M
6	SKOG	2683884.0701	-947544.6983	5689465.1548	M

9294B98HAMR.CRD
1992 EYJAFJALLAJOKULL 22-SEP-98 16:

LOCAL GEODETIC DATUM: WGS - 84 EPOCH: 1992-07-05 13:03:00

NUM	STATION NAME	X (M)	Y (M)	Z (M)	FLAG
3	HAMR	2670302.5494	-971152.9170	5691289.1915	F
4	REYN	2705472.8456	-933007.6055	5681273.9634	M
6	SKOG	2683884.0701	-947539.3971	5689465.1548	M

92xyz.final
South Iceland 1992, FINAL solution using CODE orbits (ITRF91 ref frame).

17 0s16	2705475.2092	-933010.2561	5681268.8377	p2t25
0s34	2670304.9130	-971155.5676	5691284.0658	p2t
26 0s35	2683886.4337	-947542.0477	5689460.0291	p2t

94AbHAMR.CRD
EYJAFJALLAJOKULL 21-AUG-98 09:5

LOCAL GEODETIC DATUM: WGS - 84

NUM	STATION NAME	X (M)	Y (M)	Z (M)	FLAG
7	HAMR	2670302.5494	-971152.9170	5691289.1915	M
9	SELJ	2681919.6047	-956708.2033	5688409.8692	M
11	STEI	2671552.0013	-951742.5477	5694106.6743	M

GRR92.CRD
1992 EYJAFJALLAJOKULL 22-SEP-98 16:09

LOCAL GEODETIC DATUM: WGS - 84 EPOCH: 1992-07-05 13:03:00

NUM	STATION NAME	X (M)	Y (M)	Z (M)	FLAG
3	HAMR	2670304.9130	-971155.5676	5691284.0658	F
4	REYN	2705475.2092	-933010.2561	5681268.8377	M
6	SKOG	2683886.4337	-947542.0477	5689460.0291	M

GRR94Aa.CRD
1994 EYJAFJALLAJOKULL 18-SEP-98 15:41

LOCAL GEODETIC DATUM: WGS - 84 EPOCH: 1994-05-29 12:24:30

NUM	STATION NAME	X (M)	Y (M)	Z (M)	FLAG
6	REYN	2705472.8509	-933007.5978	5681273.9768	F
2	AUST	2680944.9531	-927340.5641	5695003.1429	M
3	ENTA	2676766.0729	-931217.9584	5696308.7503	M
17	SOLH	2692559.5153	-943200.8591	5685664.8304	M
16	SOHH	2689665.4407	-939700.7809	5688175.3187	M
12	KJAL	2695261.1776	-901510.8630	5690959.3069	M
13	KRIK	2689306.2277	-916317.4065	5691660.2994	M
14	OLAF	2684728.2900	-913029.2748	5694242.1836	M
15	RJUP	2692841.8714	-907935.8103	5691131.4506	M

GRR94Aa.llh
1994 EYJAFJALLAJOKULL 18-SEP-98 15:41

LOCAL GEODETIC DATUM: WGS - 84 EPOCH: 1994-05-29 12:24:30

num	station name	latitude	longitude	H (m)
1	REYN	63.41850500	-19.02723234	301.6857
2	AUST	63.67440304	-19.08053547	1441.3574
3	ENTA	63.70111803	-19.18223286	1424.9370
4	SOLH	63.50713782	-19.30530577	275.4958
5	SOHH	63.54839203	-19.25811757	789.8493
6	KJAL	63.61622519	-18.49405588	141.7497
7	KRIK	63.62630036	-18.81532767	367.2039
8	OLAF	63.67993382	-18.78227339	287.3113
9	RJUP	63.61890482	-18.63237791	185.7406
10		NaN	NaN	NaN

GRR94Ab.CRD
EYJAFJALLAJOKULL 21-AUG-98 09:55

LOCAL GEODETIC DATUM: WGS - 84

NUM	STATION NAME	X (M)	Y (M)	Z (M)	FLAG
1	ALFT	2696288.6011	-937743.2561	5684733.6149	M
2	AUST	2680996.8547	-927340.7096	5695029.5739	R
3	ENTA	2676818.1440	-931217.7841	5696336.5822	R
4	FIMM	2681271.5392	-946205.4956	5691189.2404	M
5	HRIS	2703894.9602	-924551.6066	5683328.4798	M

6	REYN	2705472.8509	-933007.5978	5681273.9768	R
7	HAMR	2670302.5723	-971152.9418	5691289.2096	M
8	HOFD	2699486.7140	-922686.7567	5685746.5140	M
9	SELJ	2681919.6276	-956708.2281	5688409.8873	M
10	SKOG	2683884.1048	-947539.3549	5689465.1425	M
11	STEI	2671552.0242	-951742.5725	5694106.6924	M
12	KJAL	2695260.3371	-901508.7621	5690943.9989	R
13	KRIK	2689297.1396	-916312.9627	5691627.1206	R
14	OLAF	2684774.4254	-913028.6298	5694244.0118	R
15	RJUP	2692821.9719	-907907.5022	5691087.9648	R
16	SOHH	2689666.8235	-939706.4115	5688092.1513	R
17	SOLH	2692548.4123	-943194.4522	5685675.9266	R

GRR94Ab.llh 21-AUG-98 09:55
EYJAFJALLAJOKULL

LOCAL GEODETIC DATUM: WGS - 84

num	station name	latitude	longitude	H (m)
1	ALFT	63.48958388	-19.17718331	210.6368
2	AUST	63.67411349	-19.08019558	1486.8207
3	ENTA	63.70083366	-19.18188365	1471.6522
4	FIMM	63.60672929	-19.43764748	923.6627
5	HRIS	63.46075733	-18.87726418	244.0727
6	REYN	63.41850500	-19.02723234	301.6857
7	HAMR	63.62249035	-19.98564256	163.6052
8	HOFD	63.50876659	-18.87046991	276.2685
9	SELJ	63.56251773	-19.63259661	268.6016
10	SKOG	63.57649223	-19.44546658	672.6693
11	STEI	63.67710446	-19.60848245	292.1798
12	KJAL	63.61617593	-18.49402109	127.3858
13	KRIK	63.62624880	-18.81530195	333.0204
14	OLAF	63.67959157	-18.78196092	308.2245
15	RJUP	63.61895570	-18.63196526	134.3861
16	SOHH	63.54803433	-19.25821530	716.7975
17	SOLH	63.50728336	-19.30525806	279.8075
18	NaN	NaN	NaN	
19	NaN	NaN	NaN	

GRR94B.CRD 09-AUG-98 18:00
1994 EYJAFJALLAJOKULL

LOCAL GEODETIC DATUM: WGS - 84 EPOCH: 1994-09-20 13:10:15

NUM	STATION NAME	X (M)	Y (M)	Z (M)	FLAG

6	REYN	2705472.8509	-933007.5978	5681273.9768	F
5	HRIS	2703894.9601	-924551.6066	5683328.4798	M
8	HOFD	2699486.7140	-922686.7567	5685746.5140	M
10	SKOG	2683884.1048	-947539.3549	5689465.1426	M
4	FIMM	2681271.5393	-946205.4956	5691189.2404	M
7	HAMR	2670302.5494	-971152.9170	5691289.1915	M
11	STEI	2671551.9945	-951742.5516	5694106.6519	M
1	ALFT	2696288.6011	-937743.2561	5684733.6150	M
9	SELJ	2681919.6276	-956708.2281	5688409.8874	M

GRR94B.llh
1994 EYJAFJALLAJOKULL 09-AUG-98 18:00

LOCAL GEODETIC DATUM: WGS - 84 EPOCH: 1994-09-20 13:10:15

num	station name	latitude	longitude	H (m)
1	REYN	63.41850500	-19.02723234	301.6857
2	HRIS	63.46075733	-18.87726418	244.0727
3	HOFD	63.50876659	-18.87046991	276.2685
4	SKOG	63.57649223	-19.44546658	672.6694
5	FIMM	63.60672929	-19.43764748	923.6628
6	HAMR	63.62249052	-19.98564225	163.5756
7	STEI	63.67710458	-19.60848226	292.1280
8	ALFT	63.48958388	-19.17718331	210.6369
9	SELJ	63.56251773	-19.63259661	268.6017
10		NaN	NaN	NaN

GRR98.CRD
1998 EYJAFJALLAJOKULL 22-SEP-98 16:09

LOCAL GEODETIC DATUM: WGS - 84 EPOCH: 1998-07-05 13:03:00

NUM	STATION NAME	X (M)	Y (M)	Z (M)	FLAG
3	HAMR	2670302.5494	-971152.9170	5691289.1915	F
2	FIMM	2681271.5422	-946205.5036	5691189.2349	M
4	REYN	2705472.8622	-933007.5960	5681273.9750	M
7	STEI	2671552.0012	-951742.5570	5694106.6922	M
6	SKOG	2683884.1152	-947539.3642	5689465.1670	M
1	DAGM	2672538.3701	-964008.1702	5692111.0920	M
5	SELJ	2681919.6306	-956708.2272	5688409.8941	M

GRR98.llh
1998 EYJAFJALLAJOKULL 22-SEP-98 16:09

LOCAL GEODETIC DATUM: WGS - 84 EPOCH: 1998-07-05 13:03:00

num	station name	latitude	longitude	H (m)
1	HAMR	63.62249052	-19.98564225	163.5756
2	FIMM	63.60672922	-19.43764761	923.6602
3	REYN	63.41850492	-19.02723223	301.6886
4	STEI	63.67710468	-19.60848231	292.1677
5	SKOG	63.57649223	-19.44546668	672.6969
6	DAGM	63.62842539	-19.83482129	752.9054
7	SELJ	63.56251774	-19.63259658	268.6088

EYJAFJALLAJOKULL 1994Ab

Scatter Plot

Height

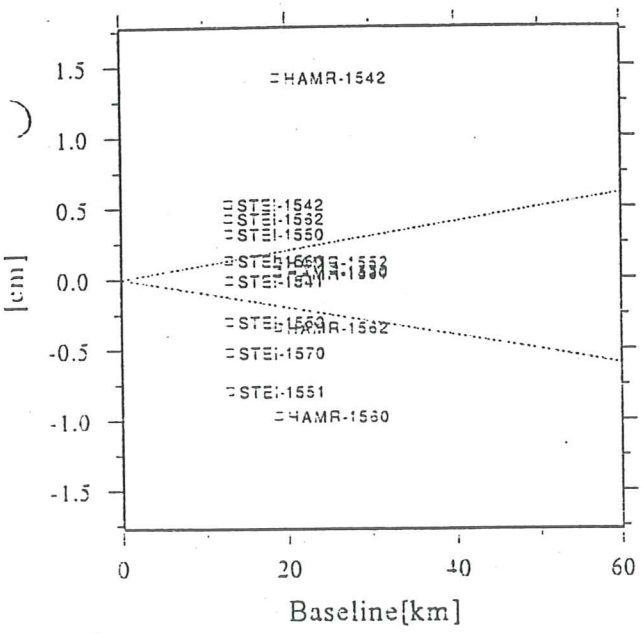

Length

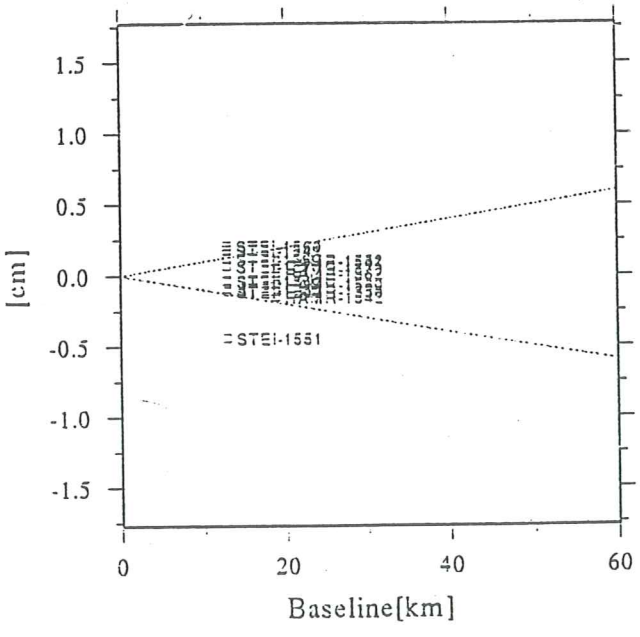

N-S

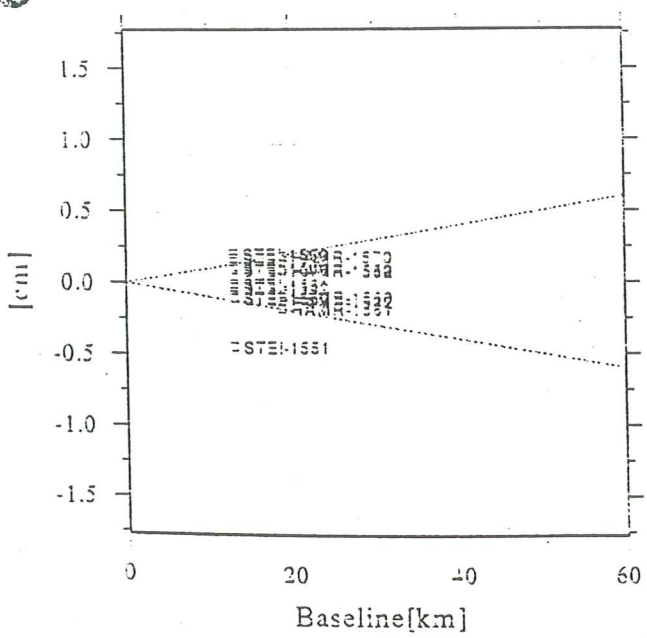

E-W

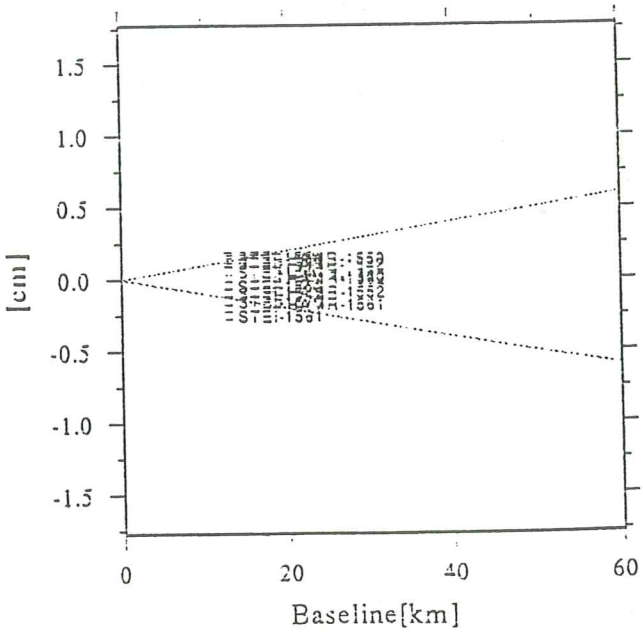

EYJAFJALLAJOKULL 1994Ab

Repeatabilities

Height

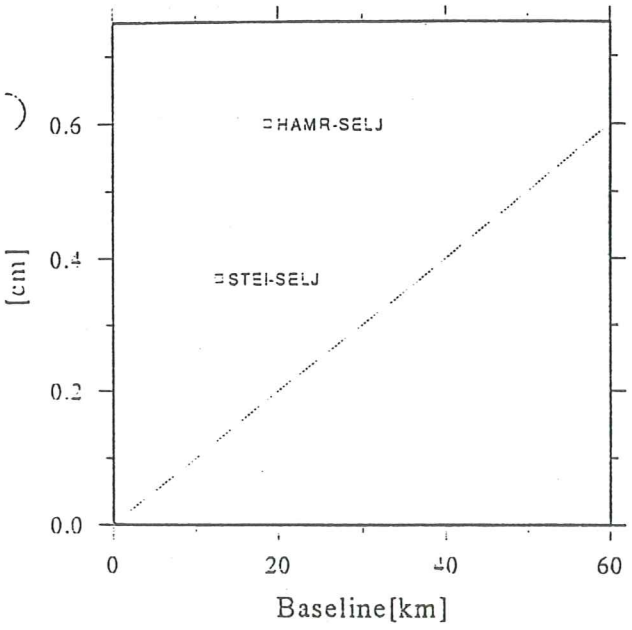

Length

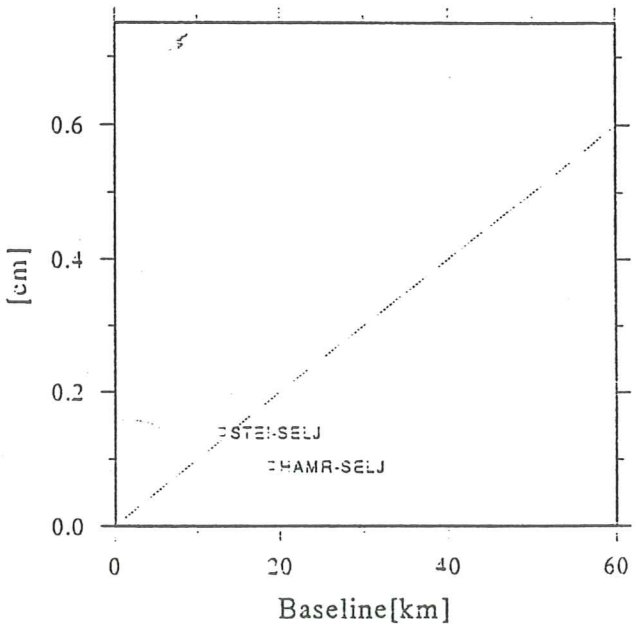

N-S

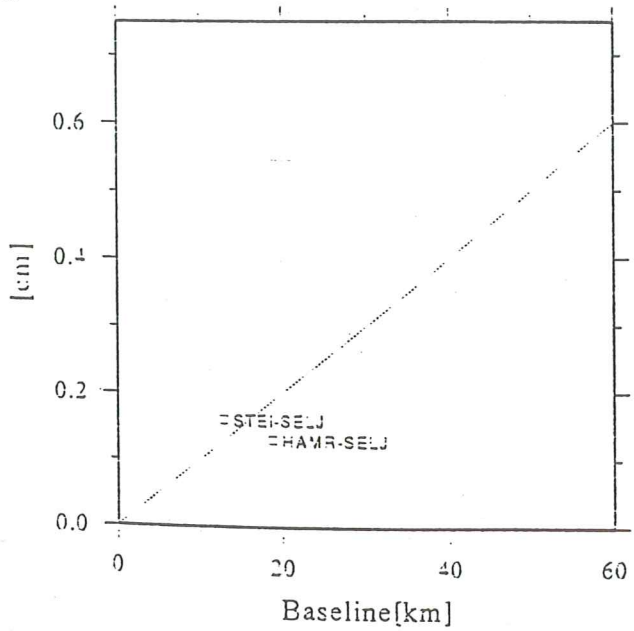

E-W

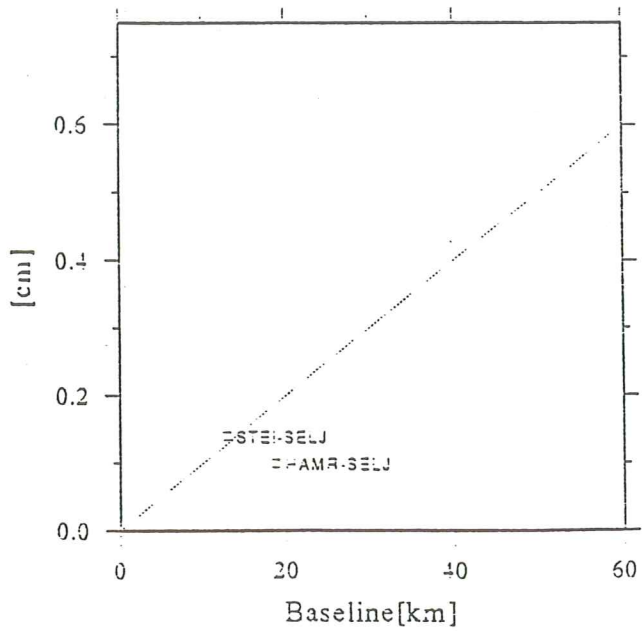

EYJAFJALLAJOKULL 1994B

Scatter Plot

Height

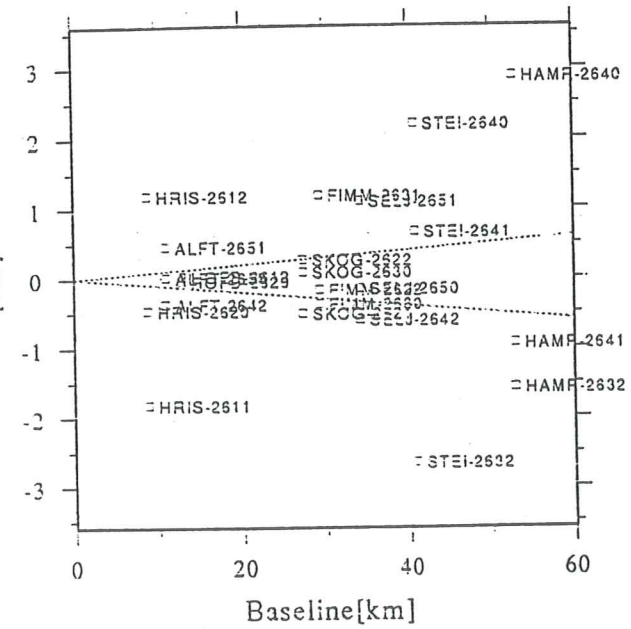

Length

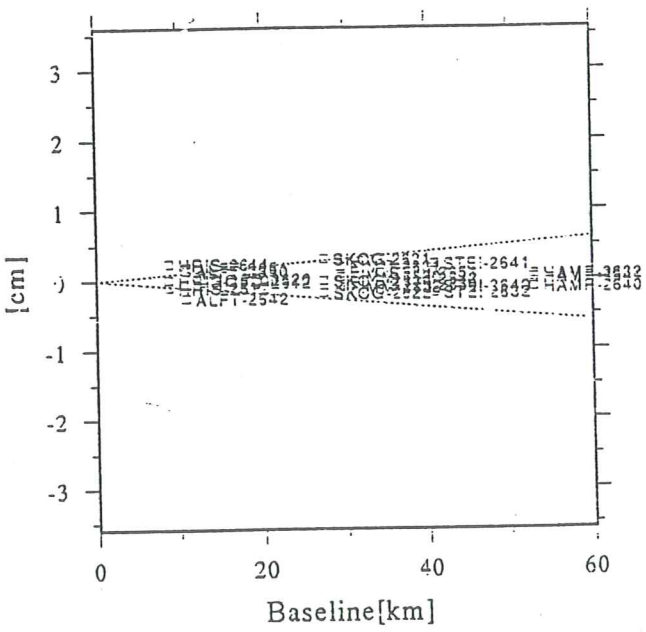

N-S

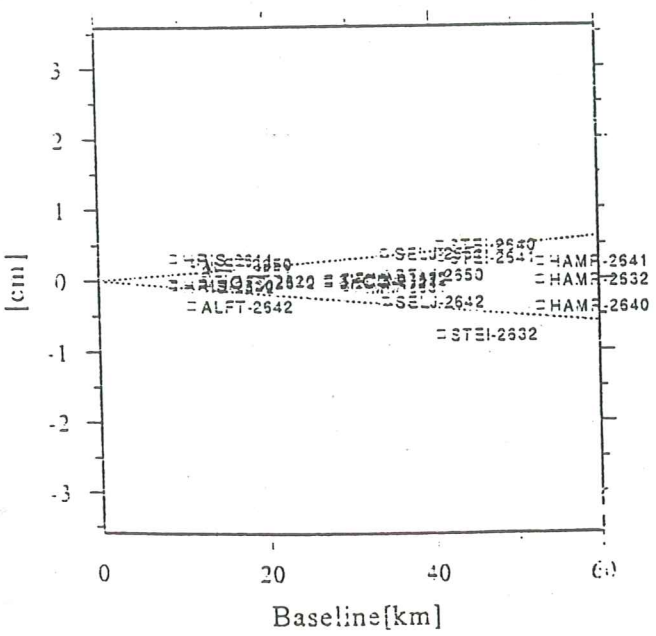

E-W

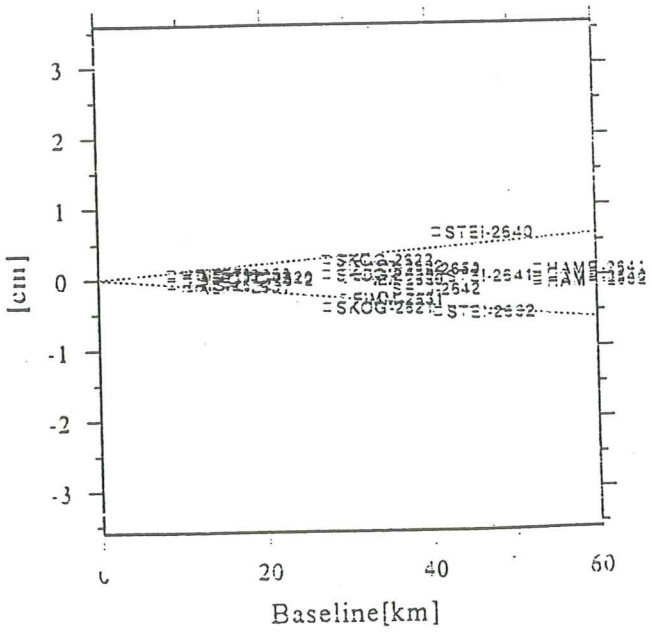

EYJAFJALLAJOKULL 1994B

Repeatabilities

Height

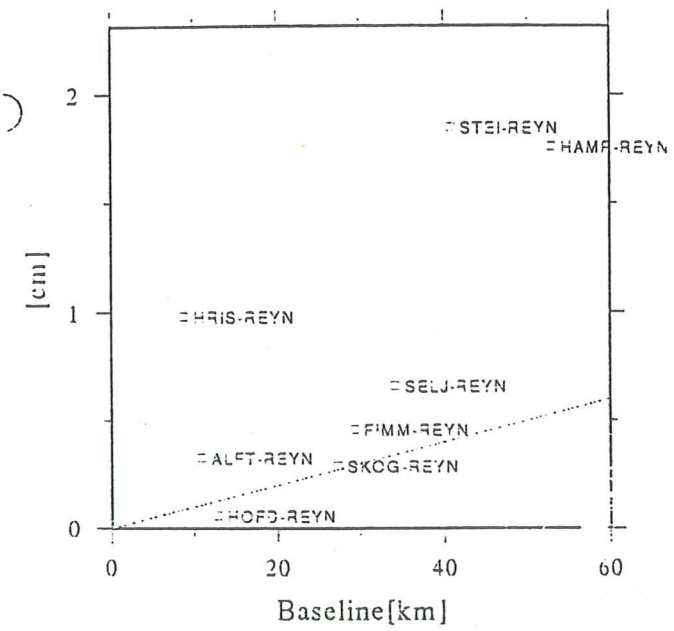

Length

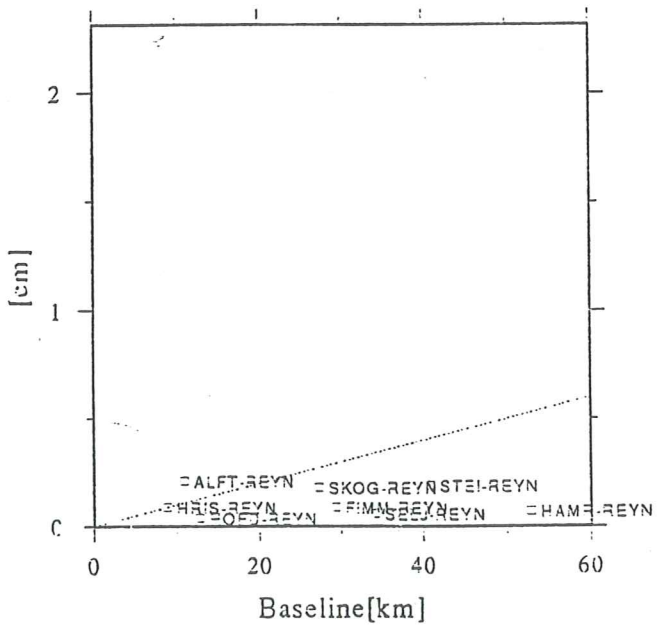

N-S

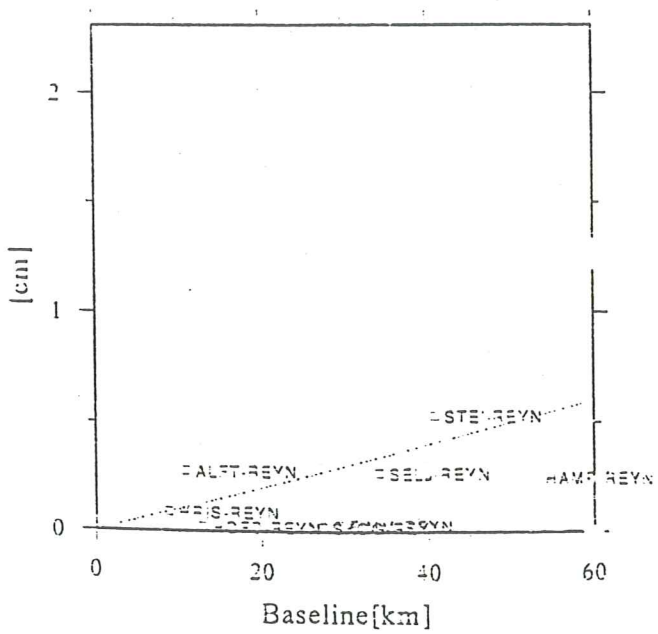

E-W

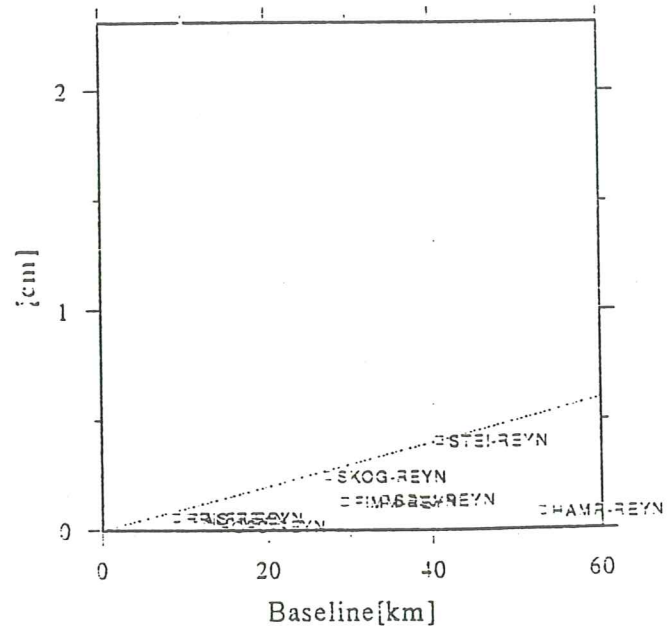

EYJAFJALLAJOKULL 1998

Scatter Plot

Height

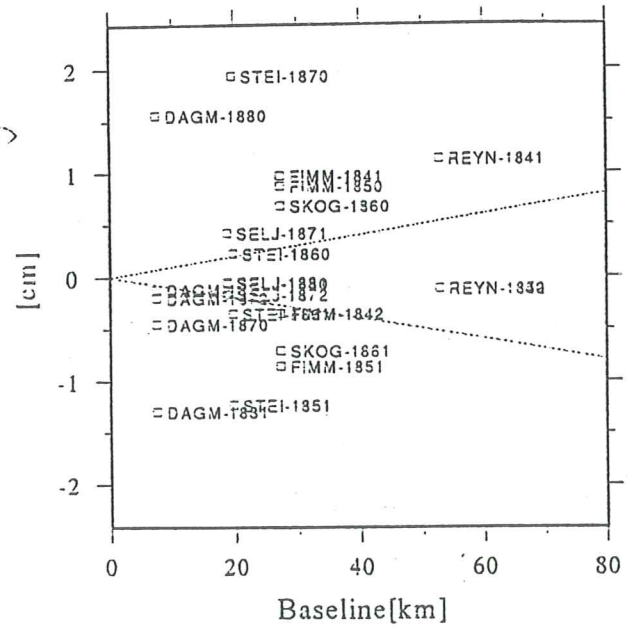

Length

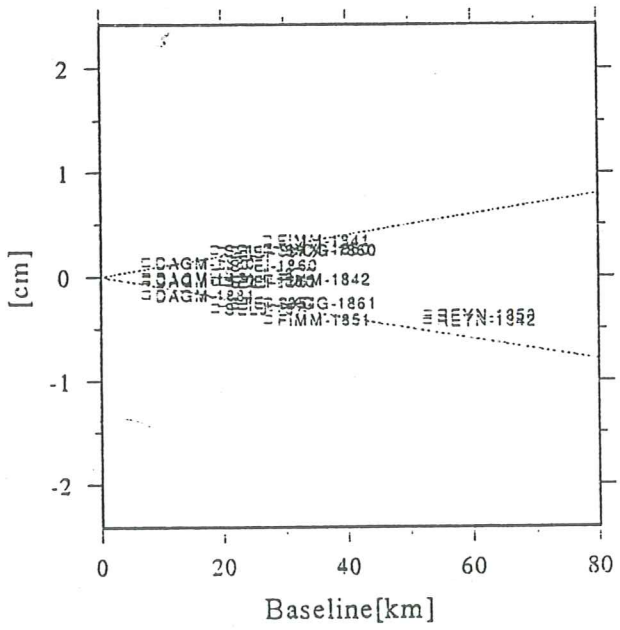

N-S

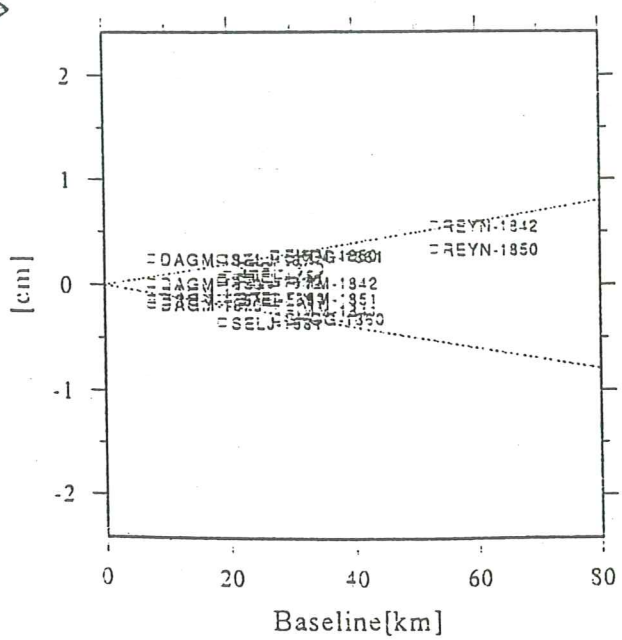

E-W

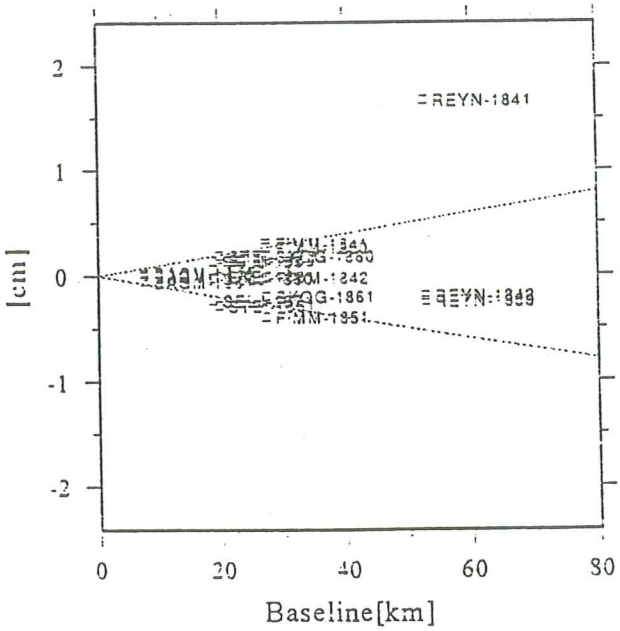

EYJAFJALLAJOKULL 1998

Repeatabilities

Height

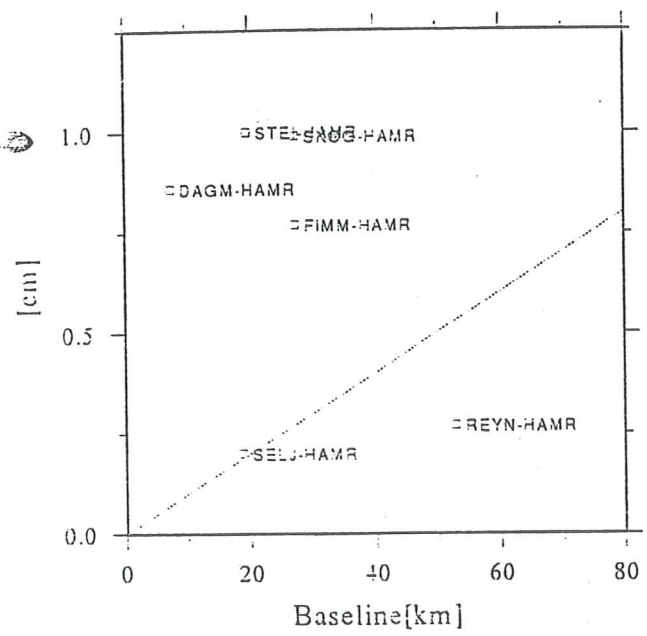

Length

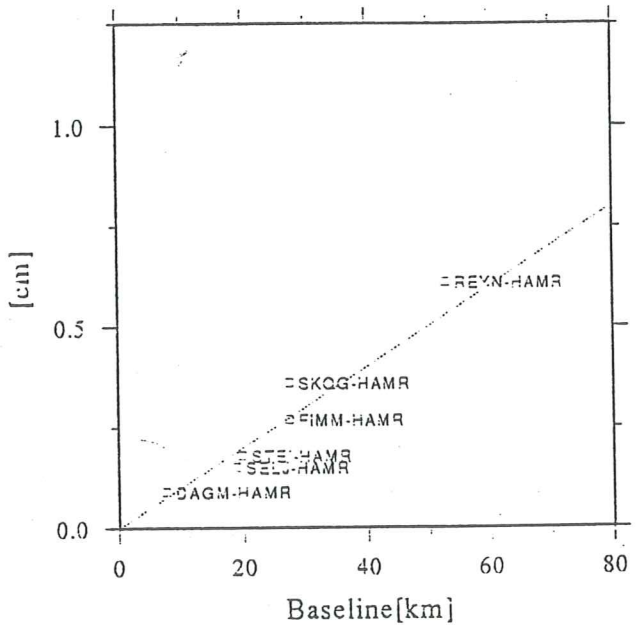

N-S

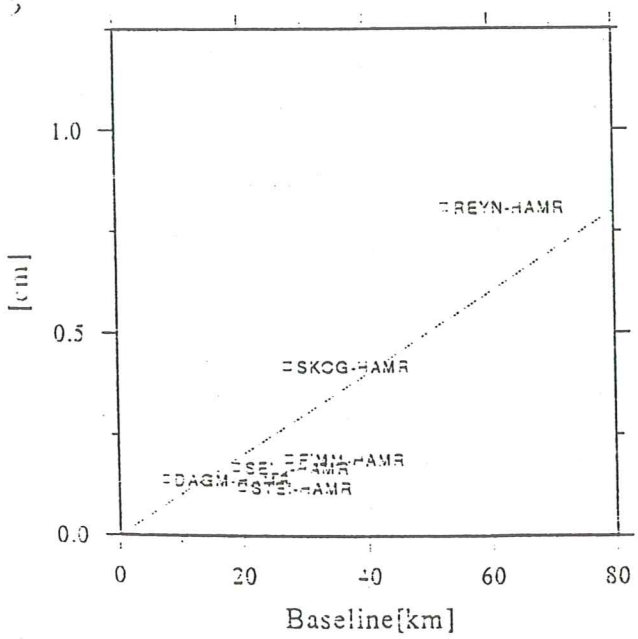

E-W

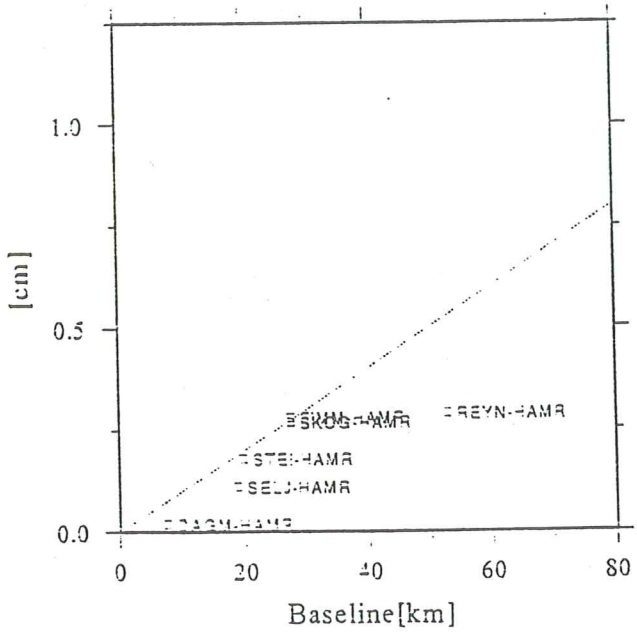

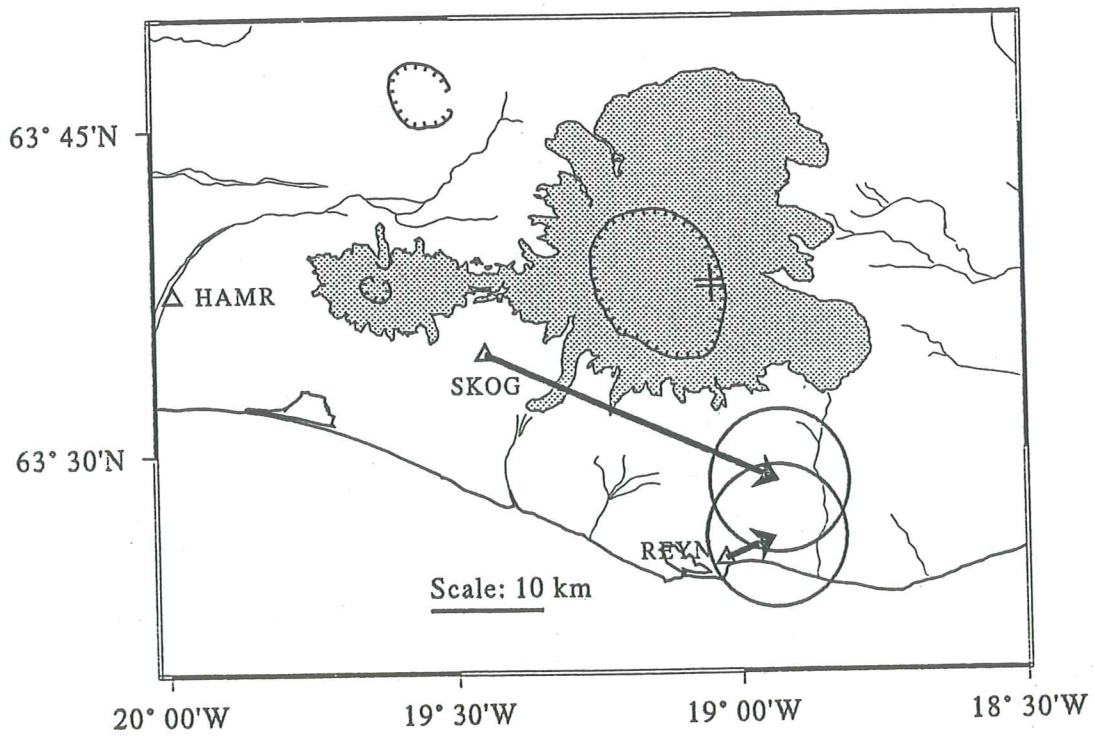
63° 45'N
63° 30'N
HAMR
SKOG
REYN
Scale: 10 km
20° 00'W
19° 30'W
19° 00'W
18° 30'W

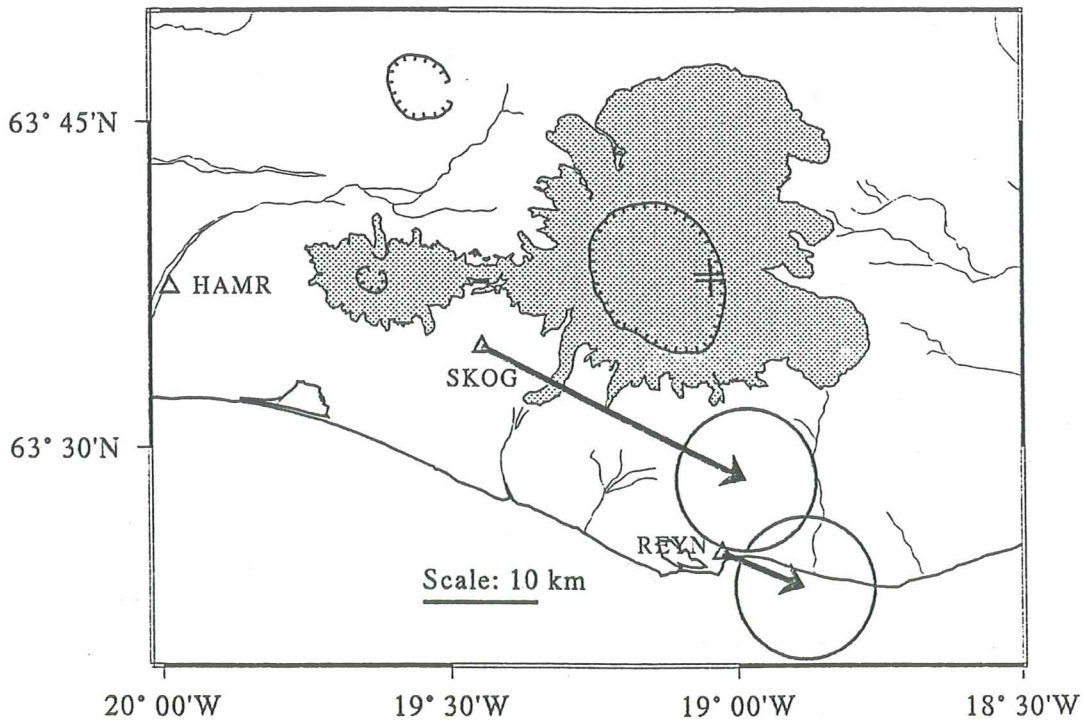
63° 45'N
63° 30'N
HAMR
SKOG
REYN
Scale: 10 km
20° 00'W
19° 30'W
19° 00'W
18° 30'W

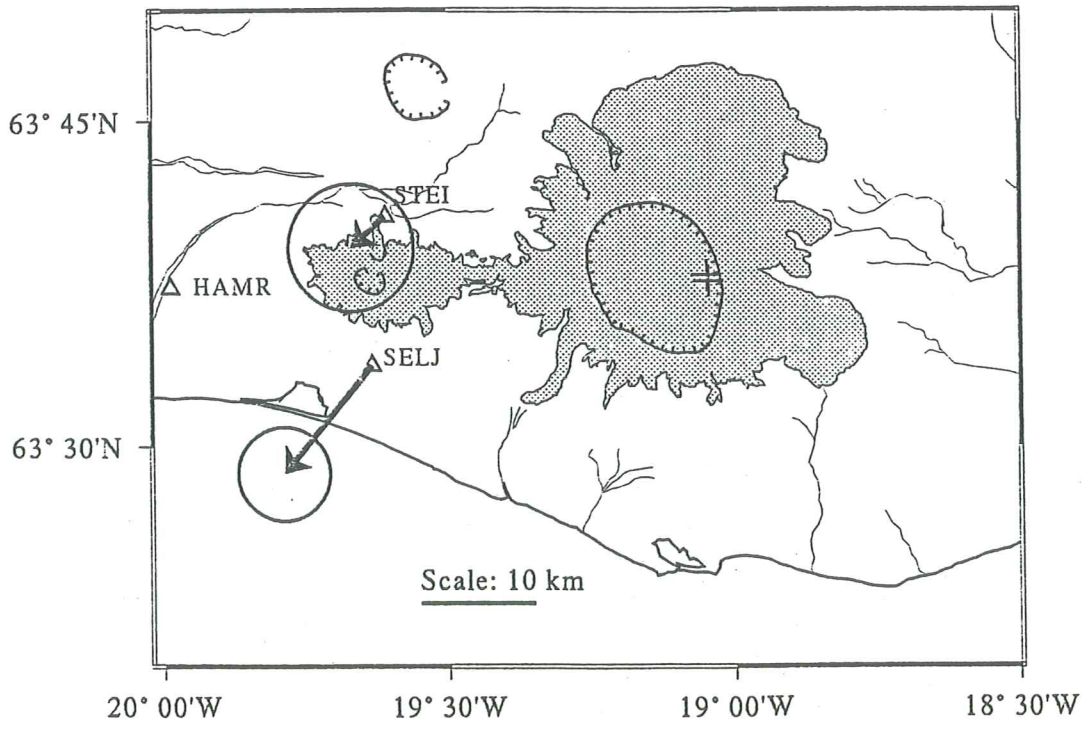
63° 45'N
63° 30'N
STEI
HAMR
SELJ
Scale: 10 km
20° 00'W
19° 30'W
19° 00'W
18° 30'W

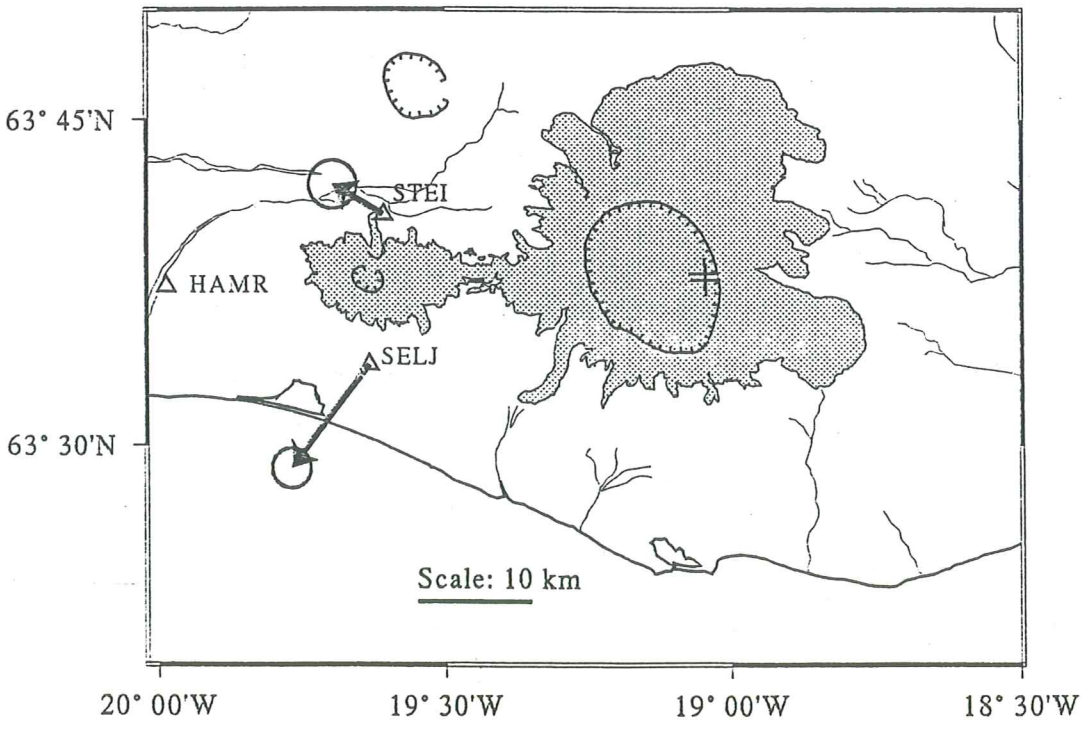
63° 45'N
63° 30'N
STEI
HAMR
SELJ
Scale: 10 km
20° 00'W
19° 30'W
19° 00'W
18° 30'W

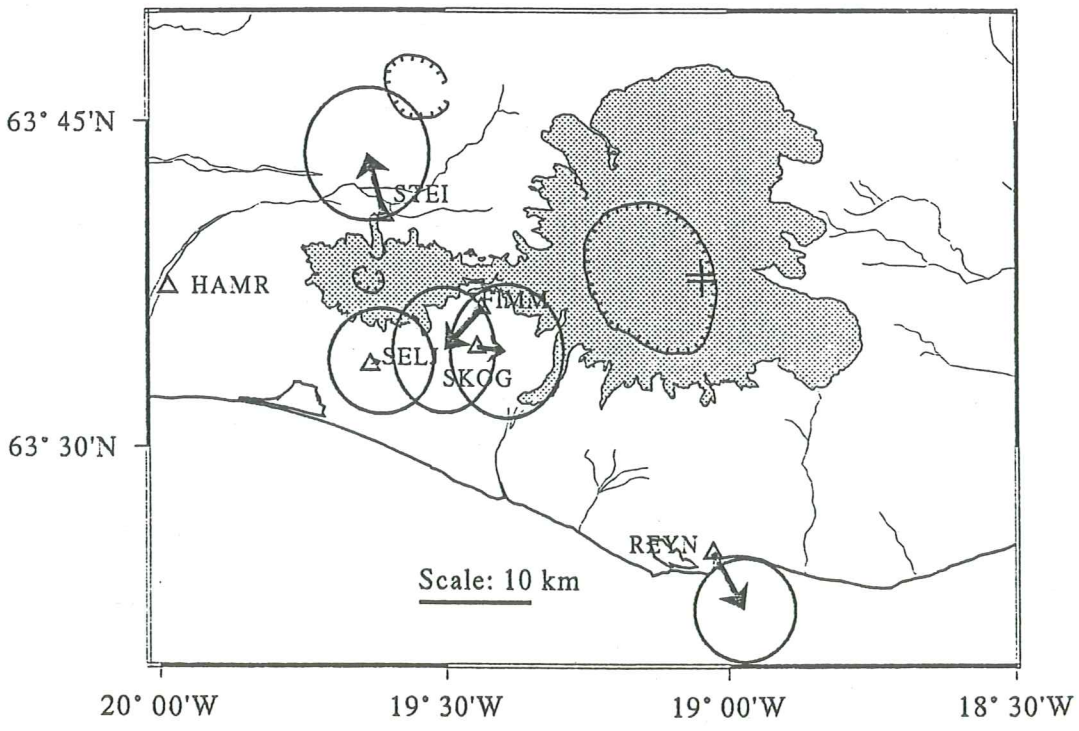
63° 45'N
63° 30'N
20° 00'W
19° 30'W
19° 00'W
18° 30'W
STEI
HAMR
HMM
SELJ
SKOG
REYN
Scale: 10 km

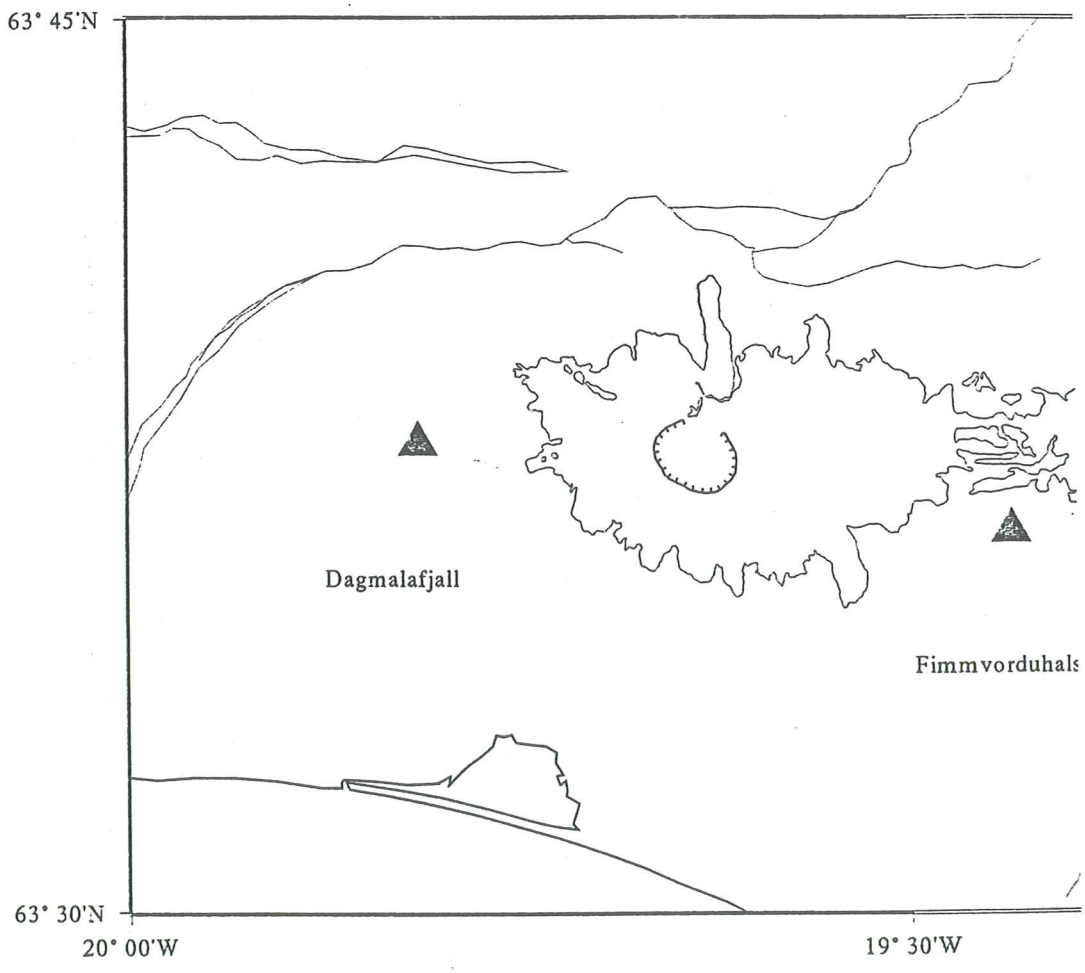

Scale: 10 km

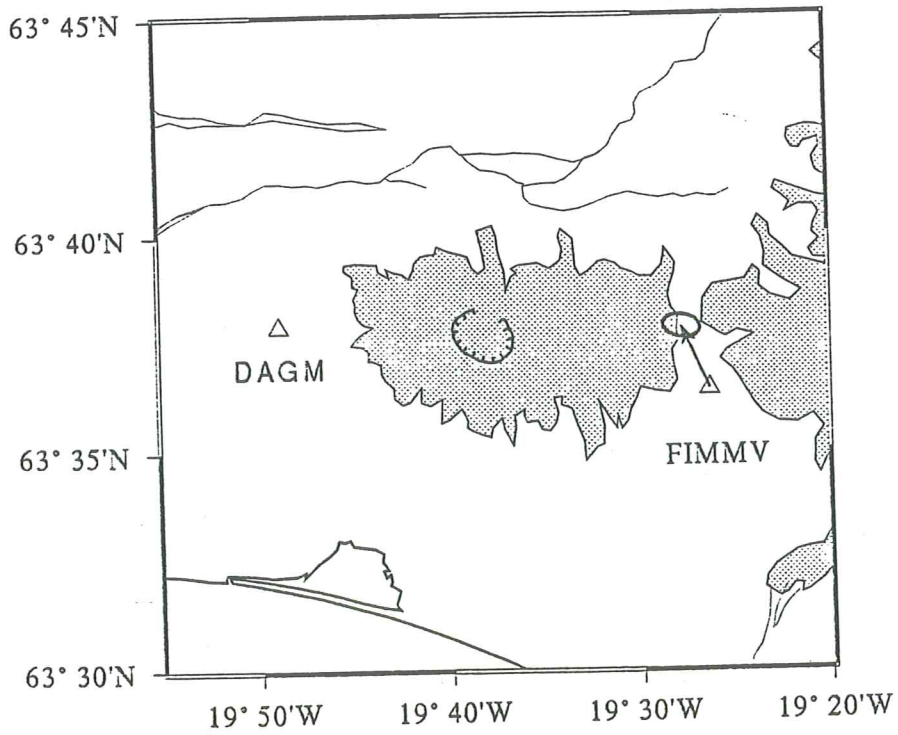

Scale: 10 km

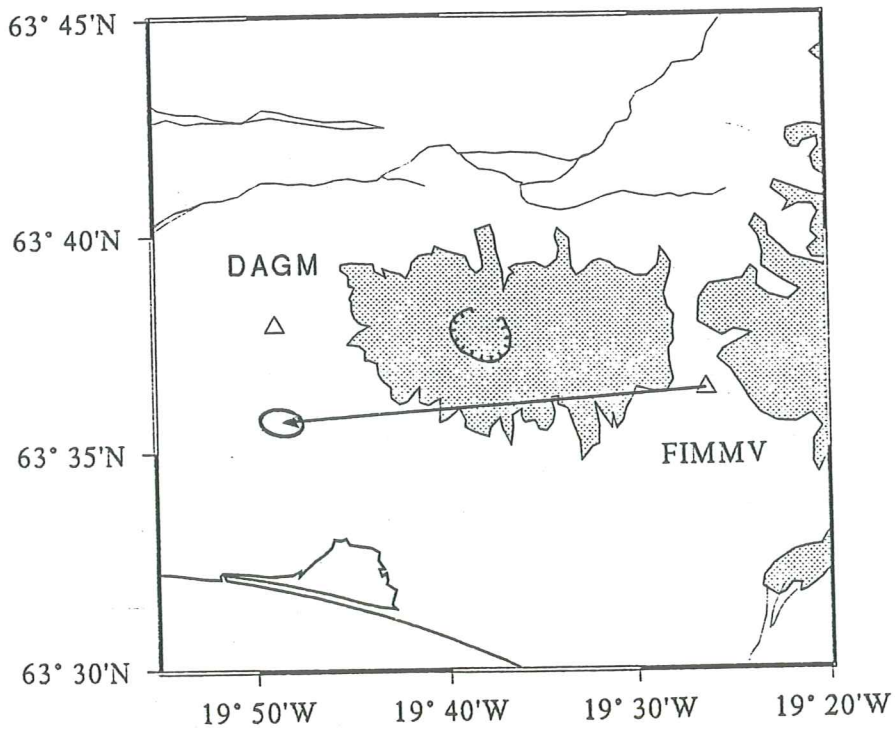

Scale: 10 km

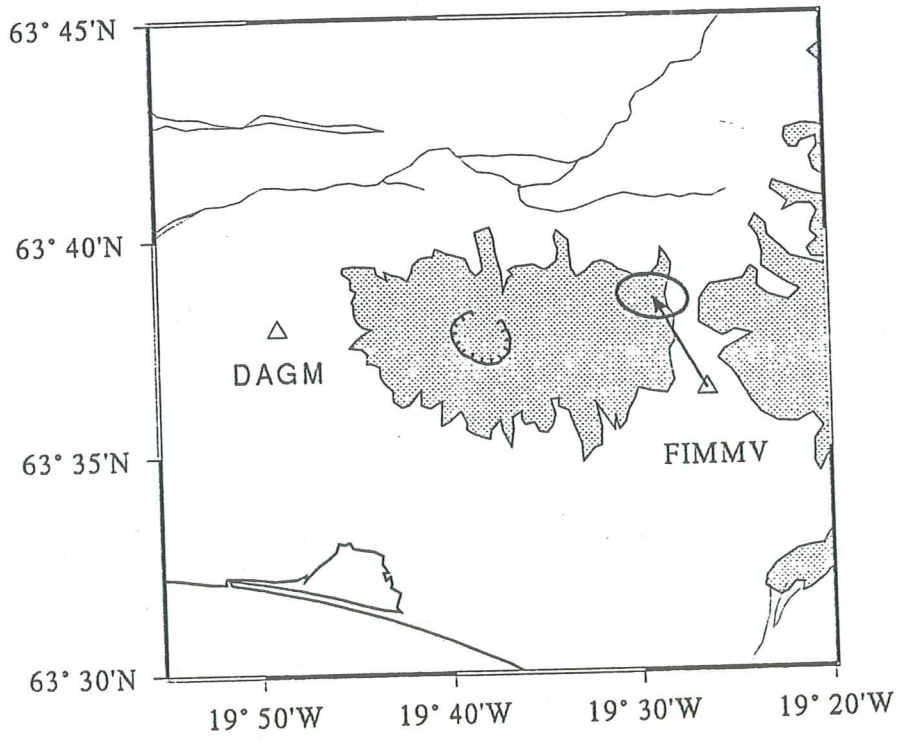

Scale: 10 km

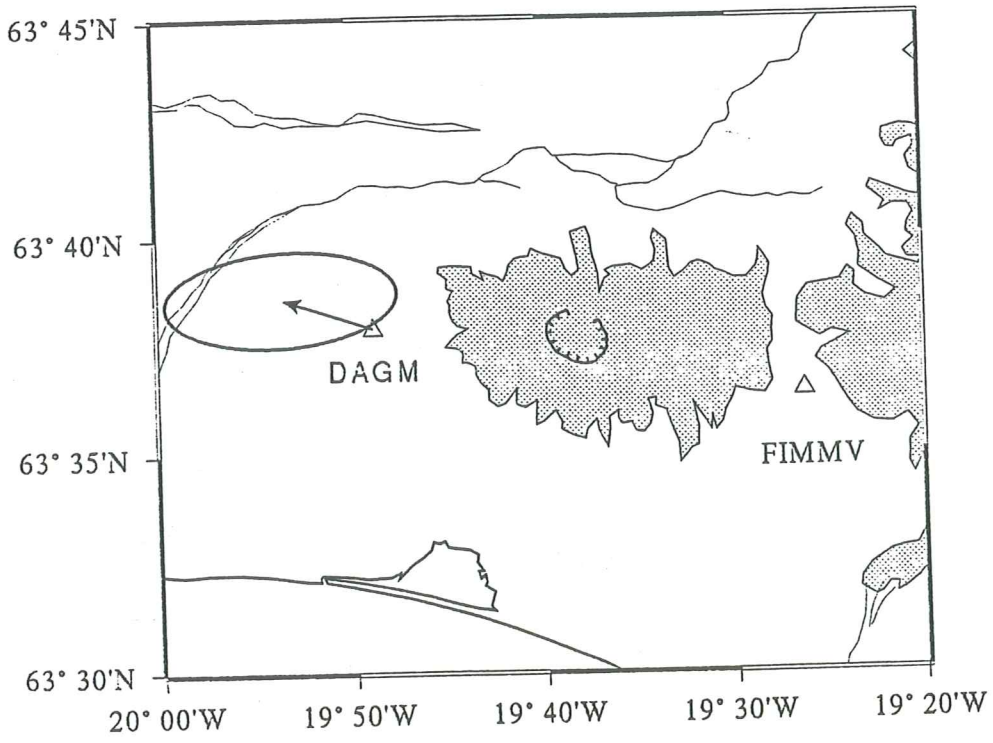
63° 45'N
63° 40'N
63° 35'N
63° 30'N
20° 00'W
19° 50'W
19° 40'W
19° 30'W
19° 20'W
DAGM
FIMMV

Scale: 10 km

1 sigma minor and major axis of uncertainty ellipsoids in the GPS measurments

	Minor (mm)	Major (mm)
1992-1994Ab		
REYN		
SKOG		
1992-1998		
REYN		
SKOG		
1994Ab-1994B		
STEI	1.73	1.73
SELJ	1.41	1.41
1994Ab-1998		
STEI	4.47	4.47
SELJ	3.32	3.32
1994B-1998		
FIMM	3.74	4.36
REYN	3.61	3.61
STEI	4.36	4.69
SKOG	4.12	4.69
SELJ	3.74	3.74

Modelled tilt for station Fimmvörðuháls at Mt. Eyjafjallajökull

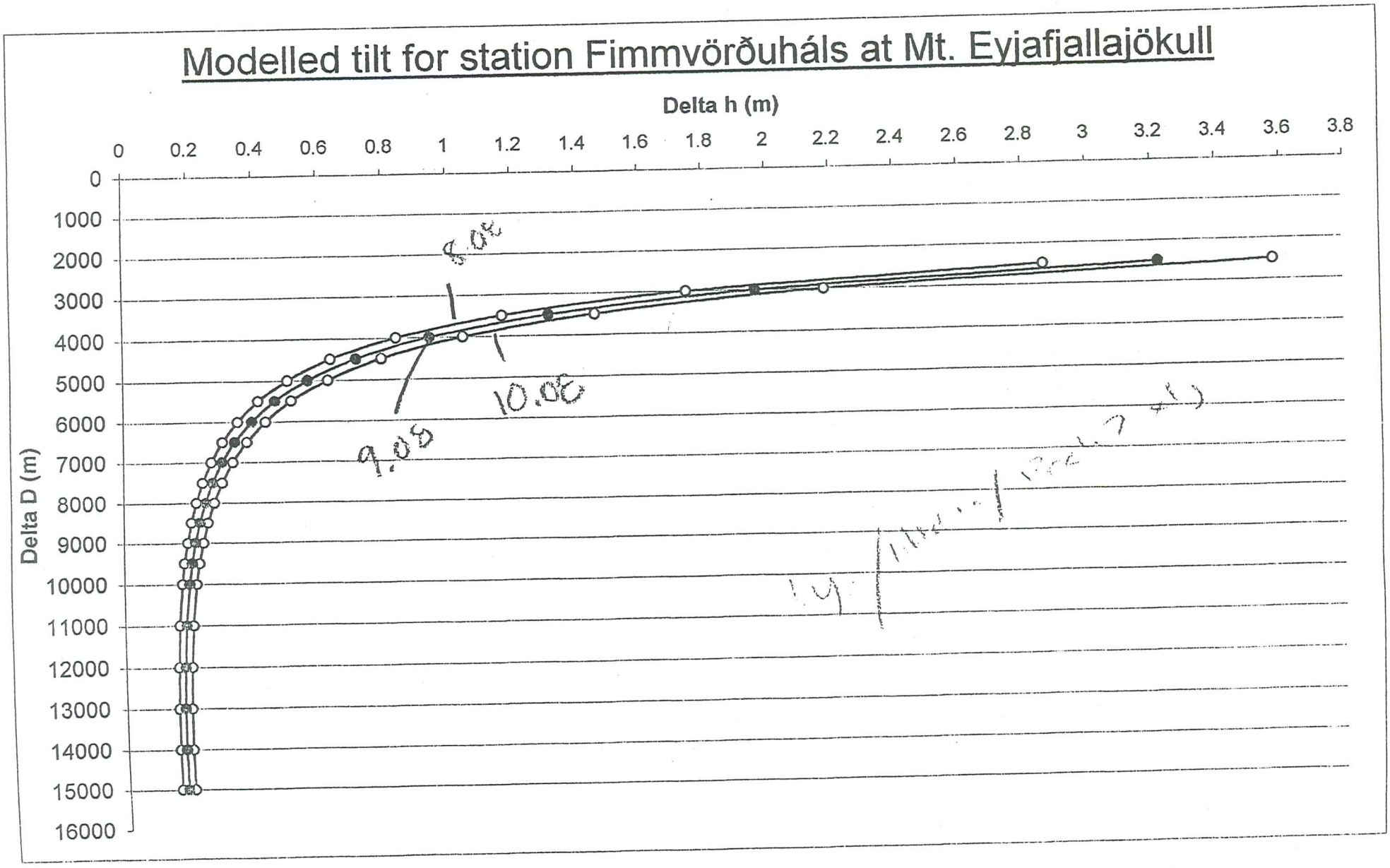

$$\Delta h_0 = tilt*R^5/-3*H^3r = tilt*((\sqrt{D^2+r^2})^5)/-3*H^3r$$

APPENDIXES

1~3

Earthquake locations with the SIL velocity model

Mean lat.: 63 39.0435; mean lon.:-19 34.27; mean D 3.8247km

day	hour	min	sec	Lat	Lon	D	nwr	gap	dmin	rms	erh	erz	Q
3	19	57	9.9	63.6532	-19.5790	5.05	16	75	2.4	0.08	0.3	0.4	a
4	0	37	45.41	63.6458	-19.5605	4.22	14	85	3.2	0.08	0.3	0.5	a
4	1	18	38.62	63.6518	-19.5333	6.32	8	240	3.1	0.03	0.7	1	c
4	1	52	32.72	63.6512	-19.5570	5.64	10	176	2.7	0.05	0.6	1	b
4	5	10	6.31	63.6495	-19.5705	5.34	19	78	2.8	0.07	0.2	0.4	a
4	5	16	16.14	63.6538	-19.5707	5.55	19	78	2.3	0.07	0.2	0.4	a
4	7	47	43.36	63.6537	-19.5712	7.35	8	160	2.4	0.06	0.8	1.1	b
4	13	22	11.14	63.6517	-19.5540	5.17	17	95	2.7	0.06	0.2	0.3	b
4	17	46	28.59	63.6448	-19.5802	4.06	14	119	3.4	0.07	0.3	0.4	b
4	23	5	42.34	63.6448	-19.5547	3.27	14	90	3.4	0.09	0.3	0.5	a
5	3	45	39.84	63.6527	-19.5600	5.42	19	89	2.5	0.08	0.2	0.4	a
5	3	46	23.29	63.6527	-19.5605	5.36	13	111	2.5	0.07	0.3	0.4	b
5	4	31	5.98	63.6512	-19.5782	4.78	19	70	2.7	0.07	0.2	0.4	a
5	5	16	22.17	63.6403	-19.6140	2.83	12	91	5.4	0.08	0.3	0.6	b
5	5	34	27.66	63.6427	-19.5335	1.3	8	123	7.3	0.06	0.2	0.9	b
5	6	7	46.3	63.6508	-19.5768	5.05	17	106	5.2	0.07	0.3	0.5	b
5	8	45	35.73	63.6415	-19.5983	2.85	11	151	5.6	0.06	0.3	0.6	b
5	13	58	27.08	63.6467	-19.5513	2.92	15	106	6.3	0.05	0.2	0.7	b
5	15	24	24.91	63.6450	-19.5722	5.17	15	105	5.8	0.06	0.3	0.6	b
5	17	5	26.42	63.6475	-19.5660	4.85	12	115	5.8	0.06	0.3	0.5	b
5	17	10	20.3	63.6482	-19.5560	4.25	13	112	6.1	0.06	0.3	0.6	b
5	22	8	48.24	63.6557	-19.5530	2.01	13	108	12.9	0.08	0.3	0.9	b
6	0	15	40.57	63.6505	-19.5520	2.25	10	107	12.4	0.07	0.3	1.1	b
6	0	41	22.52	63.6443	-19.5562	3.51	8	161	11.9	0.05	0.3	1.4	b
6	2	19	39.73	63.6538	-19.5508	2.18	15	108	12.8	0.08	0.2	1	b
6	6	42	50	63.6582	-19.5563	3.74	11	109	13.4	0.09	0.4	2.1	c
6	7	49	50.23	63.6537	-19.5600	2.24	9	157	15.1	0.07	0.4	1.5	b
6	9	17	29.41	63.6570	-19.5533	1.69	10	109	13.1	0.08	0.3	1.1	b
6	9	58	55.63	63.6563	-19.5707	2.12	14	108	12.7	0.08	0.2	1	b
6	10	42	38.37	63.6493	-19.5755	2.1	10	118	11.9	0.08	0.3	1.3	b
6	20	32	18.77	63.6500	-19.5695	4.86	19	78	2.8	0.07	0.2	0.4	a
6	20	59	9.2	63.6495	-19.5625	5.11	18	85	2.9	0.08	0.3	0.4	a
7	3	37	33.67	63.6428	-19.6112	3.63	14	104	4.1	0.07	0.3	0.5	b
7	6	45	53.82	63.6493	-19.5768	4.37	16	106	5.3	0.07	0.2	0.6	b
7	17	18	55.3	63.6537	-19.5633	2.1	13	107	12.6	0.09	0.3	1	b
7	17	52	43.86	63.6517	-19.5570	1.9	12	107	12.4	0.07	0.3	0.9	b
7	23	54	49.66	63.6545	-19.5530	2.47	11	109	13	0.06	0.3	1.2	b
8	4	7	46.86	63.6520	-19.5600	2.68	13	107	12.4	0.08	0.3	1	b
8	9	48	32.39	63.6670	-19.5745	2.38	10	114	13.9	0.07	0.3	1.2	b
8	15	7	23.67	63.6520	-19.5380	3.21	11	196	12.6	0.07	0.5	2	c
8	15	33	23.24	63.6520	-19.5712	2.85	12	161	12.3	0.05	0.4	1	b
9	1	56	24.4	63.6502	-19.5695	2.16	14	106	12.1	0.07	0.3	1	b
9	2	45	23.77	63.6577	-19.5663	2.2	14	108	12.9	0.08	0.3	1.1	b
9	7	23	25.48	63.6520	-19.5853	2.38	15	105	12.1	0.07	0.2	1	b
9	15	20	1.51	63.6473	-19.5812	4.25	14	119	5.3	0.06	0.3	0.5	b
9	15	45	22.02	63.6517	-19.5825	5.1	18	96	4.9	0.08	0.2	0.5	b

day	hour	min.	sec.	Lat	Lon	D	nwr	gap	dmin	rms	erh	erz	Q
9	18	19	47.81	63.6612	-19.5598	5.73	9	190	5	0.03	0.6	0.4	c
9	20	19	24.7	63.6563	-19.5700	6.16	17	99	5	0.1	0.3	0.5	b
10	10	11	32.76	63.6527	-19.5943	5.41	14	97	4.5	0.07	0.3	0.5	b
11	8	5	0.55	63.6575	-19.5645	5.23	10	221	5.1	0.04	0.9	0.4	c
11	12	48	37.81	63.6550	-19.5793	5.26	10	222	4.8	0.04	0.7	0.4	c
11	21	55	21.18	63.6820	-19.5670	4.35	9	188	3.8	0.09	1.4	0.7	c
12	16	27	19.33	63.6543	-19.5682	6.34	13	97	5.2	0.04	0.2	0.4	b
13	3	17	7.92	63.6482	-19.5662	5.54	14	91	5.8	0.05	0.2	0.4	b
13	21	57	0.71	63.6515	-19.6107	4.85	8	222	4.2	0.04	0.7	0.4	c
14	4	11	48.05	63.6503	-19.5907	5.37	17	95	4.8	0.06	0.2	0.4	b
14	9	40	35.08	63.6535	-19.5970	4.91	15	112	4.3	0.07	0.2	0.4	b
15	12	7	16.14	63.6482	-19.5940	4.85	17	57	3.2	0.07	0.2	0.3	a
16	7	42	24.36	63.6492	-19.5925	5.68	16	105	11.7	0.08	0.5	1.5	b
17	5	30	40.57	63.6498	-19.5847	5.02	13	105	5.1	0.07	0.2	0.5	b
17	23	0	10.09	63.6480	-19.5533	5.94	17	76	3.1	0.07	0.2	0.4	a
18	13	5	18.66	63.6478	-19.5673	5.76	13	93	3	0.06	0.3	0.3	b
19	7	32	36.31	63.6548	-19.5677	4.57	14	107	12.6	0.08	0.3	1.2	b
19	8	0	51.7	63.6508	-19.5863	5.7	11	177	2.8	0.04	0.4	0.3	b
19	9	44	42.78	63.6453	-19.5615	5.54	14	84	3.3	0.06	0.2	0.4	a
20	7	7	44.27	63.6442	-19.5708	8.5	12	105	11.4	0.11	0.8	2	b
22	1	40	40.73	63.6690	-19.5790	5.12	11	113	14	0.06	0.3	1.3	b

Earthquake locations with the MYR-N velocity model

Mean lat.: 63 38.99; mean lon.:-19 34.27; mean D: 5.5458km

day	hour	min.	sec.	Lat	Lon	D	nwr	gap	dmin	rms	erh	erz	Q
3	19	57	9.73	63.6530	-19.5770	5.67	15	75	2.5	0.07	0.3	0.4	a
4	0	37	45.25	63.6455	-19.5577	4.83	14	87	3.3	0.07	0.3	0.4	a
4	1	18	38.63	63.6478	-19.5497	5.82	8	220	3.2	0.02	0.7	1	c
4	1	52	32.66	63.6467	-19.5635	5.16	10	166	3.2	0.03	0.5	1.1	b
4	5	10	6.14	63.6497	-19.5685	5.98	19	79	2.8	0.06	0.2	0.3	a
4	5	16	15.98	63.6537	-19.5688	6.1	19	79	2.4	0.06	0.2	0.3	a
4	7	47	43.33	63.6493	-19.5743	6.72	8	154	2.8	0.05	0.7	1.2	b
4	13	22	10.98	63.6520	-19.5535	5.76	17	96	2.7	0.06	0.2	0.3	b
4	17	46	28.43	63.6457	-19.5785	4.89	14	119	3.2	0.06	0.2	0.4	b
4	23	5	42.2	63.6456	-19.5542	4.14	14	90	3.3	0.08	0.3	0.4	a
5	3	45	39.67	63.6528	-19.5565	5.95	19	93	2.5	0.06	0.2	0.3	b
5	3	46	23.12	63.6532	-19.5568	5.96	13	110	2.5	0.05	0.3	0.3	b
5	4	31	5.83	63.6513	-19.5755	5.37	19	73	2.6	0.06	0.2	0.3	a
5	5	16	22.05	63.6418	-19.6140	4.14	12	92	5.2	0.07	0.3	0.4	b
5	5	34	27.57	63.6428	-19.5287	2.29	8	124	7.5	0.06	0.3	1.2	b
5	6	7	46.13	63.6512	-19.5763	5.99	17	106	5.2	0.08	0.3	0.5	b
5	8	45	35.6	63.6425	-19.5970	4.14	11	153	5.5	0.06	0.3	0.5	b
5	13	58	26.97	63.6472	-19.5517	4.46	15	106	6.3	0.04	0.2	0.6	b
5	15	24	24.75	63.6448	-19.5722	6.14	15	105	5.8	0.06	0.3	0.5	b
5	17	5	26.26	63.6485	-19.5618	5.64	13	113	5.8	0.07	0.3	0.5	b
5	17	10	20.15	63.6488	-19.5548	5.23	13	112	6.1	0.06	0.3	0.6	b
5	22	8	48.29	63.6523	-19.5553	5.49	13	107	12.6	0.08	0.5	1.8	b
6	0	15	40.6	63.6438	-19.5572	6.49	10	106	11.6	0.06	1.2	3.6	b
6	0	41	22.45	63.6310	-19.5650	9.06	9	141	10.7	0.05	1.2	2.3	c
6	2	19	39.75	63.6505	-19.5532	5.25	15	107	12.4	0.08	0.5	1.7	b
6	6	42	49.91	63.6457	-19.5658	9.64	10	105	12.2	0.07	1	2.1	b
6	7	49	50.24	63.6518	-19.5612	4.98	9	158	14.9	0.07	0.6	2.7	c
6	9	17	29.48	63.6540	-19.5565	5.24	10	107	12.7	0.08	0.7	2.7	c
6	9	58	55.66	63.6532	-19.5738	5.38	14	106	12.4	0.08	0.5	1.9	b
6	10	42	38.42	63.6455	-19.5825	6.54	10	118	11.4	0.09	1.4	5.1	c
6	20	32	18.61	63.6502	-19.5662	5.47	19	82	2.8	0.05	0.2	0.3	a
6	20	59	9.04	63.6495	-19.5605	5.73	18	87	2.9	0.06	0.3	0.3	a
7	3	37	33.53	63.6443	-19.6098	4.65	14	104	3.9	0.07	0.3	0.4	b
7	6	45	53.66	63.6500	-19.5752	5.31	16	106	5.3	0.06	0.2	0.5	b
7	17	18	55.34	63.6492	-19.5672	5.76	13	106	12	0.08	0.6	2.1	c
7	17	52	43.92	63.6482	-19.5593	5.36	12	106	12.1	0.07	0.5	1.9	b
7	23	54	49.63	63.6527	-19.5553	4.97	11	110	12.8	0.06	0.6	1.8	b
8	4	7	46.84	63.6492	-19.5613	5.31	13	107	12.1	0.08	0.4	1.4	b
8	9	48	32.34	63.6665	-19.5757	4.51	10	114	13.8	0.07	0.5	1.8	b
8	15	7	23.61	63.6488	-19.5395	5.86	11	196	12.2	0.06	0.7	0.9	c
8	15	33	23.2	63.6495	-19.5755	5.28	12	160	11.9	0.05	0.4	1.3	b
9	1	56	24.4	63.6472	-19.5728	5.03	14	105	11.7	0.06	0.4	1.3	b
9	2	45	23.8	63.6542	-19.5700	5.75	14	107	12.5	0.07	0.5	2	c
9	7	23	25.46	63.6500	-19.5870	4.86	15	105	11.9	0.07	0.4	1.3	b
9	15	20	1.36	63.6485	-19.5797	5.21	14	118	5.3	0.07	0.3	0.4	b
9	15	45	21.86	63.6518	-19.5810	5.8	19	96	5	0.08	0.2	0.4	b

9	20	19	24.58	63.6608	-19.5692	7.82	17	103	4.7	0.09	0.3	0.4	b
10	10	11	32.76	63.6577	-19.6002	6.34	13	101	3.9	0.09	0.3	0.5	b
day	**hour**	**min**	**sec**	**Lat**	**Lon**	**D**	**nwr**	**gap**	**dmin**	**rms**	**erh**	**erz**	**Q**
11	8	5	0.37	63.6540	-19.5757	7.01	10	223	5	0.04	0.8	0.5	c
11	12	48	37.68	63.6517	-19.5928	6.7	9	223	4.7	0.06	0.7	0.4	c
11	21	55	21.07	63.6757	-19.5762	5.73	9	202	3.5	0.07	0.9	0.5	c
12	16	27	19.23	63.6588	-19.5690	7.92	13	101	4.8	0.06	0.3	0.5	b
13	3	17	7.85	63.6532	-19.5677	7.25	13	96	5.2	0.07	0.3	0.5	b
13	21	57	0.63	63.6490	-19.6240	5.84	7	222	4.3	0.05	0.6	0.4	c
14	4	11	47.99	63.6547	-19.5865	6.94	17	99	4.6	0.1	0.3	0.5	b
14	9	40	35.04	63.6580	-19.5987	6.26	14	111	3.9	0.09	0.3	0.5	b
15	12	7	16.11	63.6542	-19.5872	5.87	17	60	2.4	0.07	0.2	0.4	a
16	7	42	24.28	63.6523	-19.5867	7.72	15	105	12.1	0.1	0.7	2	b
17	5	30	40.52	63.6558	-19.5757	6.16	13	107	4.8	0.08	0.3	0.6	b
17	23	0	10	63.6532	-19.5482	7.33	17	88	2.6	0.11	0.3	0.4	a
18	13	5	18.56	63.6533	-19.5632	6.98	12	93	2.4	0.05	0.3	0.4	b
19	7	32	36.27	63.6607	-19.5638	6.06	13	108	13.3	0.07	0.5	1.9	b
19	8	0	51.64	63.6565	-19.5787	6.89	11	173	2	0.08	0.4	0.3	b
19	9	44	42.72	63.6508	-19.5522	6.55	14	96	2.8	0.08	0.2	0.4	b
20	7	7	44.12	63.6407	-19.5703	12.3	11	105	11.1	0.15	1	1.6	b
22	1	40	40.54	63.6570	-19.5792	9	9	116	12.7	0.1	0.8	1.9	b

Earthquake locations with the MYR-V velocity model

Mean lat.: 63 39.15 mean lon.:-19 33.65 mean D.:7.2936 km

day	hour	min	sec	Lat	Lon	D	nwr	gap	dmin	rms	erh	erz	Q
3	19	57	9.67	63.6593	-19.5662	6.59	15	85	1.7	0.08	0.3	0.4	a
4	0	37	45.21	63.6492	-19.5435	5.58	14	102	3.1	0.06	0.2	0.5	b
4	1	18	38.62	63.6497	-19.5425	6.17	8	230	3.1	0.02	0.7	0.9	c
4	1	52	32.69	63.6497	-19.5607	5.57	10	170	2.8	0.04	0.4	1	b
4	5	10	6.06	63.6552	-19.5595	7.03	19	91	2.2	0.07	0.2	0.4	b
4	5	16	15.9	63.6588	-19.5590	7.04	19	96	1.9	0.07	0.2	0.4	b
4	7	47	43.34	63.6510	-19.5715	7.09	8	158	2.7	0.06	0.7	1	b
4	13	22	10.92	63.6578	-19.5457	6.68	17	109	2.2	0.07	0.3	0.4	b
4	17	46	28.39	63.6493	-19.5660	5.75	13	121	2.9	0.08	0.3	0.5	b
4	23	5	42.2	63.6513	-19.5415	4.92	14	106	3	0.07	0.3	0.5	b
5	3	45	39.59	63.6580	-19.5477	7	19	109	2.2	0.06	0.2	0.4	b
5	3	46	23.05	63.6605	-19.5440	6.84	13	110	2	0.06	0.3	0.4	b
5	4	31	5.76	63.6575	-19.5667	6.48	19	84	1.9	0.07	0.2	0.3	a
5	5	16	22.04	63.6455	-19.6075	5.36	12	97	5	0.07	0.3	0.5	b
5	5	34	27.57	63.6447	-19.5163	1.88	8	128	7.8	0.05	0.3	1.3	b
5	6	7	46.03	63.6567	-19.5713	7.47	16	108	4.8	0.09	0.3	0.6	b
5	8	45	35.61	63.6465	-19.5943	5.25	10	156	5.1	0.06	0.3	0.6	b
5	13	58	26.96	63.6523	-19.5407	5.2	15	108	6.3	0.06	0.3	0.9	b
5	15	24	24.63	63.6485	-19.5752	7.81	14	106	5.5	0.5	0.3	0.4	b
5	17	5	26.19	63.6542	-19.5533	6.95	12	109	5.7	0.09	0.3	0.6	b
5	17	10	20.1	63.6555	-19.5447	6.39	13	108	6	0.06	0.3	0.6	b
5	22	8	48.12	63.6417	-19.5595	11.2	13	105	11.4	0.07	0.9	1.6	b
6	0	15	40.4	63.6355	-19.5595	11	10	104	10.7	0.07	1.1	1.8	b
6	0	41	22.34	63.6443	-19.1498	3.51	8	158	11.3	0.06	1.2	2.6	c
6	2	19	39.64	63.6448	-19.5553	10	14	106	11.8	0.09	0.8	1.6	b
6	6	42	49.71	63.6468	-19.5608	11.3	10	106	12.3	0.08	1	1.9	b
6	7	49	50.15	63.6483	-19.5643	9.95	9	159	14.6	0.07	0.8	2.1	c
6	9	17	29.3	63.6418	-19.5633	11.5	10	105	11.3	0.09	1.1	2	b
6	9	58	55.51	63.6442	-19.5785	10.9	12	104	11.3	0.08	0.8	1.6	b
6	10	42	38.28	63.6412	-19.5790	9.71	9	120	11	0.09	1.4	3.2	b
6	20	32	18.55	63.6555	-19.5567	6.44	18	95	2.2	0.06	0.2	0.4	b
6	20	59	8.96	63.6552	-19.5528	6.84	18	99	2.4	0.07	0.3	0.4	b
7	3	37	33.47	63.6500	-19.6058	6.06	14	101	3.2	0.07	0.3	0.4	b
7	6	45	53.61	63.6555	-19.5650	6.39	16	108	5.2	0.07	0.2	0.6	b
7	17	18	55.17	63.6415	-19.5717	11	13	104	11.2	0.09	0.9	1.7	b
7	17	52	43.77	63.6385	-19.5622	10.7	12	104	11	0.06	0.9	1.7	b
7	23	54	49.6	63.6615	-19.5392	4.6	10	110	13.6	0.06	0.6	4.1	c
8	4	7	46.78	63.6517	-19.5550	7.42	13	107	12.5	0.07	0.8	2.3	b
8	9	48	32.3	63.6723	-19.5612	4.69	9	115	14.6	0.04	0.5	4	c
8	15	7	23.46	63.6423	-19.5392	10.5	10	194	11.5	0.06	0.7	1.3	c
8	15	33	23.26	63.6428	-19.5793	8.03	11	198	11.2	0.04	0.8	1.5	c
9	1	56	24.39	63.6488	-19.5668	7.26	13	106	12	0.06	0.7	1.9	b
9	2	45	23.69	63.6497	-19.5727	10	14	106	12	0.07	0.8	1.7	b
9	7	23	25.41	63.6552	-19.5820	6.58	15	107	12.4	0.08	0.7	2.2	b
9	15	20	1.31	63.6533	-19.5752	6.8	14	113	5	0.1	0.4	0.5	b
9	15	45	21.76	63.6563	-19.5807	7.45	18	99	4.6	0.07	0.2	0.4	b
9	18	19	47.78	63.6853	-19.5550	7.1	9	164	4.3	0.06	1.7	0.5	c

day	hour	min	sec	Lat	Lon	D	nwr	gap	dmin	rms	erh	erz	Q
9	18	19	47.97	63.6557	-19.5588	4.45	10	193	5.4	0.07	0.7	0.5	c
9	20	19	24.85	63.6555	-19.5693	5.45	17	98	5.1	0.11	0.3	0.6	b
10	10	11	32.92	63.6520	-19.5932	4.56	14	97	4.6	0.06	0.2	0.5	b
11	8	5	0.6	63.6480	-19.5675	4.38	10	229	5.7	0.06	0.9	0.5	c
11	12	48	37.9	63.6488	-19.5795	4.37	10	226	5.2	0.04	0.7	0.4	c
11	21	55	21.22	63.6683	-19.5712	4.27	9	210	4.1	0.1	1.2	0.4	c
12	16	27	19.49	63.6538	-19.5670	5.74	13	97	5.2	0.05	0.3	0.5	b
13	3	17	8.07	63.6480	-19.5652	4.77	14	91	5.8	0.05	0.2	0.5	b
13	21	57	0.8	63.6453	-19.6105	3.97	10	164	4.9	0.04	0.5	0.3	b
14	4	11	48.21	63.6497	-19.5908	4.36	17	95	4.9	0.06	0.2	0.4	b
14	9	40	35.23	63.6522	-19.5972	3.9	15	113	4.5	0.07	0.2	0.5	b
15	12	7	16.3	63.6477	-19.5963	4.05	17	55	3.2	0.07	0.2	0.4	a
16	7	42	24.42	63.6515	-19.5897	3.23	16	105	11.9	0.08	0.2	1.2	b
17	5	30	40.72	63.6487	-19.5853	4.06	13	105	5.1	0.06	0.2	0.5	b
17	23	0	10.25	63.6470	-19.5542	5.14	17	76	3.2	0.07	0.2	0.4	a
18	13	5	18.83	63.6472	-19.5683	4.96	13	94	3	0.06	0.3	0.4	b
19	7	32	36.38	63.6552	-19.5673	2.58	14	107	12.7	0.08	0.2	1	b
19	8	0	51.86	63.6502	-19.5882	4.92	11	177	2.9	0.03	0.3	0.3	b
19	9	44	42.93	63.6453	-19.5678	5.02	14	79	3.2	0.06	0.3	0.4	a
20	7	7	44.27	63.6538	-19.5627	3.04	12	107	12.6	0.12	0.4	1.8	b
22	1	40	40.78	63.6708	-19.5780	2.76	10	112	14.2	0.05	0.2	0.9	b

GTD

Appendix 3

1. header
2. E.2
3. E.e
4. E.n

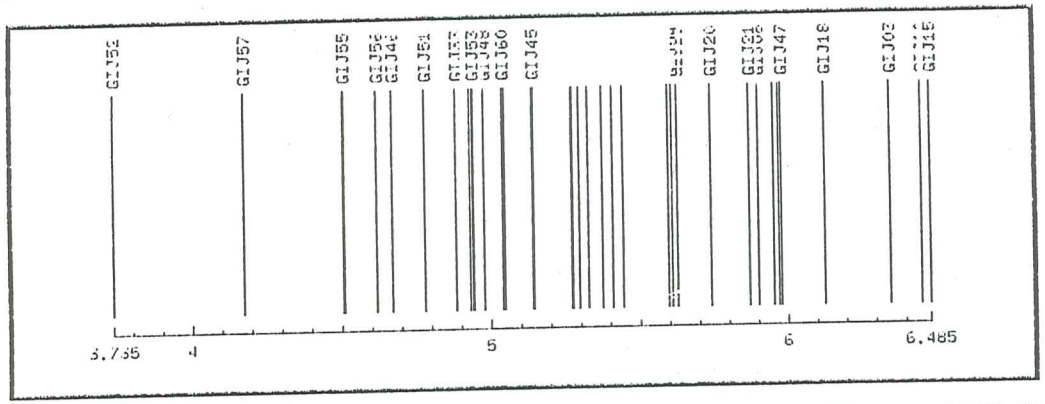

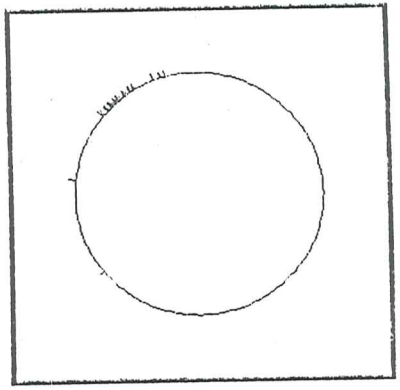

Control Parameters

Plot start time: 0.00
Plot duration: 5.00
Distance range: ALL
Azimuth range: ALL
Reduction velocity: 6
Scaling: AUTO
Trace width: 0.2
Clipping width: 0.2

Travel time model:
Travel time plot format: LINES
Tau range: 0.000 0.000
Tau interval: 0.000
P range: 0.0000 0.0000
P interval: 0.0000
Tau/P scaling: 1.00

Screendump in progress...

Time - Distance/(6.00 km/sec)
5
4
3
2
1
GIJ52
GIJ57
GIJ46
GIJ51
GIJ33
GIJ53
GIJ48
GIJ60
GIJ45
GIJ31
GIJ14
GIJ09
GIJ11
GIJ54
GIJ20
GIJ21
GIJ47
GIJ18
GIJ03
GIJ15
4
5
6
6.76
Distance (km)

Time - Distance/(6.00 km/sec)
5
4
3
2
1
GIJ52
GIJ57
GIJ55
GIJ56
GIJ45
GIJ31
GIJ14
GIJ11
GIJ20
GIJ21
GIJ47
GIJ18
GIJ03
GIJ15
4
5
6
6.76
Distance (km)

Time - Distance/(6.00 km/sec)
5
4
3
2
1
GIJ52
GIJ57
GIJ55
GIJ56
GIJ46
GIJ51
GIJ33
GIJ53
GIJ14
GIJ09
GIJ11
GIJ54
GIJ20
GIJ21
GIJ08
GIJ47
GIJ18
GIJ03
GIJ15
4
5
6
6.76
Distance (km)
Screendump in progress ...

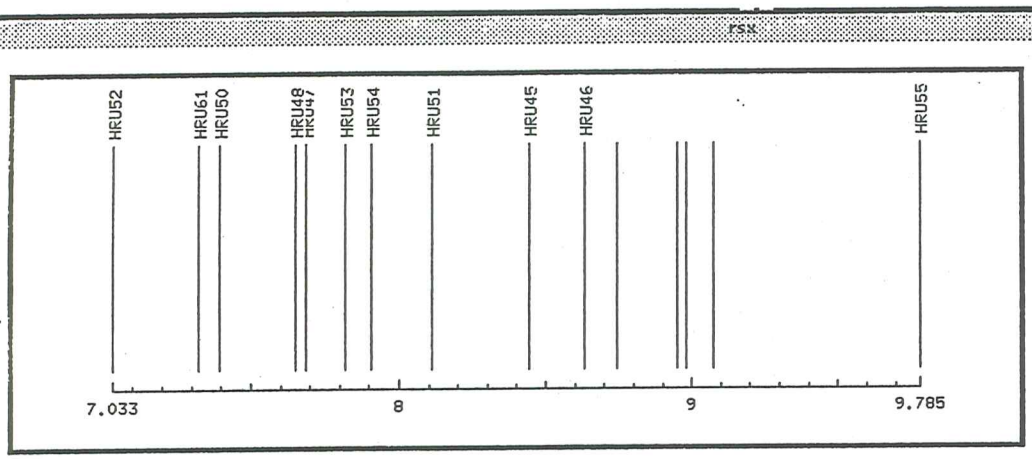

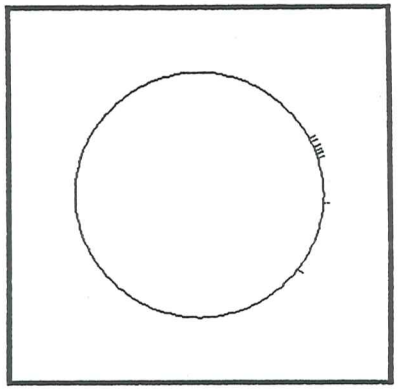

Control Parameters

Plot start time: 0.00
Plot duration: 5.00
Distance range: ALL
Azimuth range: ALL
Reduction velocity: 6
Scaling: AUTO
Trace width: 0.2
Clipping width: 0.2

Travel time model:
Travel time plot format: LINES
Tau range: 0.000 0.000
Tau interval: 0.000
P range: 0.0000 0.0000
P interval: 0.0000
Tau/P scaling: 1.00

Screendump in progress...

HRU52
HRU61
HRU50
HRU48
HRU47
HRU53
HRU54
HRU45
HRU46
HRU64
HRU56
HRU49
HRU57
HRU55
Time - Distance/(6.00 km/sec)
5
4
3
2
1
7
8
9
10
Distance (km)
Screendump in progress...

Time - Distance/(6.00 km/sec)
1
2
3
4
5
7
8
9
10
Distance (km)
HRU52
HRU61
HRU50
HRU48
HRU47
HRU53
HRU54
HRU51
HRU46
HRU64
HRU56
HRU49
HRU57
HRU55

Time - Distance/(6.00 km/sec)
1
2
3
4
5
7
8
9
10
Distance (km)
HRU52
HRU61
HRU50
HRU48
HRU47
HRU53
HRU45
HRU46
HRU64
HRU56
HRU49
HRU57
HRU55

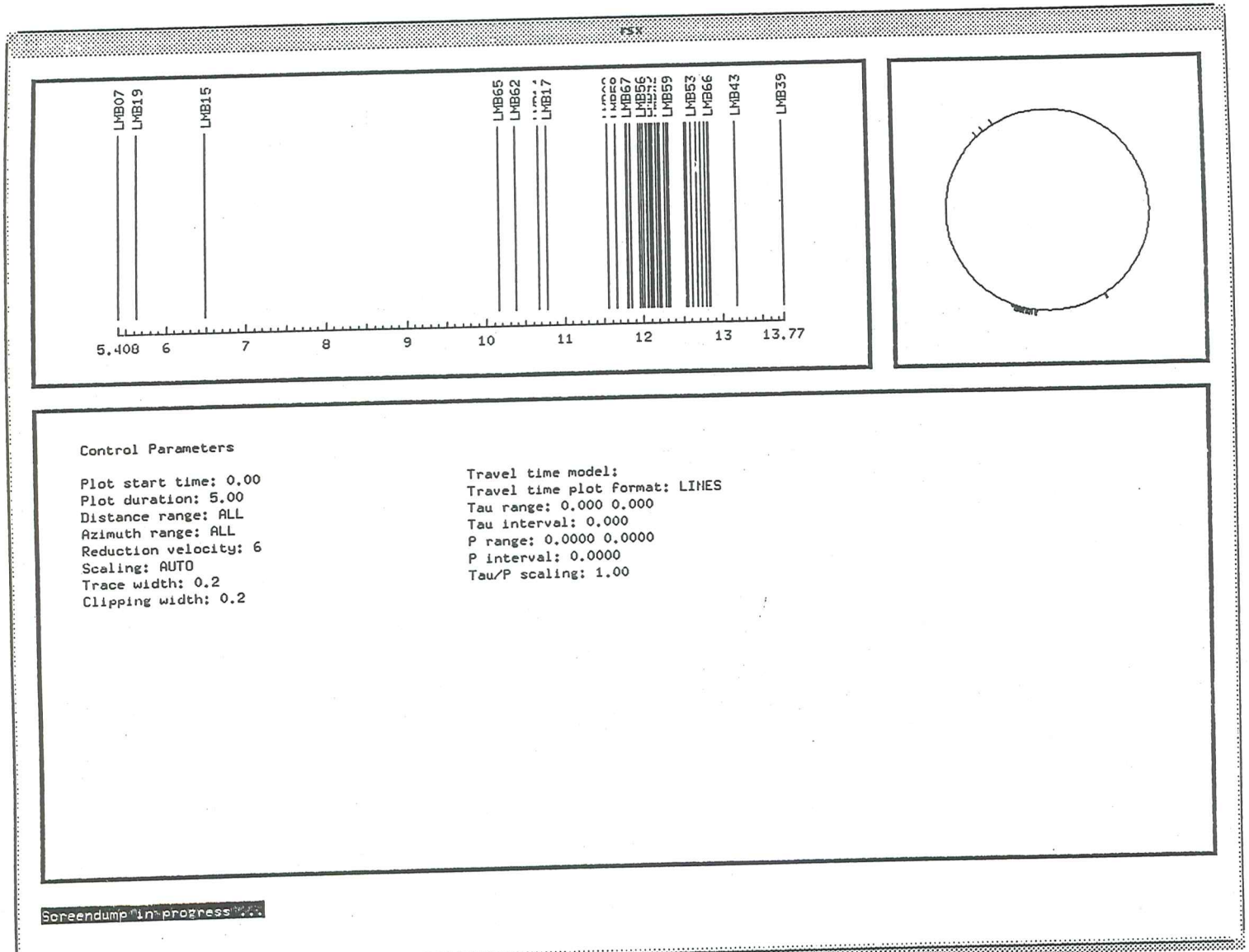

Control Parameters

Plot start time: 0.00
Plot duration: 5.00
Distance range: ALL
Azimuth range: ALL
Reduction velocity: 6
Scaling: AUTO
Trace width: 0.2
Clipping width: 0.2

Travel time model:
Travel time plot format: LINES
Tau range: 0.000 0.000
Tau interval: 0.000
P range: 0.0000 0.0000
P interval: 0.0000
Tau/P scaling: 1.00

Screendump in progress...

LMB07
LMB19
LMB15
LMB39
LMB43
LMB66
LMB53
LMB59
LMB56
LMB67
LMB17
LMB62
LMB65
Time - Distance/(6.00 km/sec)
5
4
3
2
1
Distance (km)
10
14.61
Screendump in progress ...

Time - Distance/(6.00 km/sec)
5
4
3
2
1
LMB07
LMB19
LMB15
LMB65
LMB62
LMB17
LMB59
LMB66
LMB43
LMB39
14.61
10
Distance (km)
Screendump in progress

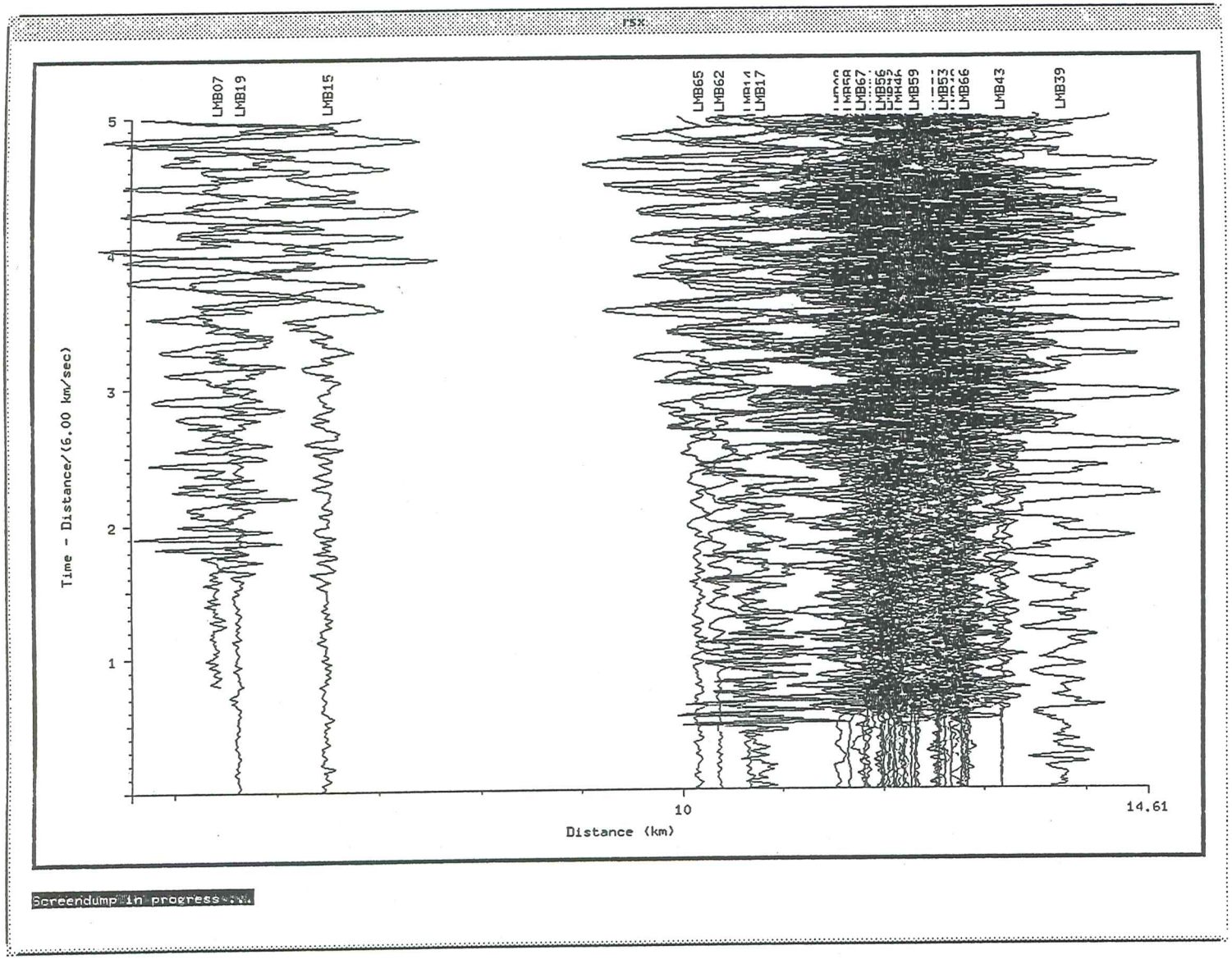
rsx
LMB07
LMB19
LMB15
LMB65
LMB62
LMB17
LMB67
LMB59
LMB43
LMB39
5
4
3
2
1
Time - Distance/(6.00 km/sec)
10
14.61
Distance (km)
Screendump in progress...

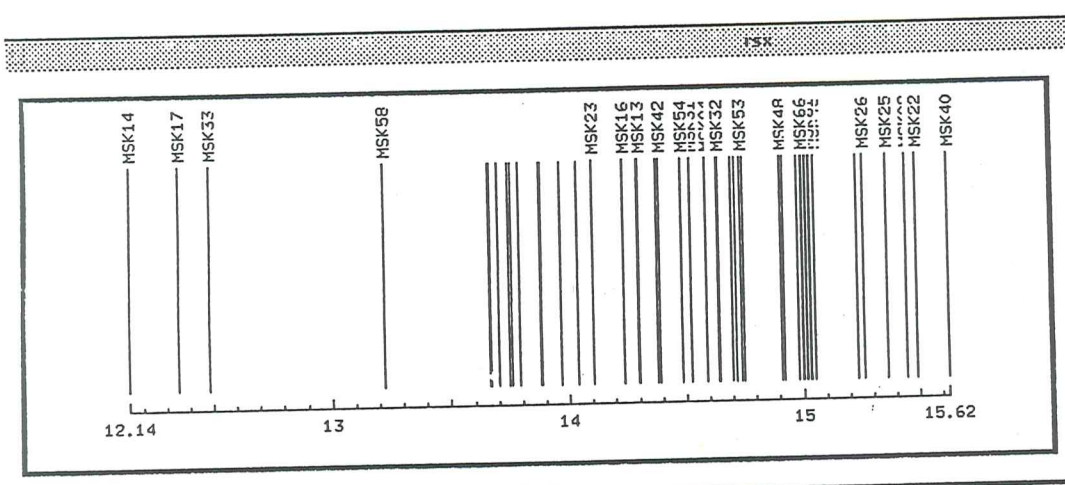

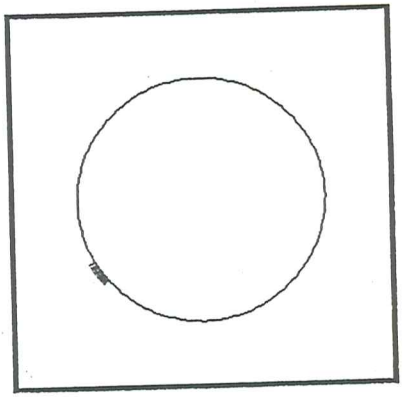

Control Parameters

Plot start time: 0.00
Plot duration: 5.00
Distance range: ALL
Azimuth range: ALL
Reduction velocity: 6.00
Scaling: AUTO
Trace width: 0.20
Clipping width: 0.20

Travel time model:
Travel time plot format: LINES
Tau range: 0.000 0.000
Tau interval: 0.000
P range: 0.0000 0.0000
P interval: 0.0000
Tau/P scaling: 1.00

Screendump in progress...

Screendump in progress...
Time - Distance/(6.00 km/sec)
1
2
3
4
5
12
13
14
15
15.97
Distance (km)
MSK14
MSK17
MSK33
MSK57
MSK60
MSK59
MSK46
MSK34
MSK23
MSK16
MSK13
MSK42
MSK54
MSK31
MSK32
MSK53
MSK48
MSK66
MSK26
MSK25
MSK22
MSK40

Time - Distance/(6.00 km/sec)
1
2
3
4
5
12
13
14
15
15.97
Distance (km)
MSK14
MSK17
MSK33
MSK58
MSK57
MSK60
MSK59
MSK46
MSK34
MSK23
MSK16
MSK13
MSK42
MSK54
MSK32
MSK53
MSK48
MSK66
MSK26
MSK25
MSK22
MSK40

Time - Distance/(6.00 km/sec)
1
2
3
4
5
12
13
14
15
15.97
Distance (km)
MSK14
MSK17
MSK33
MSK58
MSK60
MSK59
MSK46
MSK34
MSK23
MSK16
MSK13
MSK42
MSK54
MSK32
MSK53
MSK48
MSK26
MSK25
MSK22
MSK40

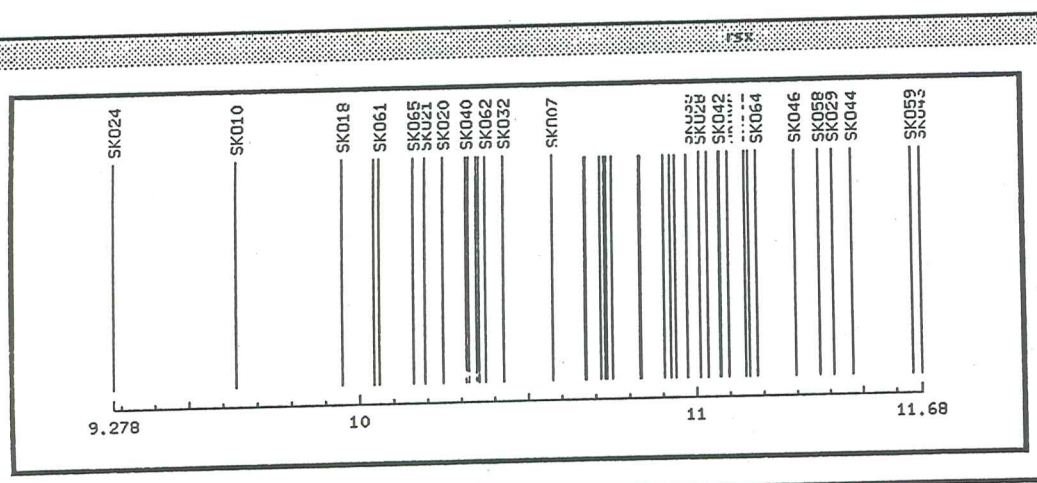

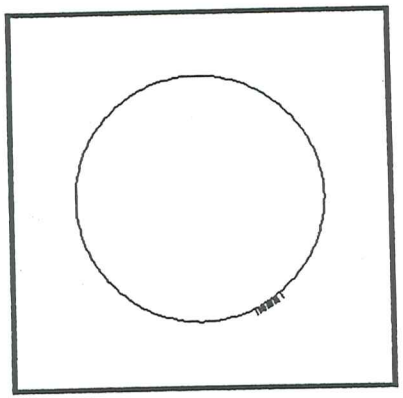

Control Parameters

Plot start time: 0.00
Plot duration: 5.00
Distance range: ALL
Azimuth range: ALL
Reduction velocity: 6.00
Scaling: AUTO
Trace width: 0.20
Clipping width: 0.20

Travel time model:
Travel time plot format: LINES
Tau range: 0.000 0.000
Tau interval: 0.000
P range: 0.0000 0.0000
P interval: 0.0000
Tau/P scaling: 1.00

Screendump in progress...

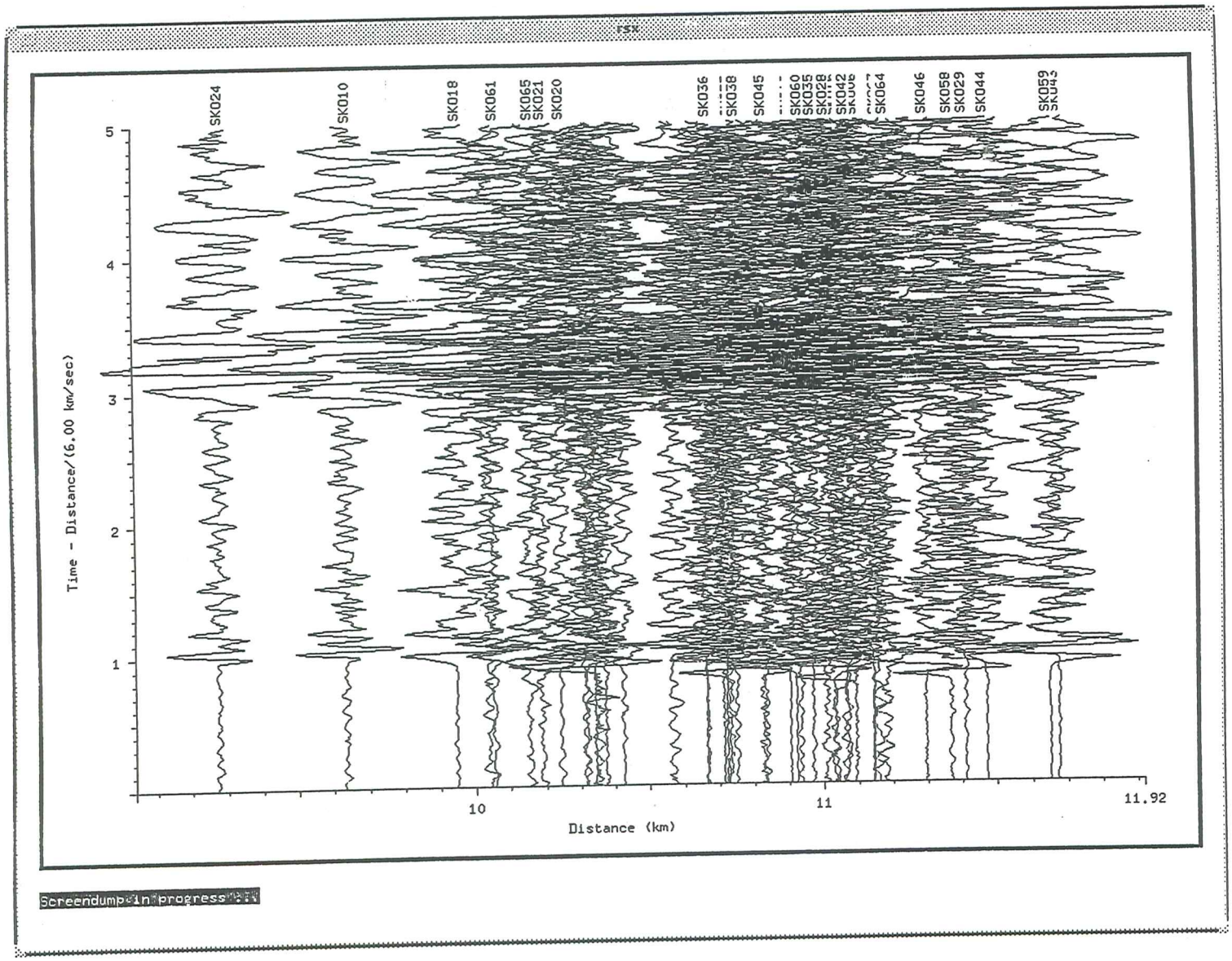
SK024
SK010
SK018
SK061
SK065
SK021
SK020
SK036
SK038
SK045
SK060
SK035
SK042
SK064
SK046
SK058
SK029
SK044
SK059
Time - Distance/(6.00 km/sec)
5
4
3
2
1
10
11
11.92
Distance (km)
Screendump in progress

Time - Distance/(6.00 km/sec)
5
4
3
2
1
SK024
SK010
SK018
SK040
SK062
SK032
SK007
SK036
SK038
SK045
SK060
SK035
SK028
SK042
SK064
SK046
SK058
SK029
SK044
SK059
10
11
11.92
Distance (km)
Screendump in progress

Time - Distance/(6.00 km/sec)
5
4
3
2
1
SK024
SK010
SK018
SK061
SK007
SK036
SK038
SK045
SK060
SK035
SK028
SK042
SK006
SK064
SK046
SK058
SK029
SK044
SK059
SK043
10
11
11.92
Distance (km)
Screendump in progress

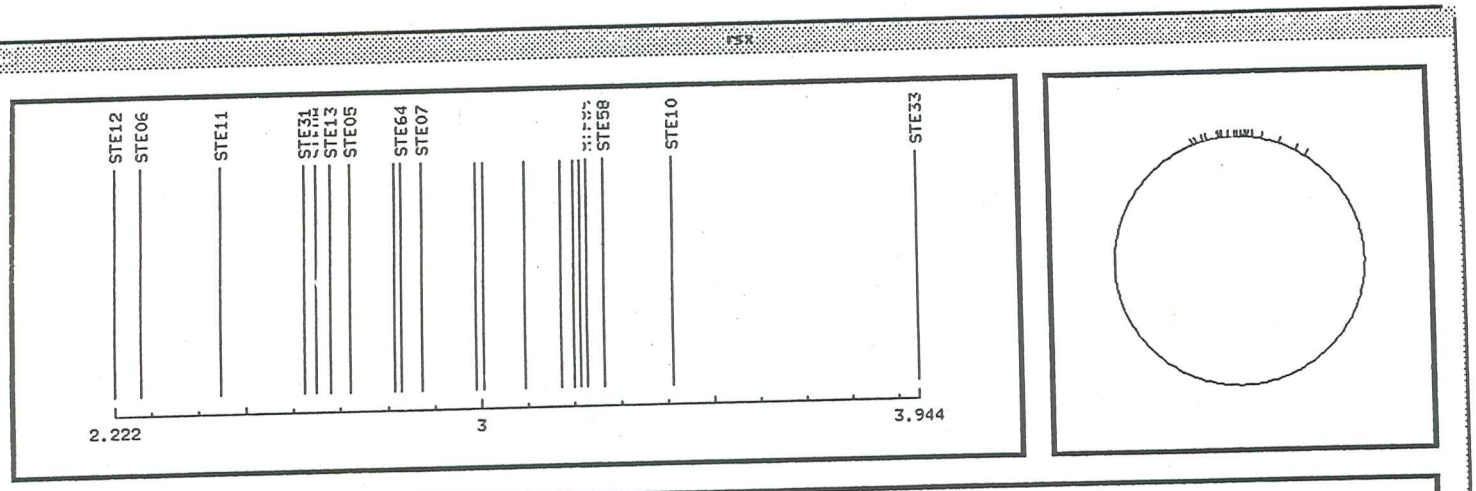

Control Parameters

Plot start time: 0.00
Plot duration: 5.00
Distance range: ALL
Azimuth range: ALL
Reduction velocity: 5.00
Scaling: AUTO
Trace width: 0.06
Clipping width: 0.06

Travel time model:
Travel time plot format: LINES
Tau range: 0.000 0.000
Tau interval: 0.000
P range: 0.0000 0.0000
P interval: 0.0000
Tau/P scaling: 1.00

Screendump in progress...

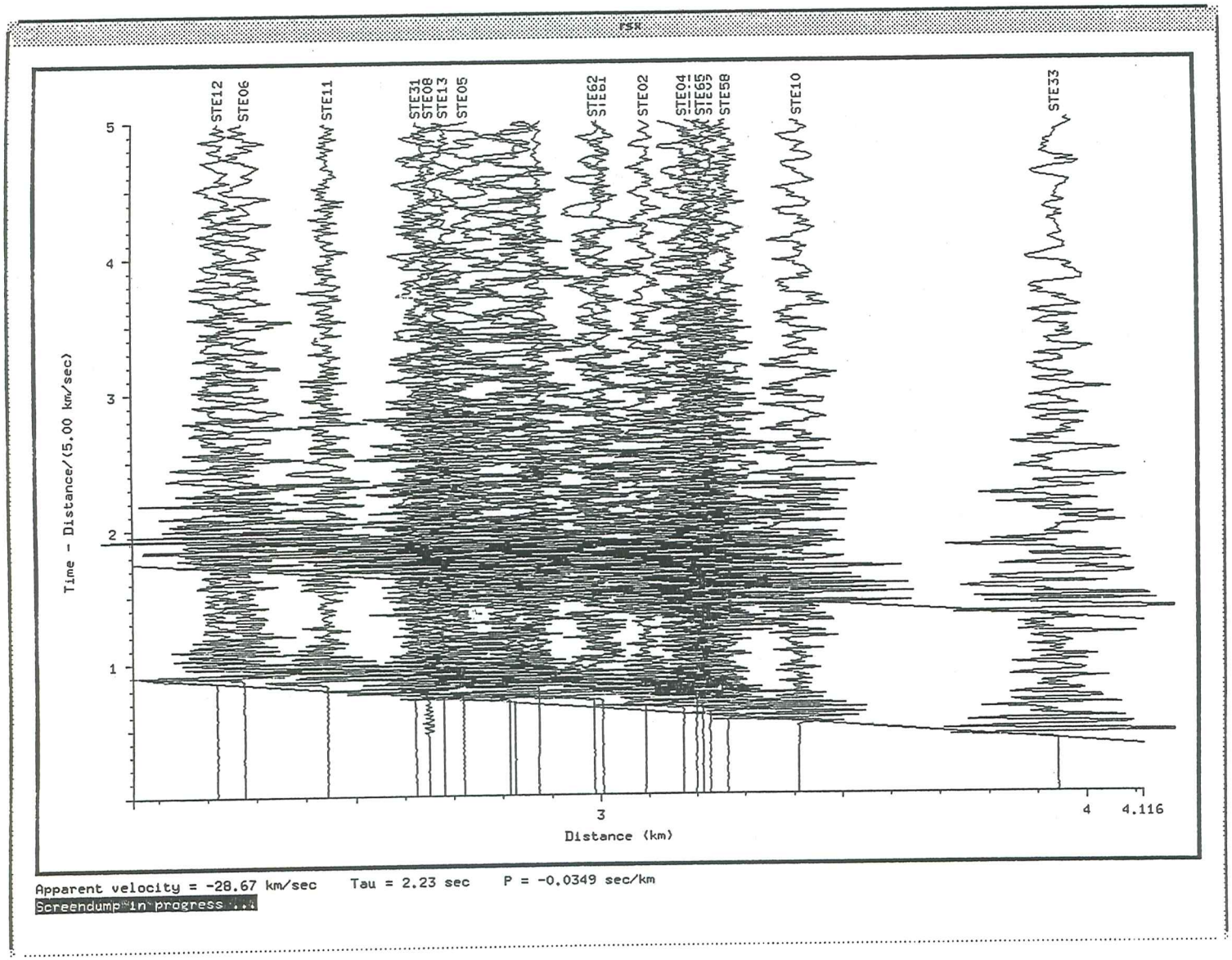

Apparent velocity = -28.67 km/sec Tau = 2.23 sec P = -0.0349 sec/km

Screendump in progress ...

Screendump in progress...
Time - Distance/(6.00 km/sec)
1
2
3
4
5
STE12
STE06
STE11
STE31
STE08
STE62
STE02
STE04
STE65
STE58
STE10
STE33
Distance (km)
3
4
4.116

Time - Distance/(6.00 km/sec)
5
4
3
2
1
Distance (km)
3
4
4.116
STE33
STE10
STE58
STE09
STE65
STE04
STE02
STE01
STE05
STE13
STE08
STE31
STE11
STE06
STE12
Screendump in progress

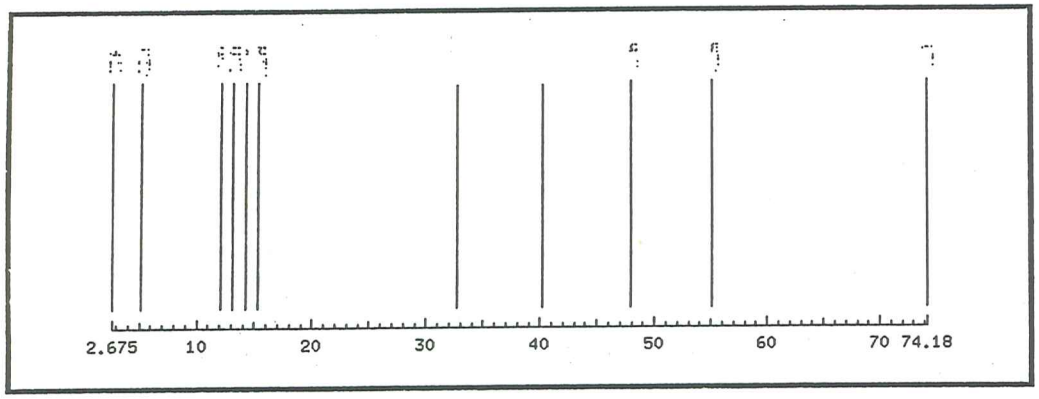

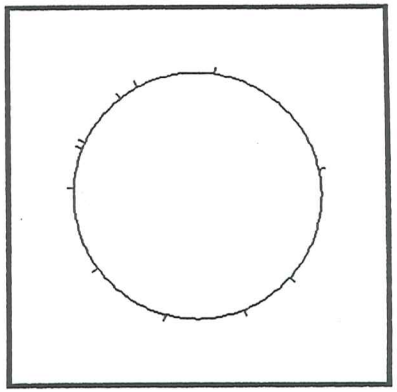

Control Parameters

Event location: -19.58 63.65
Event depth: 5.37
Event date: 1994/06/05
Event time: 4:31:05.83
Plot start time: -4.83
Plot duration: ALL
Distance range: ALL
Azimuth range: ALL
Reduction velocity: 6
Scaling: AUTO

Trace width: 0.2
Clipping width: 0.2
Travel time model: a2
Travel time plot format: LINES
Tau range: 0.000 0.000
Tau interval: 0.000
P range: 0.0000 0.0000
P interval: 0.0000
Tau/P scaling: 1.00

Screendump in progress

rsx

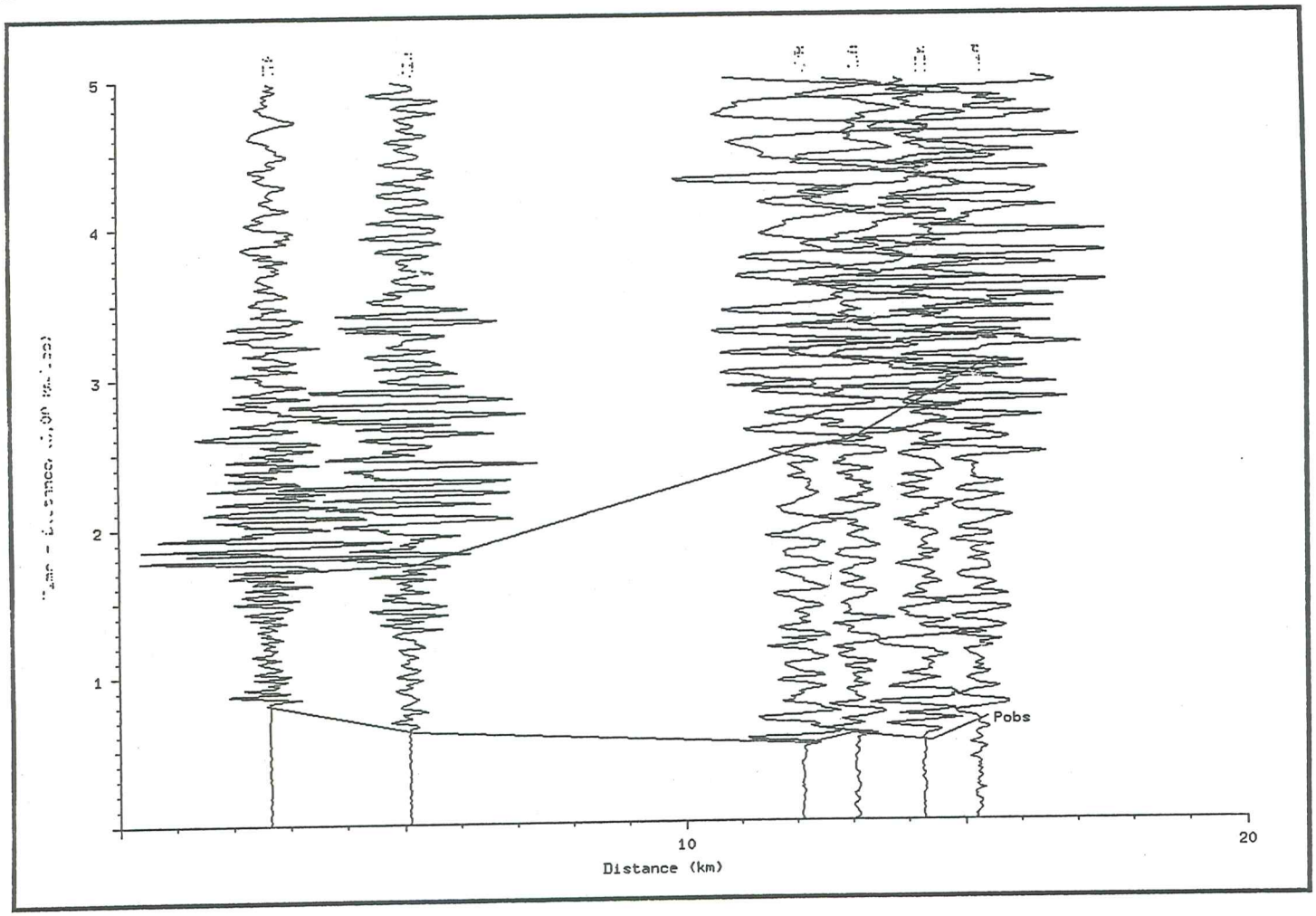

Screendump in progress...

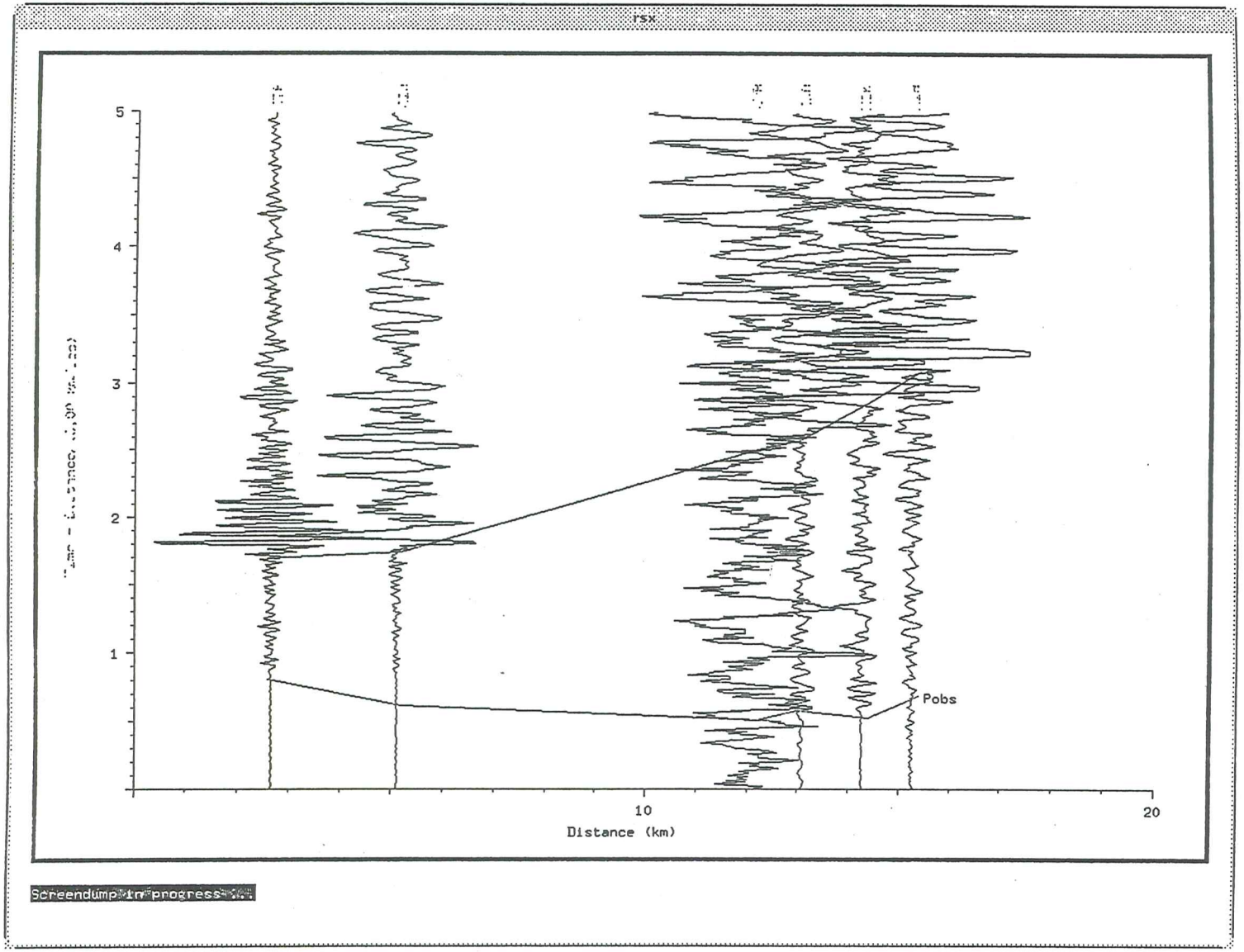
rsx
5
4
3
2
1
Pobs
10
20
Distance (km)
Screendump in progress

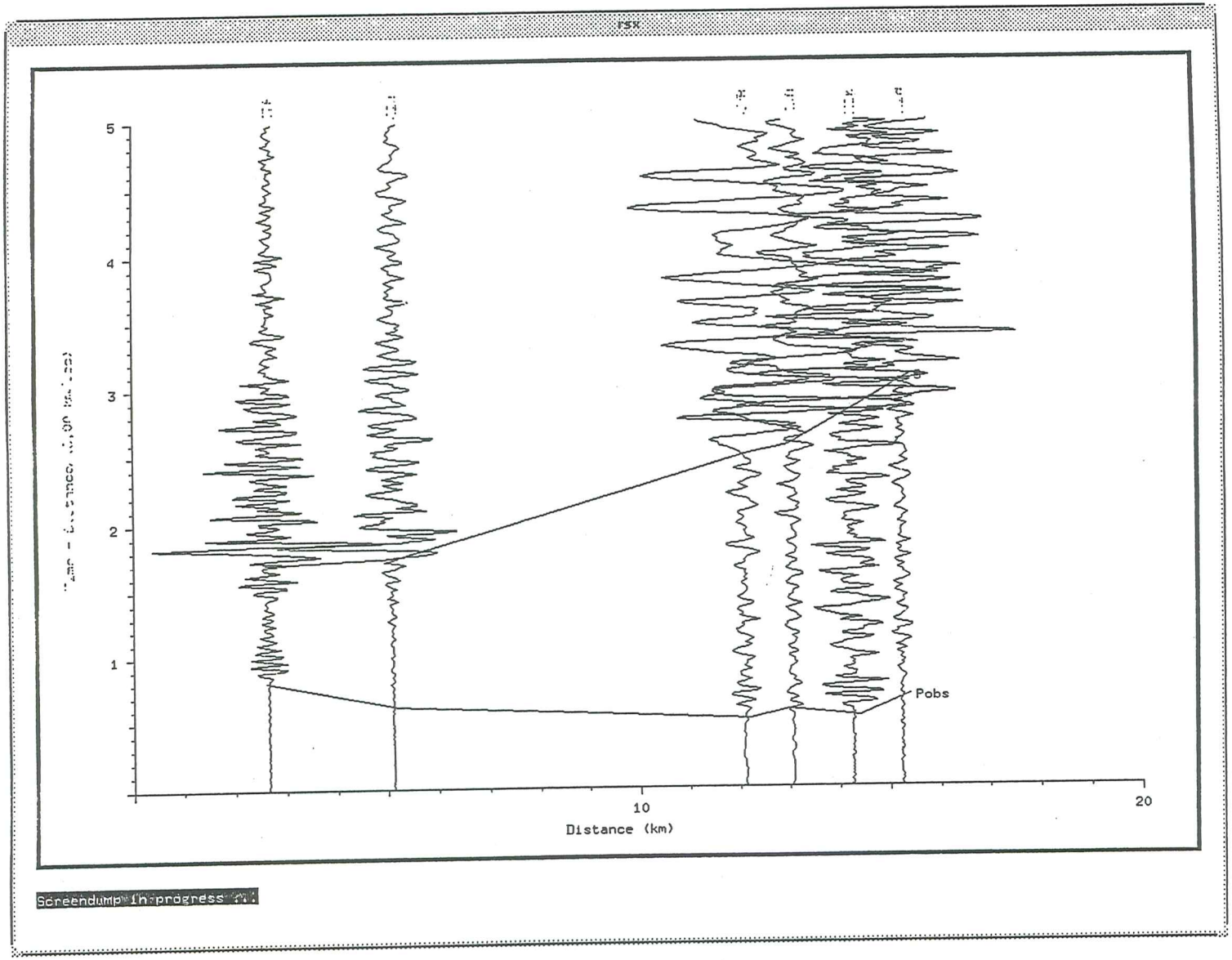
rsx
5
4
3
2
1
Pobs
10
20
Distance (km)
Screendump in progress ...

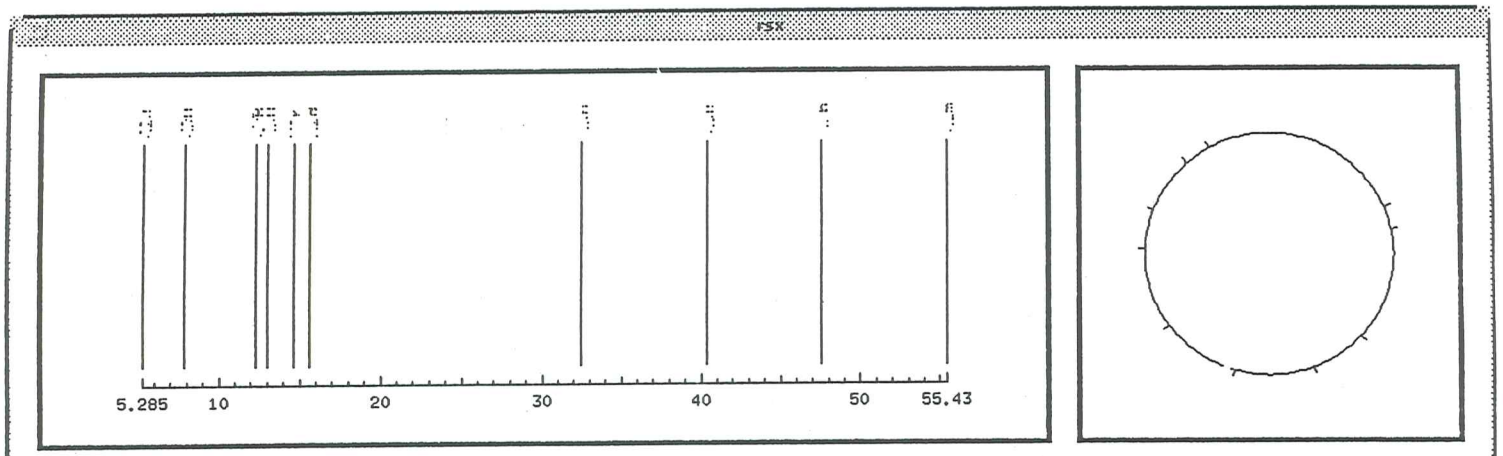

Control Parameters

Event location: -19.57 63.65
Event depth: 5.80
Event date: 1994/06/09
Event time: 15:45:21.84
Plot start time: 0
Plot duration: 5
Distance range: ALL
Azimuth range: ALL
Reduction velocity: 6
Scaling: AUTO

Trace width: 0.2
Clipping width: 0.2
Travel time model: a1
Travel time plot format: LINES
Tau range: 0.000 0.000
Tau interval: 0.000
P range: 0.0000 0.0000
P interval: 0.0000
Tau/P scaling: 1.00

Screendump in progress ...

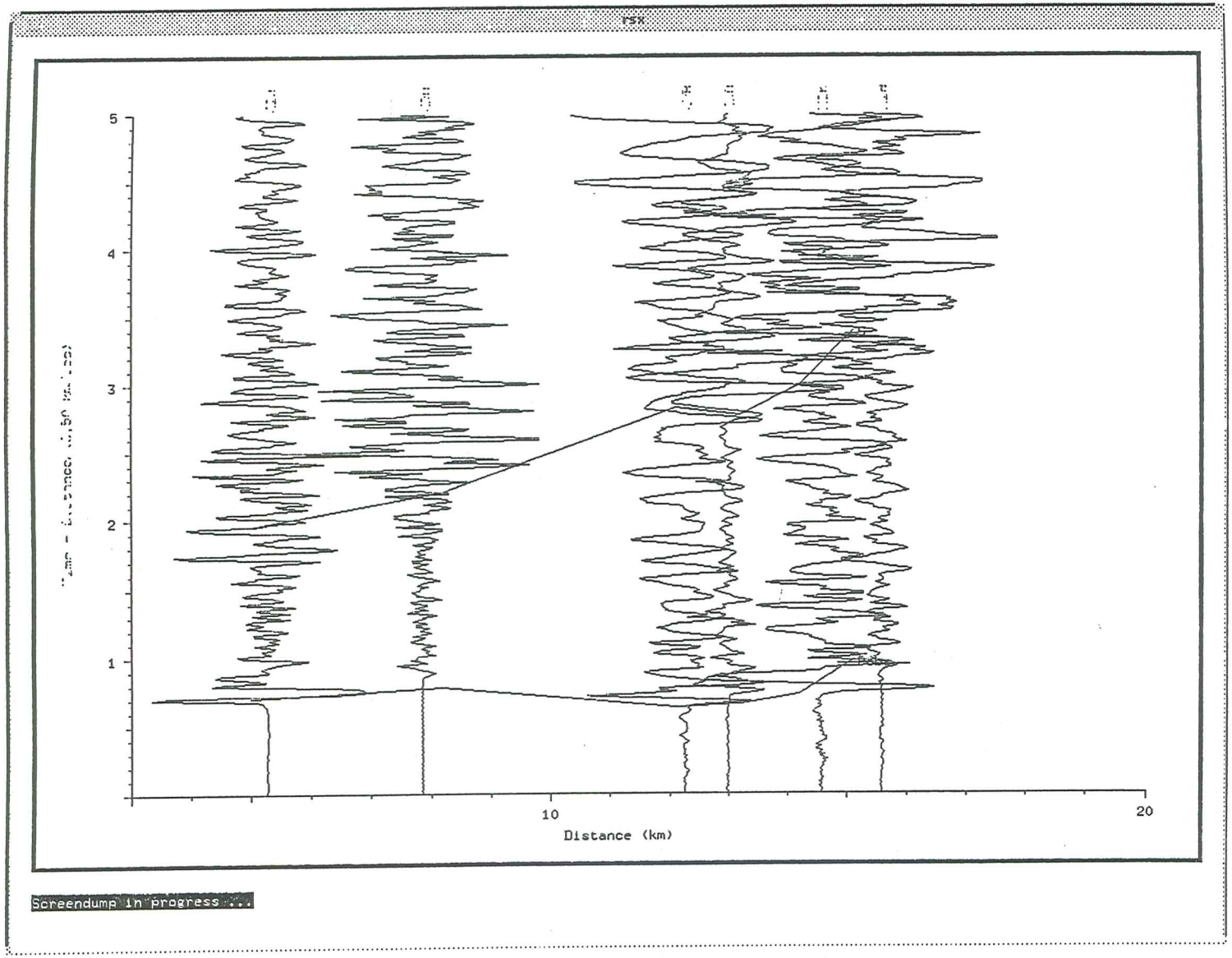
rsk
5
4
3
2
1
10
20
Distance (km)
Screendump in progress ...

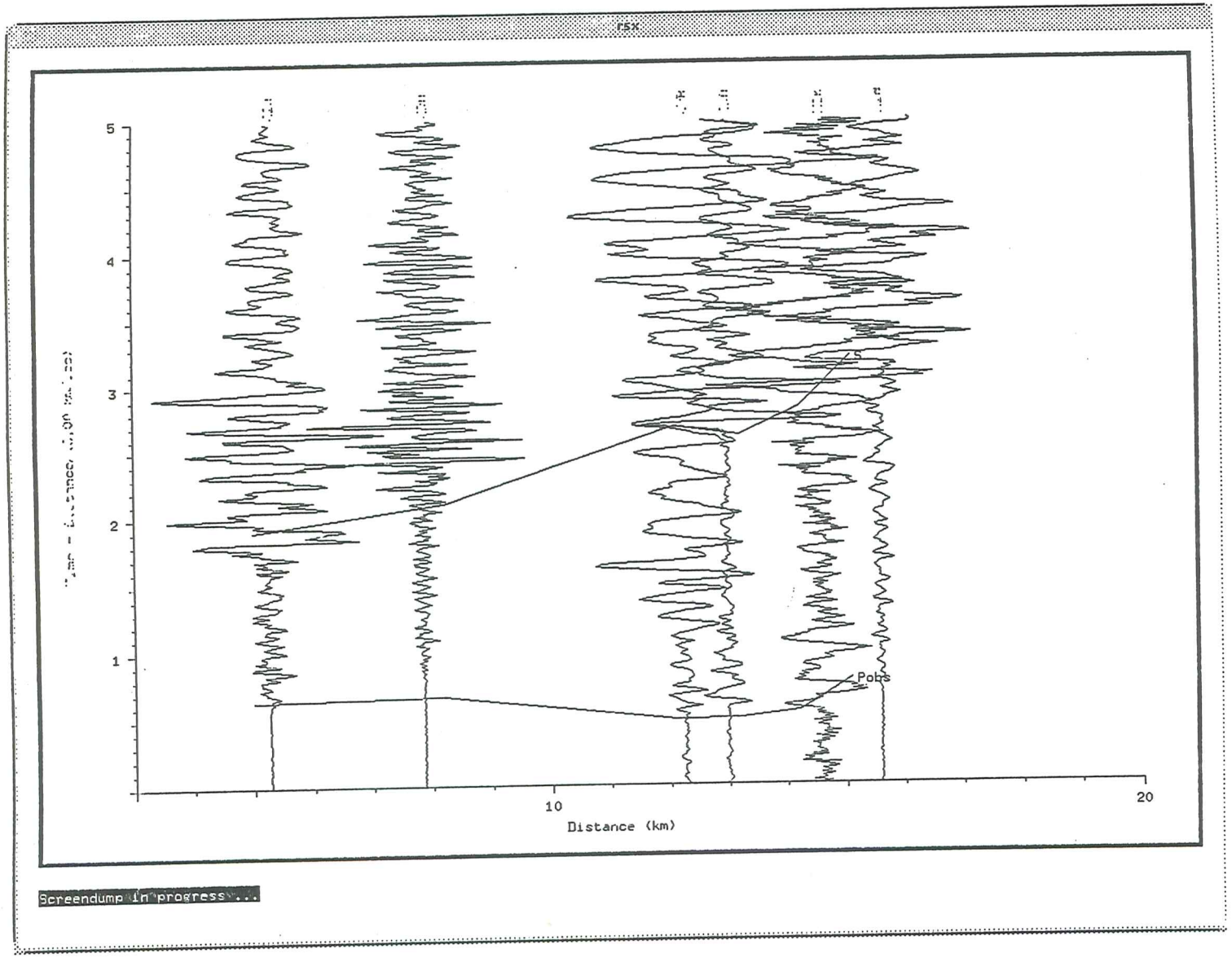
rsx
5
4
3
2
1
Pobs
10
20
Distance (km)
Screendump in progress...

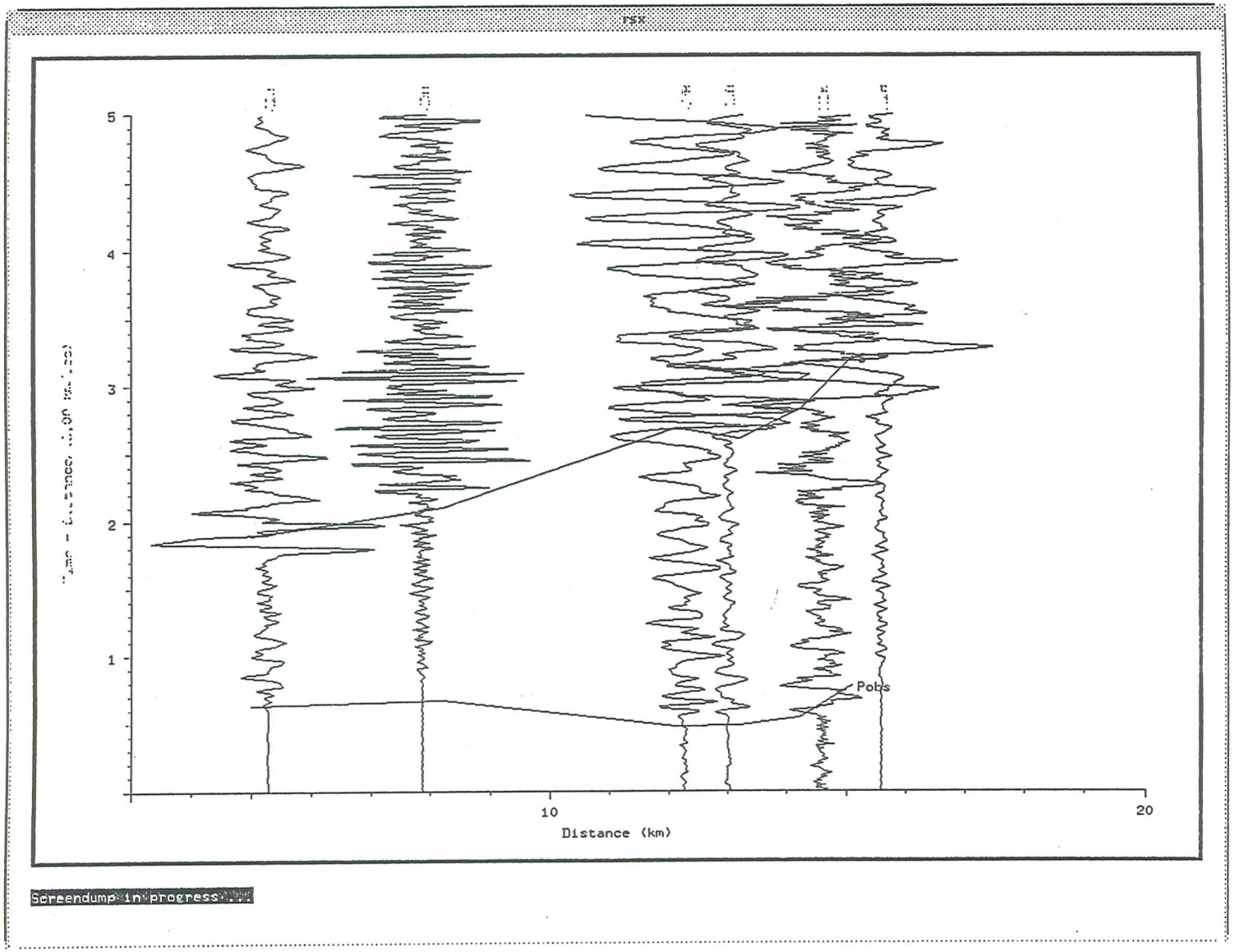
5
4
3
2
1
Pobs
10
20
Distance (km)
Screendump in progress...

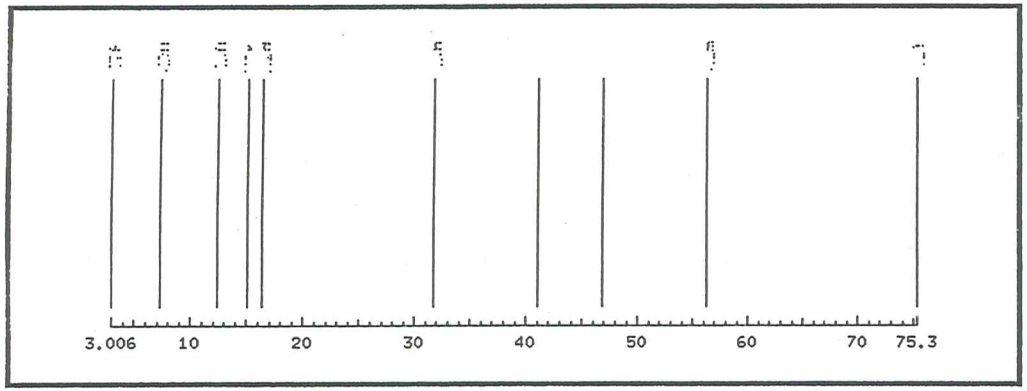

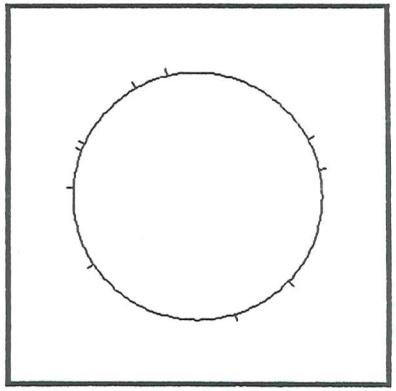

Control Parameters

Event location: -19.56 63.65
Event depth: 5.94
Event date: 1994/06/17
Event time: 23:00:10.09
Plot start time: 0.00
Plot duration: 5.00
Distance range: ALL
Azimuth range: ALL
Reduction velocity: 6.00
Scaling: AUTO

Trace width: 0.20
Clipping width: 0.20
Travel time model: a1
Travel time plot format: LINES
Tau range: 0.000 0.000
Tau interval: 0.000
P range: 0.0000 0.0000
P interval: 0.0000
Tau/P scaling: 1.00

Screendump in progress...

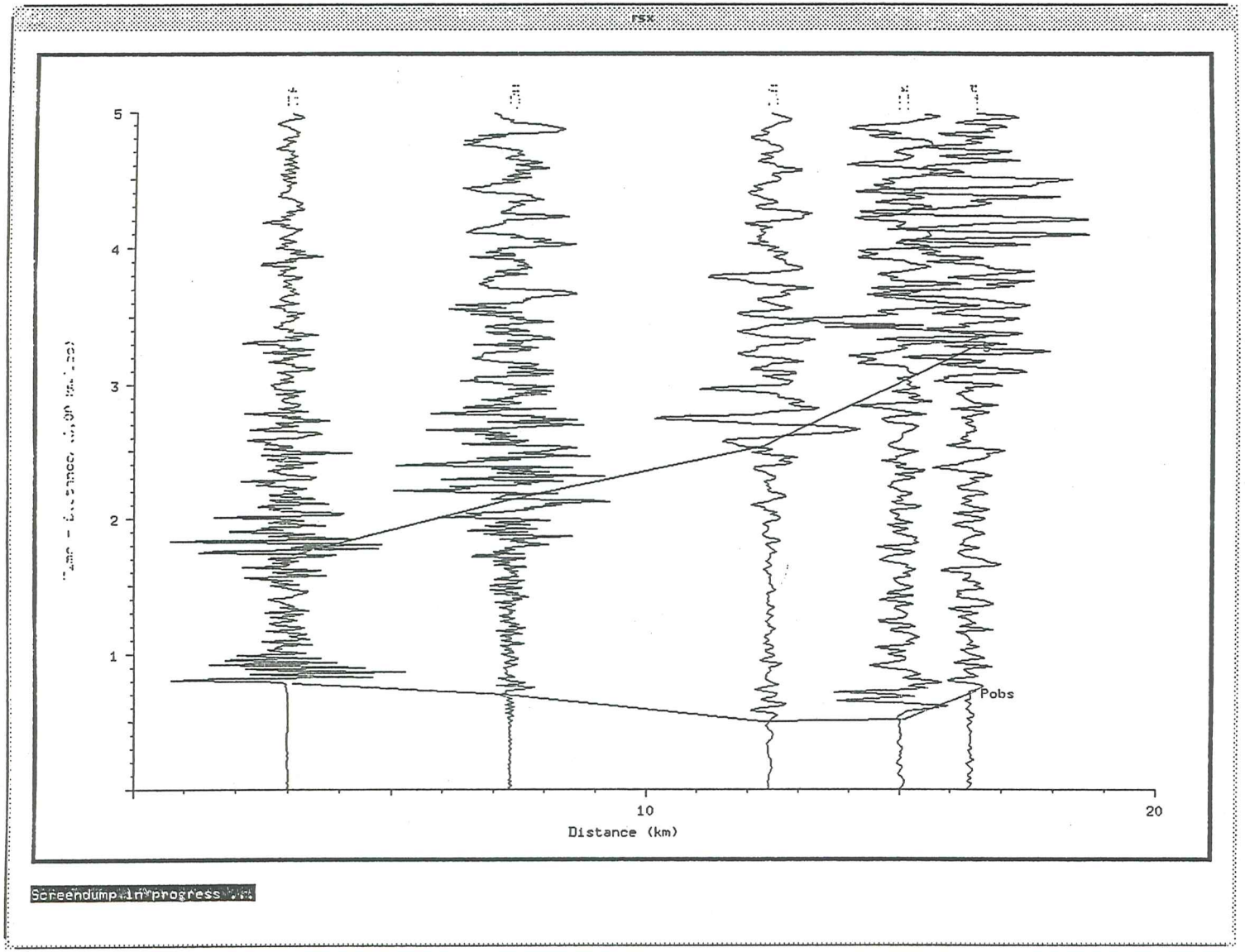
rsx
5
4
3
2
1
10
20
Distance (km)
Pobs
Screendump in progress

Screendump of progress
Time - Distance (0.00 km/sec)
1
2
3
4
5
Distance (km)
10
20
Pobs

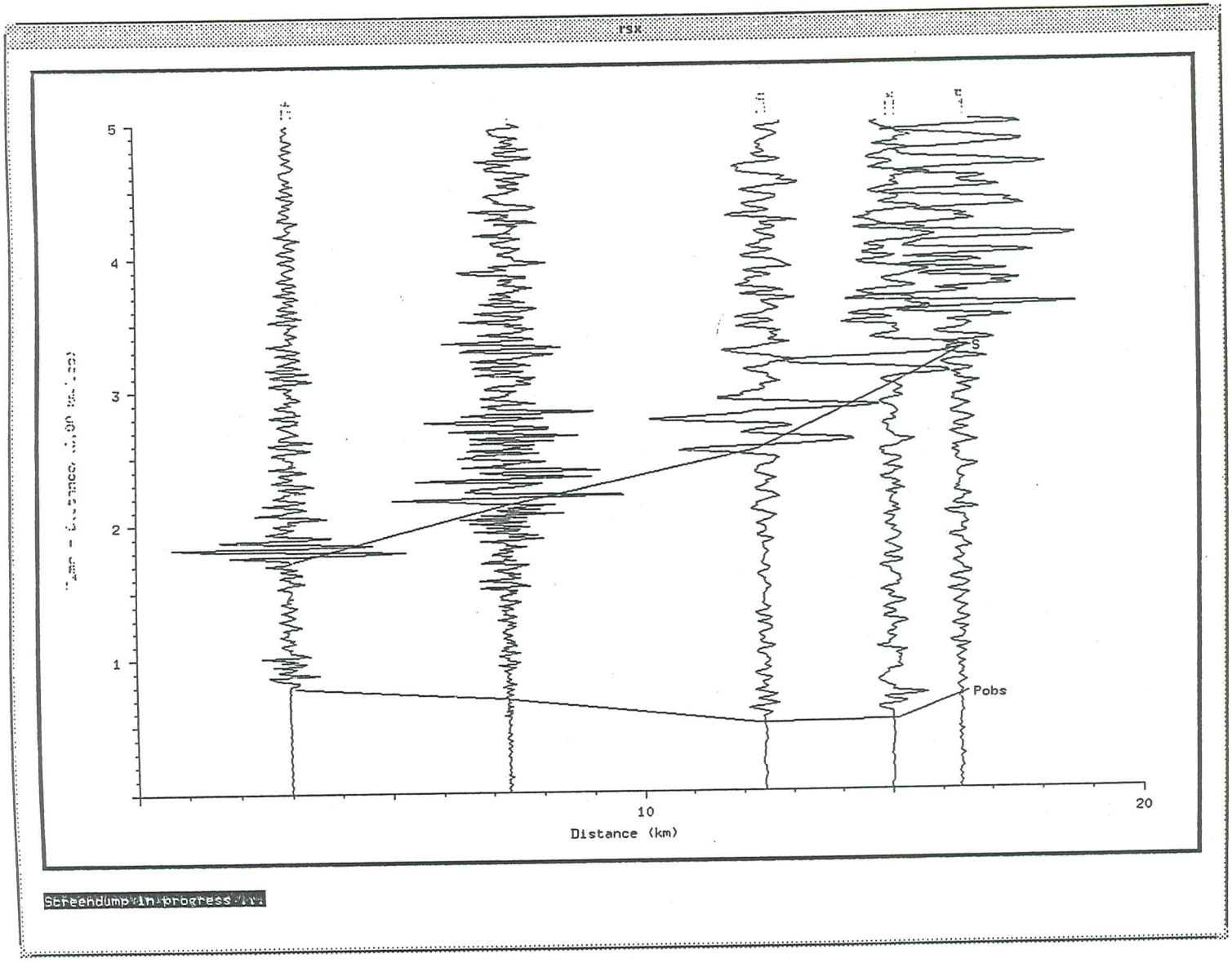
rsx
5
4
3
2
1
S
Pobs
10
20
Distance (km)
Screendump in progress

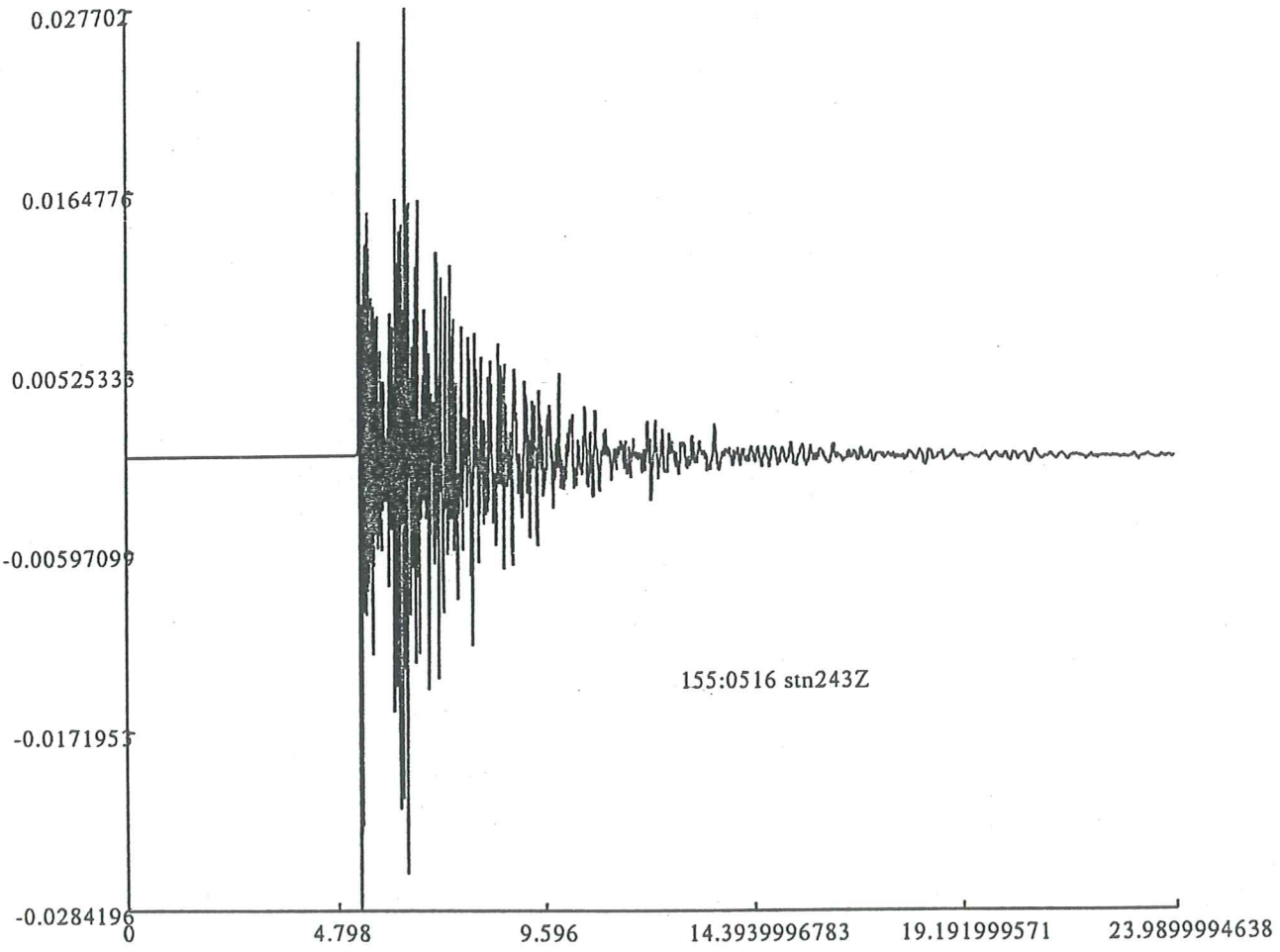
0.027702
0.0164776
0.00525336
-0.00597099
-0.0171953
-0.028419
0
4.798
9.596
14.3939996783
19.191999571
23.9899994638
155:0516 stn243Z

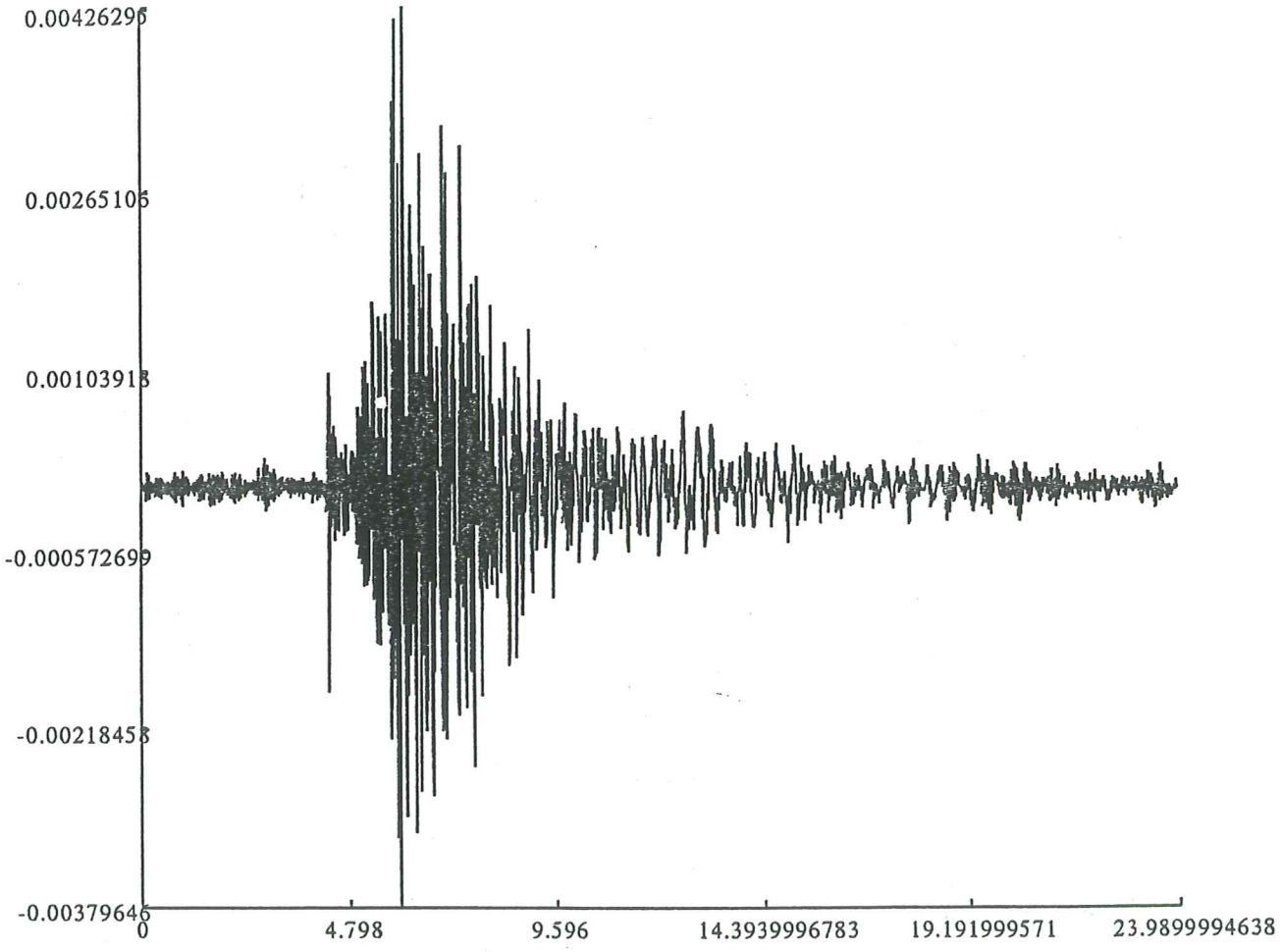
0.00426296
0.00265105
0.00103913
-0.000572699
-0.00218458
-0.00379646
0
4.798
9.596
14.3939996783
19.191999571
23.9899994638

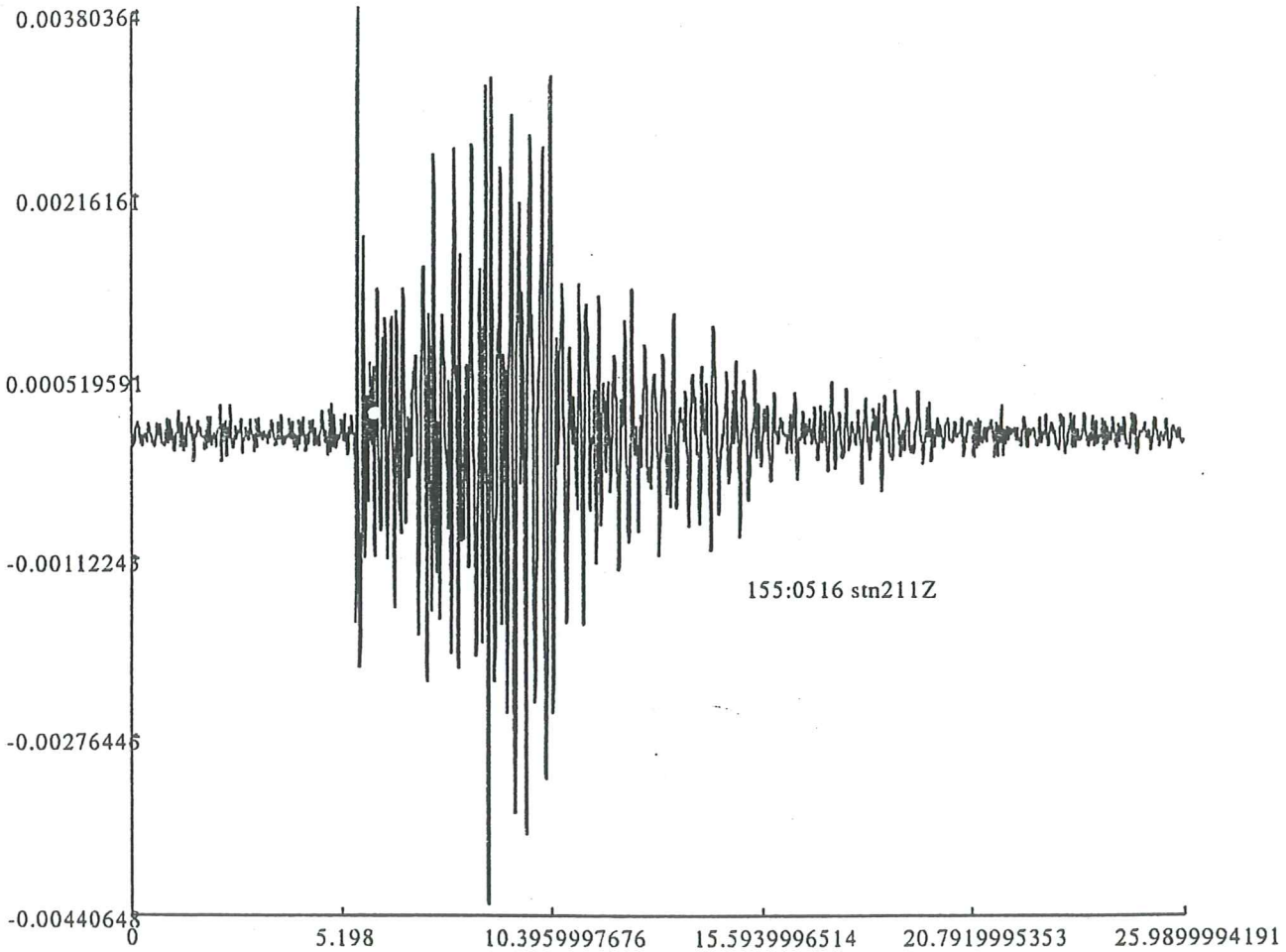

Transposed 2 12

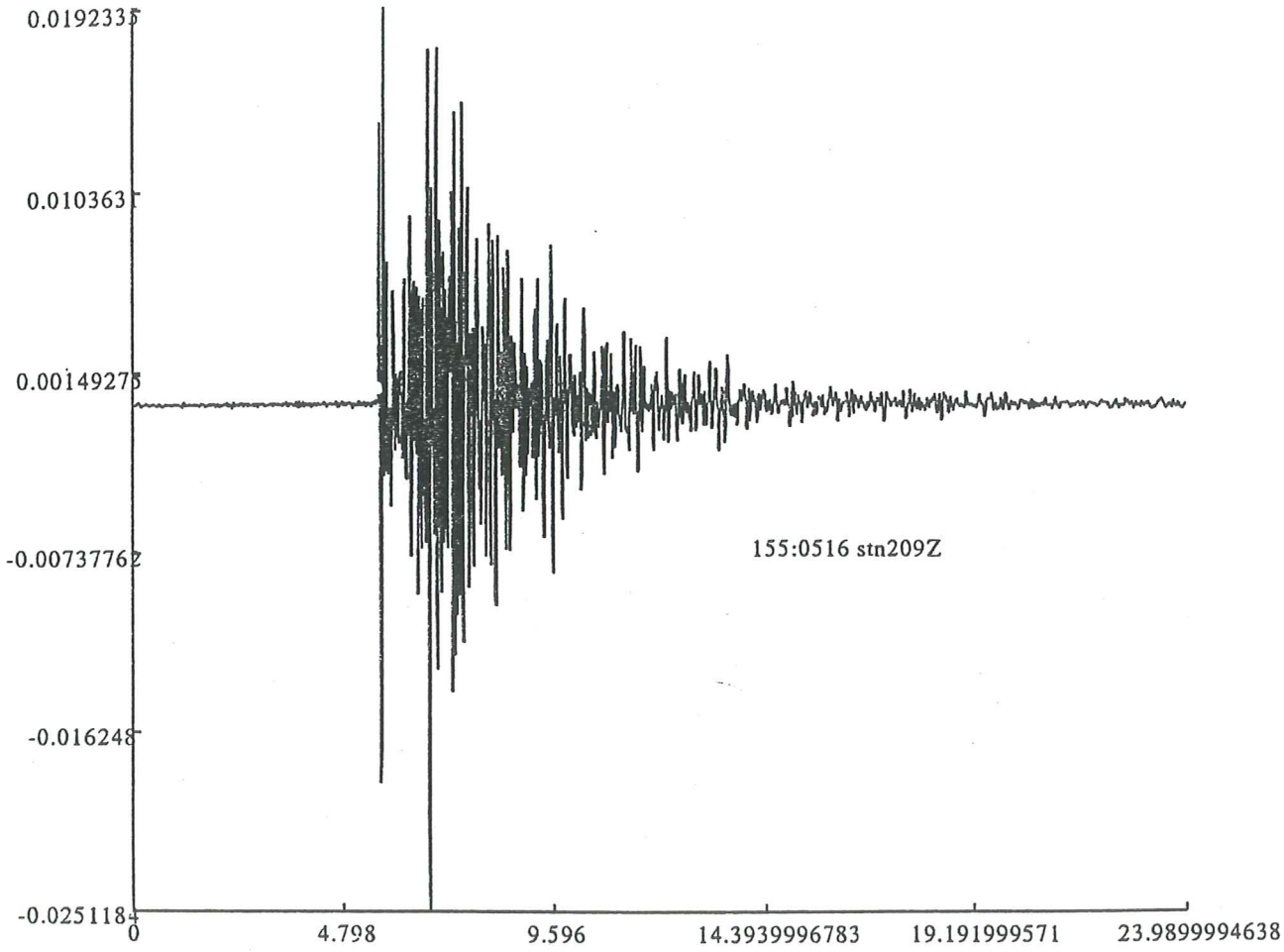
0.0192335
0.010363
0.00149275
-0.00737762
-0.016248
-0.025118
0
4.798
9.596
14.3939996783
19.191999571
23.9899994638
155:0516 stn209Z

MSC

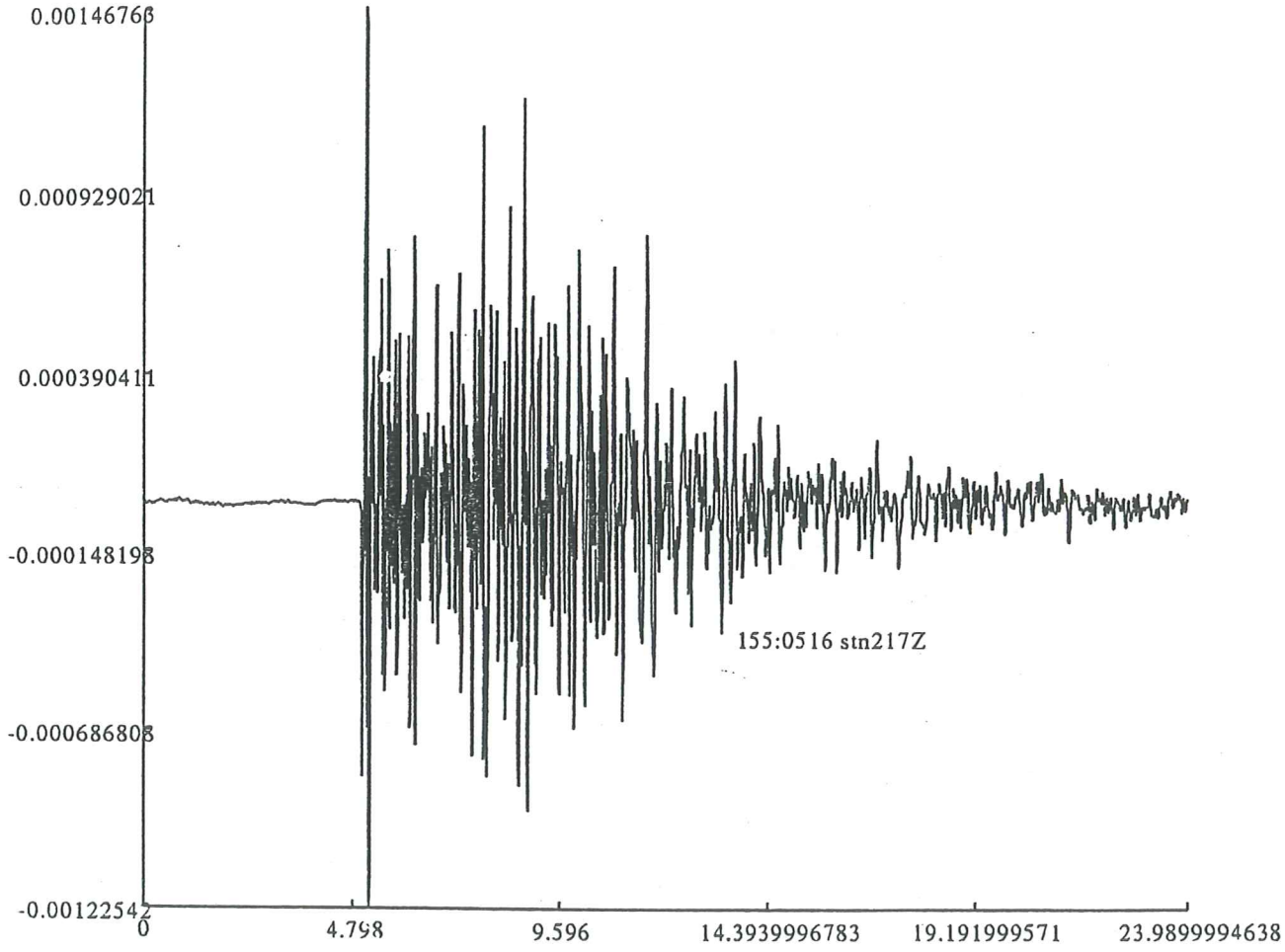
0.00146768
0.000929021
0.000390411
-0.000148198
-0.000686808
-0.00122542
0
4.798
9.596
14.3939996783
19.191999571
23.9899994638
155:0516 stn217Z

E.D. 2-12

SKO

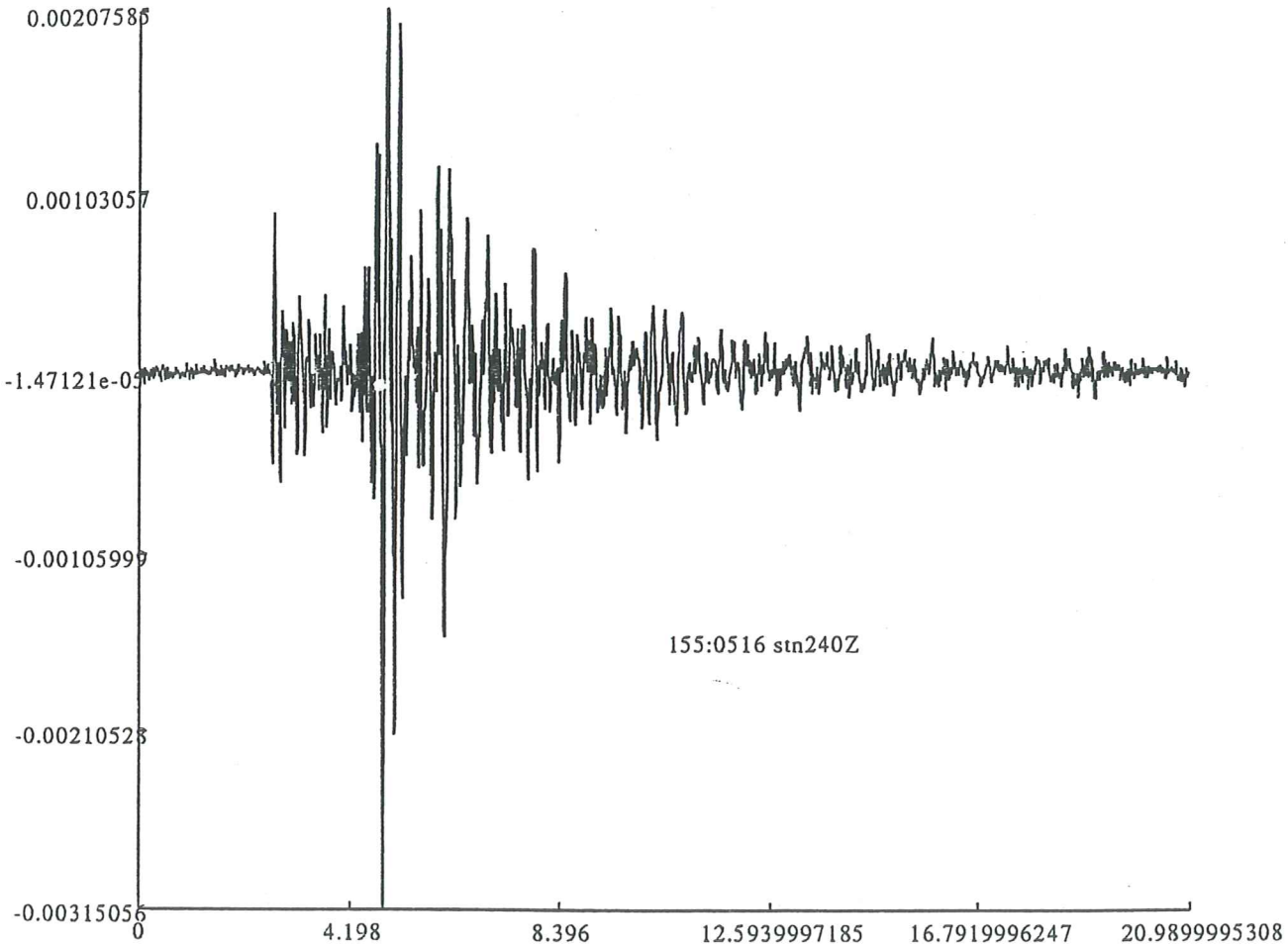
0.00207585
0.00103057
-1.47121e-05
-0.00105999
-0.00210528
-0.00315056
0
4.198
8.396
12.5939997185
16.7919996247
20.9899995308
155:0516 stn240Z